Upgrading Pyrolytic Tyre Char through Acid-alkali Demineralisation

by

Kirsty Louise Henry

Thesis presented in partial fulfilment
of the requirements for the Degree

of

MASTER OF ENGINEERING
(CHEMICAL ENGINEERING)

in the Faculty of Engineering
at Stellenbosch University

Supervisor
Dr C. E. Schwarz

Co-Supervisor/s
Prof J. F. Görgens

December 2015

DECLARATION

By submitting this thesis electronically, I declare that the entirety of the work contained therein is my own, original work, that I am the sole author thereof (save to the extent explicitly otherwise stated), that reproduction and publication thereof by Stellenbosch University will not infringe any third party rights and that I have not previously in its entirety or in part submitted it for obtaining any qualification.

Date: December 2015

I

ABSTRACT

Waste tyres are proving to be a critical environmental and social problem not only in South Africa, but worldwide; with significant hazards associated with illegal dumping, stockpiling and burning. Efforts are currently directed towards the management of waste tyres, and pyrolysis is proving to be a promising form of waste tyre recycling, with the production of potentially valuable products. Pyrolytic tyre char, in particular, is a carbonaceous solid product originating from the carbon black filler within tyres, and constituting 40% of the total product mass produced by pyrolysis. Pyrolytic tyre char, however, has an undesirable structure and is plagued by contaminants, thus considerably decreasing it value and market potential. Currently, South African waste tyre pyrolysis plants are stockpiling great quantities of char, which reduces revenue and decreases investments. The problem statement was thus that the current char produced by waste tyre pyrolysis is crude and has minimal market value or use which, in turn, reduces waste tyre pyrolysis sustainability and waste tyre recycling efforts.

A systematic approach was utilised, with a combination of literature research, experimentation, engineering design and economic evaluation methods employed to (i) investigate pyrolytic tyre char upgrading methods and product opportunities; (ii) develop and propose a process for crude pyrolytic tyre char upgrading; (iii) analyse the economic viability and appeal of the proposed crude pyrolytic tyre char upgrading process.

A thorough literature review revealed that, utilising an acid-alkali leaching process, crude pyrolytic tyre char could potentially be upgraded to a carbon black product. Industrial char and carbon black N330 were thus characterised to establish benchmark targets and process requirements, including ash content reduction from 16.24 to 1.95wt.%; BET surface area increase from $58.9m^2.g^{-1}$ to $80.22m^2.g^{-1}$; and average particle size reduction from 153.2 to 38.5μm. Furthermore, a mineralogical study revealed the ash contained approximately half silicon/silicon dioxide and half metallic components; thus substantiating the use of both an acid and an alkali.

Acids and alkalis mentioned in literature, with regards to pyrolytic tyre char demineralisation, were screened as per demineralisation ability and raw material costs. Hydrochloric acid and sodium hydroxide proved to be superior. Subsequently, significant process factors, including extraction time, extraction temperature and lixiviant concentration, were analysed through kinetic trials and sequential extractions. A final acid-alkali demineralisation process was thus established; and pyrolytic tyre char was upgraded to a carbon black product using 3x 5.0M NaOH washes at 88°C for 60minutes followed by 1x 1.0M hydrochloric wash at 80°C for 20minutes, including water washes

prior to each lixiviant wash. Additionally, 100g lixiviant was utilised per wash; with the char: lixiviant ratio decreasing from an initial 20:100 (g/g).

The upgraded pyrolytic tyre char was comparable to commercial carbon black N330 in terms of ash content (1.83wt.%) and BET surface area ($84.7m^2.g^{-1}$); however, it had much coarser particles (130.6μm).

Finally, using the proposed acid-alkali process, economic analyses were applied to an industrial process design. An industrial upgrading project cannot be eliminated as unprofitable; however project investment is not highly appealing, since the upgraded pyrolytic tyre char has to sell for a high price for the process to be economically feasible, and may not be able to compete in the relevant markets.

Two key recommendations for further research include (i) acid-alkali process optimisation aiming to reduce raw material and utility expenditures; (ii) analysing the influence of the upgraded carbon black product on tyre characteristics with the aim of suitability assessment and the requirement of a particle size reduction process.

OPSOMMING

Afvalmotorvoertuigbande blyk tans 'n kritiese omgewings- en sosiale probleem te wees, nie slegs in Suid-Afrika nie, maar wêreldwyd; met noemenswaardige gevare geassosieer met die onwettige storting, opgaring en brand daarvan. Pogings is tans gerig op die bestuur van afvalmotorvoertuigbande, en pirolise blyk tans 'n belowende vorm van herwinning van afvalmotorvoertuigbande te wees, met die produksie van potensiële waardevolle produkte. Pirolitiese motorvoertuigbandsteenkool, in besonder, is 'n koolstofryke soliede produk, afkomstig van die koolstof swart substraat in motorvoertuigbande, en wat 40% uitmaak van die totale produkmassa wat deur pirolise geproduseer is. Pirolitiese motorvoertuigbandsteenkool het egter 'n ongewenste struktuur en word geteister deur kontaminante, wat dus die waarde en markpotensiaal daarvan aansienlik verminder. Tans gaar Suid-Afrikaanse afvalmotorvoertuigbandpirolise-aanlegte aansienlike hoeveelhede steenkool op, wat inkomste verminder en beleggings laat afneem. Die navorsingsverklaring was dus dat die huidige steenkool wat deur afvalmotorvoertuigbandpirolise geproduseer is, ru is en minimale markwaarde of gebruik besit, wat op sy beurt, die volhoubaarheid van afvalmotorvoertuigbandpirolise- en herwinningspogings verminder.

'n Sistematiese benadering is gebruik, met 'n kombinasie van literatuurnavorsing, eksperimentering, ingenieursontwerpe en ekonomiese evalueringsmetodes wat gebruik is om (i) pirolitiese motorvoertuigband opgraderingsmetodes- en produkgeleenthede te ondersoek; (ii) 'n proses te ontwikkel en voor te stel vir die opgradering van ru pirolitiese motorvoertuigbandsteenkool; (iii) die ekonomiese lewensvatbaarheid en aantreklikheid van die voorgestelde ru pirolitiese motorvoertuigbandsteenkool opgraderingsproses te analiseer.

'n Deeglike literatuuroorsig het getoon dat, met behulp van 'n suur-alkali logingsproses, ru pirolitiese motorvoertuigbandsteenkool potensieel opgegradeer kan word na 'n swart koolstof produk. Industriële steenkool en koolstof swart N330 is, dus, gekenmerk om maatstafteikens en prosesvereistes te vestig, insluitend vermindering van asinhoud vanaf 16.24 - 1.95wt.%; BET oppervlakte toename van 58.9m^2.g^{-1}-80.22m^2.g^{-1}; en gemiddelde deeltjie-grootte vermindering van 153.2 - 38.5µm. Verder, 'n mineralogiese studie het getoon dat die as ongeveer 'n helfte silikon/silikondioksied en 'n helfte metalliese komponente bevat het; dus ter stawing van die gebruik van beide 'n suur en 'n alkali.

Sure en alkalië in die literatuur genoem, met betrekking tot pirolitiese motorvoertuigbandsteenkool demineralisasie, is gekeur volgens demineralisasievermoë en roumateriaalkostes. Soutsuur en natriumhidroksied het bewys om superior te wees. Daarna beduidende proses faktore, insluitende

ekstraksietyd, ekstraksietemperatuur en lixiviantkonsentrasie, is ontleed deur kinetiese proewe en sekwensiële ekstraksies. 'n Finale suur-alkali demineralisatieproses is, dus, gestig; en pirolitiese motorvoertuigbandsteenkool is opgegradeer na 'n koolstof swart produk met behulp van 3x 5.0m NaOH was teen 88 °C vir 60 minute, gevolg deur 1x 1.0m soutsuur was teen 80 °C vir 20 minute, insluitend waterwasse voor elke lixiviant was. Addisioneel, is 100g lixiviant benut per was; met 'n afname in die pirolitiese motorvoertuigbandsteenkool: lixiviant verhouding van 20:100 (g/g) per was. Die opgegradeerde pirolitiese motorvoertuigbandsteenkool was vergelykbaar met kommersiële koolstof swart N330 in terme van asinhoud (1.83wt.%) en BET oppervlakte (84.7$m^2.g^{-1}$); egter, het dit baie growwer deeltjies (130.6µm).

Ten slotte, deur die gebruik van die voorgestelde suur-alkali proses, is ekonomiese ontledings toegepas op 'n industriële prosesontwerp. 'n Industriële opgraderingsprojek kan nie uitgeskakel word as nie-winsgewend nie; maar projekbelegging is egter nie hoogs aanloklik nie, met hoë terugbetalingstydperke en lae beleggingsopbrengstariewe.

Twee belangrikste aanbevelings vir verdere navorsing sluit in (i) suur-alkali proses optimalisering gemik op die vermindering van roumateriaal- en nutuitgawes; (ii) ontleding van die invloed van die opgegradeerde koolstof swart produk op motorvoertuigbandeienskappe, met die doel op geskiktheidsevaluering en die vereiste van 'n deeltjie-grootte verminderingsproses.

DEDICATION

I devote this thesis work to my special family. Peter and Erika Henry, thank you for your continuous encouragement, upliftment and love. Your support has motivated me to achieve in all aspects of my life. I would not be where I am today without you. Matthew Henry, I will always treasure the laughs and memories we shared growing up, and that we still share. Thank you for your continuous support and friendship. Stephen Brown, your patience, love and advice has made me a stronger person. Thank you for everything.

ACKNOWLEDGEMENTS

First and foremost, I would like to express my sincere gratitude to my supervisor, Dr Cara Schwarz, whose knowledge, support and assistance has added considerably to my thesis completion and overall post-graduate experience. Allowing me the room to work in my own way has greatly increased my engineering capabilities and confidence. My co-supervisor, Prof Johann Görgens, whose insightful comments and continuous effort has taught me to 'think out of the box'.

I would like to convey my gratitude to REDISA for personal and research financial support. In particular, Dr Ziboneni Godongwana and Ika van Niekerk, for their great knowledge regarding the tyre industry and the endless provision of pyrolytic tyre char from the associated South African companies.

My research group, Devon, Katie, Malusi, Lusani, Marvin, Sithandile and Bart, have provided constant support, divulged some great tyre knowledge, and shared some good laughs through the stressful stages of completing a postgraduate degree.

My humble appreciation and respect must be given to the technical staff of Stellenbosch University. Mr Jos Weerdenburg and Anton Cordier, your relentless help and friendly smiles have made my years at Stellenbosch greatly memorable. Mr. Alvin Petersen, a special thank you for all the technical help you have provided through the years. Appreciation must also be given to Mr. Oliver Jooste and Linda Mzayifani for your punctual assistance through the years.

Thank you Mrs. Hanlie Botha, Dr Cynthia Sanchez-Garrido and Dr Angelique Laurie for the hours of analytical assistance you have provided me, especially since the char is very dirty and difficult to work with. Finally, thank you Mrs. Francis Layman for the punctual orders and going out of the way to help me with any logistical issue that came up. Mrs. Julianna Steyl, Lynette Bresler and Anita Kleinschmidt, thank you for your relevant assistance. Thank you Dr JP Barnard for ensuring my work was always backed-up.

TABLE OF CONTENTS

LIST OF TABLES

LIST OF FIGURES

LIST OF ABBREVIATIONS USED

A	Acid anion
ASTM	American Society for Testing and Materials
B	Base cation
BET	Brunauer Emmett Teller
BJH	Barrett-Joyner-Halenda
BR	Polybutadiene rubber
CCR	Cumulative cash ratio
CE	Cost effectiveness
CEA	Cost effectiveness analysis
CEPCI	Chemical Engineering Process Cost Index
CONNEP	Consultative National Environment Policy Process
CSTR	Continuously stirred tank reactor
CV	Calorific value
EA	Elemental analyser
EDX	Electron dispersive X-ray spectroscopy
EPDM	Ethylene propylene diene rubber
ICP-MS	Inductively coupled plasma mass spectrometry
ICP-OES	Inductively coupled plasma optical emission spectrometry (ICP-OES)
IR	Synthetic cis-3-4-polyisoprene rubber
IRR	Internal rate of return
IWTMP	Integrated waste tyre management plan
NPV	Net present value
NR	Natural rubber
PCT	Passenger car tyres
PET	Polyethylene terephthalate

PFD	Process flow diagram
PPB	Payback period
PT-char	Pyrolytic tyre char
PT-gas	Pyrolytic tyre gas
PVC	Polyvinyl chloride
PVR	Present value ratio
REDISA	Recycling and Economic Development Initiative of South Africa
REDOX	Reduction-oxidation
ROROI	Rate of return on investment
SBR	Styrene butadiene rubber
SEM	Scanning electron microscopy
TGA	Thermogravimetric analysis
TDO	Tyre derived oil
TEM	Transmission electron microscope
TT	Truck tyres
UPT-char	Upgraded pyrolytic tyre char
WD-XRF	Wavelength dispersive x-ray fluorescence
WT-pyrolysis	Waste tyre pyrolysis
ZAR	South African Rand

Chapter 1: Introduction and Background

1. 1.   Problem in context

Transportation is essential to the development of a country's economy as it facilitates industrial growth, communication and, evidently, the movement of goods and people. Due to the increase in opulence of the average income lifestyle, the use of convenient transport has increased substantially. The utilization of light to heavy weight road vehicles, agricultural and earthmoving vehicles, as well as aircrafts has resulted in an astounding increase in tyre production. It has been approximated that 1.4 billion tyres are manufactured internationally on an annual basis [1], with USA responsible for one third of the global production [2]. At the termination of their useful life, most waste tyres were disposed in landfills, with an estimated 4 billion tyres residing within landfills world-wide [1]. In South Africa, there is an approximated 60 million waste tyres stored in stockpiles, with an extra 10 million added to this number annually [3][4]. These statistics do not include the large number of waste tyres littered around rural communities, and in rivers and fields.

Waste tyres can become highly hazardous to their surrounding social and biological environments if not managed and disposed appropriately. Tyres disposed in landfills have associated socio-economic and environmental issues, and are an eyesore to surrounding communities [5][6]. Due to their robust characteristics, tyres do not decompose quickly [7] and, owing to their incompressibility, require a large volume of landfill space.

The high cost of waste tyre disposal in South Africa has led to the illegal dumping of units in grasslands, aquatic environments and industrial areas [7] causing associated environmental issues and related health concerns.

The storage of tyres and waste tyres in stockpiles can become residence to disease vectors [8]. Additionally, if stockpiles catch alight, not only is it costly to extinguish [7], but also cause temporary impaired vision, health problems, and environmental pollution and destruction. The smoke released by open tyre fires are of major concern as they release large quantities of noxious gases [9][10]. In South Africa, tyre fires are a common occurrence in underprivileged communities as individuals aim to produce heat or extract steel to sell [7].

In order to minimise the hazards associated with waste tyres, their accumulation must be managed. In South Africa, the White Paper Policy was established at the turn of the millennium through a process known as the Consultative National Environment Policy Process (CONNEP). This policy deals with environmental management in South Africa. In 2004, the Air Pollution Prevention Act No. 65 of

1965 was replaced by the Air Quality Management Act No. 39 of 2004, which deals with the quality of gases discharged into the atmosphere. In 2005, the Environment Conservation Act of 1989 was amended to include the management of special wastes. During 2007, the Department of Environmental Affairs and Tourism South Africa published a document regarding waste tyre regulations for public comment. [7]

As of 2012, the South African Government has accepted an integrated waste tyre management plan (IWTMP) which is managed by Recycling and Economic Development Initiative of South Africa (REDISA) [4]. This plan targets the sustainable management of waste with special emphasis on waste tyre management. The IWTMP is in accordance with the National Environmental Management Waste Act, 2008 (Act No. 59 of 2008) as stated in the Government Gazette, 17 April 2012, No. 35147. The REDISA integrated industry waste tyre management plan aims to formalise the informal tyre recycling industry by charging new tyre importers and manufacturers a fee of ZAR 2.30 per kilogram tyre they place on the South African roads. These importers and manufactures are constitutionally obligated to pay the fee as per the terms in the Waste Tyre Regulation: Part 3. The cumulative fee is then distributed throughout different operational elements of the REDISA plan including research funding, establishing tyre collection depots and recycling facilities, training personnel, and reimbursing transporters. Tyre dealerships benefit greatly by registering themselves for waste tyre collection since they are not financially responsible for waste tyre removal and processing, and it prevents waste tyre accumulation on their property. The transporters, who collect and relocate the waste tyres to depots, are monetarily compensated by REDISA. The depots receive and stockpile the waste tyres, further distributing them for recycling.

Recycling via pyrolysis is receiving much attention as a promising waste management technique owing to its simplicity and environmental benefits. Pyrolysis can be described as the degradation of inorganic material using elevated temperatures and an inert (oxygen-free) atmosphere [1], [11]–[13]. The process is associated with minimal environmental hazards since any noxious gases are caught and sold as product [1]. Energy required for pyrolysis process heating can originate from the recycling of pyrolysis products back into the process [1]. As an added benefit, pyrolysis decreases the reckless disposal of waste tyres, thus decreasing the negative environmental and health factors that accompany waste tyre pollution. Two decades of pyrolysis research has resulted in the industrial implementation of this process [14].

A waste tyre pyrolysis (WT-pyrolysis) process decomposes waste tyre crumb into a carbonaceous solid fraction, which constitutes approximately 40 percent of the total product mass, and a volatile fraction, constituting the balance, i.e., roughly 60 percent [1]. The volatile fraction, produced from

the elastomers, is condensed to form an oily product and incondensable gases. The pyrolytic tyre gas (PT-gas) is typically recycled back into the process as heat. Tyre derived oil (TDO) has been accentuated for processing since its components are greatly valuable. Pyrolytic tyre char (PT-char), however, is disillusioned by contaminants and, thus, has minimal uses to date [1][14].

Currently, there is minimal market value for PT-char in South Africa as there is a lack of resilient processes which are able to tolerate its crude nature. In South Africa, approximately 1500 tonnes of PT-char is stockpiled at WT-pyrolysis plants. For budget purposes, this PT-char is regarded as a cost to the company as it will eventually be land filled. Moreover, this limitation negatively affects the associated WT-pyrolysis economics as revenue is reduced. Shareholders recognise fragility within a process and avert/ avoid investments. Furthermore, waste tyre recycling efforts are thwarted.

For increased WT-pyrolysis sustainability and economic viability, all products should be valorised. There is thus an opportunity to increase the market value of PT-char. This can be achieved through the development and creation of a value-added product from crude PT-char through an upgrading process. The production of a valuable product from PT-char will increase WT-pyrolysis revenue, enhance investment appeal and amplify the environmental benefits. This, however, requires a great deal of research, development and economic evaluation. Determination of a valuable product which can be produced from crude PT-char is crucial. Furthermore, development of an upgrading process and product economic feasibility is essential in order to assess whether the process would be able to survive on an industrial scale.

1. 2.   Problem statement

"The current char produced by waste tyre pyrolysis is crude and has minimal market value or use which, in turn, reduces waste tyre pyrolysis sustainability and waste tyre recycling efforts".

1. 3.   Problem resolution process

The worth of crude PT-char can be increased by creating a valuable product that is able to compete within its relevant market, its production is economically viable, and has the added benefits of environmental sustainability. Refer to appendix A for a mind-map illustrating the unravelling of the research problem and emerging themes.

The first stage of this research is the determination of a valuable product which can be produced from crude PT-char. This stage is based primarily on previously published research outlining the

characteristics of crude PT-char and target products which can be produced from crude PT-char, thus showing upgrading opportunities.

Following the establishment of the degree to which crude PT-char must be transformed to create the target product, the baseline process which will be utilised for PT-char upgrading will be determined. A literature based study and intrinsic knowledge on chemical processes will be utilised to determine the baseline process.

The second stage includes process and product development: factors (process variables) that influence the baseline process will be altered so as to obtain a final product from crude PT-char with required characteristics. Safety, environmental factors and economic viability considerations will be included during process development.

Finally, an industrial process, in the form of a flow diagram, will be proposed, and a relevant economic study performed. The economic study, based on capital, manufacturing costs, revenue and tax, will show economic and investment viability over the project lifetime.

1. 4. Research objectives

The aim of this research is to add value to crude pyrolytic tyre char by achieving the following objectives:

i.   To investigate pyrolytic tyre char upgrading methods and product opportunities.
    a.   To determine a suitable target product to be produced from crude pyrolytic tyre char.
    b.   To determine a suitable baseline technique for pyrolytic tyre char upgrading.
    c.   To perform initial characterisation studies on commercial pyrolytic tyre char and target product for the attainment of benchmark characteristics.
ii.   To develop and propose a process for crude pyrolytic tyre char upgrading.
    a.   To evaluate factors which affect the pyrolytic tyre char upgrading process.
    b.   To produce a value-added product with suitable characteristics from crude pyrolytic tyre char.
iii.   To analyse the economic viability and appeal of the proposed crude pyrolytic tyre char upgrading process.

1. 5. Significance of the study

This study is significant as any efforts to alleviate a small fraction of the waste tyre management problem will have great environment and economic benefits.

WT-pyrolysis is a step into the right direction with regards to waste tyre recycling, but the performance of the process requires improvement, particularly regarding product utilization. In particular, extracting use and value from PT-char is important as it will alleviate the large stockpiles of unused PT-char; it will create revenue and increase WT-pyrolysis sustainability; and it will benefit the environment. PT-char market creation will have a cumulative effect on waste tyre recycling, thus assisting with the waste tyre management problem currently experienced worldwide.

The upgraded pyrolytic tyre char, or UPT-char, must have the appropriate characteristics required for use as a valuable product and to compete in its respective field. In the best case scenario, this research could direct industry into establishing a product which has the potential to be recycled back into tyres, thus closing the cradle-to-grave circle. This act will alleviate the consumption of raw materials and fossil fuels used to produce a tyre.

1. 6.   Scope and limitations of the research

This research is aimed specifically at creating a product of increased value from crude tyre char which has been fully pyrolysed. The study is limited to PT-char only and does not extend into creating value for TDO or PT-gas. One PT-char sample is selected based on characterisation studies.

A comparative literature survey was utilised to select the final product which is to be created from PT-char. This upgraded product was selected according to the composition of PT-char, environmental benefits, commercial value and novelty. The study is limited to creating one product from crude PT-char.

Certain characteristics of the crude PT-char were compared to those of the commercial upgraded product to determine the degree of contamination within PT-char. These characteristics were chosen according to hierarchy and limited to the availability of analytical techniques. The differences in characteristic levels were used as the upgrading benchmark.

These characteristic comparisons, as well as a literature review, are used to establish the type of upgrading process required to remove the contaminants from crude PT-char. The scope is limited to the analysis of one type of upgrading process. The overall focus of the research is to alter the characteristics of crude PT-char using additional processing measures, and not by altering the conditions WT-pyrolysis.

PT-char upgrading experimentation was limited to lab (small) scale equipment since this is the first research stage of PT-char upgrading. The experimental methodology was based on a combination of techniques described by published authors. Furthermore, the methodology was aimed at simplicity

since complex processes are associated with increased error on an experimental basis, and if scaled-up, industrial processes have increased economic viability if simple.

The PT-char upgrading process was developed by altering certain independent process variables and measuring the effective dependent variables. The independent variables were limited to those discussed in literature, which have direct relevance to PT-char and its upgrading process. The dependent variables are limited to the key characteristic differences between crude PT-char and the upgraded product (i.e., benchmark characteristics). The degrees to which the independent variables could be altered was analysed using screening comparisons and kinetic trials. Screening analyses were performed to eliminate process factors and are critical for time and monetary limitations. Kinetic trials were performed to evaluate the response of dependent variables to alterations in independent variables. Kinetic assessments are able to show a combination of responses, including reaction kinetics, system equilibrium, and yield.

Crude PT-char is upgraded by altering the process variables to achieve a final upgraded product with characteristics similar to that of its commercial equivalent. An industrial-scale process, resulting from the process development, is designed in the form of a process flow diagram (PFD). The selection, specification and design of each major process unit are estimated using scientific principles and theory that underline the design and operation of the relevant process unit. The capital cost of the industrial process is estimated using basic relationships for scaling costs and equipment size, as well as inflation forecasting using Chemical Engineering Process Cost Index (CEPCI). The manufacturing costs, including raw material, labour, utility and maintenance and repairs expenditures, are approximated. Positive revenue is produced by UPT-char retailing at ZAR 32.64/kg, further permitting a positive net present worth and an internal rate of return of 9.4%, which are requirements for attractive investment

1. 7. Definition of terms

Waste tyre: (scrap or low-grade) tyre which has met its end of useful life as it is no longer able to meet required standards and regulations, or is unsafe to use.

Waste Tyre Pyrolysis (WT-pyrolysis): the exclusive use of thermal energy to break chemical bonds within a solid, inorganic material causing the degradation or volatilization of said material within the presence of an inert (oxygen-free) atmosphere at elevated temperatures of 400°C and higher [1][11]–[13].

Crude Pyrolytic Tyre Char (PT-char): The low-value, highly contaminated carbonaceous solid fraction produced by the pyrolysis of waste tyres which has not undergone any further treatment or upgrading processes [1][15][16].

Upgraded Pyrolytic Tyre Char (UPT-char): The carbonaceous solid fraction produced by the pyrolysis of waste tyres which has undergone further treatment and/or upgrading processes to alleviate the contaminants in order to add value [1][15][16].

1. 8. Chapter overview

Chapter 2 consists of an extensive literature review covering an overview of the tyre industry and waste tyre management by recycling. A thorough analysis of waste tyre pyrolysis is investigated, including the degree to which certain conditions affect PT- char properties. Additionally, the characteristics of pyrolytic tyre char, as described by authors, are investigated, with the inclusion of current and potential uses. Finally, PT-char upgrading techniques are scrutinised, with prominence given to demineralisation via leaching, and relevant chemistry included.

Chapter 3 includes the experimental characterisation of PT- char, with emphasis directed towards heat of combustion, organic and inorganic composition, surface morphology, and porosimetry.

Chapter 4 encompasses a screening study of relevant lixiviants described by previous studies, with relevance towards demineralisation by leaching. The study is based on lixiviant demineralisation abilities and raw material costs.

Chapter 5 entails a thorough analysis of significant leaching process variables using kinetic studies and sequential extraction arrangements. Using the resultant outcomes, a process which upgrades PT-char to a valuable carbonaceous product of properties similar to that of carbon black N330 is realised.

Chapter 6 incorporates the resultant upgrading process realised in chapter 5 into an industrial process. The equipment costs, manufacturing costs, revenue, tax and cash flow are further analysed and optimised to ensure positive cash flow and investment. A sensitivity analysis of relevant factors is included.

Chapter 2: Literature Review

2.1. Literature review: study objectives

i.   To investigate (research) pyrolytic tyre char upgrading methods and product opportunities.

    a. To determine a suitable target product to be produced from crude pyrolytic tyre char.

    b. To determine a suitable baseline technique for pyrolytic tyre char upgrading.

2.2.   Brief tyre synopsis of the tyre structure an composition

2.2.1. Tyre structure

A modern tyre (figure 1) is a composite material [17] with a structure intended for a primary set of functions. These functions aim at: providing load-bearing capacity; providing damping and cushioning; transmitting driving and braking torque; providing cornering force; providing dimensional stability; resisting abrasion; generating steering response; providing resistance to low rolling; reducing noise and vibration; and providing durabilities throughout expected lifespan [18][17]. The performance and other functional requirements are fulfilled by different components of the tyre structure, namely: tread; sidewall; linear; plies; belts; and beads.
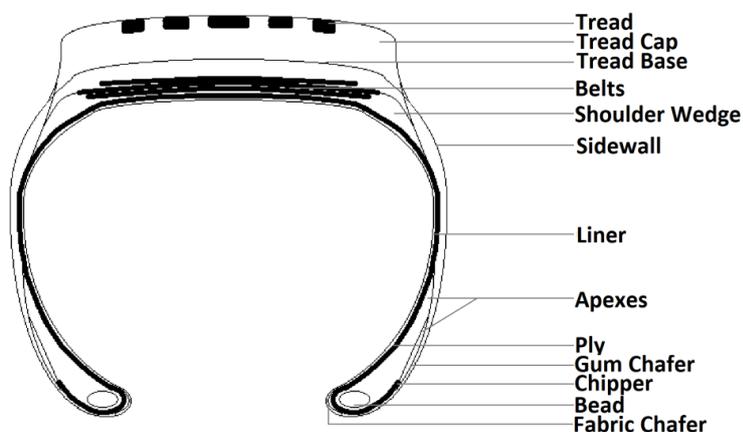
Figure 1:   **Tyre Cross Section**[1]

2.2.2. Tyre composition

The modern tyre is primarily composed of 60-65 wt.% rubber and 25-35 wt.% filler, with the rest consisting of accelerators, steel and textiles [1]. Each of these materials fulfils a specific property

---

[1] Figure 1 adapted from [17]

requirement, with each tyre component comprising of a precise, yet differing material composition [17].

The rubber components of a tyre typically consist of a varying blend of elastomers including natural rubber (NR), synthetic cis-3-4-polyisoprene rubber (IR), polybutadiene rubber (BR), styrene butadiene rubber (SBR), ethylene propylene diene rubber (EPDM), and butyl rubber [19][17]. The elastomer blend composition is dependent on the function of the tyre component as well as the elastomer chemical properties [17].

Elastomers decrease tyre degradation time as they do not readily react with ozone or oils; they resist abrasion; they augment heat dissipation through the tyre; and they increase durability and roll resistance. Elastomers also minimise structural stress and allow adhesion between different materials within the tyre [17].

Two important chemical properties render an elastomer useable as a tyre rubber, namely molecular weight and carbon chain characteristics [18]. The higher the molecular weight the stronger the rubber, thus allowing for large load bearing; however, molecular weight cannot be too high as to render processing unattainable. The hydrocarbon backbone chain must be flexible over the operational temperature range and be free of weak links. The hydrocarbon backbone must have crosslinking capabilities as the chains are comparatively weak and fail by viscous flow [18]. A process known as vulcanization (figure 2) is necessary to strengthen the elastomer by crosslinking the hydrocarbon chains with a vulcanizing agent which is usually sulphur, although peroxides and sulphur donors may be used as well [18]. Vulcanization requires the addition of activators, such as zinc oxide, which increase the rate of vulcanization.
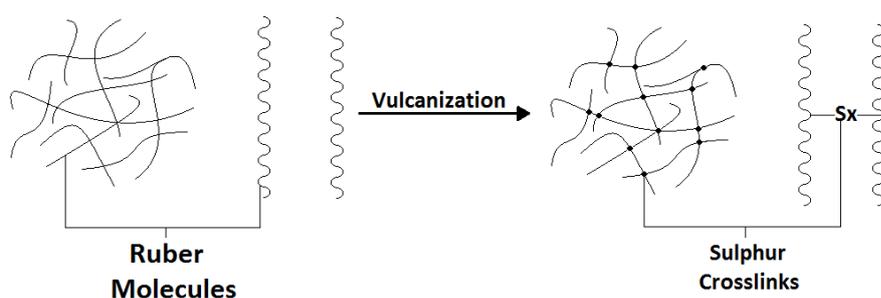
Figure 2:　　　　**Vulcanization of Rubber using Sulphur Crosslinks**[2]

Tyre filler constitutes the second largest portion of material within a modern tyre and grants the tyre its darkened colour [1]. Most importantly, the filler increases tyre strength by reinforcing the components within; and it increases tyre longevity by increasing the overall wear and heat

---

[2] Figure 2 adapted from [18]

resistance [17].It is also added to the rubber for dilution purposes, thus enhancing economic benefits by decreasing both raw rubber material and processing costs [17][18]. Impurity content, surface area and particle size are important factors considered for carbon black usage as reinforcing filler within a tyre. According to Woolard [18], a reinforcing filler is required to have an active surface with a surface area greater than $60m^2/g$, and an agglomerate size less than 50μm. The filler commonly consists of either carbon black (CB) or a mixture of CB and silicon dioxide.

Although not used solitarily for aesthetic reasons, silicon dioxide substitutes a portion of the CB for economic and environmental reasons. Having the required properties to be utilised as tyre filler, silicon dioxide is cheaper and comparatively greener than CB [1].

CB is a carbonaceous material with a specific structure, an active surface area chemically consisting of a polycondensed aromatic structure [18], and minimal impurities depending on the quality and application [20]. Structurally, tyre CB has an aciniform (grape-like) structure consisting of spherical particles (figure 3a) gathered together to form agglomerates (figure 3b) which are further fused together to make aggregates (figure 3c) [20][21]. CB aggregates used in the tyre industry range from 93-593nm [21]. CB is best suited for the tyre industry when the aggregates are irregular in shape and structure.

Particle
(a)

Aggregate
(b)

Agglomerate
(c)
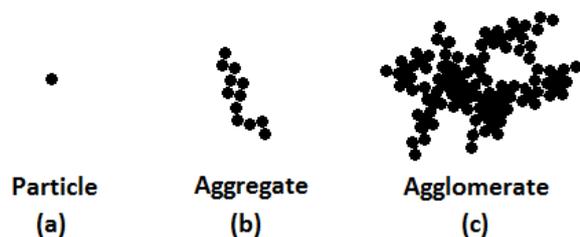
Figure 3:   Structural Form of Carbon Black[3]

CB reinforces the tyre by chemically joining the interface between rubber and carbon black [20]. The degree to which CB is able to chemically link to tyre rubber is known as surface activity. Although the precise mechanism is unknown, it is accepted that the more active the surface of a CB material is, the greater the reinforcement within a tyre [20]. The surface of CB is relatively hydrophobic [22], and is home to a variety of chemical compounds, including hydrogen, sulphur and oxygen (predominantly in the form of quinine) [20]. According to Rodgers et al. [17], the presence of oxygen and hydrogen groups on the surface of CB has a large impact on surface activity. According to Norman [20] however, the understanding by scientists of the relationship between these chemical groups and surface activity has proved intractable with limited understanding of the reactions occurring between the CB surface and the rubber. Recently, researchers have empirically observed

---

[3] Figure 3 adapted from [20]

that surface activity and the degree of reinforcement is possibly related to two attributes: the number of open edged layer planes that are exposed at the surface; and the number of unsatisfied carbon bonds associated with these exposed planes [20]. Surface area is related to surface activity and a CB with a surface area of 60-100m^2g^{-1} is considered active [20]. During tyre manufacturing, coupling agents are often added to modify the filler surface by improving dispersion and physical properties, as well as to facilitate the rubber-carbon black connection [17].

The primary load-bearing structures consist of steel cords and textiles [17]. The steel cords consist of high-carbon steel coated in brass plating. The high carbon steel specifically used in tyres consists of iron alloyed with 0.65% carbon, 0.05% chromium, 0.02% copper, 0.6% manganese, 0.25% silicon and 0.03% sulphur [17]. There are a range of textiles which are commercially available for the use as a cord within tyres including: nylon, specifically nylon 6 and nylon 6,6; polyester, particularly polyethylene terephthalate (PET); fibreglass; and aramid, which is commercially known as Kevlar [17].

Although not comprising of a large portion of the overall tyre composition, speciality chemicals are added to ease tyre processing actions, as well as to minimise tyre degradation.

Tyres can be classified into two predominant categories according to their use: truck tyres (TT) and passenger car tyres (PCT). As shown in table 1 below, the tyres differ in composition according to their specific use. For example, TT is required to be much stronger than PCT since they bear larger loads.

Table 1:   **Comparison in Composition between Truck Tyres and Passenger Tyres[4]**

	Truck Tyre (wt.%)	Passenger Tyre (wt.%)
Rubber (elastomers)	47	45
Carbon Black	21.5	22
Metal (belts and cords)	16.5	21.5
Textile	5.5	-
Zinc Oxide	1	2
Sulphur	1	1
Additives	7.5	5

---

[4] Table 1 adapted from [19]

2.3.   Waste tyre management via the implementation of WT-pyrolysis

2.3.1. Waste tyre recycling techniques

As tyres are used, so do they meet their end of useful-life. The greater the number of tyres put on the road, the greater the number of waste tyres produced. Suitable waste tyre management structures will help alleviate the large quantity of waste tyres accumulated nationally and globally, as well as diminish the associated risks. Recycling is quickly becoming a popular form of sustainable living, and waste tyre recycling is no exception. There are different recycling techniques which can be exploited to make further use of a waste tyre.

One undervalued form of waste tyre recycling is re-treading [4]. PCT are able to be re-tread once, while heavy vehicle tyres can be re-treaded thrice. Industrial and agricultural tyres can be re-treaded up to ten times.

Waste tyres are commonly repurposed as barricades on farms or as swings in playgrounds, for example, without changing their physical structure [23].

Waste tyres have a higher calorific value (CV[5]), which ranges from 27.37-40.00 MJ/kg [1][24], compared to that of coal used for electricity generation, which ranges from 20.3-24.1MJ/kg [25]. Waste tyres are, thus, often used as a solid fuel source and are able to produce large amounts of energy.

Crumbing is an established form of tyre recycling, and involves crushing and grinding of a waste tyre and the removal of steel and textile fibres [4]. Waste tyre crumb is commonly used for synthetic turfs [7], but is also used as a feed stock for WT-pyrolysis [19]. Refer to appendix B for ground tyre applications.

Owing to the large waste tyre reserve and the chemical composition of waste tyres, waste tyre pyrolysis is becoming economically and environmentally attractive. WT-pyrolysis is able produce valuable chemicals and/or energy [2].

2.3.2. Waste tyre pyrolysis: an overview

Pyrolysis as a waste management system is currently receiving much attention for two reasons: it's ability to break down solid wastes which are difficult to recycle and naturally decompose slowly, such as plastics and waste tyres; and its ability to produce products with high CVs and value potential [1].

---

[5] Calorific Values (CVs)

According to Martínez et al. [1], pyrolysis is a variety of different processes namely: reverse polymerization; polymer cracking; and thermal depolymerisation. Perry [11] described pyrolysis to be the thermal degradation of solid organic material in the presence of an oxygen-free (inert) atmosphere at elevated temperatures. In the definition described by T. Wampler [12], pyrolysis is the process whereby chemical bonds are broken using thermal energy only.

Waste tyres are pyrolysed, or decomposed, by first breaking the sulphide bonds, then further breaking the carbon bonds [13] to produce two fractions: a solid fraction, or PT-char, and a volatile fraction [1]. The volatile fraction is further processed to produce a condensable fraction, known as tyre derived oil (TDO) and an incondensable fraction, known as pyrolytic tyre gas (PT-gas) [19]. WT-pyrolysis is, in its entirety, a difficult process due to the low thermal conductivity of tyres [13], and high temperatures are necessary to decompose a waste tyre [13]. The process itself involves a succession of endothermic and exothermic reactions, with the overall process being endothermic [26][27]. There are six principle reactions that occur during WT-pyrolysis: dehydration; cracking; isomerisation; dehydrogenation; aromatisation; and condensation [28]. Due to the complexity of waste tyres, it is difficult to describe all the reactions which occur during WT-pyrolysis. However, an empirical formula, as shown in figure 4, has been proposed to describe the pyrolysis reaction scheme. It has been formulated using two key assumptions: only the organic fraction within the tyres partakes in the pyrolysis reaction(s); and 40wt.% of the tyre feed is converted into the solid pyro-char product.

100wt%
Waste Tyre
$C_{173}H_{165}O_3S_{1.5}N$
  C = 88.20wt%
  H = 6.97wt%
  O = 2.21wt%
  N = 0.59wt%
  S = 2.02wt%

Pyrolysis Process

60wt%
Volatile Fraction
$0.3453C_{285}H_{447}O_9N_3S$

40wt%
Solid Fraction
$1.1539C_{64.5}H_9S$
  C = 94.96wt%
  H = 1.12wt%
  S = 3.41wt%
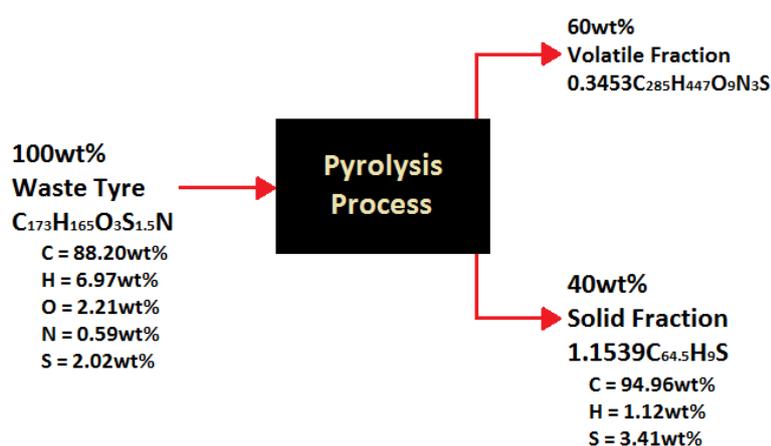
Figure 4:　　　**Pyrolysis Reaction Product Formula**[6]

The series of actions through which a waste tyre is made to pyrolytically decompose can be altered according to user-specific requirements. WT-pyrolysis can thus be further categorized into six principle sub-processes: slow pyrolysis; fast pyrolysis; flash pyrolysis; catalytic pyrolysis; microwave

---

[6] Figure 4 adapted from [1] and calculated on a dry, ash free basis.

assisted pyrolysis and vacuum pyrolysis [1]. Although these processes produce similar products, they differ in reactor technology and applied process parameters, such as heating rate, particle and volatile residence time, final temperature and yield [1].

2.3.3. Waste tyre pyrolysis products

Irrespective of the type of pyrolysis process or reactor used to degrade waste tyres, three products are ultimately produced: PT-gas, TDO and PT-char. The PT-gas and TDO originates from the volatile fraction emerging from the process, while the PT-char consists of the solid fraction. The product distribution is approximately 18-25wt.% PT-gas, 25-30wt.% oil and 35-45wt.% solid [1].

PT-gas is classified as the incondensable portion of the volatile fraction emerging from the pyrolysis reactor [29]. These incondensable PT-gases, which comprise of a paraffin and olefin rich mixture [1], originates from, and depends on, the tyre-specific elastomers [1][19]. PT-gas is predominantly formed by product pyrolysis volatiles undergoing undesirable secondary reactions which destruct long chain hydrocarbons into light, incondensable hydrocarbon PT-gases [19]. PT-gas is an attractive fuel source since is boasts high CVs [7], although the sulphur compounds must be scrubbed out before combusted [24]. According to a review conducted by Martinez et al. [1], CVs reported by authors range from 8.55-75.50 MJ/Nm^3, with most values exceeding 30.00 MJ/Nm^3. This is in agreement with Ucar et al. [16] who have reported PT-gas CVs of between 60.00-65.00 MJ/Nm^3. Upon review, Mui et al. [8] claim that PT-gas has a gross value of 30.00-40.00 MJ/Nm^3. Williams [19] claims that the CV of PT-gas can be as low as 20.00MJ/Nm^3.

TDO is a dark brown/black liquid with a rich sulphurous/aromatic odour [19]. It is chemically complex and has been fractionated into four broad groups, namely: aromatics; aliphatics; hetero-atom fraction; and polar fraction [19]. The ratio of each chemical fraction within TDO is dependent on process conditions and the tyre type and origin [1][19]. Research has focused greatly on the use of TDO as an alternative fuel as it has a high CV which is comparable to petroleum fuels [19]. Most authors have reported TDO CVs between 40.00-45.00 MJ/kg [1][2][5][16][29]; however, high CVs (49.50 MJ/kg) [19] and lower CVs (23.00MJ/kg and 26.00MJ/kg) [13] have been reported. Research has also been directed towards the extraction of valuable chemicals, such as dipentene (dl-limonene), from TDO [2][14][19][31]. Dipentene ($C_{10}H_{16}$) can be used in a variety of different applications: as an industrial lixiviant, in resins, in adhesives, in cosmetics, as dispersing agents for pigments, in fragrances and in flavourings [1]. It is generally accepted that TDO is the most valuable product emerging from WT-pyrolysis [1] since it contains dl-limonene [2].

PT-char is a highly carbonaceous, porous, solid, black material [32]–[34]. The composition of PT-char depends on pyrolysis conditions and notably on waste tyre feed. The carbon predominantly originates from the CB filler, but a small amount of carbon may also be produced by secondary reactions such as the re-polymerisation of polymer-derivatives and the dealkylation and dehydrogenation of organic vapours [1]. PT- char is not only composed of carbon, but also consists of ash and sulphur along with TDO which may be trapped within the porous structure [1][19]. The ash is comprised of two types of components: silicon/ silicon dioxide and metals [19]. The silicon/ silicon dioxide containing compounds originate from the filler as well as additives added during the tyre manufacturing procedure [1]. The metals are derived from the steel wires within the tyre which have not been removed by the tyre crumbing process, as well as from the addition of activators and other additives during tyre production [19]. As with the other WT-pyrolysis products, PT-char is also commonly used as a fuel source since it has a high CV [1][19]. CVs generally range between 28.00-35.00MJ/kg [1][19], with values between 41.70-42.66 MJ/kg [35]–[37] and as high as 71.90 MJ/kg [38] being reported. Low CVs of 14.80-15.70 MJ/kg have been reported [16][16].

2.3.4. Influence of WT-pyrolysis process parameters on PT-char

Pyrolysis processes are controlled by altering certain process parameters such as: feedstock composition, particle size, temperature, pressure, heating rate, carrier gas flow rate and type, residence time of volatiles within the reactor, and pyrolysis reaction time [1]. These parameters have a large influence on product yield and characteristics; however, pyrolysis processes are manipulated so as to increase TDO production and decrease PT-gas and PT-char yield.

Industrially implemented WT-pyrolysis processes consume a combination of brands and types of waste tyres as feedstock [19]. Each tyre brand and type accommodates differing compositions [17][19] which effect the pyrolytic product yield [16][39][40] and product composition[41]. Buekens [42] showed that feedstock influences the PT-char composition since the pyrolysis of TT produced a char with an ash content of approximately 14.32wt.%, while PCT pyrolysis produced a char with 40.3wt.% ash. Feedstock particle sizes (i.e., waste tyre crumb particle size) are closely associated with temperature, heating rate, pyrolysis reaction time and volatiles residence time [1]. During WT-pyrolysis, tyre crumb decomposes on the surface first, moving inwards towards the centre of the particle, with the decomposed elastomers moving out the carbonaceous structure as a volatile [1]. As described by Barbooti et al. [43], the depth at which heat is able to flow into a particle is dependent on pyrolysis time; therefore at a set time, a smaller particle will almost reach complete degradation (as they are regarded as being isothermal) while a coarser particle may contain a rubber

core. Partial particle decomposition will increase PT-char yield (wt.%) since more mass is left within the char, although the PT-char reactivity may be altered by the rubber core.

Pyrolysis temperature is the central process variable and, according to a review conducted by Martinez et al. [1], authors reveal 500°C to be the optimal WT-pyrolysis temperature at atmospheric pressure conditions. Temperatures greater than 500°C may cause the occurrence of undesirable secondary reactions, such as thermal cracking. Secondary reactions decrease TDO yield and increase PT-gas and PT-char mass yield. Volatiles released from elastomer decomposition can absorb on the surface of the PT-char, forming new carbonaceous products, such as tar [1][44][45]. Conesa et al. [44], found an augmented solid fraction yield as pyrolysis temperatures were increased; and Lopez et al. [46] showed that this was caused by the deposition of heavy hydrocarbon compounds on the surface. In another study, Conesa et al. [47] found nominal TDO production at 1000°C, but rather PT-gas and a solid fraction composed of approximately 37wt.% and 25wt.% PT-char and carbonaceous deposits respectively. Authors show that temperature is inversely related to PT-char CV [35] and directly related to fixed carbon content [35] and surface area [46][48].

Heating rate within a pyrolysis reactor has a large effect on temperature gradients within feedstock particles and thus, reaction kinetics [1]. As Senneca et al. [49] stated, the faster heat is added to a particle, the faster decomposition occurs and the more volatiles are cumulatively released. The fast formation and release of volatiles at a high temperature may lead to secondary reactions in the bulk gaseous phase, as well as within the porous particle [1].

The flow rate and type of carrier gas within a pyrolysis system is an important variable and allows for the control of secondary reactions. A high carrier gas flow rate reduces secondary reactions by increasing superficial gas velocity, thus decreasing the volatiles residence time within the reactor [1]. The carrier gas must be inert as the presence of, for example, oxygen will cause secondary reactions, such as combustion, thermal cracking, repolymerisation, recondensation and PT-char gasification [1]. Ogasawara et al. [50], produced a very low PT-char yield of 9wt.% when using a steam atmosphere within the pyrolysis reactor; however, the PT-char accommodated a high surface area of $1260m^2/g$. In concurrence, Betancur et al. [51] found PT-char oxidation only occurred at temperatures higher than 760°C when the carrier gas consisted of CO_2. Additionally, Lucchesi and Maschio [52] found the sulphur content to shift to the volatile fraction when a CO_2 environment was utilized.

A pressure reduction can minimise the occurrence of undesirable secondary reactions [40]. Lopez at al. [53], explained that a vacuum created a positive pressure gradient within a particle, thus

increasing volatile diffusion towards the particle surface and decreasing volatile residence time within the reactor. This minimises the formation of carbonaceous deposits on the surface of PT-char, further increasing active sites. Roy et al. [54], and Zhang et al. [40], both found the characteristics of PT-char to be similar to that of commercial CB, although still containing high ash content, when WT-pyrolysis was under vacuum.

Table 2 below illustrates the yield distribution of pyrolysis products, as found in literature, in terms of pyrolysis reactor, process temperature, heating rate and tyre feed mass. Appendix C provides a concise summary of the central trends discussed above, regarding the influence of pyrolysis process parameters on pyrolysis products characteristics and yields.

Table 2:   Distribution of Products by Different Pyrolysis Processes as found in Literature[7]

Reference	Reactor Type	Pyrolysis Temperature (°C)	Heating Rate (°C/min)	Tyre Feed Mass (g) or (kg/hr)	Oil Yield	Char Yield	Gas Yield
[55]	Fixed bed, batch	500	-	-	40.26	47.88	11.86
[56]	Fixed bed, batch	500	1200	-	58.0	37.0	5.0
[57]	Closed batch	450	30	20	~63	~30	~7
[48]	Fixed bed, batch	720	5-80	50	58.8	26.4	14.8
[58]	Fixed bed, batch	475	5	3000	58.2	37.3	4.5
[36]	Fixed bed, batch	950	~2	1ton	20.9	40.7	23.9
[37]	Fixed bed, batch	400	5 & 35	-	38.8	34.0	27.2
[59]	Fixed bed, batch	700	15	175	38.5	43.7	17.8
[60]	Fixed bed, batch	425	10	10	60	~30	~10
[61]	Fixed bed, batch, internal fire tubes	475	-	750	55	36	9
[62]	Moving screw bed	600	-	3.5-8.0kg/hr	48.4	39.9	11.7
[63]	Rotary kiln	550	-	4.8kg/hr	38.12	49.09	2.39
[46]	Vacuum, conical, spouted bed	500	-		~60	~34	~4
[35]	Rotary kiln	500	-	12-15kg/hr	45.1	41.3	13.6
[64]	Fluidised bed	740	-	1kg/hr	30.2	48.5	20.9
	Fluidised bed	750	-	30 kg/hr	31.9	38.0	28.5
	Fluidised bed	700	-	200 kg/hr	26.8	35.8	19
[65]	Fluidised bed	450	-	220g/hr	55.0	42.5	2.5
[66]	Circulating fluidised bed	450	-	5kg/hr	~52	~28	~15
[67]	Conical spouted bed	500	-	-	~62	~35	~3
[5]	Vacuum	520	-	80-180kg	45	36	6

---

[7] Table 2 redrawn from [19]

[31]	Vacuum	500	-		56.5	33.4	10.1
[40]	Vacuum	550	-	100	47.1	36.9	16
[47]	Drop tube reactor	450	-	0.03kg/hr	37.8	35.3	26.9
[68]	Fixed, wire mesh, fast reactor	860	70-90C/s	0.2	~5	~22	~73

2.3.5. WT-pyrolysis as an encouraging form of waste tyre recycling

WT-pyrolysis is a promising form of waste tyre valorisation. It is not as destructive as other thermochemical processes, such as combustion, and the products can be recovered, are manageable and can be utilised as a fuel source or refined to extract valuable chemicals [1][2][69]–[71]. The WT-pyrolysis volatiles can contain up to 50wt.% renewable material due to the presence of natural rubber within the feed stock [1]. WT-pyrolysis emits minimal toxic gases which would cause air pollution [1][5][72]; and emissions that are present include particulate release from fugitive sources and/or volatile emissions from equipment leakages. In comparison with combustion, pyrolysis releases a lower quantity of CO_2 per unit energy [1]. WT-pyrolysis is able to separate impurities [28], such as heavy metals [26] and sulphur [1], by retaining them within the solid PT-char fraction. As a result, corrosive emissions are avoided [1]. Approximately 70wt.% sulphur originally within the waste tyre feedstock partitions to the solid PT-char fraction while roughly 20wt.% and 10wt.% is contained within the TDO and PT-gas products respectively [1].

The implementation of tyre pyrolysis on a commercial basis will facilitate the management of waste tyres, increase recycling rates and creating employment [69]. Tyres which are pyrolysed are no longer available to be dumped in landfills or combusted in the open atmosphere, decreasing the hazards associated with these actions. The technology is commercially proven, reliable and has nominal health consequences [69].

2.3.6. Limitations of waste tyre pyrolysis

During process analysis, one must investigate both advantages and disadvantages in order to draw a bias conclusion and, unfortunately, WT-pyrolysis has associated limitations. Heat transfer efficiency has become a notable problem as heat cannot be distributed evenly throughout the reactor [1]. The creation of hot zones within the reactor can lead to undesirable secondary reactions [19]. Each WT-pyrolysis product formed is significantly complex in both physical and chemical aspects: TDO is composed of over 100 identified chemicals [19]; the PT-gas composition can change quickly if secondary reactions occur [1]; and the PT-char consists of a carbonaceous matrix with sulphur and ash compounds entwined within [1][33].

Although WT-pyrolysis is technically and environmentally viable, it must be economically attractive for it to be industrially implemented. Currently, there is a TDO and PT-char market deficiency since both products are unable to compete with their fossil counterparts in terms of value and quality [73]. This repels investors as a WT-pyrolysis process is unsustainable as it is unable to create (large) profits. The lack of PT-char markets creates further environmental problems as many companies dispose or stockpile the PT-char, according to REDISA representatives.

2.4. Pyrolytic tyre char

2.4.1. PT-char structure and physical properties

The physical properties of PT-char display its promising potential as a valuable product, such as fuel or CB [1]. Physically, PT-char is visible as solid, black particles of varying sizes, depending on the size of pyrolysis feedstock. The authors mentioned by Martínez et al. [1] state that the PT-char particles are much coarser in size compared to their original CB counterparts in tyres; and these PT-char particles act as nuclei during pyrolysis around which coherent solid carbon structures grow by crosslinking or cyclisation. PT-char consists of a heterogeneous, porous structure with a low surface area. Authors have demonstrated that pyrolysis temperature is inversely related to PT-char CV [35] and directly related to surface area [46][48]. The surface area of PT-char ranges from 32-116.3 m^2/g which is comparable to that of certain tyre carbon blacks, particularly: N660, N550, N351, N330, N326, N339, N375. Roy et al. [74] claim that PT-char is similar to the N300 CB series. The surface areas of tyre carbon blacks are illustrated in table 3 below. The CVs of PT-char range from 14.8-42.66 MJ/kg with a very high value of 71.90MJ/kg [38] reported. The CV of PT-char is similar to that of solid fuels, as shown in table 4 coal, and is comparable coal used for electricity generation in South Africa, which ranges between 20.3-24.1MJ/kg, depending on quality [25]. Table 5 shows a literature comparison of PT-char properties including surface area and CV.

Table 3:   **Surface Area of Tyre Carbon Blacks[8] (m^2/g)**

N110	N220	N234	N326	N330	N339	N351	N375	N550	N660	N774	N990
143	117	120	94	80	96	75	105	41	34	30	9

Table 4:   **Calorific Values of Common Solid Fuels[9] (MJ/kg)**

Anthracite	Bituminous Coal	Charcoal	Coke	Lignite	Peat	Semi Anthracite	Wood (dry)
32.5-34.0	17.0-23.5	29.6	28.0-31.0	16.3	13.8-20.5	26.7-32.5	14.4-17.4

---

[8] Table 3 adapted from [21]
[9] Table 4 adapted from [199]

Tanthapanichakoon et al. [22], found the surface of activated carbon made from PT-char to be hydrophobic. According to Kawakami et al. [75], the tensile strength, elongation and hardness of PT-char is dependent of temperature within the reactor. According to Woolard [18], a reinforcing filler is required to have an active surface with a surface area greater than 60m^2/g, and a particle size[10] less than 50μm. Pilusa and Muzenda [76] found the particles of PT-char to be much coarser than commercial CB particles, with approximately 24.3wt.% PT-char particles having a particle size larger than 425μm and 0.2wt.% having a particle size less than 38μm. In agreement, Senneca et al. [49], found the typical PT-char particle to have a size in the order of several microns, which was much coarser than the CB filler particle size. Helleur et al. [30], found the average PT-char particle size to be 30-40μm.

Table 5:   **Surface Areas and Calorific Values of PT-char found in Literature**

Reference	Pyrolysis Temperature (°C)	Surface Area (m^2/g)	Calorific Value (MJ/kg)
[46]	425	46.50	-
[44]	450	93.00	30.80
[34]	450-650	47.50	-
[77]	450	61	30.5
	475	65	30.7
[15]	500	73.47	-
[41]	500	69.50	-
[40]	500	67.96	-
[78]	500	63.00	-
[79]	500	65.20	-
[36]	500	64.00	30.50
[67]	500	83.00	29.30
[44]	500	-	31.50
[77]	500	64	30.5
	525	68	30.0
[80]	550	72.00	-
[81]	550	68.00	-
[82]	550	32.00	-
[35]	550	89.10	30.00
[83]	550	64.00	29.70
[84]	550	-	28.57
[63]	550	-	30.71
[85]	550	-	30.90
[86]	550	-	27.90
[16]	550	55.50	14.80
[16]	550	56.50	33.90
[63]	550	-	30.70
[77]	560	67	30.6
[15]	600	77.63	-

---

[10] Particle size technically refers to agglomerate size from here forth

[46]	600	116.3	-
[77]	600	65	30.2
[16]	650	60.50	15.70
[16]	650	63.50	33.40
[16]	650	60.50	15.70
	-	63.50	33.40
[15]	700	71.55	-
[82]	800	100.00	-
[15]	800	70.87	-
[16]	800	63.50	15.20
		66.00	34.20
[81]	900	61.00	-
[36]	-	-	42.00
[35]	-	-	41.70
[37]	-	-	42.66
[87]	-	-	38.00
[38]	-	-	71.90
[34]	450-650	47.5	-

2.4.2. PT-char composition

The high contaminant content within PT-char limits its versatility and economic value [19]. PT-char composition depends predominantly on the type and quality of waste tyre feedstock entering pyrolysis, as well as the pyrolytic process conditions. It is unanimously agreed upon that PT-char predominantly consists of four principle components: carbon; sulphur; and ash consisting of silicon/ silicon dioxide and metals [1][19]. Certain PT-chars can also contain TDO.

PT-char is in the form of a carbonaceous matrix [88], hence carbon constituting the largest mass portion within PT-char. Ultimate analyses have revealed a carbon mass fraction ranging from 78.76-90.60wt.%, as illustrated in table 6. Presenting a larger range, proximate analyses in table 7 shows a fixed carbon content within PT-char to range from 55.90-91.30wt.%. The carbon content originates predominantly from the CB filler within tyres, and remains as a solid pyrolytic product due to the absence of oxidation during pyrolysis [19]. Furthermore, authors have demonstrated that pyrolytic temperature is directly related to fixed carbon content [35], and carbonaceous deposits produced by volatile secondary reactions can form on the surface of PT-char [1][44][46][47].

Ultimate analyses, as shown in table 6, reveals high sulphur content within PT-char ranging from 0.8-3.41wt.%. During pyrolysis, approximately 70wt.% sulphur within the feedstock can partition to the PT-char fraction due to the thermal stability of sulphur-containing organic and/or inorganic compounds [1][34][89]. It can be in the form of sulphides which are trapped within the carbonaceous matrix [8][16][90]. Sulphur is originally added as a vulcanizing agent during the tyre manufacturing process to crosslink the elastomer chains [18][17].

Oxygen and hydrogen, which originate from the highly reactive, polycondensed aromatic structure of CB, will also be present within the carbonaceous matrix [18], as seen in table 6.

The ash content is the PT-char component which decreases its worth radically. Proximate analyses have shown that PT-char can possess an ash content ranging from 2.18-40.80wt.%, as shown in table 7. The difference in ash content arises from the difference in tyre type within pyrolysis feedstock, as demonstrated by Buekens [42]. Ash within PT-char represents heavy metals and silicon dioxide.

Silicon dioxide will be present within PT-char if it is originally present within pyrolysis feedstock due to low pyrolysis temperatures and the high boiling point of Si and SiO_2. As shown in table 8, silicon content within PT-char ranges from 0.5-2.662wt.% PT-char. Tyre companies often replace a portion of the CB filler with silicon dioxide filler for cost and environmental reasons, as discussed in section 2.2.2.

Ash within PT-char also consists of a metal fraction ranging from 1.757-8.226wt.%, as shown in table 8. It seems that aluminium, iron, zinc, calcium and potassium are exposed as major elements, while the other elements listed in table 8 are present within PT-char as minor elements. Metals are contained within the carbon matrix in their elemental form or in their corresponding oxide, sulphide or chloride form [91]. Due to the low pyrolysis temperature, metals are unable to evaporate, thus residing within PT-char product fraction at the end of pyrolysis. Metals originate from two sources: they are added as activators or other additives during the tyre manufacturing process, especially in the case of zinc; and they are in the form of steel wire which has not been liberated from pyrolysis feedstock.

Proximate analyses have also shown the containment of water and other volatiles within PT-char. As demonstrated in table 7, PT-char can encompass a moisture content ranging from 0.09-3.57wt.% and a volatile content ranging from 0.41-17.9wt.%. The volatiles are either elastomers which have not decomposed during WT-pyrolysis or TDO. These components evaporate during thermogravimetric analysis, thus showing up as volatile matter in proximate analysis results. At the conclusion of pyrolysis, as a result of cooling, volatiles condense into TDO and collect within the PT-char porous structure [92]. If PT-char does not undergo a secondary heat-treatment, TDO may remain trapped within the porous structure [33][92][93]. These condensed volatiles are proving to be a major contaminant issue for industrial producers, according to REDISA representatives.

Table 6:   **Ultimate Analysis of PT-char as found in Literature**

Reference	Pyrolysis Temperature (°C)	C (wt.%)	H (wt.%)	N (wt.%)	S (wt.%)	O (wt.%)
[94]	500	78.76	1.06	0.29	1.96	7.04
[95]	450	-	-	-	2.70	-
	600	-	-	-	2.80	-
[82]	550	83.00	1.40	0.40	1.70	13.50

[82]	800	78.50	0.50	0.30	2.40	18.30
[38]	-	-	-	-	2.98	-
[96]	-	88.19	7.23	0.23	1.80	2.55
	-	89.33	0.35	0.15	2.30	7.87
	-	89.01	0.83	0.48	2.00	7.68
	-	88.71	3.21	0.33	1.30	6.45
	-	89.70	1.61	0.42	1.60	6.67
[41]	500	82.70	0.40	<1	2.20	-
[35]	550	80.82	1.46	0.53	2.41	-
[40]	500	85.18	1.15	0.64	2.03	-
[78]	500	90.27	0.26	0.16	1.22	-
[83]	550	86.30	0.30	0.30	2.80	-
[84]	550	80.08	0.42	0.17	2.84	-
[16]	650	-	-	-	1.00	-
	650	-	-	-	2.30	-
[63]	550	85.31	1.77	0.34	2.13	-
[85]	550	89.40	0.30	1.80	0.90	-
[79]	500	86.62	1.39	0.78	2.24	-
	500	87.36	0.91	0.44	3.29	-
[97]	-	-	-	-	2.59	-
[78]	600	82.10	0.97	0.35	3.41	-
	600	81.78	0.84	0.33	2.96	-
[34]	450-650	83.50	0.90	5.10	1.60	8.90
[16]	550	-	-	-	0.80	-
	550	-	-	-	2.10	-
	650	-	-	-	1.00	-
	650	-	-	-	2.30	-
	800	-	-	-	0.90	-
	800	-	-	-	2.00	-
[36]	500	90.60	0.90	0.70	2.30	-
[44]	450	88.19	0.60	0.10	1.90	-
	500	82.17	2.28	0.61	2.32	-
[63]	550	85.31	1.77	0.34	2.13	-
[67]	500	80.30	1.30	0.30	2.70	-
[15]	500	89.17	9.69	0.29	0.85	-
	600	88.28	10.56	0.20	0.96	-
	700	88.23	10.66	0.18	0.93	-
	800	88.27	10.64	0.22	0.87	-
[77]	450	93.30	1.10	0.70	2.40	-
	475	94.80	0.90	0.70	2.60	-
	500	90.60	0.90	0.70	2.30	-
	525	95.00	1.10	0.90	2.60	-
	560	94.60	0.80	0.90	2.40	-
	600	95.90	0.80	1.10	2.30	-

Table 7:   **Proximate Analysis of PT-char as found in Literature**

Reference	Pyrolysis Temperature (°C)	Moisture (wt.%)	Volatile Matter (wt.%)	Fixed Carbon (wt.%)	Ash (wt.%)
[80]	550	0.46	0.41	90.50	8.63
[95]	450	0.90	14.20	76.30	8.60
	600	0.50	3.50	86.10	9.90
[82]	550	-	-	-	6.50[11]
	800	-	-	-	4.40[11]
[38]	-	1.22	11.20	72.00	15.70
[86]	550	0.00	5.50	78.40	16.10
[35]	550	1.28	6.92	77.22	14.58
[40]	500	-	-	-	13.25
[83]	550	0.40	1.80	91.30	12.50
[84]	550	1.00	1.20	81.30	16.50
[16]	650	-	-	55.90	40.80
	-	-	-	82.60	14.80
[63]	550	3.57	12.78	71.89	15.33
[85]	550	-	-	-	7.70
[78]	600	1.24	3.50	82.09	13.17
	-	0.26	2.51	83.41	13.82
	500	0.09	0.67	90.80	8.41
[34]	450-650	-	-	-	15.80
[16]	550	-	-	56.30	40.30
	550	-	-	82.40	14.30
	650	-	-	56.20	40.80
	650	-	-	82.60	14.80
	800	-	-	55.90	40.80
	800	-	-	84.30	13.50
[36]	500	0.40	2.80	-	11.60
[44]	450	0.37	7.78	-	8.27
	500	2.35	16.14	-	12.32
[63]	550	3.57	12.78	-	15.33
[96]	-	-	-	-	2.18
	-	-	1.77	89.30	7.93
	-	-	3.90	88.53	7.57
	-	-	17.90	76.23	5.88
	-	-	5.98	87.72	6.29
[77]	450	0.50	3.00	-	11.70
	475	0.40	2.70	-	11.60
	500	0.40	2.80	-	11.90
	525	0.40	2.80	-	12.40
	560	0.30	2.60	-	12.30
	600	0.40	2.30	-	-

---

[11] Dry basis

Table 8:   **Mineral Analysis of PT-char as found in literature**

Reference	[80]	[95]		[34]	[36]	[44]	[63]	[67]	[96]				[77]					
Pyrolysis Temperature (°C)	550	450	600	450-650	500	450	550	500	-	-	-	-	450	475	500	525	560	600
Unit	wt.%	wt.%	wt.%	wt.%	wt.%	wt.%	wt.%	wt.%	wt.%	wt.%	wt.%	wt.%	wt.%	wt.%	wt.%	wt.%	wt.%	wt.%
Al	0.130	-	-	0.138	0.15	-	1.09	-	-	-	-	-	0.3	0.2	0.3	0.4	0.2	0.3
Cu	0.008	-	-	0.034	-	-	-	-	0.0144	0.036	0.0116	0.0039	-	-	-	-	-	-
Fe	0.089	-	-	0.382	0.2	0.04	0.54	-	2.337	1.508	0.0937	0.3622	0.3	0.3	0.3	0.3	0.2	0.3
Si	2.662	-	-	-	0.42	1.69	-	-	-	-	-	-	1.0	0.9	0.9	1.1	0.5	1.4
Zn	2.525	2.924	3.3665	2.026	4.1	6.68	4.06	3.8	5.828	4.513	3.066	1.3575	3.6	3.3	4.1	3.7	4.0	3.5
Ca	0.368	-	-	0.3	1.2	0.13	-	-	-	-	-	-	0.6	0.6	1.2	1.0	1.8	0.8
K	0.142	-	-	0.08	-	-	-	-	-	-	-	-	0.1	0.2	0.1	0.1	0.1	0.1
Mg	0.086	-	-	0.074	-	-	-	-	-	-	-	-	0.6	0.6	0.9	0.6	0.4	0.6
P	-	-	-	-	-	-	-	-	-	-	-	-	0.06	0.06	0.05	0.06	0.06	0.05
Ti	-	-	-	-	-	-	-	-	-	-	-	-	0.02	0.03	0.02	0.04	0.02	0.04
Cl	-	-	-	-	-	-	-	-	-	-	-	-	0.06	0.06	0.08	0.06	0.09	0.05
Ba	-	-	-	0.007	-	-	-	-	0.0005	0.0005	0.0004	0.0002	-	-	-	-	-	-
Co	-	-	-	0.013	-	-	-	-	0.0144	0.0013	0.0006	0.0239	-	-	-	-	-	-
Cr	-	-	-	0.01	-	-	-	-	0.0025	0.0008	0.0001	0.0004	-	-	-	-	-	-
Mn	-	-	-	0.006	-	-	-	-	0.0164	0.011	0.0007	0.0027	-	-	-	-	-	-
Na	-	-	-	0.055	-	-	-	-	-	-	-	-	-	-	-	-	-	-
Ni	-	-	-	0.006	-	-	-	-	0.0027	0.0013	0.0006	0.0001	-	-	-	-	-	-
Pb	-	-	-	0.011	-	0.01	-	-	0.0077	0.0113	0.0072	0.0028	-	-	-	-	-	-
V	-	-	-	0.01	-	-	-	-	0.0004	0.0001	-	0.0024	-	-	-	-	-	-
As	-	-	-	-	-	-	-	-	0.0002	0.0001	-	0.0004	-	-	-	-	-	-
Cd	-	-	-	-	-	-	-	-	0.0006	0.0006	0.0004	0.0001	-	-	-	-	-	-
Sb	-	-	-	-	-	-	-	-	0.0014	0.0014	0.0013	0.0002	-	-	-	-	-	-
Others	0.450	-	-	-	-	-	-	-	-	-	-	-	-	-	-	-	-	-
Total (wt.%)	6.46	2.924	3.367	3.152	6.07	8.55	5.69	3.8	8.226	6.085	3.183	1.757	6.640	6.250	7.950	7.360	7.370	7.140
Total (wt.%) excluding Si	3.798	2.924	3.367	3.152	5.65	6.86	5.69	3.8	8.226	6.085	3.183	1.757	5.640	5.350	7.050	6.260	6.870	5.740

2.4.3. Current and potential applications for PT-char

The PT-char emerging from a WT-pyrolysis contains many unwanted constituents which lowers its commercial versatility and worth. Having said this, there are three main categories into which current and potential PT-char applications can fall into: supplementary fuel; adsorbent; additive.

Currently, PT-char can be used as a supplementary low-grade fuel [14][98] as it has a high CV which is comparable to other solid fuels. The large heavy metal content, however, is highly toxic to the surrounding environmental, and is carcinogenic [99]. Applications and processes must be able to manage the quantity and nature of the ash responsibly in order to abide governmental regulations [1]. In South Africa, the coal used for electricity generation must have ash content between 22.3-28.0wt.%, a sulphur capacity ranging from 0.7-1.3wt.%, a volatile content between 20.4-20.8wt.% and a CV between 20.3-24.1MJ/kg [25]. Refer to appendix F for the property specifications of coal for electricity generation in South Africa.

Many sources claim that, with the appropriate upgrading techniques, PT-char can be used as activated carbon [1]. This application seems to be one of the most promising and accepted end-use for PT-char as it has been largely and successfully reported by many authors [14]. PT-char has a high inorganic ash content, as shown in table 7 and table 8, and a low surface area, as shown in table 5, therefore, it must undergo both a demineralisation and an activation process to be upgraded to activated carbon [8]. Activated carbon has an ash content ranging from 5-20wt.% [100]. PT-char demineralization, however, requires more research to reduce costs [96]. It must be noted that metals, such as iron oxide (Fe_2O_3) can leach from activated carbon and must be removed. Surface area, pore size and pore volume are the most important characteristics of an activated carbon [8]. Surface area indicates the adsorptive properties of a porous material [8], and is most commonly calculated using the Brunauer Emmett Teller, or BET, model [101]. Pore size and volume indicate the overall adsorption capacity since the existence of micropores and mesopores improve the adsorption of large adsorbates, such a dyes [8]. As shown in table 9 below, steam and carbon dioxide are commonly used as activating agents [8]. Steam activated carbons produce a larger BET surface area in comparison to CO_2 and KOH/N_2 activated carbons. PT-char activated carbons can be used for both liquid and gaseous applications [8]. Activated carbon is commonly utilized within the water industry. PT-char activated carbon is capable of removing organic and inorganic species [8], phenol and *p*-chlorophenol [102], halogenated hydrocarbons and pesticides [103], metals such as chromium, lead and copper [30][104], dyes [22][105], and Cr^{6+} ions [8]. According to Streat et al. [102], PT-char activated carbon is comparable to coal and wood derived activated carbons in terms of adsorption. PT-char activated carbon has gas-phase applications such as the storage of gases, such

as natural gas or flammable gases such as acetylene, via adsorption using high pressures for ease of transportation [8]. Air pollution can be controlled using activated carbon since it can readily adsorb flue gas components such as SO_2 [106]. According to Brady et al. [106], PT-char derived activated carbons demonstrate a similar SO_2 adsorption rate in comparison to commercial lignite-based activated carbons. Activated carbon can also be used in batteries or fuel cells [107], and in the textile industry [30]. Refer to appendix E for the property specifications of different activated carbon series.

Table 9: **PT-char Activated Carbon Properties as found in Literature[12]**

	Reference	BET Surface Area (m^2.g^{-1})	Micropore volume (cm^3.g^{-1})
Steam	[23]	1119	0.57
		1177	0.54
	[30]	272	-
	[105]	1070	0.55
		1022	0.54
	[108]	528	-
		478	-
	[109]	640	-
	[110]	1000	0.44
		978	0.48
	[111]	1031	0.28
		888	0.25
	[106]	1031	0.28
		888	0.25
	[102]	346	-
		155	-
	[112]	607	0.01
		553	0.07
Steam	[113]	164	0.04
	[50]	1260	-
		600	-
Carbon Dioxide	[30]	270	-
	[104]	832	-
	[114]	431	-
		284	-
	[115]	813	-
		793	-
Potassium Hydroxide/Nitrogen	[103]	474	-
		411	-
	[111]	820	0.27

---

[12] Table 9 adapted from [8]

Carbon black has a much wider variety of commercial applications as an additive in comparison to activated carbon. It can be used as a pigment in inks, coating and plastics [21]. CB can be used as an additive in automotive products [21], such as tyres [18], and non-automotive products, such as conveyor belts, rubber boots or catalyst support in fuel cells [5]. If the surface activity of pyrolytic CB is sufficient, it can be used as a filler in road bitumen since it is able to improve properties such as temperature susceptibility, bitumen softening point and rutting and cracking resistance [5]. Tyre CB must have an ash content ranging from 0.1-0.4wt.% [5][116][117], a sulphur content of 0.6-1.1wt.% [5][117], and a surface area ranging from 35-123m^2/g [118]. The conversion of PT-char to tyre carbon black has not been extensively researched since it is easier to produce activated carbon. PT-char consists predominantly of CB, the filler within tyres, thus can serve as highly renewable [1]. CB has a fossil origin [1], and the volatilisation of PT-char can reduce the production of new CB, consequently reducing fossil CO_2 emissions. This is a significant environmental benefit since the tyre and rubber industry accounts for approximately 90% of the global CB market [119]. Most tyre rubber CB is produced using the furnace process which emits approximately 5.7kg CO_2 per kg CB produced [1]. Refer to appendix D for the property specifications of different CB series.

Table 10 shows a property comparison between carbon black, activated carbon and solid (coal) fuel.

Table 10:   **Major Benchmark Properties for Rubber Carbon Black, Activated Carbon and Fuel**

	Property	Value	Reference
Carbon Black	Ash Content	$0.1 - 0.4\ wt\%$	[5][117][116]
	Sulphur Content	$0.6 - 1.1\ wt\%$	[5][117]
	Nitrogen Surface Area	$35 - 123\ m^2/g$	[118]
Activated Carbon	Ash Content	$5 - 20\ wt\%$	[100]
	Surface Area	$500 - 1500\ m^2/g$	[120]
Fuel (Coal)	Ash Content	$22.3 - 28.0\ wt\%$	[25]
	Sulphur Content	$0.7 \leq x \leq 1.3\ wt\%$	[25]
	Calorific Value	$20.3 - 24.1\ MJ/kg$	[25]

2.4.4. Market value of current and potential PT-char applications

PT-char is a crude form of CB due to the contaminant content which prevents its use as activated carbon or filler, subsequently, negatively affects the market value and demand. According to REDISA representatives, there is currently no market for PT-char in South Africa, with producers stockpiling approximately 1500 tonnes with no demand. The market value for PT-char is ZAR 300/tonne, according to REDISA. In certain countries, the market value for raw PT-char can exceeds the South African price by bounds. Careddi [121] is a Chinese company which deals with waste tyres and sells PT-char for approximately US $100/tonne and claim that a new process, which can reduce the ash

content to approximately 4%, is in the development stages. The company claims that de-ashed PT-char may have a market value between US $1000-2000/tonne. Refer to table 11.

Raw PT-char can be used as an alternative fuel source, although many processes cannot handle the inorganic contaminants residing within the PT-char. Process which can withstand the inorganics can benefit substantially by using cheap PT-char as a fuel source in preference to fossil coal. In South Africa, coal used for electricity generation is valued at approximately ZAR 200.00-300.00/tonne, according to local electricity supplier [122][123], thus showing that PT-char can compete with coal on monetary terms.

The price of activated carbon depends on its adsorption characteristics and application. According to Evergreen Energy Inc. [124], the market prices for activated carbon had reached US $1000/tonne in 2011. Novinkor [125] stated that activated carbon has a market cost between US $2000-5000/tonne, depending on quality, further suggesting that a market value of US $2000/tonne is a well guided price. According to Peat Resources Limited [126], the international market for activated carbon boasts a price ranging from US $500-3000/tonne, with an average of US $1900/tonne. High quality activated carbons can sell for as much as US $9000/tonne [126]. In India, however, the price of activated carbon can range from US $750-1060/tonne [127]. It seems that the average price of US $2000 per tonne activated carbon is acceptable.

CB can be categorised into speciality and traditional CB. Traditionally CB is used as a tyre filler, nowadays CB can be made especially for applications such as use in plastics [128]. According to Asia Carbon Industries, Inc. [129], traditional CB can sell for US $1000, with speciality CB selling for US $2400. According to a study conducted by Pilusa et al. [3], the average market price for high grade CB is approximately US $661/tonne, and about US $273/tonne low grade CB according to the historical import market. This price seems to be acceptable as it is based on historical markets. It must be noted, however, that the price of carbon black production will be impacted by carbon emission taxes and the use of finite fossil fuels.

Table 11:   Market Value of Rubber Carbon Black, Activated Carbon and Fuel

Product Description	Market Value (2013-2014)	
High-grad Carbon Black	US $661/ton	[3]
Low-grade Carbon Black	US $273/ton	[3]
De-ashed PT-char	US $1000-2000/ton	[121]
Activated Carbon	US $2000/ton	[125]
Coal (Eskom)	R 200 - 300/ton	[122] [123]
PT-char as Fuel	US $100/ton	[121]
Raw PT-char	R 300/ton	

2.5. Pyrolytic tyre char upgrading analysis

2.5.1. Upgrading PT-char to carbon black

As previously discussed, PT-char has no market in South Africa since its low quality renders it unsuitable for use as a high-value product. This quality needs to be enhanced so as to increase its worth, further impacting positively on other aspects of waste tyre management by WT-pyrolysis. WT-pyrolysis product streams must be managed in a way as to extrude as much value as possible to ensure sustainability. Therefore, upgrading PT-char simply entails increasing the quality of the carbon so is can be used as a high-value produce, i.e., enhancing raw PT-char worth in terms of application and economic value.

Increasing the worth of PT-char is essential as there is a supply and demand problem in South Africa with regards to raw PT-char. There is already a large supply of PT-char stockpiled in South Africa, with the quantity increasing since pyrolysis is able to produce a PT-char yield of up to 40wt.% according to Williams [19]. The problem lies in the lack of PT-char markets, with the selling price lowered to a dismal ZAR 0.30/kg. This is predominantly due to the type and quantity of contaminants within the PT-char [19][33][92][93], rendering the product redundant to most processes. The bad design and operation of WT-pyrolysis plants add to this problem as volatiles condense within the porous structure of PT-char. This further repels potential investors from supporting WT-pyrolysis, consequently affecting the overall tyre recycling scheme. PT-char producers are burdened with large stockpiles, which signify income loss and waste.

As discussed in sections 2.4.3-2.4.4, research has shown that activated carbon and CB, which are both of high value, and can be produced from raw PT-char. These two products are produced through the demineralisation of PT-char, followed by activation, in the case of activated carbon, or size reduction, in the case of CB. Chemical activation and size reduction processes are thoroughly research and well-known [8], but the demineralisation of PT-char is less recognized, thus making it the focus of this research as it will benefit both activated carbon and carbon black industries. The target, however, will be to demineralise[13] PT-char to the point of CB rather than activated carbon for environmental and economic benefits. The production of tyre CB from PT-char will complete the cradle-to-grave lifecycle of CB in a tyre. This is important due to the fossil origin of CB and extremely

---

[13] Demineralisation refers to the removal of superfluous, mineral-based (inorganic) contaminants from PT-char (i.e. the removal of ash from PT-char).

high CO_2 emissions per kg CB produced. Although CB is not priced as high as activated carbon due to its low surface area, it is in much higher demand globally. In 2013, the world carbon black demand was 11.6 million metric tonnes [130], while the 2014 global demand for activated carbon was only 1.7 million metric tonnes. However, the profit margins for the production of each CB and activated carbon from PT-char are unknown. Therefore, the production of CB from PT-char will be analysed due to the higher demand.

Certain factors must be considered when transforming PT-char to CB. The high ash content within PT-char, as well as the inappropriate degree of aggregation (i.e. particle structure), renders it unusable in the tyre manufacturing industry [1] as it hinders the reinforcing properties within the tyre [18][76][30]. Furthermore, if the CB does not have suitable surface chemistry and reactivity, the carbon black-rubber interaction will be diminished [1] thus effecting the quality of the tyre. The heterogeneous particle structure of PT-char roots from the WT-pyrolysis process. During WT-pyrolysis, there is no distinction between the different sections of a tyre. This complicates the properties of PT-char since different tyre sections are made of different grades (series) of CB, resulting in a heterogeneous mixture of CB types and properties within the final PT-char product [1].

In conclusion, PT-char is highly heterogeneous in terms of particle size, absorption properties, ash content, surface activity and chemistry, and structure [1]. This heterogeneity is mainly attributed to the many different CBs within it, the ash content, and the complexity of the pyrolysis process [1]. These barriers prevent the recovery of this PT-char, thus decreasing the economic feasibility of WT-pyrolysis itself. An upgrading procedure must be executed to render this PT-char economically useful for the following reasons:

- WT-pyrolysis produces a large supply of PT-char which can produce an attractive income if markets are created.
- A market for PT-char must be created to increase WT-pyrolysis sustainability. This consequently creates investment attraction for both WT-pyrolysis and waste tyre recycling as a whole.
- The use of PT-char will inevitably decrease the production of waste by WT-pyrolysis, hence having environmental benefits and further increasing WT-pyrolysis sustainability.
- The ash may be recovered for possible re-use if economically feasible.
- The re-use of PT-char as CB will decrease the production requirement of fresh CB, consequently decreasing associated CO_2 emissions and the use of finite fossil sources.
- The market creation and re-use of PT-char will assist with the global waste tyre management problem.

2.5.2. Survey of PT-char upgrading techniques

Upgrading is a process whereby value is added to PT-char. As discussed above, upgrading PT-char to tyre CB is accomplished by removing contaminants, such as TDO, sulphur, metals and silicon/ silicon dioxide, from the carbon structure. This is a challenging task since the contaminants are incorporated within the carbonaceous structure [1][33], and one aims to preserve the structure of the carbon for final use as CB in the tyre manufacturing industry. Research has shown that there are three contaminant-specific techniques in which PT-char can be upgraded: consecutive pyrolysis; physical separation; and demineralization via leaching using lixiviant extraction. Each of the techniques targets a specific contaminant.

Many WT-pyrolysis plants make use of a second, consecutive pyrolysis process with the intention of extracting as much TDO from the feedstock as possible. When PT-char is submitted to a second pyrolysis operation, the volatiles (including moisture) which have condensed within the porous structure of the carbon during cooling [92], as well as elastomers which have not yet been decomposed, volatilise [34] to produce TDO and PT-gas, leaving a relatively volatile-free PT-char [33][92][93]. Martinez et al. [1] show that 500°C is the optimal temperature at atmospheric pressure conditions at which complete tyre decomposition occurs. This pyrolysis temperature is too low to the evaporate ash components, i.e., the silicon compounds and metals, therefore these constituents will remain within the PT-char [1] irrespective the number of pyrolysis processes the PT-char travels through. Although sulphur has a low boiling point of 444.7°C, most of the sulphur remains within the solid fraction during pyrolysis due to the great thermal stability of sulphur-containing organic and/or inorganic compounds formed during WT-pyrolysis [34][89]. The small amount of sulphur which is not thermally stable separates into the PT-gas fraction during WT-pyrolysis. In conclusion, a consecutive pyrolysis stage will only remove volatiles from PT-char, and not ash or sulphur due to their high thermal stability and the low operating temperatures of pyrolysis.

Physical separation is an umbrella term for different techniques used to separate components based on their physical properties such as size, shape, mass, density or magnetic state [11]. In the case of PT-char, magnetic separation and pulverisation have both been used by different authors.
The PT-char which dawns from WT-pyrolysis has been noted to contain steal wires which have not been efficiently removed during the crumbing process. For analysis or experimental purposes, many authors remove this steal magnetically [19][34][41][96][109] so as not to hamper the results. The presence of steel wire within the PT-char may become a problem in industrially implemented PT-char upgrading processes and must not be overlooked. It can simply be removed using strong magnets.

Pulverisation was utilized by Pilusa et al. [76] to decrease the raw PT-char particle size since the finer the CB particle, the stronger the reinforcement. The authors found that a 90 second pulverisation process increased the surface area significantly with 64wt.% upgraded PT-char (UPT-char) owning a particle size less than 38μm. They also stated that this pulverisation process was able to easily liberate certain ash components within the PT-char. They declared that, after grinding, silicon dioxide easily separated from CB by size fraction since the bond work index of silicon dioxide was higher than that of CB. It must be noted that Pilusa et al. [76] also made use of a leaching process to successfully reduce the metal content within PT-char.

PT-char upgrading by acid and/or alkali demineralisation, also known as acid/alkali/acid-alkali leaching, has been used for the removal of sulphur [76] and ash contaminants [14]-[16][131]. Leaching is a type of liquid-solid extraction whereby a soluble fraction is partially or totally removed from an insoluble, permeable solid phase by use of a liquid lixiviant [11][132].

Many authors have used acid demineralisation to remove the ash content of PT-char so as to decrease the catalysing effects of certain metal components during the carbon activation process [34][109]. It is apparent that sulphuric acid and, especially, hydrochloric acid are the most commonly used acids for the demineralisation of PT-char. Antoniou et al. [14], made use of alternative acids such as hydrofluoric acid, nitric acid and chlorination for the removal of ash from PT-char. Basic compounds, such as sodium hydroxide and potassium hydroxide, were shown to remove an ash fraction from PT-char [5][116][103]. Oxidizing agents, such as nitric acid and hydrogen peroxide, were used for sulphur removal by Bunthid et al. [38]. Certain authors have also used alkalis, such as KOH and NaOH for PT-char demineralisation [5][116][103].

Most authors who have demineralised PT-char have used extreme conditions which are economically infeasible, for example, high acid concentrations, long extraction times or low C:L ratios. Chaala et al. [116] performed PT-char demineralisation optimisation investigations using sulphuric acid alone. Depending on the series, CB must have a low ash content, ranging from 0.2wt.% [116] to 0.4wt.% [5] and a sulphur content of between 0.6-0.7wt.% [5]. Although successful in removing a portion of ash, no author has removed enough ash for the PT-char to reach the CB ash composition. Roy et al. [5] claim to produce a UPT-char with an ash content of 0.7wt.% and a sulphur content of 0.5wt.%, which is highly promising.

2.5.3. Motivation for further investigation into certain PT-char upgrading technique

The previously investigated PT-char upgrading techniques, namely pyrolysis, physical separation and demineralisation via leaching, each have specific advantages and shortcomings. Not only feasibility,

but economic and environmental factors must also be taken into account when establishing a method for upgrading low-value PT-char.

Pyrolysis is an industrially established form of PT-char upgrading, according to REDISA representatives. A second pyrolysis run is able to rid the PT-char of elastomers and volatiles which were not able to volatilise during the first run, yielding a solid product which is relatively volatile and water free. Unfortunately, it is unable to liberate the sulphur and ash content. This is due to the high thermal stability sulphur-containing compounds, and the high boiling points of the ash components. Advantageously, a pyrolysis process already includes a reactor, thus decreasing the need for new equipment if second pyrolysis run is required. In essence, a pyrolysis process should be designed in such a way as to optimise the elastomer volatilisation from the PT-char in one run. This will save money and energy, as well as increase the overall product yield and revenue, in comparison to two pyrolysis runs. A second pyrolysis run will not be explored further since it is, most crucially, unable to liberate ash and sulphur components from the PT-char.

PT-char has been upgraded successfully by physical separation or, more specifically, by magnetic separation and pulverisation [76].

Magnetic separation is a simple practice which aims to reduce the steel wire content within the PT-char. Most of the metal content within the PT-char is derived from steel wire within the pyrolysis feedstock; therefore, prior effort to remove the steel content will reduce metal ash within PT-char. It must be noted that, since iron is the only magnetic component that is definitely in the PT-char, a full upgrading process based solely on magnetic separation will not be viable since nonferrous metals will remain within the UPT-char. A strong magnet will assist in the removal of smaller pieces of steel wire. The utilization of magnetic separation will strongly depend on the quality of WT-pyrolysis feedstock, in terms of steel wire content, and, consequently, the quality of PT-char. The majority of authors have reported the need for steel wire removal from PT-char using magnetic separation.

Pulverisation successfully liberated a portion of silicon-containing compounds from the PT-char and reduced the particle size [76]. Moreover, the pulverisation process reported was a fast, 90 second procedure [76]. Although lucrative, pulverisation was used in addition to acid-leaching and not independently. Separation of the silicon dioxide-containing PT-char from the cleaner UPT-char may create CB product wastage in industrially implemented processes. Industrial size reduction units are expensive and energy inefficient. CB provides greater reinforcement with smaller particles, therefore a size reduction for quality purposes may be required if the UPT-char particles are coarse. It is also essential that the UPT-char product quality be reproducible and constant, especially in terms of CB particle size.

Demineralisation by acid-leaching is the most widely used upgrading procedure for PT-char. Acid-leaching has been shown to successfully reduce the ash and sulphur content within PT-char. The ash content is the greatest nuisance material within PT-char and thus, the principle elimination target. Although successful in ash reduction, no author has been able to achieve a UPT-char with the appropriate properties for use as tyre CB. Many authors have used extreme conditions to de-ash PT-char. These intense conditions, for example high acid concentrations, long extraction times or low C:L ratios, are environmentally and economically infeasible. Only one author has performed PT-char demineralisation optimisation investigations, although using sulphuric acid and sodium hydroxide only.

It is apparent that the ash content can only be reduced using an acid-alkali demineralisation process since the ash contains heavy metals and silicon dioxide-containing materials which react readily with certain acids and alkalis respectively. There is no available data concerning the comparison and optimisation of different acids.

In conclusion, a combination of techniques will be utilised to upgrade PT-char by removing sulphur and ash contaminants, and reducing the particle size, if required. Pyrolysis is not viable and will not be investigated further. Magnetic separation may be utilized if the PT-char has high steel wire content. The PT-char and UPT-char particle size distribution will be analysed, and a size reduction process will be implemented if the particles are too big causing unsuitable reinforcement, and/or there is a large variety in particle size. Acid-alkali demineralisation via leaching will be employed to extract the ash (metal and silicon-containing compounds) components from the PT-char. Since, to date, no author has compared the extraction performance of different acids, performed process optimisation comparison for different acids, or proposed an upgrading process for PT-char, this will be the core theme for this research.

2.6.   Pyrolytic tyre char upgrading by acid-alkali demineralisation

2.6.1. PT-char demineralisation by acid-alkali leaching: an understanding

Lixiviant extraction is a universal term which described the separation of two immiscible liquids or the separation of a soluble component from an insoluble solid [11]. PT-char demineralisation will make use of the latter, whereby the soluble ash component will be separated from the solid, insoluble, carbonaceous matrix.

Henley et al. [132] characterised liquid-solid extraction, as the process whereby a soluble fraction is partially or totally removed from a solid material by use of a liquid lixiviant. Perry et al. [11] describe

leaching as the removal of a soluble portion, in the form of a solution, from a permeable solid phase with which it is incorporated. Voeste et al. [133] interpreted leaching as partially or totally dissolving a solid in a suitable lixiviant using chemical reactions to create solubility. Couper et al. [134] express leaching as a process whereby solutes are removed from a mixture with a solid by contacting it with a lixiviant. Leaching can, thus, be described as the partial or complete separation and removal of a soluble fraction from the integration within a permeable solid phase by contact with a suitable lixiviant.

As shown in figure 5 below, the feed material is in contact with a lixiviant during leaching. The feed material, which is heterogeneous in composition and structure [133], consists of a solid, permeable phase which holds the leachant. In general, the solid phase can be in the form of a large, insoluble, porous structure; or it can consist of small, porous particles with a large surface area; or surface activated. The leachant is the soluble substance which is to be separated from the solid phase [133]. It is integrated within the solid phase by means of chemical bonds, an adsorption mechanism or it is mechanically held within the porous structure [11]. The lixiviant is the medium which separates and holds the leachant [133]. After the leaching process has been completed, two phases are present, as shown in figure 5: an extract phase which consists of lixiviant and a portion of leachant; and, in the case of PT-char, the product which contains the solid phase and a decreased portion of leachant.

During a leaching process, the lixiviant initially invades the pores of the solid structure and comes into intimate contact with the soluble leachant. During lixiviant-leachant contact, the leachant dissolves into the lixiviant forming a concentrated solution of metal-ligand complexes. Many mechanisms of mass transfer have been proposed to explain the movement of leachant from solid phase into lixiviant [135]. The partition of leachant to the lixiviant during a leaching process is dependent on certain process variables, as discussed in section 2.6.3 below. After the leaching process has been completed, a small amount of lixiviant, which contains some leachant, is retained by the solid material. This retention is caused by adhesive forces and is the reason why no separation process can perform a total (100%) extraction [133]. Further separation processes must be completed to recover the leachant and/or the solid material from the lixiviant. Coffee brewing and laundry cleaning are examples of the leaching processes that occur in everyday life [133].
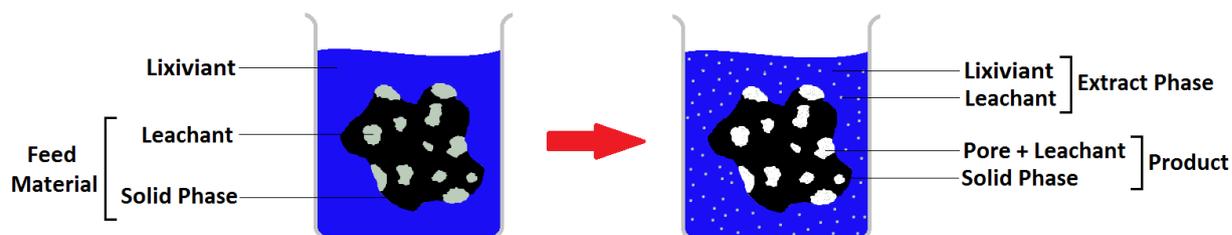
Figure 5: **The Leaching Process**

2.6.2. Chemistry conducting PT-char demineralisation by acid-alkali leaching

Brief Overview

The inorganic content within PT-char consists of the following components: aluminium, copper, iron, silicon dioxide, zinc, calcium, potassium, magnesium, barium, cobalt, chromium, manganese, sodium, nickel, lead, vanadium, arsenic, cadmium, and antimony (table 8). Metals are readily able to replace hydrogen from an acid or from water, if the metal is highly reactive [136]. Acids [14]–[16] and alkalis [116][5][103] have been successfully used to remove certain ash components from PT-char, therefore certain acids and alkalis will be used as lixiviants to extract the ash components described above from the PT-char.

Acid and Alkali Dissociation Chemistry

An acid dissociation reactions is shown in reaction 1[14] below [137]. Since the positive charge of the unbound H$^+$ ion is concentrated in such a small volume, it is able to strongly attract surrounding water molecules, consequently forming a hydronium ion (H_3O^+) through covalent bonding [137]. An alkali is a substance that produces OH$^-$ ions when dissolved in water, as illustrated in reaction 2[15] below [137].

$$AH_{(g \; or \; l)} + H_2O_{(l)} \; \rightarrow \; A^-_{(aq)} + H_3O^+_{(aq)} \qquad \text{[Reaction 1]}$$

$$BOH_{(l)} + H_2O_{(l)} \; \rightarrow \; B^+_{(aq)} + OH^-_{(aq)} \qquad \text{[Reaction 2]}$$
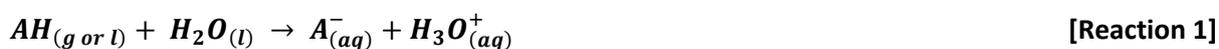
Acids and alkalis can both be classified as strong and weak, depending on their degree of dissociation within water. A strong acid or alkali dissociates completely into their representative ions, while a weak acid or alkali partially dissociates [137]. The partial dissociation of weak acids or alkalis is explained by the state of equilibrium: the reverse reaction, or reassociation reaction, of a

---

[14] A represents acid anion in reaction
[15] B represents base cation in reaction

weak acid or alkali quickly balances the forward reaction, or dissociation reaction, therefore, only a small portion of ions are produced [137]. A strong acid or alkali dissociated completely thus producing a large portion of ions since the forward reaction is highly favoured. Sulphuric acid is known a diprotic acid as it is able to lose two H⁺ ions. It first acts as a strong acid and loses the first H⁺ ion to form HSO_4^-, after which it acts as a weak acid and only a small portion of SO_4^{2-} is formed. The variation in acid strength can be quantitatively described by an equilibrium constant, known as the acid-dissociation constant, K_a [138]. K_a describes the extent to which H⁺ ions have been produced, or how far to the right the reaction has proceeded to reach equilibrium [138]. As a result, the stronger the acid, the greater K_a will be. K_a is temperature dependent and emphasizes the species whose concentrations significantly alter during dissociation [138], as shown in equation 1 below. It must be noted that K_b is the equivalent term for an alkali.

$$K_a = \frac{[H_3O^-][A^-]}{[HA]}$$
[Equation 1]

Since acids and alkalis dissociate in water, they can furthermore be classified as electrolytes. Strong acids and alkalis are strong electrolytes and are able to conduct current well, whereas weak acids and alkalis conduct only a small amount of current and are, thus, weak electrolytes [137]. The ability of an electrolyte to conduct current allows for the electronic measurement of pH, which can be interpreted into H⁺ or H_3O^+ ion activity, as shown in equation 2 [138]. Table 12 shows the characteristics and dissociation constants.

$$pH = -\log[H_3O^+]$$
[Equation 2]

Table 12:   Properties of Select Acids and Alkalis[16]

Acid/Alkali	Classification	Molecular Formula	Lewis Structure	K_a K_b	Reference for PT-char Demineralisation
Hydrochloric Acid	Strong Acid	HCl	H—Cl:	1.3E+6	[131] [22] [34] [82] [33] [92] [14] [109] [15] [16] [103] [94]
Nitric Acid	Strong Acid and Oxidizing Agent	HNO₃	H—O -O: N+ :O:	2.4E+1	[14]
Sulphuric Acid	Strong Acid	H₂SO₄	:O: H—O—S—O—H :O:	1.0E+3 1.2E-2	[14] [76] [116] [5]

---

[16] Table 12 based on [200] [201]

Hydrofluoric Acid	Weak Acid and Oxidizing Agent	HF	H—F̈:	7.2E-4	[14]
Sodium Hydroxide	Strong Alkali	NaOH	Na—Ö—H	0.631	[116] [5]
Potassium Hydroxide	Strong Alkali	KOH	K—Ö—H	0.316	[103]
Acetic Acid	Weak Acid	CH$_3$COOH	$$H \quad :\ddot{O}:$$ $$\quad | \quad \|$$ $$H—C—C—\ddot{O}—H$$ $$\quad |$$ $$\quad H$$	1.75E-5	-
Hydrogen Peroxide	Oxidizing Agent	H$_2$O$_2$	H—Ö—Ö—H	2.4E-12	[38]

Amphoterism Properties of PT-char Ash Components

When assessing leaching chemistry, it is important to consider the leachant properties, and not just the acid or alkali. In the case of PT-char, the reactants include metals and oxides, as listed in table 8. An amphoteric substance has the ability to act as an acid or base, thus able to react with both an alkali and an acid [139]. Most metals and metal ions are basic and only able to react with an acid. Aluminium and zinc, however, are amphoteric and are able to react with both [116]. Similarly, certain oxides may also be amphoteric. Two oxides are commonly present within a tyre are zinc oxide (ZnO) and silicon dioxide (SiO$_2$). ZnO is an amphoteric oxide, and is able to react with both an acid and a base. SiO$_2$, however, is not amphoteric, but rather slightly acidic, and can only react with a substance that has a basic characteristic [140]. SiO$_2$ is also known to react with hydrofluoric acid, although it reacts with the fluoride ion in the solution, and not the H$^+$ ion. Aluminium, magnesium and titanium form oxide layers immediately upon exposure to air and, thus, will partly be in oxide form. Magnesium oxide is not amphoteric, while aluminium oxide and titanium oxide are. Furthermore, chromium and iron oxides, particularly Fe$_2$O$_3$, are also amphoteric in nature.

Reduction-Oxidation Reactions

The reaction between the acid or alkali and the leachant occurs through reduction-oxidation reactions, commonly known as REDOX reactions, are the net movement of electrons from one reactant to another [136]. The electron(s) move to the reactant with the greater attraction for electron(s), therefore REDOX reactions are the gain (reduction) or loss (oxidation) of electrons from a species [136]. The overall redox reaction of an element or compound can be balanced using two half-reactions: a reduction half-reaction and an oxidation half-reaction [136]. Half-reactions are quantified using a measure known as Standard Reduction Potential (E$_h$), which can be defined as the

readiness of a species to gain an electron(s). The higher the E_h, the more a species is susceptible to being reduced. A REDOX pair can be formed by pairing two half-reactions based on their E_h. Refer to M. S. Silberberg [141] for a list of standard electrode potentials.

There are three types of REDOX reactions: combination reaction; decomposition reactions; and displacement reactions [136]. The sulphur within the PT-char may undergo a combination reaction, generally shown in reaction 3 [136] below, and combine with oxygen to form sulphur dioxide or sulphur trioxide, or with hydrogen, to form hydrogen sulphide [136]. Similarly, NaOH is able to react with sulphur producing water soluble sodium thiosulphate [142].

$$A + B \rightarrow AB \hspace{6cm} \textbf{[Reaction 3]}$$

When a metal reacts with an acid, it displaces the hydrogen from the acid or water [136], therefore the type of reaction which will occur during PT-char demineralisation will be displacement REDOX reactions. Single displacement, or substitution reactions, as shown in reaction 4 [136] below, involves the substitution of a single element for an element(s) in a compound [136]. Double displacement reactions, also known as metathesis reactions, involve the exchange of ions between reactants, as shown in reaction 5 below [136].

$$A + BC \rightarrow B + AC \hspace{5cm} \textbf{[Reaction 4]}$$

$$AB + CD \rightarrow AD + CB \hspace{5cm} \textbf{[Reaction 5]}$$

The metals within PT-char react with the acid forming a salt and hydrogen, as shown in reaction 6 [136], and will react with a alkali as shown in reaction 7 [136]. When in solution, however, complex ions may be present, with water molecules as the respective ligand, and the acid anion as the counter ion.

$$M_{(s)} + AH_{(g\ or\ l)} \rightarrow MA_{(aq)} + H_{2(g)} \hspace{3cm} \textbf{[Reaction 6]}$$

$$M_{(s)} + BOH_{(l)} \rightarrow MOH_{(aq)} + B_{(aq)} \hspace{3cm} \textbf{[Reaction 7]}$$
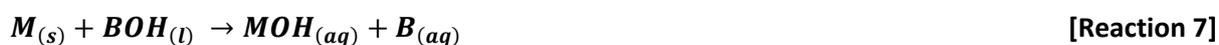
The reactivity of a metal depends on its strength as a reducing agent [136]. The most reactive metals, which are in group 1 on the periodic table, are able to displace hydrogen from water. Figure 6 below is based on the activity series of metals, and shows the reactivity of certain metals relative to hydrogen. The metals which appear below hydrogen on the reactivity series cannot displace hydrogen from any source. Similarly, an alkali, such as NaOH, is only able to react with species which are situated above sodium on the reactivity series [143]. It must be noted that silicon and silicon dioxide, which are present within PT-char, are only able to react with HF and NaOH, if NaOH is hot and concentrated, as discussed above. After a reaction between silicon dioxide and sodium

hydroxide, sodium silicon dioxidete is formed according to reaction 8 [144] below. Reaction 9 below illustrates the reaction between SiO_2 and HF.

$$SiO_{2(s)} + 2NaOH_{(aq)} \rightarrow Na_2SiO_{3(aq)} + H_2O_{(l)} \qquad \text{[Reaction 8]}$$

$$SiO_{2(s)} + 6HF = SiF_4 + H_2O \qquad \text{[Reaction 9]}$$
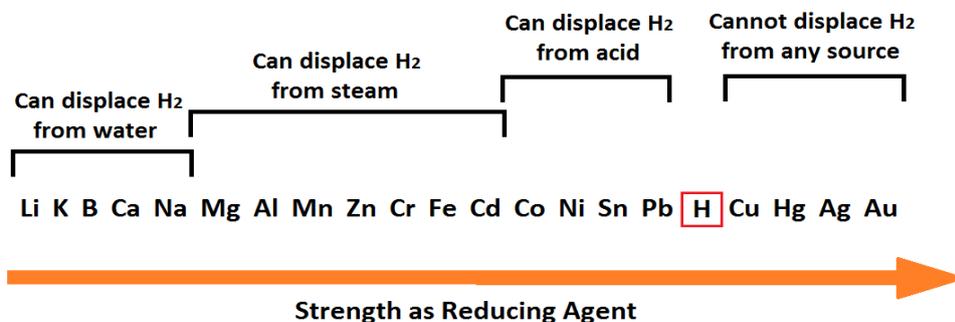
Figure 6: **Reactivity Series of Metals**[17]

Solution Chemistry

During PT-char demineralisation, after the reaction, the metal salt must be transported out of the carbonaceous structure, and this is done through the utilization of the acid as a carrier [133]. After formation, the metal salt dissolves into the bulk acid according to specific solubility rules, as listed in table 13 below. Solubility is dependent on temperature, and most solids experience an increased solubility at higher temperatures [145]. Although temperature effects the solubility equilibrium, solubility behaviour cannot be determined using a single measure since it is highly complex [145].

Table 13: **Solubility Rules**[18]

Rule	Compound	Solubility	Exception
Common group 1 ions	Li^+ ; Na^+ ; K^+	Soluble	-
Ammonium ion	NH_4^+	Soluble	-
Common nitrates	NO_3^-	Soluble	-
Common acetates	CH_3COO^-	Soluble	-
Most perchlorates	ClO_4^-	Soluble	-
Common chlorides	Cl^-	Soluble	Ag^+ ; Pb^{2+} ; Cu^+ ; Hg_2^{2+}
Common bromides	Br^-	Soluble	Ag^+ ; Pb^{2+} ; Cu^+ ; Hg_2^{2+}
Common Iodides	I^-	Soluble	Ag^+ ; Pb^{2+} ; Cu^+ ; Hg_2^{2+}

---

[17] Figure 6 adapted from [136]
[18] Table 13 adapted from [202]

Common fluorides	F^-	Soluble	Pb^{2+} ; Group 2
Common sulphates	SO_4^{2-}	Soluble	Ca^{2+} ; Sr^{2+} ; Ba^{2+} ; Ag^+ ; Pb^{2+}
Common metal hydroxides	OH^-	Insoluble	Group 1 ; Larger members of group 2 (beginning with Ca^{2+})
Common carbonates	CO_3^{2-}	Insoluble	Group 1 ; NH_4^+
Common phosphates	PO_4^{3-}	Insoluble	Group 1 ; NH_4^+
Common sulphides	S^{2-}	Insoluble	Group 1 ; Group 2 ; NH_4^+

2.6.3. Factors effecting leaching

The chemistry of a leaching process is complex and there are many variables which will affect the yield and viability. These factors, which may alter process thermodynamics, reaction kinetics and/or product properties, can be classified into three groups: factors caused by the leaching system; factors influenced by the leachant and/or lixiviant; and factors caused by the solid structure [135].

Factors caused by the leaching system are closely related to the lixiviant used during leaching. Systematic variables include temperature, pressure, residence time, C:L ratio, and lixiviant movement (system agitation) [135].

Generally, temperature, residence time and system agitation are directly proportional to the amount of leachant extracted from the solid structure, i.e., the yield [135]. If the temperature and residence time are increased while the system is agitated, the leachability and yield will increase [135]. Xue et al. [146] claim that an increase in temperature will increase leaching efficiency over a certain time period. The leaching rate will decrease over time due to the decrease in reagent concentration. An increase in temperature leads to a decrease in lixiviant viscosity, thus allowing the lixiviant to move through the porous structure with less effort. Lixiviant density decreases with increasing temperature, thus lowering the solubility [147]. The effect of temperature on a system will depend on which phenomenon is limiting: porous structure and size of pores, or solubility of leachant in lixiviant [135].

Pressure has little effect on solids and liquids since they are relatively incompressible, but it has a large effect on gases [148][149]. Teramoto et al. [150] discussed the decrease in mass transfer coefficient of a He/p-xylene system which may be attributed to a change in liquid viscosity. The authors claim that pressure had minimal influences on the investigated liquid systems.

All processes are related to time. Depending on reaction kinetics, a process yield may increase as time increases. If the residence time of the solid in the lixiviant is high, the lixiviant will be able to extract more leachant, assuming slow reaction kinetics. The exact dependence of time on

leachability may be a function of other factors, for example, size, shape and porosity of solid particle, as well as rate limitations such as mass and concentration limitations.

Fluid motion is a mass transfer mechanism [132]. The movement of a fluid causes the formation of a boundary layer. A large increase in fluid flow, i.e., a high Reynolds number, decreases the boundary layer thickness since there is less time for it to grow [151]. A thin boundary layer will cause a higher mass transfer rate since there is less obstruction to mass movement. The movement of fluid decreases the build-up of concentration, thus increasing solubility by maintaining a concentration gradient [135]. Xue et al. [146] discussed the effect of stirring speeds on leaching efficiency. The authors showed that increasing the movement will increase the leaching efficiency. The leaching efficiency increased due to the suspension of particles and the reduction in mass transfer boundary layer on the particle surface. They also found that, after a certain speed, there was no difference in leaching efficiency as stirring speed increased. This showed that the leaching reaction was not under external diffusion control. An increase in fluid velocity will increase the heat-transfer coefficient between the surface of the solid particle and the fluid [152].

C:L ratio has a large effect on the saturation of a system. Saturation occurs when a lixiviant cannot dissolve any more solute, i.e., it is at maximum capacity [145]. Excess lixiviant allows for more leachant to be dissolved in it, thus decreasing the occurrence of saturation [135]. Excess lixiviant may also allow for lixiviant recycling within the system. Xue et al. [146] showed that an increase in weight ratio increased leaching efficiency.

Leachant and lixiviant factors may include leachant redox potential, lixiviant pH, lixiviant and leachant polarity, and leachant composition [135].

The lixiviant pH and the leachant redox potential are strongly related [135]. As discussed previously, the greater the lixiviant, or acid, pH, the more H^+ ions are available to react with metals within the PT-char. Lixiviant pH also effects the solubility of the leachant if the leachant dissociates into is respective cation or anion via redox half-reactions [136]. The anions of certain salts may form the conjugate base of a weak acid, thus causing protonation. Protonation can increase the solubility of a salt at a low pH.

The leachant composition i.e., the type of atoms/molecules to be extracted, have many properties which influence the leaching process [133]. The Standard Reduction Potential, the polarity and solubility are all dependent on the elemental composition of the leachant. Polarity of a substance plays an important role in solubility, since like dissolves like. A solute and a lixiviant must have similar polarities for dissolution to occur. At molecular levels, the forces created (molecular interactions) between the solute and the lixiviant must be equivalent in strength to the forces which are destroyed within both the lixiviant and solute [153].

There are a variety of different requirements that a lixiviant must realise. Since a lixiviant will not fulfil all the requirements, certain compromises must be made and the most important requirements must be realised. A mixture of different lixiviants can be used to attain special characteristics. Selection of a lixiviant will depend on the physico-chemical nature of the solid, the characteristics of the lixiviant, regeneration of the lixiviant, recovery of desired components from leaching solution, and economics [133]. Important lixiviant requirements are listed below [133]:

- High dissolving capacity.
- Selective dissolving capacity towards the desired components of the solid and no other constituents.
- Low specific heat.
- Low relative density.
- Low heat of vaporization.
- Non-flammable.
- Gaseous concentrations do not lie within flammability limits.
- Non-toxic.
- Environmentally friendly or minimal environmental harm.
- Non-corrosive.
- Ability to infiltrate into solid medium easily.
- High removal of diffusant from extract and extraction residue without affecting odour or taste.
- Chemically defined.
- Homogeneous.
- Chemical and thermal stability.
- Constant boiling point which is not too high.
- Low price.
- Low viscosity.

The solid structure has a large influence not only on lixiviant extraction processes, but also in catalysis. The surface conditions of the solid such as activity, surface area and porosity, as well as composition, homogeneity and solid size and shape effect leachability [135].

The activity of the surface is caused by the presence of active species, such as oxygen [116]. These species may react with the lixiviant causing either the hindrance or facilitation of lixiviant extraction [135]. An impenetrable layer may form over the surface, preventing any extraction, or the reactivity of the lixiviant may be increased, thus increasing the extraction.

The solid structure must be composed of a material that is inert and will not react with the lixiviant [135]. Most structures are not homogeneous, especially in the case of ores and PT-char from pyrolysis processes. If the substance to be extracted only coats the surface, extraction is simplified. If the substance to be extracted is distributed throughout the structure, it may be difficult and take time for the lixiviant to percolate through the solid and extract the leachant.

The shape and size of the solid has an impact on leachability since it may cause a barrier and obstruct the percolation of the lixiviant into the solid to extract the leachant [135]. Xue et al. [146] demonstrated that decreasing the particle size will increase the rate of leaching efficiency. The authors explained that these results were attributed to the effect of increased reaction surface area. If the solid is brittle, agitation may decrease particle size through ablation.

The surface area is strongly dependent on the shape and size of the solid, as well as the porosity. The higher the surface area the larger the contact between the lixiviant and, thus, the leachant embedded in the solid [135]. The higher the contact area, the better the extraction yield due to the absence of obstructive barriers.

The pore size, in terms of length and diameter, will serve as an obstruction to extraction in comparison to the full exposure of the leachant to the lixiviant [135]. The pore size and shape will either completely obstruct the (large) lixiviant molecule movement or partially obstruct the (small) molecule movement into the solid [152]. This shows that the porosity has a strong effect on diffusion within the solid [135]. Dissolution of leachant from the solid structure may change the porosity of the solid.

2.6.4. Fluid-particle kinetics

During solid-fluid reactions, the diffusion of molecules into pore voids is obstructed by different resistances. In general, these resistances are dependent on the solid-fluid reaction causing the solid particle to either shrink with time due to the formation of flaking ash (figure 7a); or the particle size may remain unchanged due to the formation non-flaking ash or solid product (figure 7b) [154]. Ash, in this case, is the reacted, or converted, material, which may be inert, and may either remain on the particle, or leave (flake) the particle [154].
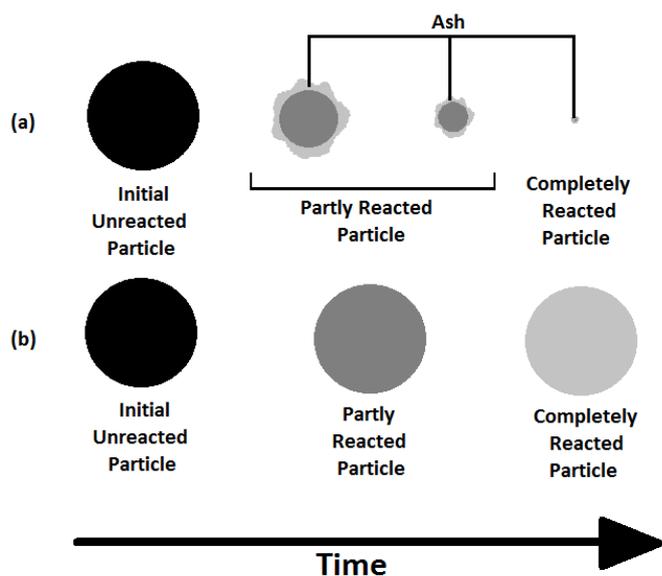
Figure 7:   **Reaction Behaviour of a Particle**[19]

Considering the above represented solid particle reaction behaviours, there are two idealized models which are able to represent non-catalytic particle reactions: the progressive-conversion model; and the shrinking-core model [154].

The progressive conversion model (PCM), which is represented by Figure 7b above, recognises the fluid movement into and through the particle, and the continuous, progressive conversion of solid reactant to product throughout the particle [154]. Although the fluid-solid reaction occurs throughout the particle, the reaction occurs at different rates at different locations within the particle [154].

The shrinking-core model (SCM), which is illustrated by Figure 7a above, anticipates the initial fluid-particle reaction to be on the particle surface, and slowly moving toward the particle core [154]. After a particular particle area has reacted, the converted material (ash) is left behind [154]. The ash is either able to flake off the particle, thus reducing the particle size; or it remains on the particle, preventing the particle from decreasing in size. Whether the ash leaves the particle or not, the unreacted particle core slowly decreases in size as time progresses [154]. In most cases, the SCM model estimates reality more accurately in comparison to the PCM model [154].

When particle size remains constant, there are five consecutive stages which commonly occur during a shrinking-core reaction, as shown in figure 8, [155]–[157]:

---

[19] Figure 7 adapted from [154]

1. Diffusion of fluid reactant A through the film (boundary layer) surrounding the particle to the particle surface.

2. Diffusion of fluid reactant A through ash layer to the surface of the unreacted core.

3. Reaction of reactant A with solid reactant B at reaction surface.

4. Diffusion of products C from unreacted core surface through ash layer to solid exterior surface.

5. Diffusion of products C through film (boundary layer) surrounding the particle to bulk fluid.
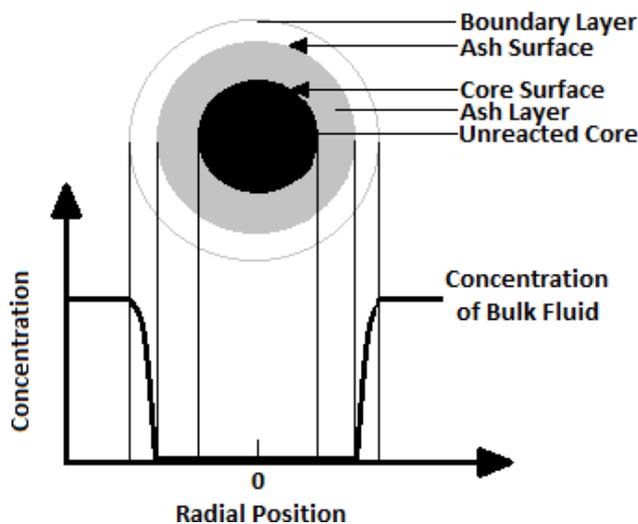
Figure 8:   **The Shrinking-Core Reaction[20]**

Each of the above diffusion stages will have a different magnitude of resistance, and may vary greatly from one another [154]. The stage with the greatest resistance to movement will be rate-controlling, although a combination of resistances are usually taken into account. During the reaction between a solid and a fluid, a concentration difference between the bulk fluid and the particle provides a driving force for mass transfer between the two phases [152]. A temperature difference within the boundary layer surrounding the particle is the driving force for heat transfer [152]. When particle size remains constant, either film diffusion, ash diffusion or chemical reaction is rate controlling [154].

When the boundary layer around the particle is rate-controlling, the concentration gradient will decrease from bulk fluid, through the boundary layer, and to the particle surface (or ash surface) [154].

Similarly, a concentration gradient will form through the ash when stage II is rate-controlling [154]. There will be no concentration gradients through the boundary layer or unreacted core, with the boundary layer and bulk fluid concentrations equivalent, and the unreacted core concentration gradient zero.

---

[20] Figure 8 adapted from [154]

Finally, the chemical reaction can be the controlling resistance. When this occurs, the reaction progression is impervious to the ash or boundary layer, and the rate is directly related to the available unreacted core surface area [154]. There are, in essence, no gradients within the particle when the chemical reaction is rate controlling.

When the ash layer is able to flake off the unreacted particle core, stages II and IV are not present since the vacant ash layer does not present any movement resistance [154]. The rate-limiting effect of the boundary layer surrounding a shrinking particle is dependent on fluid properties, particle size and relative velocity between bulk fluid and particle size [154].

Being an idealized model, there are a few limitations associated with the SCM. An intermediate behaviour between SCM and PCM may occur when the reaction occurs along a diffuse front rather than strictly between the ash layer and the unreacted core of the particle [154]. Considerable temperature gradients can occur within the particle during fast reactions where the energy (heat) release is high [154]. A continuous reaction model may better suit reality either when a fluid is in contact with a highly porous solid while a slow reaction is occurring since the reaction may occur throughout the solid; or when a solid particle is not in contact with a fluid and heat singularly converts the solid particle to products [154].

Certain generalities are present to assist in the prediction of the rate-limiting step. Since chemical reactions are temperature-sensitive, temperature alterations can enable the distinction between chemical reaction as the rate-limiting step, or ash/boundary layer as rate-limiting [154]. Kinetic experiments enable the distinction between different rate-limiting steps by comparing how well graphical results fit certain models. The models are listed below in equations 3-6 below.

Rate-limiting step is Interfacial chemical reaction rate:

$$k_r t = 1 - \frac{2}{3} X - (1 - X)^{\frac{2}{3}}$$ [Equation 3]

Rate-limiting step is film diffusion:

$$k_f t = X$$ [Equation 4]

Rate-limiting step is ash/ product layer diffusion:

$$k_a t = 1 - (1 - X)^{\frac{1}{3}}$$ [Equation 5]

Rate-limiting step is pore diffusion:

$$k_p t = 1 - (1 - X)^{\frac{2}{3}}$$ **[Equation 6]**

Generally speaking, when a hard, ash layer forms around a solid particle during fluid-solid reaction, the ash layer is rate-limiting and the boundary layer resistance is negligible [154]. In the case of ash layer resistance, an increase in temperature and particle size may cause the rate-limiting stage to shift from reaction controlling to ash-layer diffusion controlling. When ash flakes from the core, a temperature increase may reallocate rate control from reaction control to boundary-layer control [154]. When boundary layer resistance is considerable and controls, the reaction is not sensitive to temperature, but rather particle size and solid-fluid relative velocity.

The general mechanisms of fluid-particle kinetics are well studied [152] [154], however, no research is available regarding PT-char kinetics.

2.6.5. Analysis of literature regarding PT-char demineralisation by leaching

PT-char demineralisation kinetics has not been discussed in literature, however, PT-char demineralisation by acid- and/or alkali-leaching has been successful. Table 14 illustrates a thorough analysis of literature pertaining to PT-char demineralisation. One particular study must be noted: Roy et al. [3] and Chaala et al. [141] demineralised PT-char using H_2SO_4 followed by NaOH. The authors achieved an UPT-char ash content of 3.06wt.% using 1N H_2SO_4 and 5N NaOH. The ash was extracted using 10mL acid per 1g raw PT-char at 60°C for 30 minutes. They also found that the ash content merely increased by 1wt.% when the acid was recycled and reused thrice.

Eight acids, alkalis and oxidizers have been discussed by authors with regards to PT-char demineralisation: five acids, namely sulphuric acid, hydrochloric acid, nitric acid, hydrofluoric acid and formic acid; two alkali, namely sodium hydroxide and potassium hydroxide; and one oxidizer, namely hydrogen peroxide.

Sulphuric acid and hydrochloric acid were most commonly referenced by authors and are most successful in removing a large portion of ash from PT-char. Additionally, although being very strong acids, they are commonly used in industrial processes, such as car battery and PVC[21] manufacturing, and thus, process design factors such as safety, equipment and environmental protection and compatibility have been implemented on an industrial scale. Nitric acid and hydrofluoric acid act as both an acid and oxidizing agent which make them powerful PT-char demineralising agents. Nitric

---

[21] Polyvinyl Chloride

acid is a stronger acid in comparison to hydrofluoric acid, which is classed as a weak acid. Conversely, the F^- ion of hydrofluoric acid is an extremely strong oxidizing agent, especially in comparison to NO_3^-. Both acids have been known to remove ash from PT-char [14]; while sulphur has been shown to be removed by nitric acid [38] and hydrofluoric acid is able to dissolve silicon dioxide. On an industrial scale, nitric acid is used in the manufacturing of inks and dyes and explosives, depending on the stability of the nitro compounds. The stability of the nitro compounds produced by nitric acid is of concern; however, impurity removal from PT-char by nitric acid is promising since nitric acid acts as both a strong acid and strong oxidizer. Hydrofluoric acid is the precursor to many pharmaceutical products, however, it is extremely dangerous to work with and thus, for safety reasons will not proceed further in this research. Hydrogen peroxide has not been specifically used to demineralise PT-char, but it has been successfully used to remove sulphur from TDO [38]. The sulphur within TDO is thermally instable which is why it vaporised and partitioned to the TDO during WT-pyrolysis. The sulphur within PT-char, however, is thermally stable and may be difficult to liberate. Since nitric acid has been shown to release sulphur from PT-char [38], hydrogen peroxide may also be able to alleviate sulphur since it is a stronger oxidizing agent.

Formic acid is a weak carboxyllic acid and has been used to successfully remove sulphur from TDO [38]. However, as discussed above, the sulphur with PT-char X is thermally stable and difficult to liberate and since formic acid is so weak, it may be ineffective. Acetic acid, however, is a stronger and more structurally complex carboxyllic acid in comparison to formic acid. Acetic acid is not only able to react with sulphur, it will also able to target the metallic ash within PT-char since it able to dissolve metals, and any non-polar oils which may be present within the porous structure. Additionally, acetic acid has been utilised for soil remediation [158].

Two alkali, namely potassium hydroxide and sodium hydroxide, have been discussed by authors [5][116][103] with regards to PT-char demineralisation. Both alkalis are known to react with silicon dioxide; however, sodium hydroxide has been shown to be more successful, as it is stronger than potassium hydroxide. Additionally, it is utilised successfully to dissolve SiO_2 in many different fields, particularly mineral processing.

In summation, hydrochloric acid, sulphuric acid, nitric acid, hydrogen peroxide, acetic acid and sodium hydroxide show PT-char demineralisation potential and will proceed further in this study.

Table 14:   **Overview of PT-char Demineralisation as found in Literature**

Reference	Acid/Alkali Type	C:L Ratio	Acid/Alkali Concentration	Extraction Temperature	Extraction Time	Agitation	Final Ash Content	Ash Removed	Comment
[116] [5]	H$_2$SO$_4$ & NaOH	3:1 – 15:1[22]	0.1N – 10N[23]	20-60°C[24]	10-60min[25]	Vigorous stirring	3.06 wt.%	11.54wt.%	Acid reused thrice, giving demineralised PT-char ash content of 1% higher than when fresh acid used.
[34]	HCl	30mL/g	1M		24hr		7.4%	8.4%	
		30mL/g	3M		24hr		9.9%	5.9%	
		5mL/g	1M		6hr		27.9%	-12.1%	
		5mL/g	1M		24hr		7.9%	7.9%	
		5mL/g	3M		6hr		6.4%	9.4%	
		5mL/g	3M		24hr		6.6%	9.2%	
		17.5mL/g	2M		15hr		8.0%	7.8%	
		30mL/g	1M		6hr		8.6%	7.2%	
		30mL/g	3M		6hr		10.6%	5.2%	
[33] [92]	HCl	100mL/g	1M	60°C	60min	Continuous stirring	1.11% w/w 3.16% w/w	1.24 0.43	Different co-pyrolysis chars used

[22] Optimal found to be 10mL/g

[23] Optimal found to be 1N for H$_2$SO$_4$ and 5N for NaOH

[24] Optimal found to be 60°C

[25] Optimal found to be 30 minutes

[14]	HCl		2N	70°C	3hr	Stirred			Parameters sourced from review by Antoniou et al.
	HF + Cl			Elevated	24hr + 1hr				
	HCl	3:1	3M		18hr				
	HCl		1M						
	HCl		1N		24hr				
	H_2SO_4		1N		24hr				
	HNO_3		4M						
[15]	HCl		2N	70°C	3hr	Stirred	2.97	9.24	PT-char pyrolysed at different temperatures were used as feed.
							2.63	9.06	
							2.78	8.73	
							2.80	9.10	
[109] [77]	HCl		5M	Boiling point	90min		1.6	10.10	PT-char pyrolysed at different temperatures were used as feed.
							2.1	9.50	
							1.5	10.4	
							2.0	10.4	
							1.1	11.2	
							2.6	9.5	
[131]	HCl		1M						
[76]	H_2SO_4		70wt.%	60°C	90min		1.30		
[94]	HCl		1M				10.89		
[103]	HCl & KOH	250mL acid	0.5N	85°C	30min		0.5wt.%[26]	2.5wt.%	
[22]	HCl	2-3g/100mL	1M	Room	1day				
[82]	HCl		5% solution						
[16]	HCl		10% solution	100°C	2hr		4-5wt.%[27] 38wt.%[28]	10wt.% 2wt.%	

---

[26] KOH incorporation removed ash: ash removed using 4KOH/tire
[27] Truck tyres utilized to produce PT-char
[28] Passenger car tyres utilized to produce PT-char

2.6.6. Commercial leaching methods: a brief overview of process concepts

Lixiviant extraction is a popular industrial separation method, especially in the hydrometallurgical field [133]. Industrial lixiviant extraction separations usually make use of multiple extraction stages for increased efficiency, and the lixiviant is cleaned and regenerated for further use for cost and process viability purposes [132]. Commercial extraction processes can be categorized into two types: batch extraction and continuous extraction [133].

Batch extraction can be subdivided into two methods, namely the displacement method and the enrichment method [133]. Batch (pot) extractors and rotating extractors are commonly used for batch extraction [133].

Although being the oldest method, the displacement method is very simple, making it popular [133]. This method consists of several batch extractors connected in series, with a feed of fresh lixiviant entering each batch extraction unit, as shown in figure 9a. This arrangement is known as a cross-flow arrangement and it requires a large concentration difference. Cross-flow extraction is commonly used when the nature of the solid feed material does not allow for the use of other processing methods. In each process unit, the solid material is first thoroughly mixed with the fresh lixiviant. After the mixing process, the solid material is allowed to settle. If the solid and liquid phases are unable to separate sufficiently using a sedimentation process, other process such as extraction, filtration or centrifugation can be employed. The extract solution is removed from the process while the solid material enters the next batch extraction unit for another stage of extraction. A disadvantage of the displacement method is the high recovery cost as the number of extraction stages increase.

The enrichment method also makes use of several batch extractors connected in series, but consists of a single feed of fresh lixiviant [133]. The lixiviant flows counter-currently through each batch unit, entering the unit which contains almost fully extracted solid material and leaving the unit containing the fresh solid material feed, as shown in figure 9b. This operation approach is known as counterflow battery extraction or enrichment process. The cost and consumption of utilities are much lower for the enrichment method in comparison to the displacement method.
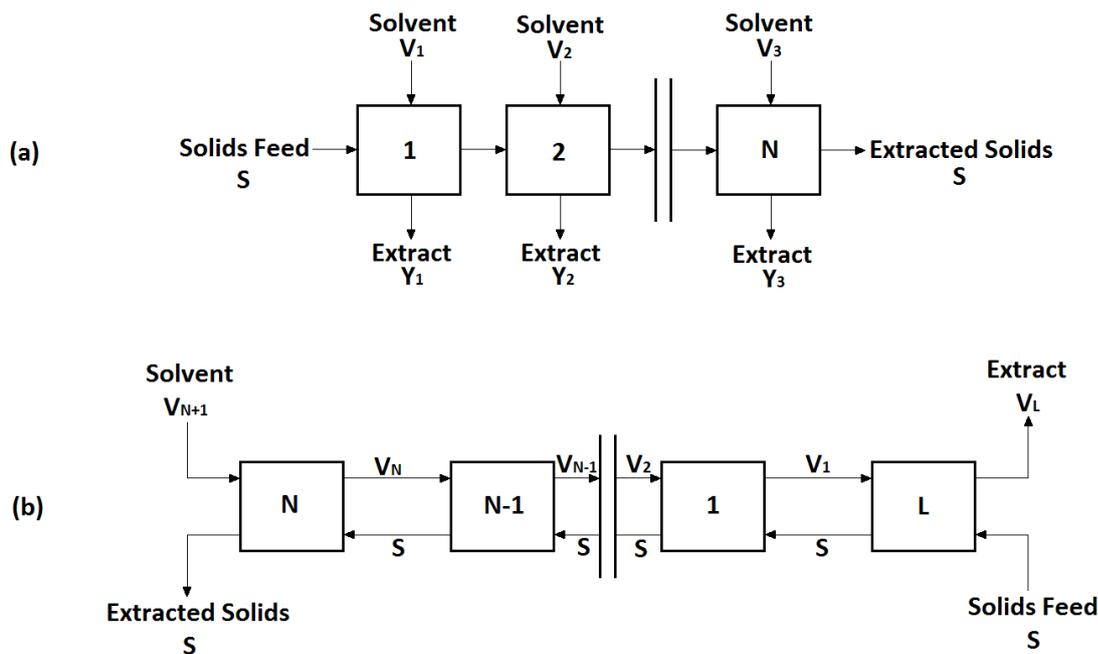
Figure 9: **(a) Continuous, Counter-current, Ideal-stage Leaching System; (b) Cross-flow, Ideal-stage Leaching System**[29]

Continuous extraction makes use of a percolation system which requires a highly permeable feed material to allow the lixiviant to pass through it using self-filtration [133]. The feed is exposed to minimal mechanical stress and the extract solution has low fines content. There are a variety of continuous extraction units available: Bollmann bucket-elevator extractor; continuous countercurrent percolation extractors; rotation extractor or carousel extractor; De smet reflex extractor; Lurgi sliding-cell extractor; De smet LM extractor; crown Iron extractor.

2.7. Conclusions of literature review

The objectives of the literature review were to determine a suitable target product which can be produced from crude PT-char, and to establish an upgrading technique.

It is well established that the high contamination level within PT-char renders it low-value, further discouraging any market worth. In its crude form, PT-char can be utilised as a solid fuel if the process is able to manage the toxic ash remnants correctly. If upgraded, PT-char can be transformed into activated carbon or carbon black.

A distinct trend between published articles shows that PT-char can successfully be transformed into activated carbon using a demineralisation process followed by activation. Authors have thoroughly studied the activation process; however, no work has been focused on the demineralisation process.

---

[29] Figure 9 adapted from [203]

Many authors have used extreme variable values, such as long extraction times and high lixiviant concentrations, to remove the metal content within PT-char on lab-scale equipment, which are infeasible on an industrial scale.

To date, there has been no published work regarding the kinetic relationships of variables which effect PT-char extraction efficiency.

The transformation of PT-char to carbon black has been suggested by many authors, although only two articles have investigated this topic. Pilusa and Muzenda [138] utilised highly concentrated sulphuric acid to remove the metal components of PT-char, followed by a grinding process to remove the silicon/ silicon dioxide content. Chaala et al. [141] demineralised PT-char using a sulphuric acid wash followed by a sodium hydroxide wash to extract their metal and silicon/silicon dioxide components respectively. There are a few shortcommings observed wtihin the literature. There are no comparisons between the extraction efficiency different lixiviants, and authors seem to use either hydrochloric acid or sulphuric acid. It is clear that both an acid and an alkali should be employed to extract the different ash components; however, there is no information regarding the sequence in which the acid-alkali extraction should occur. No process has been developed which removes the required ash content from PT-char to form CB using chemical separation only. Furthermore, no economic analyses have been performed on any process which converts PT-char to CB and, thus, it is unclear whether it is more economically viable to produce CB or activated carbon from PT-char.

The following research will aim at adressing these shortcommings.

- Each lixiviant which has been discussed by authors with direct relevance to PT-char demineralisation will be compared by studing their individual extraction efficiency and economic viability. This will give a clear, novel view on which lixiviant is superior at ash extraction.

- The kinetic relationships of relevant extraction variables will be analysed in order to gain in-depth, novel knowledge of the PT-char extraction process. This will further enable the selection of the most suitable conditions at which the extraction process should operate.

- The acid-alkali wash sequence will be analysed so as to develop a novel process using solely chemical separation processes. An economic analysis will be performed on an industrial scale verision of the developed chemical process so as to determine if the conversion of PT-char to carbon black is economically viable.

Chapter 3: Pyrolytic Tyre Char Characterisation

3.1.   PT-char characterisation: study description

Literature has shown that PT-char may differ substantially in physical characteristics and chemical compositions. There is no current information regarding the properties of the commercially produced PT-char provided for this research, therefore a characterisation study must be performed. This study focuses on establishing the properties of PT-char and CB for use as benchmark targets.

3.2.   PT-char characterisation: study objective i.c.

To investigate (research) pyrolytic tyre char upgrading methods and product opportunities by performing initial characterisation studies on commercial pyrolytic tyre char and target product for the attainment of benchmark characteristics.

3.3.   PT-char characterisation methodology

3.3.1. Materials required for pyrolytic tyre char characterisation

Two PT-chars, namely PT-char X and PT-char Y, were obtained from two different industrial South African suppliers. CB N330 was chosen for comparison since it is a moderate carbon black and both Williams [19] and Martinez et al. [1] discussed its comparability to PT-char. TT crumb, as obtained from an industrial South African supplier, was utilised for a heat of combustion comparisons as it is currently used in industry as a solid fuel source.

3.3.2. Analytical experimental procedure

Heat of Combustion

The CV of PT-char was analysed using a pressurised CAL2k ECO bomb calorimeter. The sample, which weighed between 0.25-0.30g, was fully combusted using a pure oxygen environment at a pressure of 2100kPa for 10 minutes. A correction factor was applied to account for work done, heat lost, and for the difference in density between tyre char and coal, as shown in equation 7, section 3.3.3.

Proximate, Ultimate and Mineralogical Composition

The proximate analysis was completed using Mettler Toledo TGA/DCC1. The analytical method utilized was a modified version of ASTM[30] E1131-08, adapted according to the properties of PT-char.

0.1g PT-char was heated to 750°C according to the trend shown in appendix G.

The mineralogy study was performed using PANalytical Axios WD-XRF. The analytical method was adapted according to the properties of PT-char. The inorganic components within PT-char were oxidised at approximately 950°C[31] and the relative weights analysed.

The ultimate analysis was executed using LECO TruSPEC Micro elemental analyser. The analytical method was adapted according to the properties of PT-char. Oxygen was measured and not calculated by means of subtraction.

Surface Morphology

The surface characteristics of PT-char was analysed using Zeiss EVO® MA15 Scanning Electron Microscope with Oxford Instruments® X-Max 20mm EDX detector and Oxford INCA software. The surface of the PT-char sample is first covered with a thin layer of gold for conductivity. Under reduced pressure, the samples were identified with secondary electron images and the composition was identified using EDX. The 20kV beams had a current of 20nA and a working distance of 8.5mm. The counting time was 10 seconds live-time. Pure cobalt was used periodically to correct for detector drift.

Porosimetry

The particle size distribution was analysed using Micromeretics Saturn DigiSizer 5200 laser diffraction system. The analytical method used was based on ISO[32] 13320 and the refractive index for carbon was used since PT-char is predominantly carbon.

The surface area and pore dimensions were determined using Micromeretics 3Flex nitrogen adsorption at 77K. The surface area was calculated using the BET method, while the pore dimensions were determined using the BJH method.

---

[30] American Society for Testing and Materials
[31] A temperature of 950°C was determined through method development.
[32] International Organization for Standardization

3.3.3. Relevant equations

Table 15:　　　**Description of Unknowns within Equations 7-8**

Equation Unknown	Description	Position in Procedure
m_{sample}	Mass of the sample used for calorific value measurement	Initial measurement
$CV_{measured}$	Calorific value measured using the bomb calorimeter	Result
$CV_{corrected}$	Corrected calorific value	Result

$$CV_{corrected} = \frac{(CV_{measured})(m_{sample}) + 0.0713}{1.0037(m_{sample})}$$　　　**[Equation 7]**

$$STDEV = \sqrt{\frac{\sum(x - \bar{x})^2}{2}}$$　　　**[Equation 8]**

3.4.　Results and discussion of PT-char characterisation study

Heat of Combustion

An energy analysis of PT-char X, TT crumb and a South African coal was determined[33]. Table 16 shows the average CVs of each material. The CV of PT-char X was found to be 27.50MJ/kg. This is agreeable with reported values in literature, which range from 14.8-71.90MJ/kg, as shown in table 5. The heat produced when combusting TT crumb is very high, with a CV value of 37.41MJ/kg. This is in conformity with published values described in table 5. The energy produced by a South African coal was measured to be approximately 25.52MJ/kg, which is in concordance with the benchmark range of 20.3-24.1MJ/kg [25], as discussed in table 10. It is clear that both PT-char X and TT crumb produce a large amount of energy when combusted. Both PT-char X and TT crumb have a much higher CV than commercial coal used for electricity generation, thus showing that combustion is a feasible option for the reuse of waste tyre or crude PT-char X [1][159].

Table 16:　　　**Calorific Values of PT-char and Coal**

Sample	Unit	Value	Standard Deviation
PT-char X	MJ/kg	27.50	0.015
TT Crumb[34]	MJ/kg	37.41	0.180
RSA Coal	MJ/kg	23.53	0.012

---

[33] Due to incomplete pyrolysis, PT-char Y contains high elastomer content which is similar to that of TT crumb, therefore the CV of TT crumb was analysed rather than PT-char Y as incomplete pyrolysis is economically infeasible – refer to page 64 for further substantiation.

[34] Steel and fabric free basis

Proximate, Ultimate and Mineralogical Composition

An ultimate analysis (CHNO) was performed on PT-char X and CB N330 using an elemental analyser (EA). Sulphur was not analysed using EA due to calibration limits. PT-char Y was not included due to EA material processing difficulty. The standard deviation is described by repeated measures and deviations from calibration. Refer to table 17 for the ultimate analysis results; and section 2.4.2 for relevant literature.

The carbon content constitutes the largest portion of both PT-char X and CB N330, with values of 81.43wt.% and 96.18wt.% respectively. This is in agreement with the TGA results discussed below in table 18. The PT-char X carbon content is supported by literature since the value fall within the published range of 78.5-98.9wt.%.

The hydrogen content in PT-char X, which is 0.58wt.%, is slightly higher than that of CB N330, which is 0.18wt.%, as shown in table 17. The PT-char X hydrogen content is in agreement with the published range of 0.26-10.66wt.%.

Nitrogen constitutes the lowest mass within both PT-char X and CB N330, as shown in table 17, with values of 0.58wt.% and 0.17wt.% respectively. The nitrogen content within PT-char X is supported by literature as it falls within the range of 0.1-5.1wt.%.

The oxygen content within PT-char X, as measured by EA, is 3.15wt.%, while in CB N330, it is 2.04wt.% (table 17). These values are supported by literature.

The CB N330 has a sulphur capacity of 1.8wt.%. The sulphur content within PT-char X analysed to be 7.28wt.% using WD-XRF and 1.98wt.% using SEM-EDX. Published sulphur contents of PT-chars range from 0.8-3.41wt.%, thus showing that the WD-XRF measurement is not in agreement with any literature. WD-XRF is highly susceptible to matrix errors. These errors may be caused by the utilisation of coal as the calibration standard since there are no available PT-char standards. The difference in structure between coal and PT-char may be causing this large deviation from publications. A total of 9 different spectrum analyses were used for the SEM-EDX and, since it is supported by published findings, it will be used as the sulphur content of PT-char X.

Table 17:   **Ultimate Analysis of PT-char X and CB N330**

	Unit	PT-char X		CB N330	
		Value	Standard Deviation	Value	Standard Deviation
C	wt.%	81.430	1.089	96.176	0.480
H	wt.%	0.583	0.024	0.176	0.011
N	wt.%	0.317	0.004	0.167	0.026
O	wt.%	3.153	0.117	2.038	0.050
S	wt.%	1.983	0.328	1.803	0.031
Total	wt.%	**87.466**	**1.562**	**100.36**	**0.598**

A proximate analysis was performed on CB N330, PT-char X and PT-char Y. Refer to table 18 for the proximate analysis results; and section 2.4.2 for relevant literature. The standard deviation is described by repeated measures.

Although considerably low, PT-char X has double the water content than CB N330 and PT-char Y. The moisture content within PT-char X falls within the range of 0.09-3.57wt.% and is, thus, in agreement with literature.

The volatile content, excluding water, within PT-char X is 1.38wt.%, and is in agreement with published values, with range from 0.41-17.9wt.%. The volatile content within PT-char Y, which is 64.68wt.%, is considerably higher than the published range for PT-char. This value, however, coincides with the volatile content within waste tyre crumb, which ranges from 63.8-73.9 [15][80][110].

The fixed carbon contents measured by TGA are in agreement with the ultimate analysis results discussed in table 17. The carbon content of PT-char Y is not in agreement with published values for a PT-char. It is, however in agreement with the carbon content found in waste tyres, which ranges from 25.00-35.00wt.% [1].

The ash content within PT-char X is 16.24wt.%, and within PT-char Y is 6.67wt.%. These values are in agreement with authors who have thoroughly analysed PT-char ash contents to range from 2.18-40.80wt.%. Furthermore, PT-char produced from PCT has an ash content of 40.80wt.%, while PT-char produces from TT has an ash content of 14.80wt.% [16], thus showing that PT-char X is predominantly made from TT. The ash content within CB N330 is 1.95wt.%.

Table 18:   **Proximate Analysis of CB N330, PT-char X and PT-char Y**

	Unit	PT-char X		PT-char Y		Carbon Black N330	
		Value	Standard Deviation	Value	Standard Deviation	Value	Standard Deviation
Water	wt.%	0.644	0.009	0.251	0.019	0.349	0.003
Volatiles[35]	wt.%	1.38	0.019	64.675	0.202	0.657	0.023
Fixed Carbon	wt.%	81.737	0.241	28.408	0.174	97.047	0.063
Ash	wt.%	16.239	0.251	6.665	0.048	1.947	0.083
Total		100.00	0.520	100.00	0.443	100.00	0.172

The mineralogy study aimed at analysing the variety and quantity of inorganic, or ash, composition within PT-char X and CB N330. PT-char Y was not included due to WD-XRF material processing difficulty. The standard deviation is described by repeated measures and deviations from calibration. Zinc was not measured via WD-XRF due to a lack of appropriate calibration; however, it is known to be in its oxide form as zinc oxide is an activator added to tyres during manufacturing. Refer to section 2.4.2 for relevant literature.

The mineralogical results produced by WD-XRF are in oxide form, as expressed by the 'oxide mass' column in table 19. Using stoichiometry, the mass of the elemental metal can be calculated as a percent of the oxide, as described by the 'metal mass' column. It must be noted that the metals can be in their elemental form or in their corresponding oxide, sulfide or chloride form [91]. It is certain, however, that a large portion of silicon is present in its oxide form in PT-char since silicon dioxide is added to the tyre as a filler, and WT-pyrolysis is unable to destruct its strong covalent structure or evaporate it [160]. Additionally, aluminium, magnesium and titanium all form oxide layers immediately upon exposure to air, therefore, a small portion of these elements will be in their oxide forms.

PT-char X consists predominantly of iron, silicon dioxide, sodium and calcium, with aluminium and potassium also making up a large portion of the inorganic content. This is in partial agreement with referenced work since the presence of zinc and sodium were found to be deviations when comparing the major inorganics within PT-char X and those found in literature. Firstly, due to analytical constraints, zinc was not analysed, although it is suspected to exist in large portions, and in its oxide form [18], within PT-char. Furthermore, the sodium content is not well represented by literature as Chan et al. [34], were the only authors to the analyse sodium content within PT-char X, implying that other authors found it present in minor quantities or not present at all, or they did not analyse it due to certain constraints. CB N330 comprises essentially of iron, silicon, sodium and

---

[35] Volatiles excluding water

magnesium, as shown in table 19. This is in agreement with Long et al. [21], who stated that carbon black has been found to contain inorganics including calcium, copper, iron, manganese, potassium, lead, arsenic, chromium, selenium and zinc. Copper, lead, arsenic, and zinc were not analysed, while selenium was found to be below detection limits for CB N330.

The quantity of inorganics found in PT-char X is comparable to what has been discussed in literature, however; the iron, silicon dioxide and sodium content within PT-char X are slightly higher than reported values. Due to the lack of published information regarding the magnitude of inorganic material found in carbon black, the quantities reported in table 19 cannot be compared other findings. Iron and silicon, however, make up half the inorganic content within CB N330.

The total inorganic (ash) content within PT-char X and CB N330, as analysed by WD-XRF, are shown at the bottom of table 19. Two values are illustrated under the metal mass column for both PT-char X and CB N330: the upper value is the sum total of all inorganics if in elemental form; the lower value is the sum total of all inorganics in elemental form, except silicon which is in its oxide form.

Table 19:   **Major Mineralogical Composition of PT-char X and CB N330**

	Unit	PT-char X			CB N330		
		Oxide Mass	Metal Mass	Standard Deviation	Oxide Mass	Metal Mass	Standard Deviation
Fe_2O_3	wt.%	5.70	3.99	0.087	1.09	0.762	1.365
SiO_2	wt.%	8.47	3.96	0.987	0.90	0.421	1.250
Na_2O	wt.%	1.93	1.43	0.202	0.15	0.111	5.740
CaO	wt.%	1.81	1.29	0.168	0.10	0.071	1.565
K_2O	wt.%	0.42	0.35	0.044	0.06	0.050	11.335
Al_2O_3	wt.%	0.43	0.23	0.068	0.02	0.011	2.055
P_2O_5	wt.%	0.25	0.11	0.084	0.02	0.009	4.140
TiO_2	wt.%	0.17	0.10	0.009	0.01	0.006	8.535
MgO	wt.%	0.11	0.07	0.172	0.19	0.115	3.225
Cr_2O_3	wt.%	0.06	0.04	3.655	0.05	0.034	3.655
MnO	wt.%	0.04	0.03	0.001	0.01	0.008	6.29
Total	wt.%	**19.39**	**11.60** **16.11**[36]	**0.1770**	**2.6**	**1.60** **2.08**[36]	**0.335**

Table 20 shows a comparison between the total ash content analysed by TGA and analysed by WD-XRF. It is difficult to conclude which elements are in their oxide form and which are not. It is known, however, that SiO_2 will be in a large portion within PT-char as it is tyre filler. Also, Al, Mg Ti form oxide layers upon exposure to air.

---

[36] Including SiO_2 and not elemental silicon

If all the inorganics were in their oxide form, the WD-XRF ash results show to be much higher than the TGA ash results. Similarly, if all the inorganics were in their elemental form, the WD-XRF ash results show to be much lower than the TGA ash results. The ash content analysed by TGA is most comparable to the WD-XRF results when summating the inorganics in their elemental form, except for silicon which is in its oxide form (SiO_2). Considering this the ash content within PT-char X as measured by TGA is 0.13wt.% higher than that analysed by WD-XRF; while the ash content within CB N330 as measured by TGA is 0.13wt.% lower than that analysed by WD-XRF. This is most likely due to TGA producing an ash result which is in its oxide form. It is, therefore, most accurate to say that the inorganics are predominantly in their elemental form, except silicon which is predominantly in its oxide form, with a small portion in its elemental form. This is substantiated by stoichiometry calculations which show that 4.5wt% oxygen is required for all silicon to be in its oxide form, however, the EA measured on 3.15wt.% oxygen. Additionally, Al, Ti and Mg will exist chiefly in their elemental form, with a small portion in oxide form.

Ultimately, the ash content within PT-char X is approximately 16.1wt.% according to both TGA and WD-XRF. Half the ash content is silicon/ silicon dioxide (8.47wt.%), and the rest consists of a mixture of metallic inorganics, most likely in their elemental form. It is recommended that further analysis be performed on PT-char so as to certify whether the inorganics are in their oxide, sulphide or chloride form. However, it must be noted that XRD[37] analyses have been performed to study the chemistry of ZnO [161] and its transformation to ZnS [91] [116].

Table 20: **Comparison between the Ash Content analysed by TGA and by WD-XRF**

	Unit	PT-char X	Carbon Black N330
TGA: ash	wt.%	16.239	1.947
WD-XRF: total oxide mass	wt.%	19.390	2.600
WD-XRF: total elemental mass	wt.%	11.600	1.600
WD-XRF: Metal elemental mass and SiO$_2$	wt.%	16.110	2.080

In order to verify the results, table 21 observes the total organic and inorganic composition of PT-char X and CB N330, which should equate to approximately 100wt.%. The total organics included the summation of C,H,N,O,S using the ultimate analysis results. The total inorganics included the summation of the WD-XRF ash components in their elemental form so as to avoid oxygen summation repetition. The mass analyses performed on PT-char X tallies to a total of 99.066wt.%, while the matter analysed in CB N330 adds to a total of 101.96wt.%. Considering the high degree of PT-char X heterogeneity in terms of particle size, concentration and matrix structure, the results

---

[37] X-ray Diffraction

represented in table 21, and consequently the proximate analysis, the mineralogical analysis and the ultimate analysis, describe PT-char X and CB N330 well and are acceptable.

Table 21:   Sum total of Inorganics and Organics for PT-char X and CB N330

	Unit	PT-char X		CB N330	
		Value	Standard Deviation	Value	Standard Deviation
Total Inorganics (elemental form)	wt.%	11.60	1.770	1.60	0.335
Total Organics (including oxygen)	wt.%	87.47	1.562	100.36	0.598
Total Mass	**wt.%**	**99.07**	**3.33**	**101.96**	**0.93**

Comparison between PT-char X and PT-char Y

The compositional analyses of PT-char X and PT-char Y show that PT-char X is a completely pyrolysed char, while PT-char Y is either partially pyrolysed or not pyrolysed at all.

The carbon content of PT-char Y (28.41wt.%) is much lower than literature values reported for a PT-char, but is in agreement with the filler content within tyres, which ranges from 25.0-35.0wt.% [1]. PT-char Y also accommodates a very high volatile content (64.68wt.%) as measured by TGA. This measurement is comparable to volatile contents within waste tyre crumb, which range from 63.8-73.9 [15][80][110]. Additionally, Undri et al. [96] found the volatile contents of partially pyrolysed PT-chars to be 17.9wt.% and 5.98wt.%, and originating from composed elastomers. Visually, the PT-char Y particles felt soft and spongy, and did not leave any residue on glove surface. These findings accentuate the perception that PT-char Y has either undergone partial pyrolysis or, more importantly, the supplier has provided waste tyre crumb rather than PT-char.

The inorganic contents of PT-char X, however, are in agreement with all literature values reported for a PT-char. According to Undri et al. [96], a hydrogen content less than 1wt.% is attributed to residual TDO within the porous structure of PT-char caused by the cooling of the pyrolysis reactor [33][92][93]. Hydrogen content greater than 1wt.% was ascribed to the presence of elastomers; which translates to an incomplete WT-pyrolysis process. Since PT-char X has hydrogen content less than 1wt.%, it has undergone complete pyrolysis but does contain a portion of TDO within its porous structure. This is in agreement with the low volatile content within PT-char X. Furthermore, on visual inspection, PT-char X had had hard, brittle, coarse particles which left a dark black residue on the glove surface. These findings show that PT-char X is fully pyrolysed.

Surface Morphology

The surface morphology of CB N330, fully pyrolysed PT-char X and partially pyrolysed PT-char Y were analysed using SEM-EDX, as shown in figure 10 below. Particle size can be approximated by comparing particle populations, as well as single particles. Figure 10a, c and f show particle populations of CB N330, PT-char X and PT-char Y respectively. The particle size of the CB population is much smaller in comparison to PT-char X and PT-char Y. Additionally, the particle size distribution of both PT-chars are heterogeneous.

Figure 10b, d and h show a single particle of CB N330, PT-char X and PT-char Y respectively. It must be noted that the CB N330 particle can be seen in figure 10a, bottom left corner. The CB N330 particle is approximately 35µm in size, while the PT-char X and PT-char Y particles are 400µm and 200µm respectively; thus showing that CB has a much smaller particle size in comparison to PT-char. The differences in CB N330 and PT-char particle sizes may be a result of high pyrolysis temperatures [82]. Furthermore, carbonised rubber and tarry products from by secondary reactions [82] may cause the original CB particles from the tyre to bind together during pyrolysis [105]. Hofman and Pietrzak [82] found PT-char particle sizes to be highly irregular with a wide array particle diameters. Helleur et al. [30] made use of SEM for particle size analysis. Due to the heterogeneous nature of PT-char, particle size analysis by SEM is not accurate.

Figure 10e illustrates PT-char X particles with a macropore structure. During WT-pyrolysis, the macropores are formed by the core-to-surface progression of volatile elastomeric species within a tyre particle [105]. Subsequent to macropore creation, organic material fills the pores [96], giving the solid, rough surface morphology of a PT-char particle, as shown figure 10d. Furthermore, a comparison between figure 10d and figure 10g illustrates the difference in surface morphology between a particle which has undergone complete pyrolysis and one which has undergone partial pyrolysis: smoother surfaces are attributed to the presence of elastomers which have not yet decomposed, whilst rough surfaces are attributed to PT-char and a lack of smooth elastomers [161]. This can be seen particularly in figure 10h: the upper part of the particle is rough and elastomers have volatilised, while the lower portion of the particle is smooth and the elastomers are intact. It must also be noted that, as discussed in section 2.2.2, tyres are composed of a blend of different elastomers [17][19], each having different kinetics and boiling points, which augment the sporadic structures of PT-char particles. The micrographs of figure 10 show grey areas and bright spots. EDX was used to analyse the bright surface area of the PT-char X particle in figure 10d and the bright spot at the bottom of the PT-char Y particle in figure 10. As shown in table 22, the particle in figure 10d is predominantly composed of zinc, oxygen and sulphur, most likely in the form of zinc oxide or zinc

sulphide. Zinc oxide is added during tyre manufacturing as a vulcanizing agent [18], and has the tendency to transform to zinc sulphide with increasing pyrolysis temperatures [161][91][96][116]. The bright spot on the particle in figure 10g contains major elements aluminium, silicon and oxygen. The silicon and oxygen are most likely in the form of silicon dioxide [96] since it is a present in a tyre as filler [1][17][18]. These results are in agreement with Undri et al. [96] who noted that the bright spots in SEM images are caused by backscattering due to the presence of metals. They showed that the bright spots had a higher metal composition, including Fe, Zn, Co, Cr, Cu, Si and Mg, than the grey areas.

Table 22: **SEM-EDX Composition Results for Bright Spots on PT-char Particles, in terms of wt.%**

	Na	Mg	Al	Si	S	K	Fe	Cu	Zn	O	Total
Figure 10d	3.98	1.09	1.63	9.44	13.05	0.73	1.68	2.9	24.34	41.16	**100**
Figure 10g	1.17	0.56	17.24	22.41	1.04	6.69	2.97	0.54	1.48	45.9	**100**

(a)

(b)

(c)

(d)

(e)

(f)

(g)

(h)
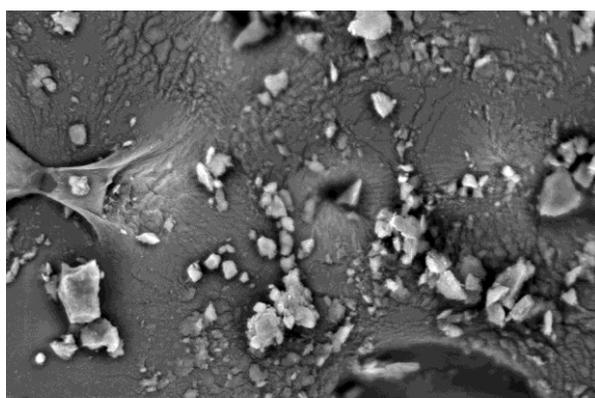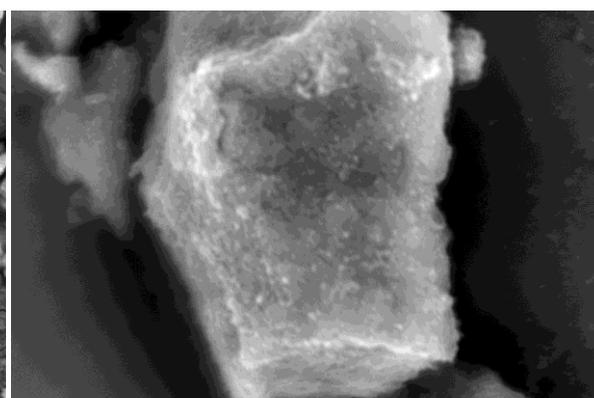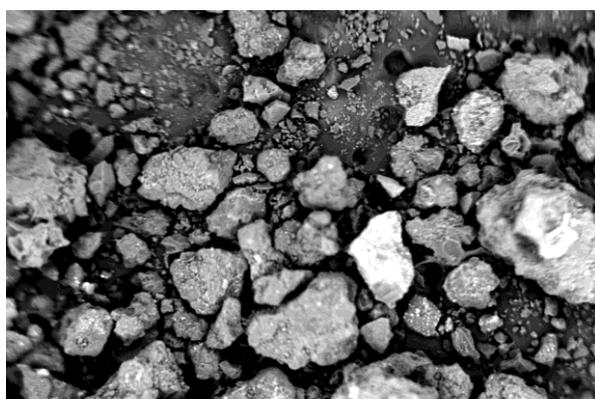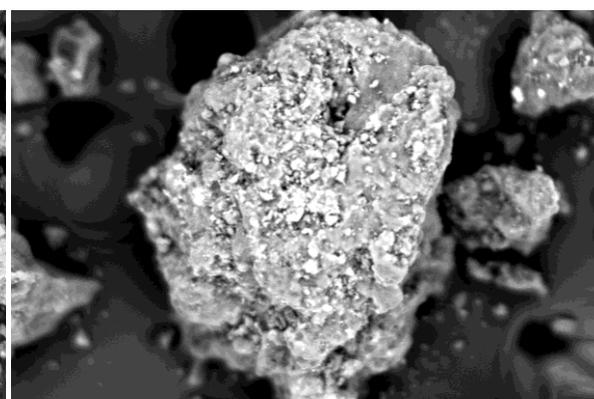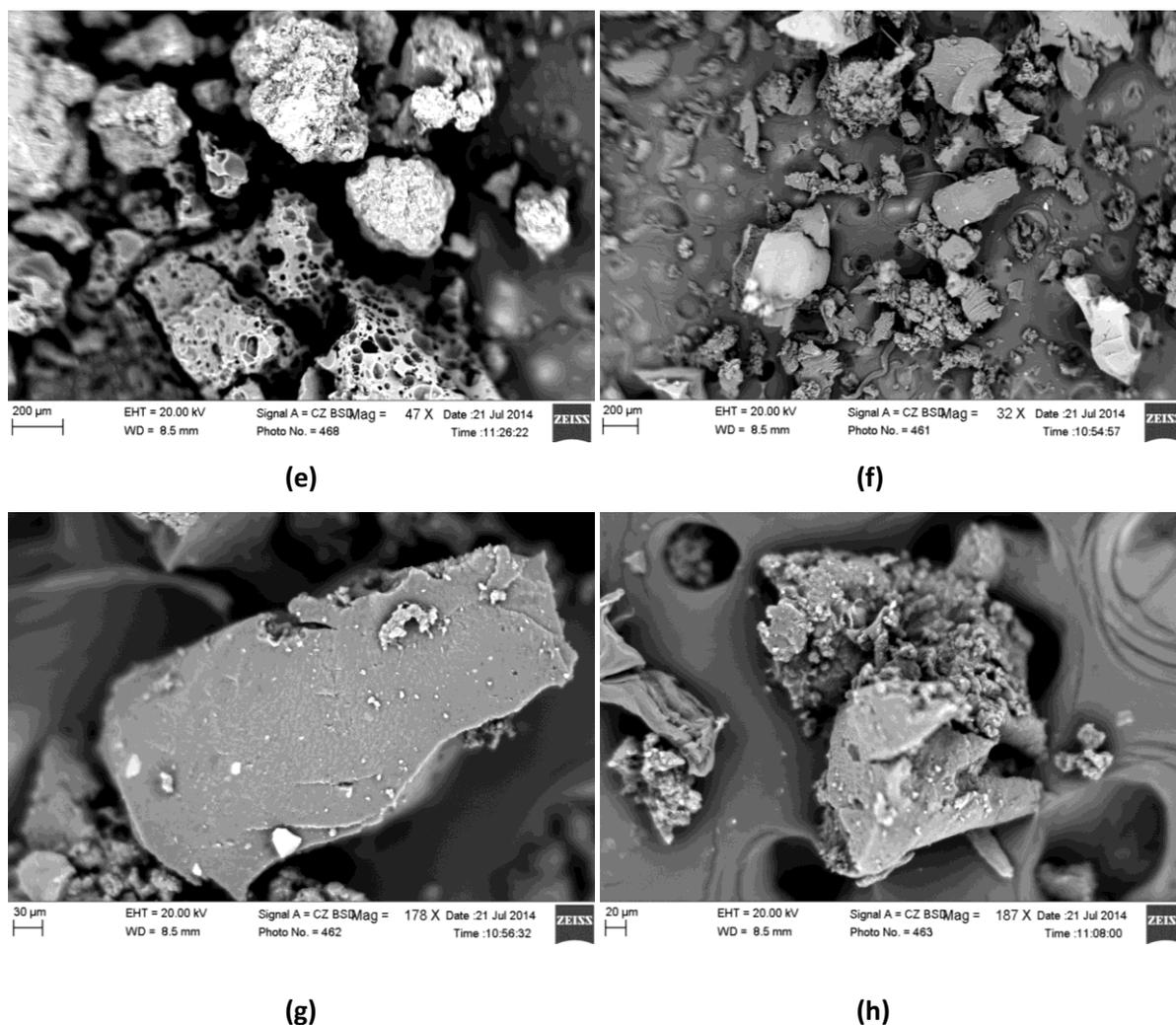
Figure 10:   **(a) SEM Image of Carbon Black N330 Particle Population (b) SEM Image of Carbon Black N330 Particle (c) SEM Image of PT-char X Particle Population (d) SEM Image of PT-char X Particle (e) SEM Image of PT-char X Macroporous Particle Structure (f) SEM Image of PT-char Y Particle Population (g) SEM Image of PT-char Y Particle (h) SEM Image of Decomposing PT-char Y Particle**

Particle Size Distribution and Porosimetry

The particle size distribution was measured using laser diffraction on a volume frequency basis.

Figure 11 illustrates the sample particle population distribution of CB N330, PT-char X and PT-char Y, in terms of percent finer. It can be seen that most CB N330 particles are less than 100µm in size, while the majority PT-char Y particles are greater than 100µm. Figure 11 also shows that, within the range of 1-100µm, CB N330 has the most evenly distributed particle size. As listed in table 23, 59.6% of the CB N330 particle population has a size ranging from 1-10µm. In comparison, PT-char X has a larger population particle size, with 35.3% of the particles accommodating a size greater than 100µm. In relation, the PT-char Y particle population size comprises of the largest cumulative particle size range, with 96.8% of the sampled particles measuring greater than 100µm. Particle size

distribution statistics, as shown in table 24, further substantiates the above discussed observations. The average particle size for CB N330, PT-char X and PT-char Y is 38.52μm, 153.2μm and 738.9μm, showing that CB N330 has the smallest average particle size while PT-char Y has the largest. The median shows that 50% of the particle population occurs at a size less than 3.585μm, 139.2μm and 775.9μm for CB N330, PT-char X and PT-char Y respectively. The particle size which most commonly occurs (i.e., mode) within the CB N330 particle population is 2.677μm, while 212.6μm and 949.8μm are the most commonly occurring particle sizes in the PT-char X and PT-char Y populations respectively.

The particle size of PT-char X is greater than commercial CB N330, which in agreement with literature. This is caused by the formation of carbonised rubber and other tarry products during high temperature WT-pyrolysis binding the small CB particles together[1][45][47][48][82][49][105]. PT-char X and PT-char Y particle size distributions were irregular compared to CB N330, which is in agreement with literature[82]. The average particle size of PT-char Y is much larger than PT-char X. This is due to the presence of solid elastomers in PT-char Y. Due to the incomplete pyrolysis of PT-char Y, elastomers have not decomposed to leave behind CB skeleton, thus producing a final PT-char particle with a greater size. PT-char X particles are much smaller since they contain no elastomers and only the CB skeleton is present.
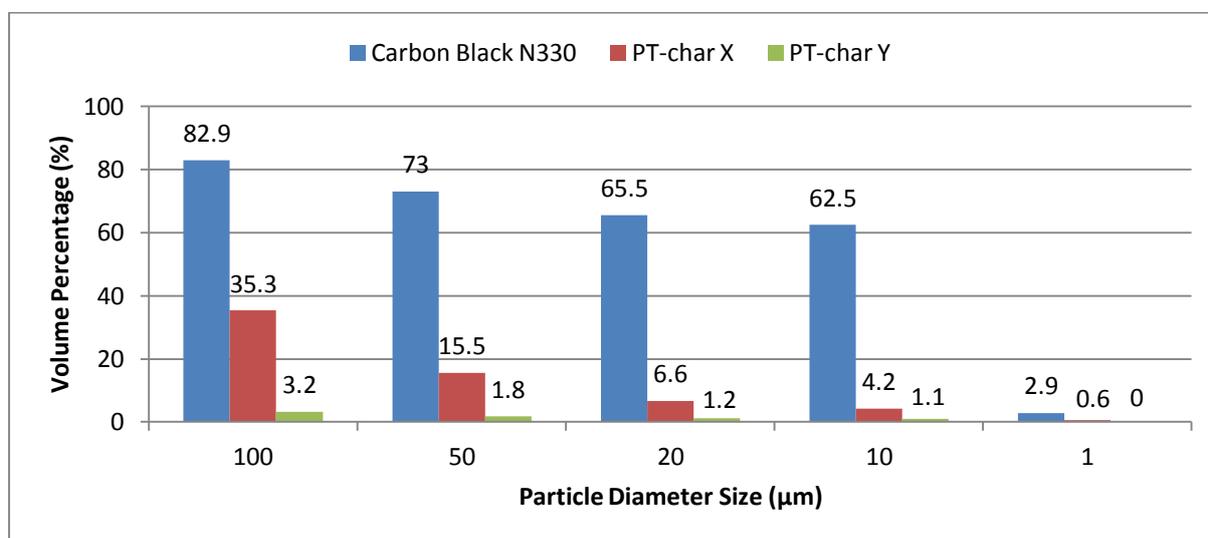
Figure 11:   **Particle Size Representation in terms of Percent Finer of Sampled Particle Population**

Table 23: **Particle Population Cumulative Size Range Distribution**

Particle Size Range (μm)	PT-char X (%)	PT-char Y (%)	CB N330 (%)
>100	39	96.8	17.1
100-50	30	1.4	9.9
50-20	16	0.6	7.5
20-10	6	0.1	3
10-1	8	1.1	59.6
<1	1	0	2.9

Table 24: **Particle Size Distribution Statistics**

		PT-char X		PT-char Y		Carbon Black N330	
	Unit	Value	Standard Deviation	Value	Standard Deviation	Value	Standard Deviation
Mean	μm	153.2	5.118	738.9	63.77	38.52	17.12
Median	μm	139.2	5.276	775.9	89.26	3.585	0.435
Mode	μm	212.6	19.87	949.8	59.63	2.677	0

The particle and pore surface areas were measured using nitrogen gas adsorption and desorption isotherms, and calculated using both BET and BJH methods.

The resultant trends illustrated in the isotherm linear plots, depicted appendix J, show that the pore size analysis must originate from the adsorption branch. The adsorption isotherm analysis is added to table 25 and table 26 for comparison purposes. Refer to section 2.4.1 for relevant literature.

The BET surface area of CB N330 (table 25) is approximately $80.22m^2.g^{-1}$, which is to be expected [5][19]. The BJH adsorption isotherm shows that the pore surface area of CB N330 is $74.81m^2.g^{-1}$, which is slightly less than the BET value, showing that the pores do not encompass the entire surface area of the structure[162]. The BET and BJH adsorption surface areas of PT-char X do not differ significantly, and are approximately $58.93m^2.g^{-1}$ and $58.76m^2.g^{-1}$ respectively. This shows that the entire surface area comprises of a pores. This is supported by literature since the surface areas of PT-char generally range from $32-116.3m^2.g^{-1}$. The BJH adsorption surface area of PT-char Y is approximately $3.08m^2.g^{-1}$.

Overall, two key observations are present: the two PT-chars have different surface areas, and CB N330 has a larger surface area compared to PT-char X. PT-char Y has a very low surface area due the presence of elastomers, which have a characteristic smooth texture as discussed previously in figure 10g. This is in agreement with Teng et al. [115] who discuss the presence of elastomers reducing the available surface area. The surface area of the original tyre CB is reduced due the presence of impurities within PT-char such as: volatiles entrapped within the porous structure

[30][33][115]; the formation of carbonaceous products and/ or inorganic materials [14][34][80] on the surface of PT-char during WT-pyrolysis; and elastomers which have not yet decomposed during WT-pyrolysis [161] [96]. Many authors have noted that surface area increases when the inorganic impurities are removed [1][5][14] [115][30][33][34][80]. Additionally, the surface area of PT-char X is similar to that of CB N440, which has a surface area ranging from 43-69 $m^2.g^{-1}$ [163], rather than N330 [1].

Table 25:   **Surface Area Analysis of CB N330, PT-char X and PT-char Y**

	Unit	PT-char X	PT-char Y	CB N330
BET surface area	$m^2.g^{-1}$	58.9316	3.3244	80.2244
BJH adsorption cumulative pore surface area	$m^2.g^{-1}$	58.758	3.084	74.808
BJH desorption cumulative pore surface area	$m^2.g^{-1}$	55.0192	1.7763	80.5584

The pore size analysis is shown in table 26 below. The resultant trends illustrated in the isotherm linear plots, depicted appendix J, show that the adsorption measurement is most accurate for pore size analysis although desorption values are added to table 26 for comparison measures. The trends also show that CB N330 and PT-char X have distinctive mesoporous structure with poorly developed micropores [105]. PT-char Y has characteristic of cylindrical and spherical pores and the pores have a disordered, lamellar structure, with a slit and wedge shape [162].

The pore volume for PT-char X is 0.49$cm^3.g^{-1}$ and the pore diameter is 17.92nm. These values are in agreement with the range of values reported in literature [34][80][96][105]. CB N330 has a significantly larger pore size, while PT-char Y has the smallest pore size. Pore size is strongly related to surface area, therefore, these two properties will show the same observable trend and, thus, similar reasoning can be concluded with regards to the presence of elastomers and other impurities.

Table 26:   **Pore Size Analysis of CB N330, PT-char X and PT-char Y**

	Unit	PT-char X	PT-char Y	CB N330
BJH adsorption cumulative pore volume	$cm^3.g^{-1}$	**0.486442**	**0.003396**	**0.811579**
BJH desorption cumulative pore volume	$cm^3.g^{-1}$	0.492437	0.002988	0.824733
BET adsorption average pore diameter	**nm**	**17.92**	**3.93**	**41.22**
BET desorption average pore diameter	nm	25.71	3.67	41.21
BJH adsorption average pore width	**nm**	**33.11**	**4.40**	**43.40**
BJH desorption average pore width	nm	35.80	6.73	40.95

3.5. Conclusions and recommendations of PT-char characterisation study

The principle objective of this study was to analyse UPT-char product opportunities and gain a greater knowledge of commercial PT-char characteristics. It was previously established that PT-char could be used as solid fuel or upgraded to carbon black, therefore, the principle objective of this study was implemented by comparing crude PT-char obtained by commercial entities to carbon black N330 and a South African coal. Comparison allows for the establishment of benchmark characteristics of which the UPT-char must meet in order to be utilised at tyre CB. It also shows the intensity required by the upgrading process. Four different characteristic studies were concluded: heat of combustion, composition, surface morphology, and porosimetry.

The heat of combustion study showed that both crude PT-char and TT crumb released more energy than a commercial coal burnt for electricity generation in South Africa, translating to the conclusion that crude PT-char can be used as an energy source. However, the large quantity and quality of ash, as well as the sulphur content, must be considered when combusting PT-char, as it harm the relevant process units and surrounding environment.

The composition of PT-char X and PT-char Y was the most important study as it gave insight into the impurity quality and quantity. The low volatile content illustrated by the TGA results concluded that PT-char X had undergone complete pyrolysis, whereas the large volatile content (64.7wt.%) and SEM imaging of PT-char Y indicated that it had not been completely pyrolysed. Furthermore, the low organic hydrogen content (<1wt.%) confirmed that PT-char X had undergone complete WT-pyrolysis. Consequently, PT-char Y will not partake further in this research and PT-char X will be used at the subject for process and product development studies.

The inorganics, or ash, content within PT-char is regarded as the principle impurity group as it greatly hinders the reinforcing properties within the tyre if reutilised as tyre carbon black. Comparison of the ash contents within PT-char X (16.24wt.%) and CB N330 (1.95wt.%) show that approximately 14.29wt.% ash must be removed from PT-char X in order to meet the target quality of CB N330. The mineralogical study, completed using WD-XRF, showed that the inorganic (ash) composition consisted predominantly of iron, silicon or silicon dioxide, sodium and calcium; with approximately half the ash content dominated by a mixture of silicon and silicon dioxide, and the rest consisting of metals. The correlates to the type of lixiviants which must be utilised: sodium hydroxide or hydrofluoric acid is able to react with silicon dioxide; while the metals are able to react with acids or

alkalis, depending on their amphoteric properties. Another important impurity is sulphur, of which PT-char X contained approximately 1.98wt.% and CB N330 consisted of 1.8wt.%.

Structurally, PT-char X had a larger particle size distribution and BET surface area compared to CB N330. Upgrading PT-char X to a CB product would require the BET surface area to increase from $58.9m^2.g^{-1}$ to $80.22m^2.g^{-1}$, and a reduction in average particle size from 153.2-38.5μm. Additionally, CB N330 displayed a highly uniform particle size distribution, whereas PT-char X did not. Previous research has shown that a reduction in ash content will augment the surface area of PT-char.

A method and appropriate standard for PT-char sulphur analysis using WD-XRF should be developed. It is also recommended that the degree to which each ash component is in its elemental/oxide form within PT-char be determined through XRD.

Chapter 4: Acidic Lixiviant Screening for Upgrading Pyrolytic Tyre Char

4.1. Acid-alkali screening: study description

By definition, screening is a trial experimental procedure used to condense a large selection of variables. Each variable is assessed and the variable(s) which are best suited for the particular purpose are identified and selected according to specific results. Typically, upper and/or lower limits are tested during experimental screening trials.

The overall purpose of this particular research is the development of a process which is able to upgrade of low-value, crude pyrolytic tyre char (PT-char) to a value-added product. In the previous sections, it has been established that, upgrading crude PT-char to carbon black is greatly appealing. Characterisation studies have further illustrated that the ash content of PT-char X must be reduced by 14.29wt.%, while the surface area must increase from $58.9m^2.g^{-1}$ to $80.22m^2.g^{-1}$ to render the upgraded product similar to that of CB N330. Additionally, the characterisation studies have confirmed that the ash comprises of silicon, silicon dioxide and metals; further showing the possibility of acid-alkali leaching as a promising upgrading technique for ash removal.

Acid-alkali leaching, as described in section 2.5, has been proven to remove portions of ash from PT-char. A large number of acids and alkalis[38] have been discussed by authors with regards to PT-char demineralisation, as shown in table 14. In this particular study, analysis of hydrochloric acid, sulphuric acid, nitric acid, hydrogen peroxide, acetic acid and sodium hydroxide will be performed by means of a screening procedure; hence, lixiviant type will be the only variable which will be altered and screened. Two types of screening procedures will be concluded: demineralisation screening and an economic screening. The demineralisation screening will assess the quantity of impurities removed by individual lixiviants and by sequential acid-alkali demineralisation. The economic screening, which will compare the cost of each lixiviant required to produce the results from the demineralisation screening trial. The economic screening will, ultimately, be based on a cost effectiveness analysis (CEA).

---

[38] Acids and alkalis collectively referred to as lixiviants

4.2.   Acid-alkali screening: study substantiation

To date, there is no published data comparing the PT-char extraction efficiency of different lixiviants, thus making this work novel. A reduction in the number of lixiviants considered is required since the technicality of process and product development renders the analysis of a large number of lixiviants impractical and unworkable.

4.3.   Acid-alkali screening: study objective ii.a.

To develop and propose a process for crude pyrolytic tyre char upgrading by evaluating factors which affect the pyrolytic tyre char upgrading process.

4.4.   Acid-alkali screening: methodology

4.4.1. Methodology overview

The acids discussed in literature will partake firstly in the demineralisation screening, followed by the economic screening.

The demineralisation screening is based on experimental procedure aimed at reducing the ash content within PT-char X using. Two sets of experiments were conducted, namely single acid extraction and sequential acid-alkali extraction. The lixiviant type was the independent variable. The constant variables include: PT-char type; solid-lixiviant mixture agitation speed; C:L mass ratio; extraction temperature; extraction time; and lixiviant concentration. Refer to table 27 for the extraction conditions, which are based on literature. The two dependent variables analysed include total mass and total ash extracted from PT-char. Since fully pyrolysed PT-char X was used as feed, its properties, as analysed in chapter 3, were used as the initial baseline, particularly 16.24wt.% ash and 1.98wt.% sulphur. Similarly, the properties of CB N330 are the benchmark targets, particularly 1.95wt.% ash and 1.80wt.% sulphur.

The economic screening procedure, which was based on a CEA, included assessing and comparing the cost of the raw lixiviants, as the cost factor, required to achieve the extraction results attained in the demineralisation screening trial.

Table 27:   **Comparison of Relevant Experimental Variables for Single Lixiviant Extraction and Acid-alkali Sequential Extraction**

	Extraction Temperature	Extraction Time	Lixiviant Concentration	C:L Ratio
Single lixiviant extraction	20°C	24hr	5M	10:100 (g/g)
Acid-alkali sequential extraction	80°C	1hr	1M	10:100 (g/g)

4.4.2. Methodology substantiation

Demineralisation screening reveals the exclusive extraction effectiveness of each lixiviant, as well as the feasibility and combined effectiveness of sequential acid-alkali washes. The lab scale demineralisation screening methodology and apparatus was designed for simplicity and based on a combination of techniques described in literature [34][90][93][164]–[173]. PT-char X was sampled according to the cone and quartering technique[39] so as to minimise error [174]. The particle size of PT-char X was not altered before the experimental procedure since the removal of ash during extraction may increase surface area and decrease particle size, thus reducing size reduction processing requirements. Solid-lixiviant mixture agitation speed was kept constant for equipment limitation purposes. The lone lixiviant extraction conditions aimed at maximum impurity extraction, regardless of the economic and processing constraints. It must be noted that an ambient extraction temperature was selected due to the hazards associated with hot acid extraction for extended periods of time. These variables were adjusted for sequential acid-alkali demineralisation since the aim was to test the feasibility. The demineralisation process itself consisted of three sections, namely pre-treatment, demineralisation, and post-treatment. Pre-treatment aimed at removing moisture from the feed PT-char X, while post-treatment removed moisture from UPT-char X. This is vital so as to prevent inaccurate mass measurement results. The balance was calibrated before each experimental run.

The economic screening procedure made use of the assumption that the extraction process of each acid can be scaled up perfectly, the economic analysis used the price of 10t[40] acid used to extract 1t PT-char X. The lowest of six prices for each lixiviant[41] which partook in the demineralisation screening trial were located using Alibaba.com. The price of NaOH was obtained from Dow Chemical Company.

---

[39] PT-char size segregation induced sampling error; therefore it was minimised as much as possible.
[40] Metric tonnes
[41] Of the same purity

4.4.3. Chemicals, materials and equipment required for acid-alkali screening

Table 28: **Description of chemicals required for demineralisation screening**

Chemical Description	Quantity
PT-char X	120g
Nitrogen gas	1 bottle
Distilled water	2.5L
Sulphuric acid, 5M	200g
Hydrochloric acid, 5M	200g
Nitric acid, 5M	200g
Acetic acid, 5M	200g
Sodium hydroxide, 5M	200g
Hydrogen peroxide, 5M	200g

Table 29: **Description of materials and glassware required for demineralisation screening**

Material/ Glassware Description	Quantity
Measuring cylinder, 250mL	1
Beaker, 2L (for mixing lixiviant concentrations)	1
Weigh boat, large	24
Lab spoon spatula	1
Chemical grade Schott bottle with PP[42] lid, 250mL	12
Filter paper, 150mm diameter, 10µm	36
Glass funnel, short stem	36
Erlenmeyer Flask	36
Plastic wash bottle	1
Watch glass (200mm diameter)	12
Centrifuge sample bottles, 15mL	24
Ceramic crucibles	26

Table 30: **Description of equipment required for demineralisation screening**

Equipment Description	Quantity
Magnet	1
Vacuum oven	1
Balance, 4 decimal, 250g maximum	1
Water bath with lid	1
Magnetic stirrer	1
Magnetic bead	12
Thermometer, 250°C	1
Muffled furnace	1

---

[42] Polypropylene

4.4.4. Experimental apparatus
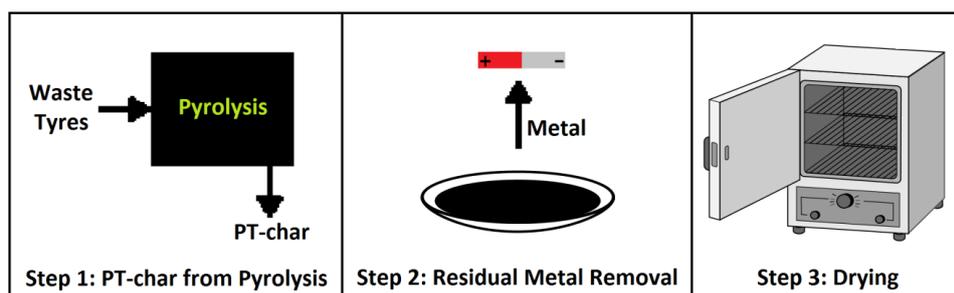
Figure 12: **PT-char Pre-treatment Experimental Apparatus**
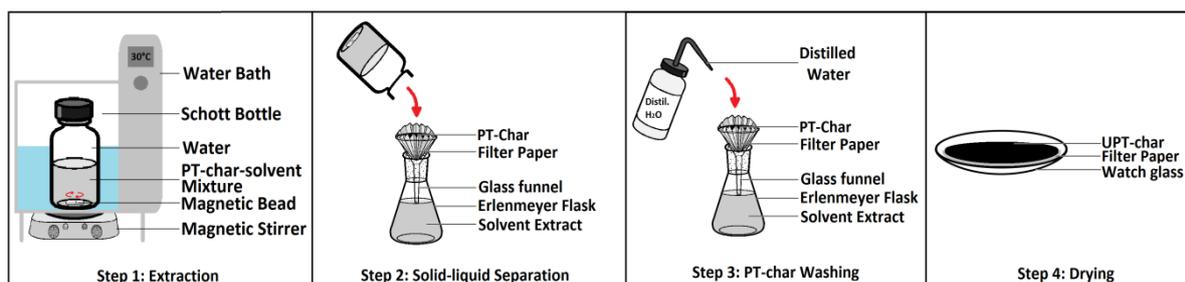
Figure 13: **PT-char Demineralisation Experimental Apparatus**
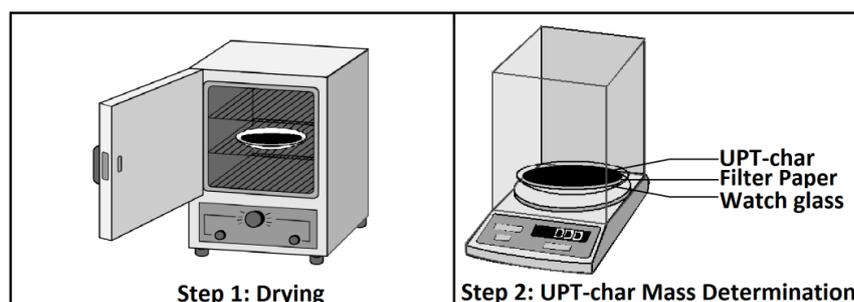
Figure 14: **PT-char Post-treatment Experimental Apparatus**

4.4.5. Demineralisation experimental procedure

The demineralisation screening experimental procedure described below is for one PT-char X demineralisation run by one lixiviant. The process must be repeated a total of 12 times: twice for all six lixiviants described above, namely: sulphuric acid, hydrochloric acid, nitric acid, acetic acid, hydrogen peroxide and sodium hydroxide. It must also be sequentially repeated for the acid-alkali experiments; therefore, including repeats, the procedure must be duplicated another 12 times.

The process starts with PT-char X pre-treatment, then moves onto the principle demineralisation process, followed by PT-char post-treatment and the ash determination procedure. The control is raw PT-char X. Mass lost on the magnetic bead and in the weigh boat are all taken into account. The extraction temperature, C:L (g/g) ratio, extraction time, and lixiviant concentration are stated in table 27.

PT-char Pre-treatment Procedure

1. Remove residual steel from raw PT- char X sample using a strong magnet, if required.
2. Place raw PT-char X sample in a vacuum oven at 110°C for 24 hours under a nitrogen atmosphere.
3. Proceed to the demineralisation procedure.

PT-char Demineralisation Procedure

1. Set water bath to the desired **extraction temperature** and turn on magnetic stirrer.
2. Weigh and record the magnetic bead and place bead inside clean Schott bottle.
3. Weigh, record and place 100g lixiviant of the required **concentration** in Schott bottle. Ensure lid is tight and bottle sealed.
4. After the water bath has gained thermal equilibrium, place the Schott bottle in the water bath and allow it and the lixiviant to heat up to the desired temperature for 20 minutes. Ensure that the Schott bottle is directly above the magnetic stirrer plate so as to ensure agitation.
5. After heating the lixiviant, measure the required PT-char mass, as per the **C:L ratio (g/g),** and slowly add into the Schott bottle with the hot lixiviant:
   a. Weigh and record the mass of the weigh boat.
   b. Weigh and record mass PT-char X as per the **C:L ratio (g/g)**.
   c. Add PT-char to hot lixiviant in Schott bottle and place back into water bath. Ensure no spilling and lid is tight and bottle sealed. Place Schott bottle is directly above the magnetic stirrer plate in the water bath so as to ensure agitation.
   d. Weigh and record the mass of the weigh boat after adding the PT-char to the lixiviant.
6. Leave the Schott bottle in the heating bath on the magnetic stirrer for the required **extraction time**.
7. Weigh and record three pieces of filter paper and fold each filter paper appropriately so it fits in a glass funnel. Place each glass funnel atop an Erlenmeyer flask.
8. Weigh and record a watch glass.
9. After the extraction time has been completed, turn off the magnetic stirrer and pour the PT-char-lixiviant mixture (Schott bottle contents) onto the three filter paper setups. Allow the lixiviant to filter and separate from the PT-char.
10. Pour the filtered, cool lixiviant back into the Schott bottle so it can collect residual PT-char from the Schott bottle. Pour on to the filter paper.
11. Using distilled water; ensure all the PT-char mass is out the Schott bottle and on the filter paper.

12. Wash loose PT-char off unclean magnetic bead and allow bead to dry. Weigh and record the bead mass once dry.

13. Thoroughly clean the PT-char by allowing distilled water to filter through the PT-char on the filter paper.

14. After the PT-char has been thoroughly cleaned with distilled water, place the three filter papers with now, UPT-char, on the watch glass and proceed to the post-treatment procedure.

PT-char Post-treatment Procedure

1. Place watch glass (with filter paper and UPT-char) into vacuum oven for 24 hours at 110°C under a nitrogen atmosphere.

2. After drying, weigh and record the watch glass, filter paper and UPT-char. Sample the UPT-char.

3. Proceed to the ash determination procedure.

PT-char Ash Determination Procedure

1. Record the mass of a clean, dry ceramic crucible.

2. Measure 1g extracted UPT-char and place it into a clean ceramic crucible.

3. Place crucible and UPT-char into the muffled furnace and set the furnace to heat up to 900°C[43] at a rate of 45°C/min and let the final temperature hold for 40min in the presence of air.

4. Wait for the furnace to cool down to room temperature.

5. Weigh and record the mass of the crucible and ash contents within the crucible from the muffled furnace.

4.4.6. Experimental uncertainty

Numerically proceeding through the experimental methodology described above, there are different sources of error which may alter experimental results.

The heterogeneous nature of PT-char and the analysis of a sample of PT-char and not the entire population introduce random error to the experimental results. This is minimised by utilising the cone and quartering sampling technique [174] and sampling a portion of PT-char which is free from bias and is well represented of the entire particle population in terms of particle size.

The mixing of molar solutions introduces both random and systematic errors. Parallax associated with reading the water meniscus in the measuring cylinder is reduced by reading the volume measurement horizontally, and not at an angle. Observational error, which is the difference between

---

[43] 900°C was determined through trial runs and was necessary due to the crucible shape.

the true measurement and the measurement observed by the reader, is minimised by accurately obeying the measurement marking on the glassware and abiding specific techniques constantly throughout the experimental procedure. The acid mass measurements were measured to the closest 0.001g. Additionally, the molar solutions were well mixed and allowed to cool in a closed container to prevent error associated with concentration gradients and the evaporation of water caused by heat of solution.

Systematic errors associated with instrument calibration and drift were reduced by calibrating each instrument (electronic balance and thermometer) before each set of readings or if ambient temperature alters substantially. Since there was no available standard to calibrate the thermometer and balance, the accuracy of these instruments were checked by comparing them with other instruments of high quality. To prevent displacement of the zero reading of the balance, it was re-zeroed often. Error associated with temperature readings were minimised by allowing the probe to gain equilibrium with the surroundings. The fluctuation in mass measurements were minimised by drying all samples and preventing mass loss through percolation, and by allowing mass measurements to stabilise.

Through preliminary experiments, it was determined that there was only mass lost via the weigh boat and magnetic bead. The error associated with mass loss was minimised by measuring the mass lost and including it in relevant equations and calculations.

Overall personal experimental error was reduced by performing preliminary experiments and practising the required techniques, however, it can never be eliminated.

4.4.7. Relevant screening equations

Table 31:   **Description of Unknowns within Equations 9-14**

Equation Unknown	Description	Position in Procedure
m_{PTchar}	Initial mass of feed PT-char X including mass losses (g)	Demineralisation procedure, step 5
$m_{UPTchar}$	Final mass of UPT-char X after extraction and drying in vacuum oven (g)	Post-treatment procedure, step 2
$m_{extracted}$	Overall mass extracted from PT-char by lixiviant (g)	Result
$\%m_{extracted}$	Percent overall mass extracted from PT-char by lixiviant (wt.%)	Result
$m_{UPTchar\ in\ crucible}$	Mass of UPT-char X in ceramic crucible before muffled furnace (g)	Ash determination procedure, step 2

ma	Mass of ash in crucible after muffled furnace (g)	Post-treatment procedure, step 5
$\%ma_{extracted}$	Percent ash extracted from UPT-char X by lixiviant (wt.%)	Result
$\%ma_{feed}$	Percent ash in feed PT-char X (wt.%)	Result
$m_{difference}$	Difference between the mass extracted from the PT-char and the ash extracted from identical PT-char (g)	Result
CE_{Ash}	Cost effectiveness of an acid based on the wt.% ash extracted from PT-char X	Result
CE_{Mass}	Cost effectiveness of an acid based on the wt.% overall mass extracted from PT-char X	Result
C_{5Macid}	Cost of 5M acid	Result

$$m_{extracted} = m_{PTchar} - m_{UPTchar} \qquad \text{[Equation 9]}$$

$$\%m_{extracted} = 100\left(\frac{m_{extracted}}{m_{PTchar}}\right) \qquad \text{[Equation 10]}$$

$$\%ma_{\text{extracted}} = \%ma_{feed} - \left(100\left(\frac{ma}{m_{UPTchar\ in\ crucible}}\right)\left(\frac{m_{UPTchar}}{m_{PTchar}}\right)\right) \qquad \text{[Equation 11]}$$

$$m_{difference} = \%m_{extracted} - \%ma_{extracted} \qquad \text{[Equation 12]}$$

$$CE_{Ash} = \frac{cost\ factor}{effect\ factor} = \frac{C_{5Macid}}{(\%ma_{feed} - \%ma_{\text{extracted}})} \qquad \text{[Equation 13]}$$

$$CE_{Mass} = \frac{cost\ factor}{effect\ factor} = \frac{C_{5Macid}}{\%m_{extracted}} \qquad \text{[Equation 14]}$$

4.5. Results and discussion of acid-alkali screening

Assumptions

- The mass of dust and other particles which settle on the PT-/ UPT-char have been assumed negligible since special precautions were made to prevent airborne contamination. The adsorption of humidity by PT-char or UPT-char is assumed negligible as they have hydrophobic properties. Washing using deionised water was performed thoroughly so as to assume no extraction products remained within the UPT-char. The feed PT-char X has an ash content of 16.24wt.%.

- It was assumed that the chemicals and demineralised water did not contain contaminants, particularly solids, and the specifications, particularly in terms of purity, were accurately represented by the labelling provided by the supplier. All materials utilised have repeatable characteristics, as described by the relevant suppliers and manufacturers. Filter paper and watch glass mass assumed to stay constant during drying.

- The reaction only occurred between the respective lixiviant and PT-char, since all equipment and materials were chemically inert towards the lixiviants. Extraction by the deionised water has been tested to be negligible since any ash extracted by the water would've already been removed by the relevant lixiviant. It is assumed that no reactions occurred during the drying stages of the methodology.

Demineralisation Screening

Hydrochloric acid, sulphuric acid, nitric acid, hydrogen peroxide, acetic acid and sodium hydroxide partook in individual demineralisation screening, after which the three superior acids then proceeded to acid-alkali sequential extraction. Each experiment was replicated, i.e., run 1 and run 2 represented on figure 15, figure 16 and figure 17, and the error bars represent the standard deviation between each run. Relevant data is listed in appendix K.

Figure 15 below illustrates the total mass extracted (wt.%) by each lixiviant. Hydrochloric acid and nitric acid prove superior in comparison to sulphuric acid, acetic acid and hydrogen peroxide. Although similar, hydrochloric acid extracts, on average, 0.89wt.% more than nitric acid, establishing superiority in terms of total mass extracted from PT-char X. By comparison, sulphuric acid proves to be most inferior as it extracts only 6.61wt.% total mass, while hydrochloric acid extracts almost double this amount (13.84wt.%). Figure 15 shows that sodium hydroxide extracts a more mass than sulphuric acid, acetic acid and hydrogen peroxide, however, not as much as nitric acid or hydrochloric acid. The low standard deviations show that the experiments are repeatable. Thus far, it can be seen that hydrochloric acid and nitric acid are most efficient in extracting mass from PT-char X, where as sulphuric acid, acetic acid and hydrogen peroxide extract much less mass.
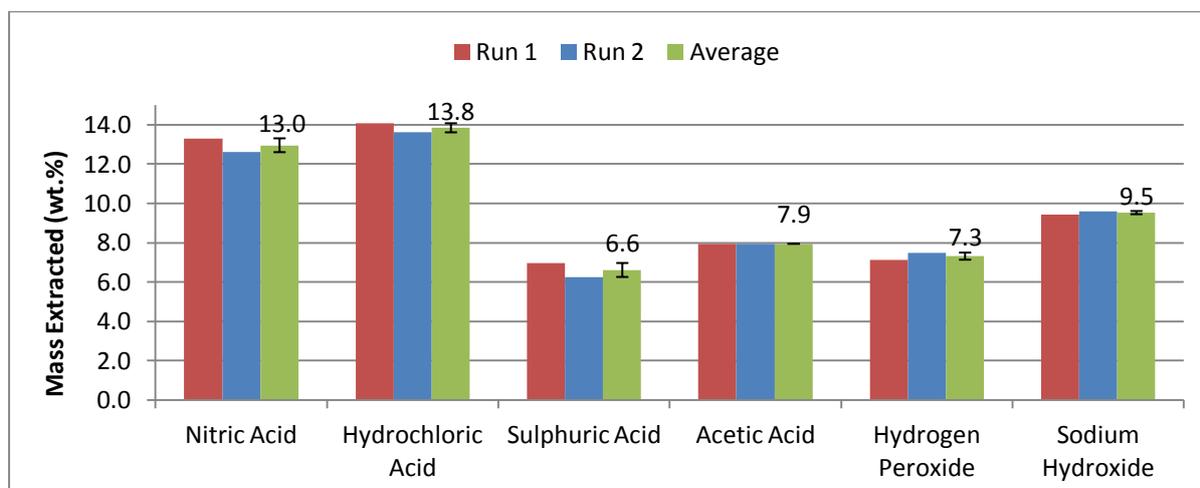
Figure 15: **Total Mass Extracted from PT-char by Respective Lixiviants**

Figure 16 below illustrates the ash extracted (wt.%) from PT-char by each lixiviant, with relevant data is listed in appendix K. The objective is to decrease the ash content within PT-char in order to meet the benchmark requirements of carbon black (1.95wt.%). Nitric acid, hydrochloric acid and sulphuric acid extract the most ash, with average quantity ash extracted being 11.2wt.%, 11.4wt.% and 10.9wt.% respectively. Acetic acid and hydrogen peroxide remove similar, but low quantities of ash, i.e. 7.4wt.% and 7.2wt.% respectively. The low standard deviations show that the experiments are repeatable. In summation, hydrochloric acid is the strongest and hydrogen peroxide is the weakest acidic lixiviant in terms of ash removal.
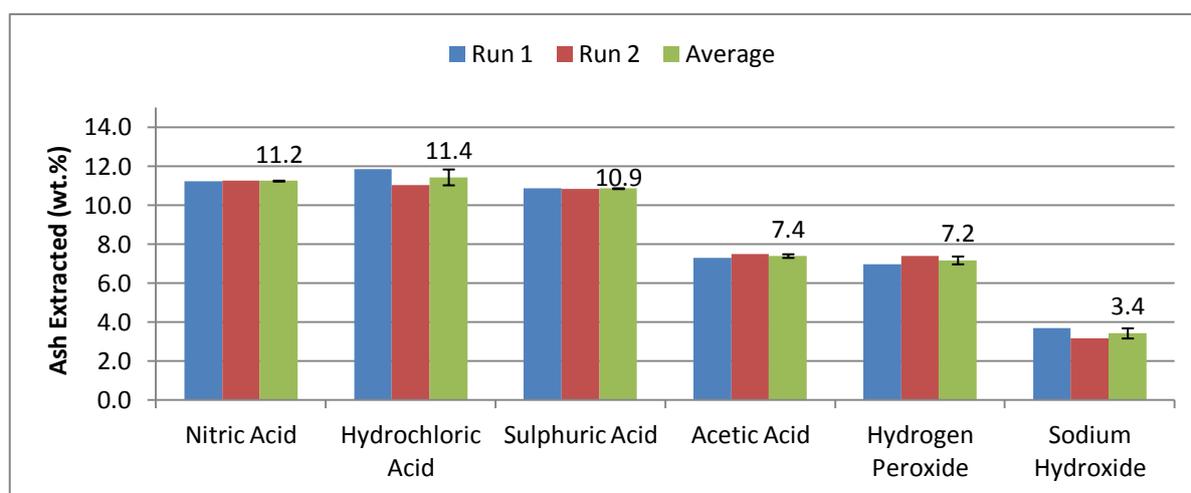
Figure 16:   **Total Ash Extracted from PT-char by Respective Lixiviants**

Overall, hydrochloric acid, nitric acid and sulphuric acid extracts the most ash from PT-char X as they are strong acids and harbour K_a values of 1.3E+6, 2.4E+1 and 1.0E+3 respectively (as illustrated in table 12figure 6). Since hydrochloric acid has the largest K_a value of the three acids, it is comprehensible that it extracts the most ash of all the screened acids. It dissociates more readily than the other acids, thus producing the greatest magnitude of H^+ ions to react with the metals within PT-char X. Sulphuric acid and nitric acid extract similar ash masses, although nitric acid extracts more overall mass compared to sulphuric acid[44]. When sulphuric acid decomposes, H^+ and HSO_4^- are formed, while nitric acid dissociates to form H^+ and NO_3^-. When comparing these two acids sulphuric acid has a higher K_a value than nitric acid indicating that sulphuric acid readily releases more H^+ ions which are able to reduce more metals within PT-char. However, oxidizing agents HSO_4^-, SO_4^{2-} and NO_3- are also present in their respective aqueous acidic solutions. The standard electrode potential of HSO_4^-, SO_4^{2-} and NO_3- are 0.17V, 0.1576V and 0.9275V respectively, thus showing NO_3- is able to react and oxidize with many more ions in comparison HSO_4^- and SO_4^{2-}. The combined effect

---

[44] This conclusion considers the false sulphuric acid mass reading caused by the uptake of surrounding water, as discussed subsequently.

of the H^+ ion and the NO_3^- oxidizing agent from nitric acid extracts much more mass from PT-char X in comparison to the combined effect of the dissociated ions of sulphuric acid.

The low dissociation levels of acetic acid and hydrogen peroxide render them poor PT-char extraction lixiviants, with K_a values of 1.75E-5 and 2.4E-12 respectively. Although hydrogen peroxide is a very strong oxidizing agent (1.776V) and contains a particularly unstable peroxide bond within its structure, it extracts only a small portion of ash from PT-char. This may be due to its very slow decomposition rate (low K_a) which is accentuated by the cool, acidic conditions at which extraction occurs. However, certain compounds, especially transition metals, tend to catalyse decomposition. Sodium hydroxide is only able to extract a small portion of ash due to its largely basic properties, as discussed in detail below.

The difference between total mass extracted, as shown in figure 15, and the total ash extracted, as illustrated in figure 16, is analysed further in table 32. If the total mass extracted is greater than the ash extracted, an alternative compound ('non-ash'), in addition to the ash, is removed by the lixiviant. It is clear, from table 32 below, that the acids are able to remove a mass portion from PT-char X which is not ash. Hydrochloric acid shows to have removed the largest portion of 'non-ash' (2.40wt.%, on average) from PT-char X, while hydrogen peroxide removes the least amount of 'non-ash' (0.14wt.%, on average). One large inequality observable is that sulphuric acid extracts more ash than overall mass, as represented by a negative difference in table 32. This negative value is equivalent to a false increase in the total UPT-char mass[45] caused by the uptake of humidity by sulphuric acid remnants on the filter paper, since sulphuric acid is intensely dehydrating [175]. Additionally, this increase in mass cannot be connected to a solubility phenomenon since sulphates are soluble, as discussed in table 13.

Table 32:   Comparison of Extracted Mass and Extracted Ash Quantities of Screened Lixiviants

	Unit	Mass Extracted from PT-char (wt.%)	Ash Extracted from PT-char (wt.%)	Difference between mass and ash extracted
Nitric Acid	wt.%	12.955	11.241	1.714
Hydrochloric Acid	wt.%	13.842	11.431	2.411
Sulphuric Acid	wt.%	6.610	10.853	-4.243
Acetic Acid	wt.%	7.947	7.396	0.551
Hydrogen Peroxide	wt.%	7.314	7.174	0.141

The 'non-ash' component is interrogated further by analysing the sulphur content within the extracted chars. Nitric acid, hydrochloric acid, sulphuric acid and acetic acid are excellently

---

[45] As described by $m_{UPTchar}$ in Table 31

compatible[46] with carbon [176], which is the reason the selection of sulphur analysis[47]. Conversely however, hydrogen peroxide is moderately[48] compatible with carbon [176] and, although slow, corrosion does occur. Having said this, Bunthid et al. [38] made use of PT-char incorporated with hydrogen peroxide to successfully remove sulphur from the naphtha fraction of TDO, thus showing it readily reacts with sulphur rather than carbon. Table 33 below illustrates the SEM-EDX sulphur analyses of the PT-chars extracted by each acid[49]. It is observed that PT-char X which had been extracted by HCl and by H_2O_2 contained the lowest sulphur content, with 0.86wt.% and 0.77wt.% respectively. This is in agreement with HCl results since HCl has extracted a large portion of mass from PT-char X which is not ash; however, H_2O_2 only removes a small portion of mass which is not ash, thus showing that certain ash components may be in their chloride form. The sulphur within the HNO_3 and CH_3COOH extracted PT-char makes up a larger mass portion in comparison to the feed PT-char. This shows that the respective acids did not extract enough sulphur so as to decrease the sulphur mass percent. However, if HNO_3 and CH_3COOH were to extract no sulphur, the sulphur contents within their extracted PT-chars would be 2.187wt.% and 2.099wt.% respectively. Since the PT-char extracted by HNO_3 has lower sulphur content than 2.187wt.%, HNO_3 extracted a portion of sulphur; however, using the same argument, it cannot be concluded that CH_3COOH extracted sulphur.

Table 33:   **SEM-EDX Sulphur Analyses of PT-char X Extracted by Screened Acids**

	Unit	Sulphur	Standard Deviation
Feed PT-char X	wt.%	1.983	0.328
Nitric Acid	wt.%	2.009	0.864
Hydrochloric Acid	wt.%	0.860	0.089
Sulphuric Acid	wt.%	1.059	0.120
Acetic Acid	wt.%	2.090	0.153
Hydrogen Peroxide	wt.%	0.770	0.087

The three outperforming acids, namely hydrochloric acid, nitric acid and sulphuric acid, proceeded further to sequential acid-alkali demineralisation, where PT-char encountered acid extraction followed by NaOH extraction. A larger error accompanies sequential extraction experiments in

---

[46] Excellently compatible implies there is virtually no effect, with a low corrosion rate of less than 0.05mm per annum [176]

[47] This is comprehensible since any volatiles within PT-char are significantly removed by the vacuum oven during the pre- and post-treatment stages of the methodology.

[48] Moderately compatible implies softening, weakening or swelling may occur with a corrosion rate between 0.5mm and 1.3mm per annum [176]

[49] Sulphur removal by NaOH explored further in section 5.6

comparison to single extraction experiments as the chance for error doubles with two lixiviant washes.

Figure 17 show that sequential extraction using hydrochloric acid surpasses nitric acid and sulphuric acid. This is in accordance to the results described by figure 15 and figure 16, and can be ascribed to the same reasons stated above.
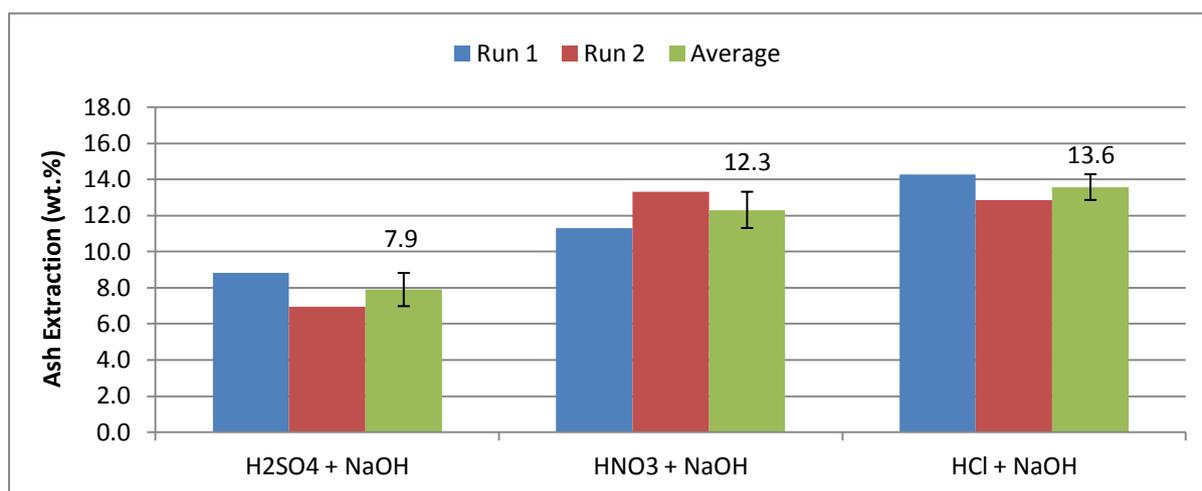
Figure 17:   **Total Ash Extracted by Sequential Acid-alkali Extraction**

Table 34 shows a comparison between the results from single extraction versus sequential extraction in terms of ash content within UPT-char. Although the single extraction experiments use different conditions to the sequential extraction, the fact that sequential extraction withdraws more ash at less severe conditions in comparison to single extraction, shows competitiveness between the conditions and allows for the examination of comparative conclusions.

Acid-alkali sequential extraction removes more ash when hydrochloric acid and nitric acid are used compared to single extraction using the same acids. This increase can be explained by analysing the presence of oxides within the ash composition and their amphoteric properties. There are two oxides which are added to a tyre during manufacturing, namely zinc oxide (ZnO) and silicon dioxide. With regards to SiO_2 in particular, the electronegativity between the atoms is very strong, causing stable covalent bonds rather than ionic bonds [144]. Due to the absence of ionic bonds, SiO_2 does not dissociate and is, thus unable to react with the H^+ ion of a dissociated acid. SiO_2 is weakly acidic and only able to react with a strong alkali such as sodium hydroxide or the fluoride ion of HF [144]. The hot, concentrated sodium hydroxide utilized for the sequential extractions provides enough energy to break the silicon and the oxygen bond to form sodium silicon dioxidete, generally expressed by the formula of $mNa_2O.nSiO_2$ [140]. The dissociation of sodium silicon dioxidete in

water is very complex and depends on the type of sodium silicon dioxidete present (Na_2SiO_3[50] versus Na_4SiO_4[51] versus $Na_2Si_2O_5$[52]). In general, Na_2SiO_3 and Na_4SiO_4 dissociate in water via a hydrolyzation reaction [140].

Table 34 shows the amount of ash extracted by sodium hydroxide during sequential extraction, calculated by means of difference. The observable trend shows that the more ash the acid is able to remove, the more ash sodium hydroxide removes. Refer to section 5.6 for further discussions regarding sequential extraction.

In conclusion, an acid-alkali wash consisting of hydrochloric acid and sodium hydroxide is a viable option for the reduction of ash within PT-char.

Table 34: **Comparison between Ash Contents within UPT-char by Single Extraction and Sequential Extraction**

	Ash Extracted from PT-char (wt.%) - Single Extraction	Ash Extracted from PT-char (wt.%) - Sequential Extraction	Ash Content (wt.%) extracted by NaOH during Sequential Extraction
Hydrochloric Acid	11.431	13.562	2.131
Nitric Acid	11.241	12.301	1.060
Sulphuric Acid	10.853	7.889	-2.964
Sodium Hydroxide	3.431	-	-

Economic Screening

The economic screening aimed at analysing the cost effectiveness of hydrochloric acid, sulphuric acid, nitric acid, hydrogen peroxide, acetic acid and sodium hydroxide. Since the effectiveness of the acid is described by both ash extraction and overall mass extracted during the demineralisation screening trial, both these outcomes will be used for separate CEAs.

Figure 18 below compares the lowest relative cost of each acid at a concentration of 5M. In comparison, it is clear that hydrochloric acid is the cheapest, while acetic acid is significantly more costly. The relatively high costs of nitric acid, hydrogen peroxide and acetic acid decrease their economic viability substantially. It is also clear that sodium hydroxide is cheaper in comparison to the screened acids. It must be reiterated that the price of a 5M acid concentration is used for consistency and comparison purposes alone.

---

[50] Metasilicon dioxidete
[51] Orthosilicon dioxidete
[52] Dimetasilicon dioxidete
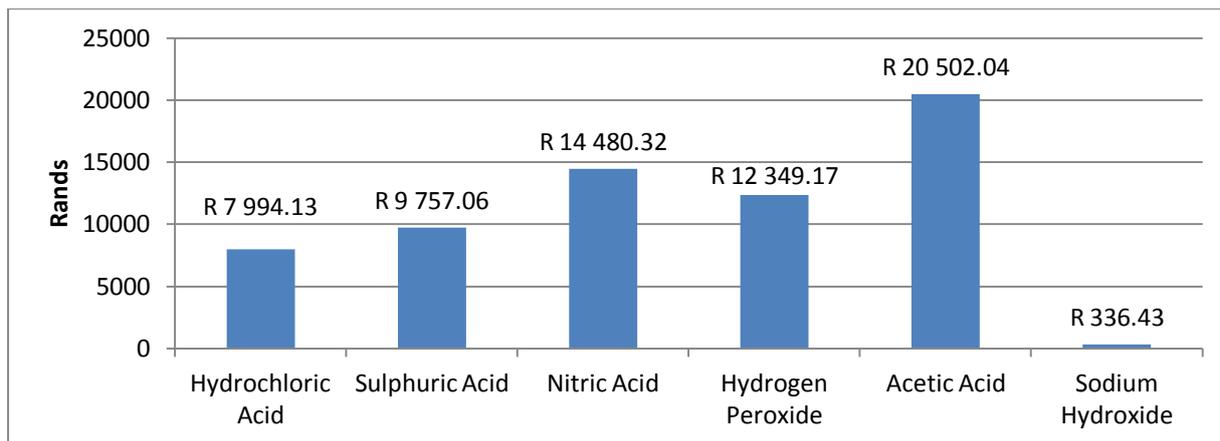
Figure 18: Relative Cost of 10t Raw Lixiviant required to extract 1t PT-Char as per Demineralisation Screening Process Factors

Figure 19 illustrates the cost effectiveness ratio of each acid, using the wt.% ash removed by the acid during the demineralisation screening trials as the effect factor. In this instance, the most cost effective acid, which is represented by the lowest CE ratio, is hydrochloric acid. The least cost effective acid is acetic acid. This is in agreement with previous results since acetic acid does not extract as much ash as hydrochloric acid and it is more expensive than the other screened acids. Although hydrogen peroxide extracts less ash in comparison to acetic acid, it is still more cost effective to use it rather than acetic acid since it is much cheaper. Sodium hydroxide is the most cost effective as it is inexpensive and able to extract ash from PT-char X at the given conditions.
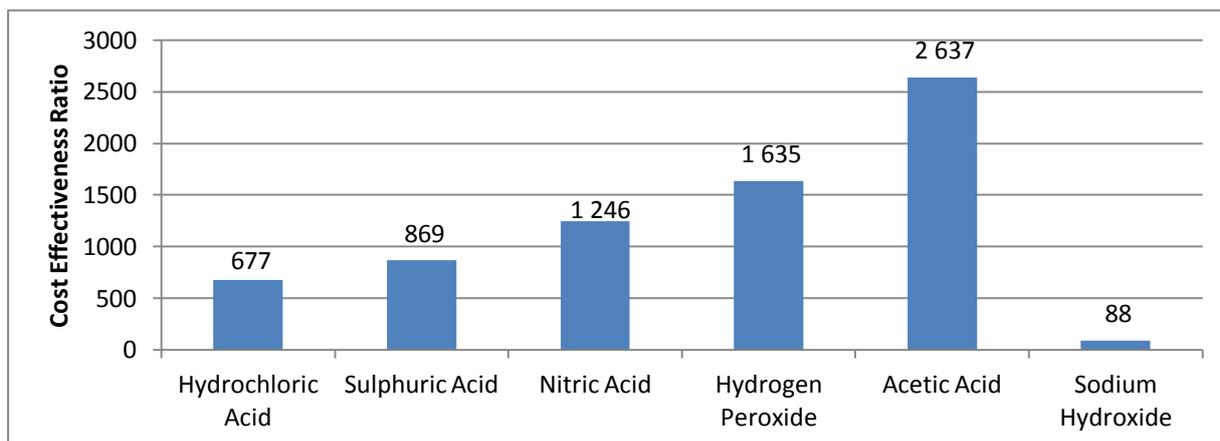
Figure 19: Cost Effectiveness Ratio of Screened Lixiviants based on Total Ash Extraction (wt.%)

Figure 20 below depicts the cost effectiveness ratio of each acid using the wt.% total mass removed by the acid during demineralisation screening trials as the effect factor. In this case, as with figure 19, hydrochloric acid is the most cost effective acid, and acetic acid is the least cost effective acid. It is clear that, when using ash extraction as the effect factor, the acids are less cost effective than

when using overall mass extraction as the effect factor. This is due to the fact that the overall mass extracted accounts for the entire impurity content removed by the acid, whereas ash extracted is only a portion of impurities extracted by the acid. Additionally, nitric acid extracts more impurities in total compared to sulphuric acid, which is why it is more cost effective to use if the outcome is based on the overall mass extracted. Conversely, if the outcome is based on ash extracted, sulphuric acid is more cost effective than nitric acid. However, due to the dehydration properties of sulphuric acid, the overall mass extracted by sulphuric acid showed to be less than the ash extracted, as discussed in table 32. This has an impact on the CEA, in particular when comparing cost effectiveness of nitric acid and sulphuric acid. Assuming that, as a lower limit, sulphuric acid is only able to extract ash from PT-char. Equating the wt.% ash extracted by sulphuric acid to its overall wt.% mass extracted, sulphuric acid will be more cost effective than nitric acid. Sodium hydroxide is more cost effective compared to acetic acid since it is cheaper.

Based on this CEA, hydrochloric is the most cost effective acid in comparison to the others independent of whether ash extracted or overall mass extracted was used as the outcome. On the contrary, acetic acid showed to be the least cost effective due to its high cost as an acid.
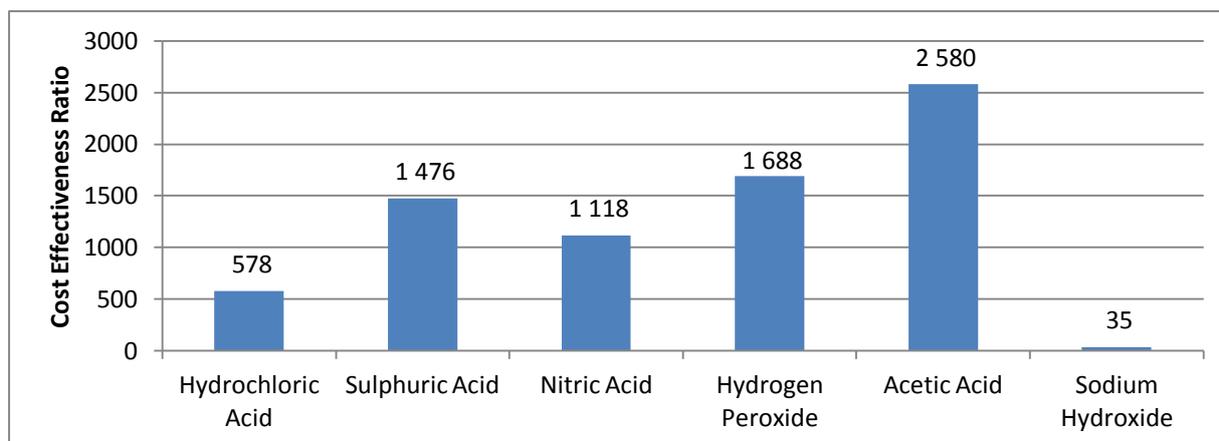
Figure 20:   **Cost Effectiveness Ratio of Screened Lixiviants based on Total Mass Extracted (wt.%)**

Overall Performance Analysis of Screened Acids

There were four principle screening assessments which the acids participated in: total mass extracted from PT-char X, total ash extracted from PT-char X, CE ratio based on ash extraction, and CE ratio based on mass extraction. Sequential extraction was performed to assess the viability of an acid-alkali demineralisation process. In order to analyse the overall performance of each acid, they were rated on a scale from 1-5 for each screening assessment. A rating of five was awarded to the most superior acid within each assessment, with the rating decreasing to 1 as performance

deteriorated. A grand total of 20 can be achieved if the acid is unsurpassed in all screening assessments.

Table 35 shows the performance rating of each acid which participated in the four assessments of the screening procedure. Hydrochloric acid outperformed all the other acids during each screening trial, while acetic acid and hydrogen peroxide underperformed significantly. Nitric acid outperformed sulphuric acid; however, this result may be contradictory due to the uptake of moisture by sulphuric acid producing a false result for total mass extracted from PT-char. The comparison between demineralisation effectiveness of sulphuric acid and nitric acid would have to be studied further for concrete conclusions; however, since HCl outperformed both nitric acid and sulphuric acid in all screening assessments, this would be a futile endeavour, although a possible recommendation for future research.

Table 35:   **Performance Rating of Acids based on Screening Trials (5=best, 1=worst)**

	Total Mass Extracted from PT-char (wt.%)	Ash Extracted from PT-char (wt.%)	CE Ratio (Ash)	CE Ratio (mass)	TOTAL
Hydrochloric Acid	5	5	5	5	20
Sulphuric Acid	1	3	4	3	11
Nitric Acid	4	4	3	4	15
Hydrogen Peroxide	2	1	2	2	7
Acetic Acid	3	2	1	1	7

4.6.   Conclusions and recommendations of acid-alkali screening

The key objective of this study was to evaluate factors which affect the process, lixiviants in particular. Based on literature, sulphuric acid, hydrochloric acid, nitric acid, hydrogen peroxide, acetic acid sodium hydroxide partook in the screening analysis. Two forms of screening were completed namely, demineralisation screening and economic screening.

The demineralisation screening consisted of single lixiviant leaching and sequential acid-base leaching. It was found that HCl removed the most overall mass and the most ash in comparison to the other acids, with 13.8wt.% and 11.4wt.% extraction respectively. H_2O_2, however, showed the worst extraction capacity, with the overall mass and ash extraction efficiencies of only 7.3wt.% and 7.2wt.% respectively. In terms of sulphur extraction, hydrochloric acid and hydrogen peroxide extracted the most sulphur, with extracted PT-chars containing 0.86wt.% and 0.77wt.% sulphur respectively. While nitric acid removed the least sulphur and acetic acid removed no sulphur. HCl-NaOH sequential extraction proved to be superior, with 13.6wt.% ash extraction.

The economic screening analysed the cost effectiveness of each acid by combining their relative ash extraction capacity and their raw material costs. It was found that HCl was the cheapest and, since it proved to have the greatest extraction capacity, it is the most cost effective acid to use for PT-char acid-alkali demineralisation. Hydrogen peroxide and acetic acid proved to be the worst, while sulphuric acid and nitric acid are highly competitive. Sodium hydroxide proved to be greatly cost effective.

Overall, it is clear that HCl is the most cost effective acid to utilise for PT-char acid-alkali demineralisation since it was able to extract more overall mass and ash compared to H_2SO_4, HNO_3, H_2O_2 and CH_3COOH and is the cheapest raw material. It will, therefore, partake further in process and product development, alongside sodium hydroxide.

Chapter 5: Upgrading Pyrolytic Tyre Char using Acid-alkali Leaching: Process and Product Development

5.1. Process and product development: study overview and description

Developing a new chemical process requires in-depth knowledge of the influence a particular variable has on the process and product characteristics. This is required to obtain the most favourable process operating conditions.

Previous chapters have established that the conversion of crude PT-char to carbon black through demineralisation by acid-alkali extraction is a promising technique for increasing the value of PT-char. In order to upgrade PT-char X to CB N330, the ash content of PT-char X must be reduced by 14.29wt.%, the surface area must increase from $58.9m^2.g^{-1}$ to $80.22m^2.g^{-1}$, the sulphur content must be reduced from 1.98wt.% to 1.80wt.%, and the average particle size must be reduced from 153.2-38.5μm. Screening trials have proved that hydrochloric acid and sodium hydroxide are the most cost effective lixiviants to use for acid-alkali demineralisation. Utilising this information, the next research phase is development of an acid-alkali demineralisation process which is able to produce a UPT-char product with characteristics comparable to that of CB N330.

The first obstacle is to establish if carbon black of acceptable[53] characteristics can be created from PT-char. The influence of process variables on ash extraction, particularly the limits of variable influence, will be performed using kinetics. This particular kinetic study will examine and compare lixiviant type (HCl and NaOH), lixiviant concentration and extraction temperature over a time intervals of 5, 10, 20, 60 and 100 minutes. After establishing the most desirable process variable conditions and the boundary conditions, further sequential-extraction experiments will be conducted so as to establish if, and, at which variable conditions carbon black of acceptable properties can be produced from PT-char.

---

[53] Acceptable in that the properties of upgraded PT-char are similar to those of carbon black.

5.2.   Process and product development: study substantiation

A kinetic study will be performed using the preferred lixiviants (HCl and NaOH) to address the shortcomings of published literature and provide technical information for industrial process design.

5.3.   Process and product development: study objective ii.a. and ii.b.

To develop and propose a process for crude pyrolytic tyre char upgrading by evaluating factors which affect the pyrolytic tyre char upgrading process and producing a value-added product with suitable characteristics from crude pyrolytic tyre char.

5.4.   Process and product development: a brief literature review

As of date, no kinetic studies have been published with regards to PT-char acid-alkali leaching using HCl and NaOH. However, kinetic studies have been performed on the leaching of coal, ores and spent catalysts using HCl and/or NaOH. Due to the differences between PT-char and coal, ore and spent catalysts properties, such as matrix and composition, the leaching efficiency cannot be compared, but the leaching kinetic behaviour may be comparable.

When using HCl to leach ores and spent catalysts, it has been agreed upon that increasing temperature and concentration increases the percent metal leached; and, after a certain period of time, the leaching curves reach a plateau and the process has reached equilibrium [177][178][179]. Additionally, according to Cui et al. [177], an increase in HCl concentration will allow for the reduction in extraction time while still producing the similar results.

NaOH has been successfully used to demineralise PT-char in an acid-alkali sequential extraction procedure. Chaala et al. [116], who performed this demineralisation process, found the optimal extraction conditions to be 5M NaOH at a temperature of 60°C, extracting for 30min using 10mL NaOH per gram PT-char, as discussed in section 2.6.5. NaOH has also been used to successfully extract silicon and silicon dioxide from coal and fly ash [180][181]. In agreement, the authors stated that NaOH concentration and extraction temperature was directly proportional to ash removal.

Impurity content, surface area and particle size are important factors considered for carbon black usage as reinforcing filler within a tyre. According to Woolard [18], a reinforcing filler is required to have an active surface with a surface area greater than $60m^2/g$, and a particle size less than 50μm.

5.5. Process and product development methodology

5.5.1. Methodology overview

The analysis progression is shown in figure 21. The kinetic experimental procedure consisted of four independent variables: lixiviant type (HCl and NaOH); extraction time; lixiviant concentration; and extraction temperature. The relevant treatment conditions are depicted in table 36 for time periods of 5, 10, 20, 60, 100minutes. The constant variables include PT-char type (PT-char X), atmospheric pressure; solid-lixiviant mixture agitation speed; C:L mass ratio (20:100 g/g); and PT-char particle size. The dependent variables analysed included total mass extracted and ash content within UPT-char, which was translated to percent ash extracted. The baseline and benchmark conditions are the properties of PT-char X and CB N330 respectively. The experimental methodology used was similar to that used for the demineralisation screening procedure, as stated in section 4.4.5., however; differing in the variable values and analysis progression.

Extraction Time Determination:	Extraction Temperature Determination:	Lixiviant Concentration Determination:	Attaining Benchmark Requirements:
Kinetic influence of temperature and concentration reveals optimal extraction time.	Influence of temperature on ash extraction from PT-char at optimal extraction time reveals optimal extraction temperture.	Using the determined optimal extraction time and temperature, the optimal lixiviant concentration was determined using both kinetics and sequential extraction results	Using the determined lixiviant concentration, extraction time and temperature, PT-char was upgraded to UPT-char with CB properties using sequential extration.

Figure 21:   Logical Progression of PT-char Variable Analysis

Table 36:   Variables used for kinetic analysis of PT-char acid-alkali leaching

	Lixiviant Concentration	Extraction Temperature
HCl	0.01M 0.1M 0.5M	60°C
	0.1M	20°C 40°C 60°C
NaOH	1M 3M 4M	60°C
	3M	30°C 60°C 80°C

5.5.2. Methodology substantiation

A kinetic study was chosen as it allows for the simultaneous comparison of the effect of two variables, of which one is time. It is able to reveal additional information about the chemical system, such as rate controlling mechanisms, the point at which chemical equilibrium is reached and yield attainment.

The same methodological substantiation, as discussed in section 4.4.2, holds. The variable values, however, differ since this kinetic study aims at analysing the effect of the variables rather than the effectiveness of the lixiviants. The constant, independent and dependent variables were chosen chiefly according to literature. The C:L ratio is kept at 20:100 (g/g) so as to increase throughput. According to Chaala et al. [116], ash extraction reached a plateau after 10ml/g.

Three values of concentration and temperature were analysed to improve external validity and to strengthen conclusions. These three values were selected according to literature. The centre point values were chosen according to literature and experimentation.

Chaala et al. [116] found PT-char demineralisation to be most favourable when utilizing a concentration of 0.5M H_2SO_4. Cui et al. [177] examined the kinetics of coal demineralisation using HCl concentrations ranging from 3-6mol/L. Olanipekun [179], studied the kinetics of ilmenite ore demineralisation using 7.2 – 9.6M HCl concentrations. Since coal and ore consist of a much denser and harder matrix than PT-char, a high HCl concentration may not be necessary. Additionally, a concentration of 0.5M H_2SO_4 was sufficient for PT-char demineralisation. Therefore, as a starting point, HCl concentrations of 0.1M, 0.5M and 1.0M were chosen for the kinetic trials.

Chaala et al. [116] tested NaOH concentrations ranging from 1M-10M and found PT-char demineralisation to be most favourable when utilizing a concentration of 5M NaOH a prior an H_2SO_4 wash. Similarly, Yang et al. [180] demineralised coal using 1-6.1M (4-20wt.%) NaOH. As a starting point, NaOH concentrations of 1M, 3M and 4M were elected for the concentration kinetic experiments, especially since HCl is stronger than the H_2SO_4 used by Chaala et al. [116].

Chaala et al. [116] used temperatures of 20°C, 40°C and 60°C for demineralisation of PT-char, and found 60°C to be optimum for both HCl and NaOH. Cui et al. [177], tested coal extraction using HCl at temperatures ranging from 40°C-106°C. They noted that inert layers may surround the particle at temperatures above 90°C, preventing HCl from reaching the reactive zones of the coal particle. Similarly, Olanipekun [179] tested ilmenite ore extraction at temperatures varying from 70-90°C and noted that temperatures higher than 90°C were unsuitable as HCl corrosion rates escalated and loss of HCl vapour was high. Using the same rationale discussed above regarding HCl concentration, the extraction behaviour of HCl at 20°C, 40°C and 60°C were analysed.

Yang et al. [180] removed SiO_2 from coal using 2.7M NaOH at temperatures ranging from 150-210°C and achieved an ash content less than 0.3wt.%. Wang et al. [181], tested NaOH extraction at temperatures of 25-99°C and found 90°C to be optimum when analysing the leaching rate of SiO_2 from fly ash. Since Chaala et al. [116] and Wang et al. [181] found 60°C and 90°C to be sufficient in extracting ash from PT-char and fly ash respectively; and an ash content lower than 1.9wt.% is unnecessary as that is the benchmark for CB N330 (table 18), the extraction behaviour of NaOH at 30°C, 60°C and 88°C will be analysed.

5.5.1. Chemicals, materials and equipment required for PT-char acid-alkali leaching kinetics

Table 37:   **Description of chemicals required for kinetic trials**

Chemical Description	Quantity
PT-char X	3600g
Nitrogen gas	1 bottle
Distilled water	40L
Hydrochloric acid, 0.1M	7000g
Hydrochloric acid, 1.0M	1000g
Hydrochloric acid, 3.0M	1000g
Sodium hydroxide, 1M	1000g
Sodium hydroxide, 3M	7000g
Sodium hydroxide, 4M	1000g

Table 38:   **Description of materials and glassware required for kinetic trials[54]**

Material/ Glassware Description	Quantity
Measuring cylinder, 250mL	1
Beaker, 2L (for mixing lixiviant concentrations)	1
Weigh boat, large	180
Lab spoon spatula	1
Chemical grade Schott bottle with PP[55] lid, 250mL	10
Filter paper, 150mm diameter, 11µm	540
Glass funnel, short stem	30
Erlenmeyer Flask	30
Plastic wash bottle	1
Watch glass (200mm diameter)	10
Centrifuge sample bottles, 15mL	360
Ceramic crucibles	20

---

[54] Schott bottles, glass funnels, Erlenmeyer flasks, watch glasses and ceramic crucibles to be reused for each experiment – 10plate magnetic stirrer enables 10 experiments to be performed simultaneously.
[55] Polypropylene

Table 39:   **Description of equipment required for kinetic trials[56]**

Equipment Description	Quantity
Magnet	1
Vacuum oven	1
Balance, 4 decimal, 250g maximum	1
Oil bath with lid	1
Magnetic stirrer	1
Magnetic bead	10
Thermometer, 250°C	1
Muffled furnace	1

5.5.2. Experimental apparatus

Refer to section 4.4.4 for the experimental apparatus required for PT-char kinetic trials.

5.5.3. Experimental procedure

The relevant treatment conditions are depicted in table 36 for time periods of 5, 10, 20, 60 and 100minutes. Including repeats, a total of 90 kinetic experiments for each HCl and NaOH performed, therefore the pre-treatment, demineralisation, post-treatment and ash determination procedures must each be repeated 180 times in total.

PT-char Pre-treatment Procedure

Refer to section 4.4.5 for PT-char pre-treatment procedure.

PT-char Demineralisation Procedure

The PT-char demineralisation procedure described to section 4.4.5 is similar to the procedure used for the kinetic trials, however, a few differences must be noted. Firstly, in section 4.4.5, the water bath must be set at the temperatures described in table 36, as stated in step 1. The PT-char used in step 6 and 6b must be increased to 20g. The extraction time described in step 10 will be 5, 10, 20, 60 and 100minutes, and not 24hr. The concentrations used for the kinetic demineralisation procedure alter according to table 36 and not 5M lixiviant as described in section 4.4.5.

PT-char Post-treatment Procedure

The same post-treatment procedure as described in section 4.4.5 is used for the kinetic experiments. For the sequential experiments, however, the entire acid-alkali extraction sequence must be

---

[56] Schott bottles, glass funnels, Erlenmeyer flasks, watch glasses and ceramic crucibles to be reused for each experiment – 10plate magnetic stirrer enables 10 experiments to be performed simultaneously.

completed before proceeding to the ash determination methodology. An amended post-treatment procedure for sequential extraction is described below.

1. Place watch glass (with filter paper and PT-char) into vacuum oven for 24 hours at 110°C under a nitrogen atmosphere.
2. After drying, weigh and record the watch glass, filter paper and UPT-char.

If the sequential extraction has not been completed, proceed to step 3 below. If the sequential extraction has been completed, proceed to step 5 below.

3. Carefully scrape the PT-char from the filter paper into the weigh boat and proceed to step 5.a of the demineralisation procedure for the next extraction step of the sequential extraction. After scraping all the PT-char off the filter paper, weigh the watch glass and used filter paper.
4. Proceed to the ash determination procedure.

PT-char Ash Determination Procedure

Refer to section 4.4.5 for PT-char ash determination procedure.

5.5.4. Experimental uncertainty

The uncertainties associated with the experiments conducted within this section are similar to the errors indentified in section 4.4.6, with regards to acid-alkali screening, since similar experimental methodologies are used. However, additional experimental uncertainties are associated with kinetic trials and sequential extractions.

The kinetic experiments conducted within this study are predominantly based on extraction time. It must be noted, however, that the stated extraction times do not include filtration time. Since the filtration time for the lixiviants are less than 1 minute, the exclusion of filtration time does not significantly impact the extraction efficiency. Additionally, the lixiviants cool down quickly during filtration, further reducing any extraction that occurs.

Sequential extractions have increased associated uncertainties since multiple extractions are performed on a single PT-char sample. As previously stated, analysing small sampled quantities rather than the entire population has associated inaccuracies. Additionally, mass lost caused by sample transferral from filter paper to the sequential extraction may cause inaccuracies. However, experimental repeats and accounting for mass lost on the filter paper and watch glass during calculations reduces error. All samples were sampled according to the cone and quartering technique.

5.5.5. Relevant equations

The dependent variable analysed in this kinetic study include the mass extracted from PT-char, and the ash content within the final UPT-char. The equations relevant to calculating this ash content are identical to those demonstrated in section 4.4.7, specifically equations 9-12.

Table 40:   **Description of Unknowns within Equations 15-21**

Equation Unknown	Description	Position in Procedure
X	Fraction ash extracted	Result
t	Time	-
k_r	Interfacial chemical reaction rate coefficient	Result
k_f	Film diffusion rate coefficient	Result
k_a	Ash/ product layer diffusion rate coefficient	Result
k_p	Liquid phase pore diffusion rate coefficient	Result
R	R coefficient	Result

$$X = \frac{\%ma_{\text{extracted}}}{100}$$ [Equation 15]

$$k_r t = 1 - \frac{2}{3}X - (1-X)^{\frac{2}{3}}$$ [Equation 16]

$$k_f t = X$$ [Equation 17]

$$k_a t = 1 - (1-X)^{\frac{1}{3}}$$ [Equation 18]

$$k_p t = 1 - (1-X)^{\frac{2}{3}}$$ [Equation 19]

$$R = \frac{\sum(x-\bar{x})(y-\bar{y})}{\sqrt{\sum(x-\bar{x})^2 \sum(y-\bar{y})^2}}$$ [Equation 20]

$$E_a = -R\left[\frac{\partial \ln k}{\partial\left(\frac{1}{T}\right)}\right]_P$$ [Equation 21]

5.6.   Results and discussion of process and product development

Assumptions

The same assumptions described in sections chapter 4.5 are relevant within this section. During the kinetic experiments, filtration time was not included in the time taken for the lixiviant to extraction PT-char (i.e., extraction time) as it was very fast. It is also assumed that the characteristics of CB

N330 previously analysed are constant throughput industry. Finally, the employment of shrinking core models requires the assumption that all particles are spherical.

Hydrochloric Acid Kinetic Behaviour

Figure 22 and figure 23 illustrate the kinetic effect of HCl concentration and extraction temperature respectively. Three kinetic behavioural responses are observable, namely: the rate of ash extraction from PT-char; the point at which equilibrium has been reached; and the quantity of ash extracted from PT-char.

The rate of ash extraction, as depicted by the gradient in figure 22 and figure 23, is very fast from 0-5 minutes, slowing down dramatically after 10minutes. Furthermore, figure 22 shows that increasing HCl concentration from 0.1-1.0M increases the mass quantity of ash removed from PT-char X by 11.3% from 0-5 minutes more than an increasing in HCl extraction temperature from 20-60°C, which removes 4.9% ash. There is no significant impact on rate after 10 minutes for both HCl concentration and HCl extraction temperature, as depicted by similar slopes. These trends are in agreement with metal leaching of ores [182]–[184]. Additionally, Ho et al. [185], discussed the fast extraction rates to be attributed to the driving force of fresh lixiviant promoting the leachant to preferentially move to the lixiviant phase of the system if reaction conditions are favourable.

Chemical equilibrium is attained at approximately 10minutes in both systems, as illustrated by the formation of a plateau in figure 22 and figure 23. Gerald et al. [183], illustrated similar results when leaching iron ore. The inconsistent rise in ash extraction observed at 60 minutes in both figure 22 and figure 23 shows that there is more ash within PT-char which has been extracting for 60 minutes, compared to 20 minutes. This is postulated to be caused by either the re-formation of ash by a reverse reaction, or the formation of a new insoluble solid, either of which would be faster than the rate at which ash is extracted. Figure 24 graphically illustrated this hypothesis, and further study is recommended.

Extraction yield, in terms of ash removed from PT-char X, increases with an increase in HCl concentration and with extraction temperature. An increase from 0.1M-1.0M HCl increased ash extraction by approximately 20.2% after 100minutes, to give a final extraction efficiency of 52.7% at 1.0M HCl. Increasing the extraction temperature from 20-60°C increased the quantity extracted by only 2.0%, giving a final ash extraction yield of 32.5%. These trends are in agreement with literature [116][183][186]. In particular, Chaala et al. [116], found an increase sulphuric acid concentration from 0.1-0.97M increased extraction by 7.58%, which is half of what HCl is able to extract; and found an increase in extraction temperature from 20-60°C increased extraction by 3.3%, which is slightly higher than what was found for the HCl system.
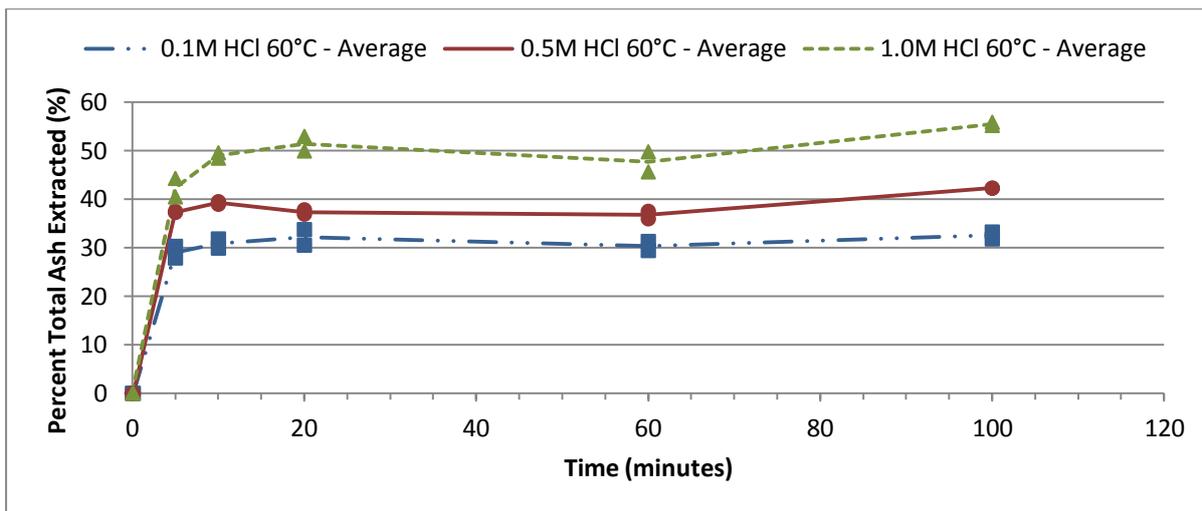
Figure 22: Kinetic Effect of various Hydrochloric Acid Concentrations in terms of Percent Total Ash Extracted (%)
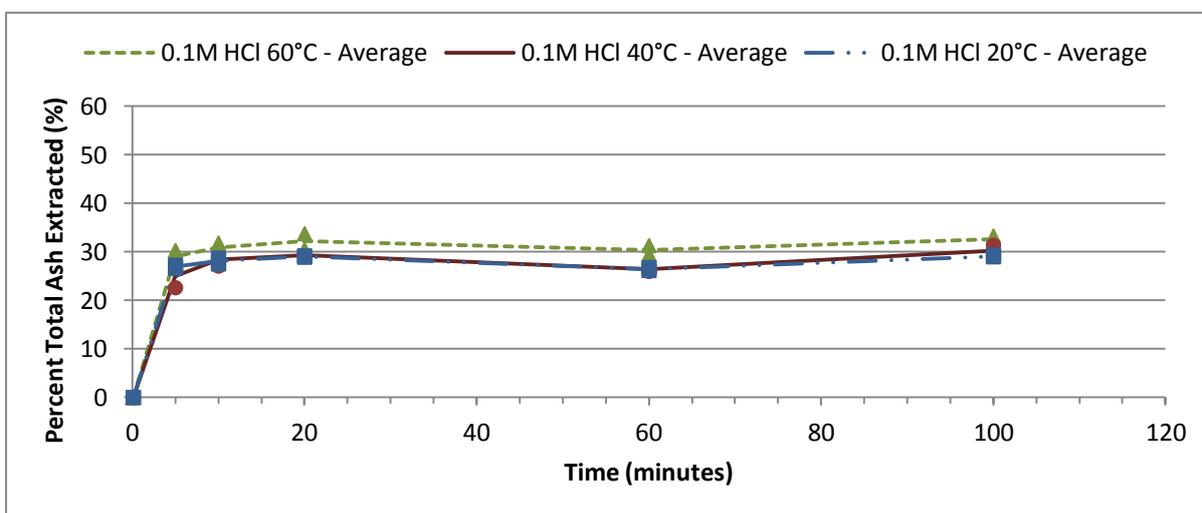
Figure 23: Kinetic Effect of various Hydrochloric Acid Extraction Temperatures in terms of Percent Total Ash Extracted (%)
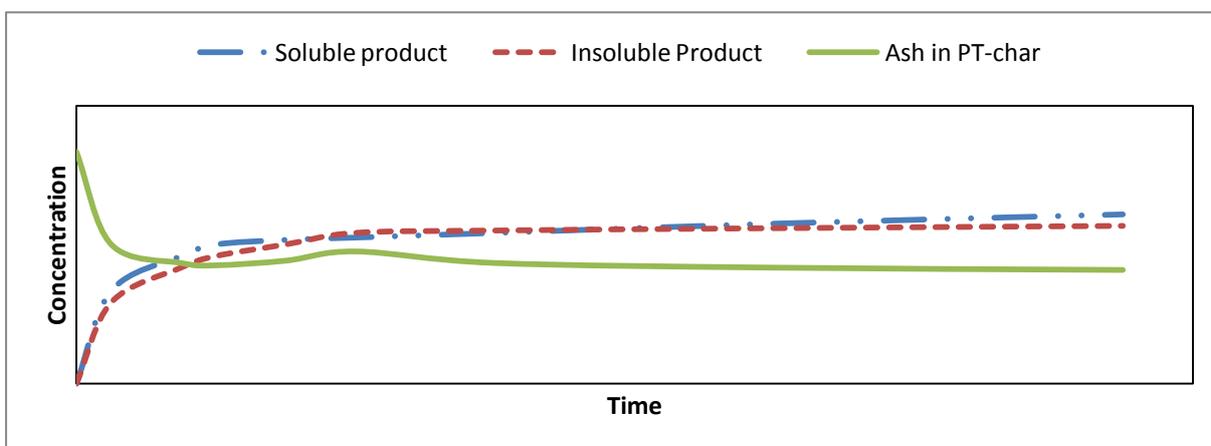
Figure 24: Postulation Product Formation causing the Increase in PT-char Ash Content at 60 minutes

The HCl kinetics were further examined by analysing the reaction rate controlling mechanism. The rate constants for different control models were calculated, namely: interfacial chemical reaction control; film diffusion control; product layer diffusion control; and control by the liquid phase diffusion through the porous structure. Using linearised plots, rate constant were analysed from 5-20 minutes for different HCl extraction temperatures (as per equation 21), with the assumption that the particles are spherical [183].

Table 41 and table 42 show the resultant rate constant, k, and the correlation coefficient, R^2, of the linear correlation plots (refer to appendix L for each plot). As can be seen by the lowest rate constant[57] and the largest correlation coefficient, interfacial chemical reaction is most likely to be the controlling mechanism as it fits the experimental data best. Using the interfacial chemical reaction control rate constant and the Arrhenius equation, the activation energy was calculated to be 10.97kJ/mol, which shows that an increase in temperature increases the rate of reaction. This is substantiated by literature as both Marafi et al. [187] and Van der Merwe et al. [182] attribute fast extraction rates to control by interfacial chemical reactions.

Theoretically, this is acceptable since control by film diffusion is minimised by the agitation of the PT-char-lixiviant suspension, reducing the formation of a boundary layer [132][151]. Additionally, control by diffusion through product layer formation is minimised due to the solubility of chlorides, thus forming no product layer accumulation around the particles [145]. Furthermore, diffusion of the lixiviant through the porous structure of PT-char is, also, very fast due to the large surface area and porosity of the particles, and the presence of metals on the surface of the PT-char particles.

Table 41:   Kinetic Rate Constants (k) of Rate Control Models for Hydrochloric Acid[58]

	Interfacial Chemical Reaction Control	*Film Diffusion Control*	*Product Layer Diffusion Control*	*Liquid Phase Diffusion through Pore Control*
	$1-\frac{2}{3}x-(1-x)^{\frac{2}{3}}$	x	$1-(1-x)^{\frac{1}{3}}$	$1-(1-x)^{\frac{2}{3}}$
20°C HCl	**3.00E-06 min^{-1}**	2.00E-04 min^{-1}	8.00E-05 min^{-1}	2.00E-04 min^{-1}
40°C HCl	**8.00E-06 min^{-1}**	6.00E-04 min^{-1}	2.00E-04 min^{-1}	4.00E-04 min^{-1}
60°C HCl	**5.00E-06 min^{-1}**	4.00E-04 min^{-1}	2.00E-04 min^{-1}	3.00E-04 min^{-1}

---

[57] A low (small) rate constant correlates to a slow speed. $k = min^{-1}$
[58] Refer to appendix L for relevant linear correlations

Table 42:   **Correlation Coefficients (R^2) of Rate Control Models for Hydrochloric Acid[58]**

	Interfacial Chemical Reaction Control	Film Diffusion Control	Product Layer Diffusion Control	Liquid Phase Diffusion through Pore Control
	$1 - \frac{2}{3}x - (1-x)^{\frac{2}{3}}$	x	$1 - (1-x)^{\frac{1}{3}}$	$1 - (1-x)^{\frac{2}{3}}$
20°C HCl	**0.9336**	0.9281	0.9282	0.9281
40°C HCl	**0.9397**	0.9253	0.9258	0.9256
60°C HCl	**0.8377**	0.8259	0.8263	0.8261

The HCl kinetic results show HCl concentration, particularly the reactant H^+ ion, is the limiting factor of this system and controls ash extraction from PT-char X. This is greatly substantiated by the increase ash reduction when HCl concentration is increased; by the constant equilibrium attainment at 10minutes regardless of HCl concentration; and by the possibility of interfacial chemical reaction control. Furthermore, HCl concentration has a greater effect on ash extraction than extraction temperature.

In most systems which house chemical reactions, after a certain time period, the transformation of reactants into products slows down as there are fewer reactants available for reaction [188]. An increase in HCl concentration correlates to an increase in number of reactant ions within the system. The more molecules which are present within a system, the higher the probability of collision frequency, resulting in an increased extent of reaction [189]. Similarly, increasing the temperature of the system increases the kinetic energy of the molecules present, resulting in an increased extent of reaction [189]. However, since HCl is so strong, the ash is easily accessible (as seen in figure 10) and the metals are not covalently (or strongly) bonded, the probability of collision is already very high, thus causing the extent to which the reaction proceeds to approach its maximum. This is further encouraged by the fact that an increase in temperature does not result in a large increase in ash extraction, thus showing that the extent of reaction is nearing its maximum since an increase in collision probability has no large effect on product formation.

Sodium Hydroxide Kinetic Behaviour

Figure 25 and figure 26 illustrate the kinetic effect of NaOH concentration and extraction temperature respectively. The behavioural responses of HCl extraction and NaOH extraction are similar.

The rate of ash extraction by NaOH shows a fast initial extraction rate between 0-5 minutes, followed by a slower, intermediate rate between 5-20 minutes. An increase in NaOH extraction temperature has a larger effect on reaction rate from 0-5 minutes compared to an increase in NaOH concentration. An increase NaOH concentration from 1-4M at 60°C increases ash leaching from PT-

char X by 12.13% during the first 5 minutes of extraction. Correspondingly, an increase in 3M NaOH extraction temperature from 30-88°C increases ash extraction by 19.57% from 0-5 minutes. After 5 minutes, the effect of temperature and concentration does not significantly impact the rate of ash extraction. These trends are in agreement with Wang et al. [181] who studied the kinetic leaching of silicon dioxide from fly ash slag using NaOH.

Chemical equilibrium is attained after approximately 10 minutes in both chemical systems, and an increase in NaOH concentration or extraction temperature does not have a significant effect on the time at which equilibrium is attained. This is in agreement with Wang et al. [181]. The linear inconsistencies between 5-100 minutes is not constant for each run, therefore further conclusions regarding the trend cannot be made.

Extraction yield, or ash content removed from PT-char X, increases as NaOH concentration and system temperature increases. After 100 minutes, an increase from 1M-4M NaOH increased ash extraction by 21.70%; while an increase in temperature from 30-88°C increased ash extraction by 15.5%. Additionally, the difference in ash extracted by 3M NaOH and 4M NaOH is not largely different, showing the approach of a concentration boundary limit. Chaala et al. [116], did not study the kinetics of a PT-char system, although they did observe an increase in ash extraction of 2.75% when the concentration of NaOH was increased from 1-5M, with no considerable ash extraction increase from 5M-10M at an extraction time of 30minutes. Wang et al. [181] increased the rate of SiO_2 leaching from 34.75-96.08% by increase the extraction temperature from 25-99°C. Furthermore, Yang and Das [180] showed that increasing NaOH extraction temperature from 150-210°C at constant 10% NaOH concentration decreased the ash content from 0.23-0.05% within coal; and increasing the concentration from 4-20% at a constant temperature of 190°C reduced the ash content from 0.42-0.06%.
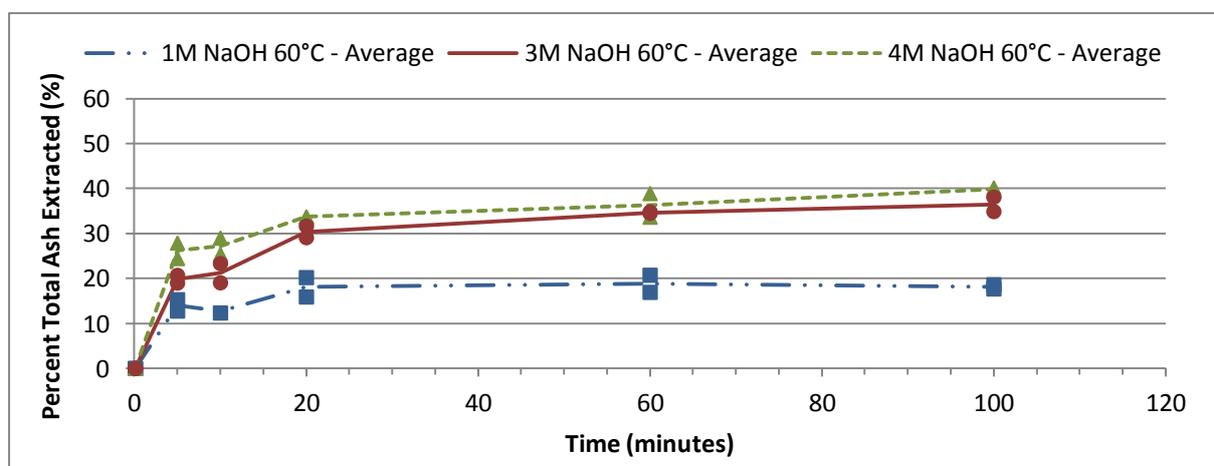

Figure 25:   **Kinetic Effect of various Sodium Hydroxide Concentrations in terms of Percent Total Ash Extracted (%)**
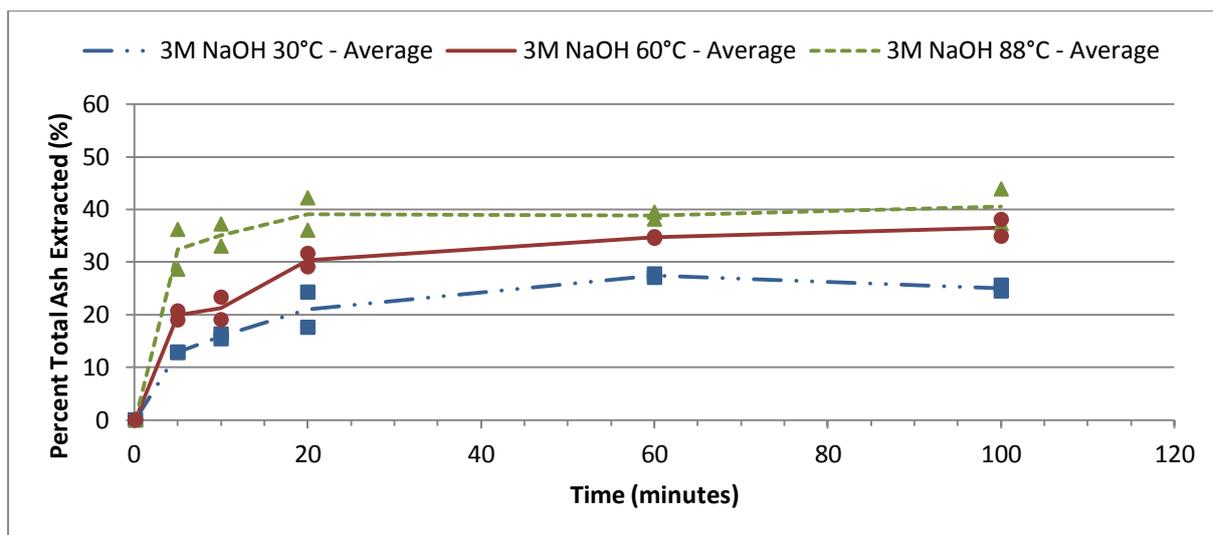
**Figure 26:** **Kinetic Effect of various Sodium Hydroxide Temperatures in terms of Percent Total Ash Extracted (%)**

The reaction rate controlling mechanism was examined further in the same manner described previously with regards to HCl kinetics.

Table 43 and table 44 list the resultant rate constant, k, and the correlation coefficient, R^2, respectively of the linear correlation plots described in appendix M. As with HCl leaching, the highest correlation coefficient and the smallest rate constant show that interfacial chemical reaction is most likely the control mechanism as it best fits the NaOH kinetic experimental data. It must be noted that, at 60°C, the reaction is most likely diffusion controlled. Since the rate constants are smallest for interfacial chemical reaction control, the corresponding rate constants and the Arrhenius Equation, the activation energy, which computed to be 4.24kJ/mol, shows that reaction rate increases with increasing temperature. This is substantiated by literature [187][182] and the same reasoning described for the HCl control mechanism apply.

Table 43: **Kinetic Rate Constants (k) of Rate Control Models for Sodium Hydroxide[59]**

	Interfacial Chemical Reaction Control	Film Diffusion Control	Product Layer Diffusion Control	Liquid Phase Diffusion through Pore Control
	$1 - \dfrac{2}{3}x - (1-x)^{\frac{2}{3}}$	x	$1 - (1-x)^{\frac{1}{3}}$	$1 - (1-x)^{\frac{2}{3}}$
30°C NaOH	**3.00E-06 min⁻¹**	5.00E-04 min⁻¹	2.00E-04 min⁻¹	3.00E-04 min⁻¹
60°C NaOH	**3.00E-06 min⁻¹**	4.00E-04 min⁻¹	1.00E-04 min⁻¹	2.00E-04 min⁻¹
88°C NaOH	**4.00E-06 min⁻¹**	3.00E-04 min⁻¹	1.00E-04 min⁻¹	2.00E-04 min⁻¹

---

[59] Refer to appendix M for relevant linear correlations

Table 44:   Correlation Coefficients (R^2) of Rate Control Models for Sodium Hydroxide[59]

	Interfacial Chemical Reaction Control	Film Diffusion Control	Product Layer Diffusion Control	Liquid Phase Diffusion through Pore Control
	$1-\frac{2}{3}x-(1-x)^{\frac{2}{3}}$	x	$1-(1-x)^{\frac{1}{3}}$	$1-(1-x)^{\frac{2}{3}}$
30°C NaOH	**0.9997**	0.9810	0.9816	0.9813
60°C NaOH	0.9913	**0.9954**	0.9953	**0.9954**
88°C NaOH	**0.9803**	0.9665	0.9671	0.9668

The NaOH kinetic results show NaOH concentration is the limiting factor for the same reasons pertaining to the HCl system; however, extraction temperature plays an important role during the reaction between SiO_2 and NaOH.

The probability of collision frequency increases with increasing concentration and temperature [189]. In a system where NaOH extracts SiO_2, an increase in temperature increases extraction more so than an increase in concentration due to the properties of the reactants. Characteristically, SiO_2 is covalently bonded in a lattice formation, with a bond energy of 368kJ/mol[190]. This relates to a large amount of energy required to break the Si-O bond. Additionally, a covalent bond has a high electron density causing repulsion of other molecules, such as NaOH. The collision between NaOH molecules and Si-O bonds is not enough to cause a reaction; the collision must have the required energy to break through the electron density repulsion and further break the bond. Therefore, the temperature of the system must be high enough to supply the collision with enough energy for a reaction to occur when a collision happens, after which, an increase in number of NaOH molecules will further increase the reaction rate as collision frequency increases. This is shown in figure 25 and figure 26 by the greater increase in extraction caused by temperature increase in comparison to concentration increase.

Determination of Suitable Process Variable Levels for Acid-alkali Demineralisation of PT-char

Four predominant process variables have been utilised during this kinetic study, namely C:L ratio, extraction time, extraction temperature and lixiviant concentration. The previous kinetic studies have shown the influence of temperature, time and concentration on ash extraction from PT-char X. Using these results, an in-depth analysis will follow, with the aim of revealing the value of each variable at which the acid-alkali demineralisation process will proceed.

C:L ratio is an important parameter in leaching processes as it has a significant impact on ash extraction. It is in general agreement that a reduction in solids percentage within a leaching system increases ash extraction [116][181]. Industrially, a low solids content relates to a higher cost per unit solids processed, therefore a C:L ratio of 20:100 (g/g) will be utilised throughout the rest of experimentation. This ratio will, thus, result in moderate ash extraction, but increased product throughput within an industrially implemented process. Additionally, this ratio will decrease slightly after sequential extraction since each lixiviant wash will result in ash removal and, thus, weight reduction.

Extraction time was thoroughly analysed during HCl and NaOH kinetic analysis. Industrially, a low extraction time is attractive as this will result in increased product throughput per unit time, further resulting in increased revenue. A low extraction time must be manageable in terms of process control and operation and must not be at the expense of yield. Figure 27 observes the quantity of ash extracted at time intervals for the central points of HCl (0.1M, 60°C) and NaOH (3M, 60°C). The extraction time trend for HCl shows that the quantity of ash extracted at 10minutes and 60minutes are similar; while the ash extraction capacity at 20minutes and 100minutes are similar. However, the quantity ash extracted at both 20 and 100minutes is approximately 2.0% higher than at 10 and 60minutes. Since 20 minutes is more economically feasible than 100 minutes, 20 minutes will be used as the HCl extraction time. The extraction time trend for NaOH shows a steady increase in PT-char X ash extraction from 10-60 minutes, with a small difference between 60 and 100 minutes. As with HCl, 60 minutes is more economically viable in comparison to 100 minutes and, therefore, NaOH extraction time of 60minutes will be used.
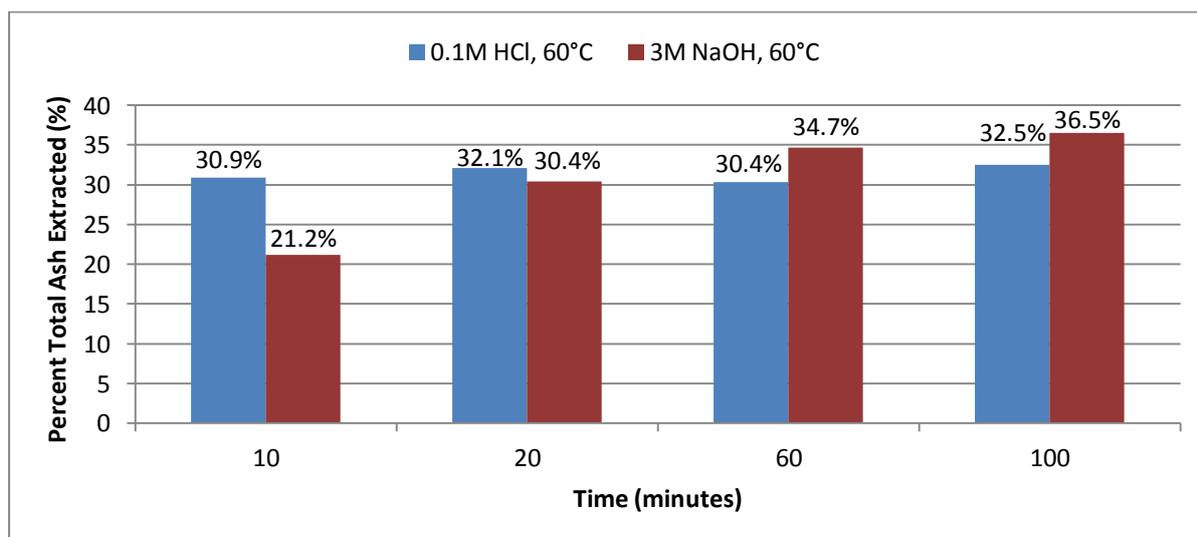
Figure 27: **Comparison of Percent Total Ash Extracted at Specific Time Intervals for Hydrochloric Acid and Sodium Hydroxide Kinetic Central Points**

The influence of extraction temperature on PT-char ash extraction for HCl and NaOH was analysed in the kinetic studies above. On an industrial scale, the temperature increase of a process stream is common practice. However, process safety becomes a concern when corrosive chemicals, such as acids and alkali, require heating. Additionally, special construction materials are required for corrosive chemicals. The temperatures utilised during PT-char demineralisation will most likely not influence corrosion or the energy balance significantly.

Figure 28 below shows the ash extraction trend caused by increasing extraction temperatures of a 0.1M HCl system extracting for 20minutes and a 3.0M NaOH extracting for 60minutes. T1, T2 and T3 represent 20°C, 40°C and 60°C for HCl and 30°C, 60°C and 88°C for NaOH. The results shown included 0.1M HCl. In a system where HCl is the lixiviant, a temperature increase from 20°C-40°C does not greatly influence the quantity ash extracted. However, an increase from 40°C-60°C increases ash extraction from 29.3-32.1wt%. An HCl extraction temperature of 60°C will be utilised for further experiments as it allows for the greatest quantity of ash to be extracted from PT-char X. In a NaOH system, there is a steady increase of 7.3% and 4.1% when temperature increases from 30°C-60°C and from 60°C-88°C respectively. A NaOH extraction temperature of 88°C will, thus, be used as the largest amount of ash is extracted at this temperature.
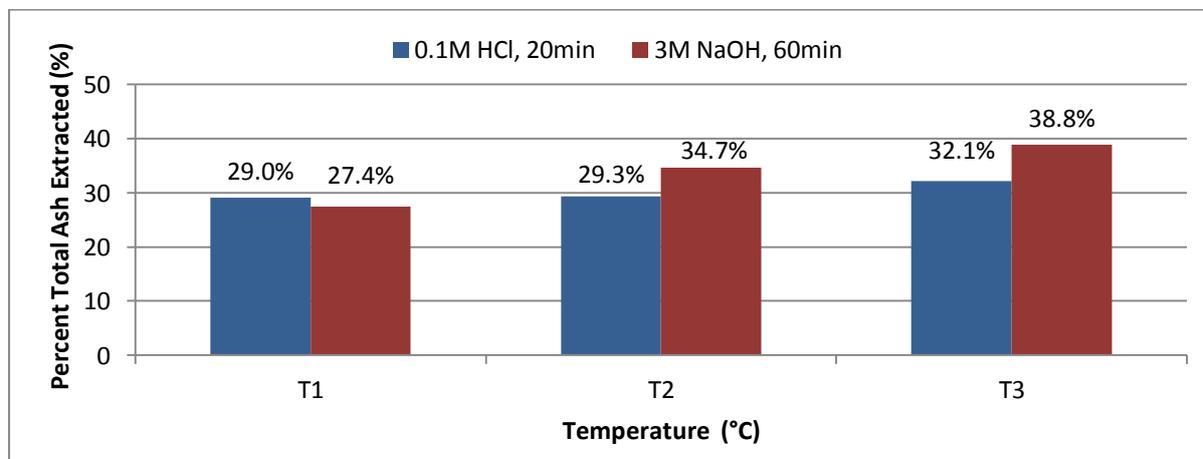
Figure 28:   **Comparison of Percent Total Ash Extracted at Specific Temperatures for Hydrochloric Acid and Sodium Hydroxide**

Lixiviant concentration largely influences PT-char ash extraction, with HCl targeting the metals having a basic nature and NaOH targeting the impurities with an acidic nature, particularly SiO_2. As demonstrated by the TGA and mineralogical studies in table 18 and table 19 respectively, PT-char X has a silicon dioxide content of approximately 8.47wt.% and a metal content of 7.15wt.%. If all the silicon dioxide content were to be extracted by NaOH, 54.2% of the total ash content must be removed; and 45.8% ash must be removed by HCl if all the metals were to be extracted from PT-char X. At the predetermined 20min extraction time and 60°C extraction temperature, the most suitable

lixiviant concentration is determined by analysing single vs. multiple lixiviant washes at low and high concentrations since one lixiviant wash may not remove the required ash content. It must be noted that a C:L ratio of 20:100 (g/g) was utilised.

The kinetic results of HCl (figure 22) shows that 1.0M HCl at 60°C for an extraction time of 20minutes is able to extract 51.44% of the ash content, which meets the benchmark requirement, as shown in figure 29 and table 45. Showing promise, 0.1M HCl is able to extract 31.13% ash (at the same extraction temperature and time); however, two 0.1M HCl extractions were unable to remove the required ash content of 51.44%. Three 0.1M HCl extractions are, most likely, required; however, this will relate to increased capital and reduced product throughput which may not balance the savings made on the low HCl concentration. Using these results, a single 1.0M HCl wash was chosen to target the metal content within PT-char X.

The kinetic results of NaOH show that a single NaOH wash at 88°C for 60minutes is unable to extract the required 54.2wt% ash, even at a concentration of 4.0M. However, since Chaala et al. [116] noted the boundary condition of NaOH concentration was 5.0M in a PT-char extraction system, the concentration of NaOH was increased to 5.0M. As shown in figure 30 and table 45, 5M NaOH at 88°C, extracting for 60 minutes, extracts only 38.4wt% ash and not the required 54.2%. Since both the temperature and the concentration of the NaOH system are at their boundary limits, sequential extraction is the next alternative to increase ash extraction. As demonstrated in figure 30 below, a double NaOH wash (44.3% extraction) and a triple NaOH wash (51.2wt% extraction) still do not meet the required 54.2wt% ash extraction. However, economic infeasibility will increase further if a fourth NaOH wash were to be added to the extraction sequence therefore, the acid-alkali demineralisation process will utilise three 5.0M NaOH washes at 88°C for 60minutes extraction time. Additionally, if combined with an HCl wash, three NaOH wash may be sufficient due to the amphoteric nature of certain ash components.
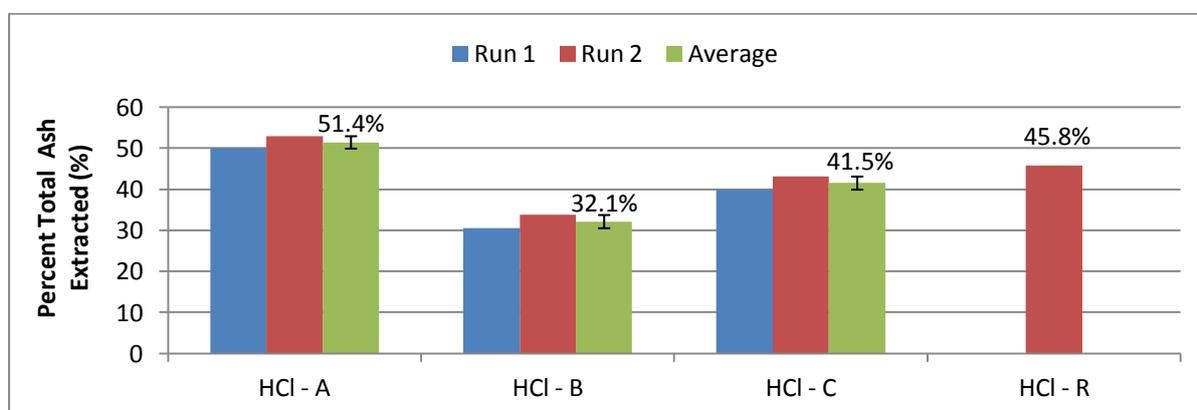
Figure 29: **Comparison of Percent Total Ash Extracted for Single and Double Hydrochloric Acid Washes**
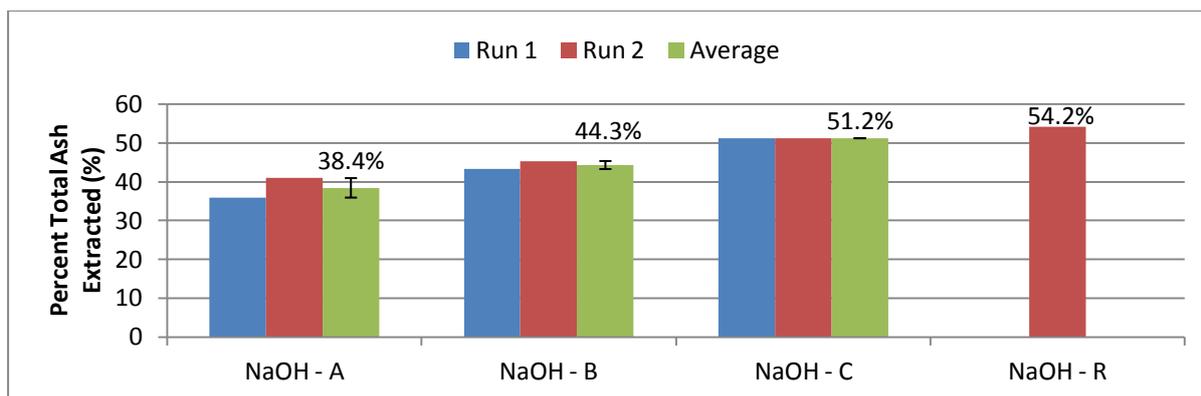
Figure 30: **Comparison of Percent Total Ash Extracted for Single, Double and Triple Sodium Hydroxide Washes**

Table 45: **Variable Description and Key for Figure 30 and Figure 29**

Graphical Description	Variable Description	Number of Extractions	Quantity Removed: Run 1 (%)	Quantity Removed: Run 2 (%)	Quantity Removed: Average (%)
NaOH – A	5M NaOH, 88°C, 60min, 20:100 (g/g)	1	35.92	40.95	38.43
NaOH – B	5M NaOH, 88°C, 60min, 20:100 (g/g)	2	43.27	45.35	44.31
NaOH – C	5M NaOH, 88°C, 60min, 20:100 (g/g)	3	51.22	51.22	51.22
NaOH – R	Overall SiO_2 Removal Requirement	-			54.23
HCl – A	1.0M HCl, 60°C, 20min, 20:100 (g/g)	1	49.93	52.95	51.44
HCl – B	0.1M HCl, 60°C, 20min, 20:100 (g/g)	1	30.54	33.74	32.13
HCl – C	0.1M HCl, 60°C, 20min, 20:100 (g/g)	2	39.93	43.12	41.52
HCl – R	Overall Metal Removal Requirement	-			45.77

Acid-alkali Demineralisation Sequence Analysis

As analysed and discussed above, the following process variable values and sequential washes have been selected thus far: one 1.0M HCl wash at 60°C for 20 minutes using 20g char and 100g HCl; and three 5.0M NaOH washes at 88°C for 60 minutes using 20g char and 100g NaOH. In order to analyse and optimise the combined effect of HCl and NaOH on ash extraction of PT-char X, sequential extractions using different wash sequences were analysed. Three NaOH washes (represented by B) were combined with one HCl wash (represented by A) in the following combinations: A-B-B-B; B-A-B-B; B-B-A-B; B-B-B-A.

The ash extraction capacity of each of the above acid-alkali combinations are illustrated in figure 31. Firstly, it is clear that B-B-B-A combination extracts the largest quantity ash; while a combination of B-A-B-B extracts the least. Additionally, an initial acid wash (A-B-B-B) is unable to extract as much ash in comparison to a final acid wash (B-B-B-A). With the exception of A-B-B-B, the results further show that an increase in initial NaOH washes increases the overall ash extracted. The increase in ash extraction, however, is not linear; with two initial NaOH washes (B-B-A-B) increasing ash extraction by 4.8%, while three initial NaOH washes (B-B-B-A) increasing the ash extraction by 3.6%. Figure 31 clearly demonstrates that the sequence in which the acid-alkali washes are performed effects the efficiency of the individual lixiviant ash extraction efficiency, with a combination of B-B-B-A exhibiting the greatest extraction efficiency.
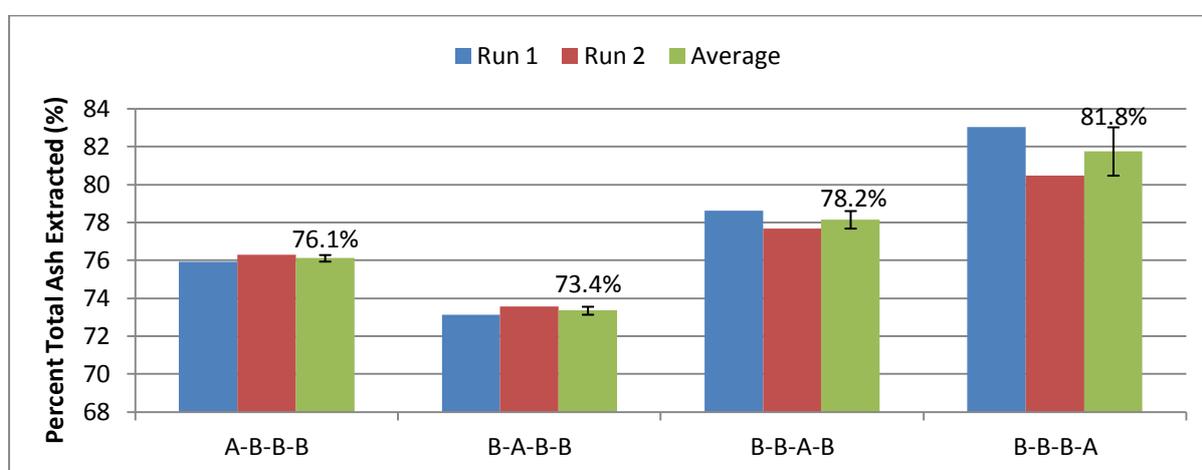
Figure 31:   Analysis of Acid-alkali Sequential Extraction of PT-char X

For further wash sequence analysis, the combinations analysed above were broken down into single, double and triple extractions as demonstrated in figure 32.

Analysing the individual results, a single HCl wash extracts 13.0% more ash than a single NaOH wash, illustrated by A and B in figure 32 respectively[60]. However, the extraction effectiveness is reduced if the respective lixiviant is utilised second in a sequence, as shown by a comparison between A, B, AB, BA in figure 32. HCl extracts 25.5% less ash if a NaOH wash precedes it; while NaOH extracts 76.8% less ash if an HCl wash precedes it. Similarly, when three NaOH washes precede an HCl wash, the HCl wash extracts 40.47% less ash; while NaOH extracts 51.76% less ash when one HCl wash precedes them. This observation, as summarised in table 46, clearly shows that using three NaOH washes first is more efficient in removing ash from PT-char than using an HCl wash first.

Single, double and triple NaOH extractions are compared in figure 32. It can be seen that the ash extraction increases by 5.9% when PT-char X is submitted to a second NaOH wash; further increasing by 6.9% when submitted to a third NaOH wash. This is due to the presence of a fresh lixiviant per

---

[60] Previously shown in Figure 29 and Figure 30

every wash, and a decreasing C:L ratio with increasing NaOH washes, thus increasing extraction. Furthermore, many authors have found the surface area to increase with impurity removal [1][5][14][30][33][34][80][115], thus increasing the solid-lixiviant contact area, further increasing extraction.

A comparison between figure 31 and figure 32 shows that combination B-A extracts slightly more ash than combination A-B-B-B and B-A-B-B. It is unclear as to why this occurs, and may be subject to further investigation. However, it must be noted that PT-char is a heterogeneous material, and four lixiviant washes has increased associated error compared to two lixiviant washes. Further investigation into this observation was rendered irrelevant since neither A-B-B-B nor B-A-B-B were able to extract the most ash from PT-char X.
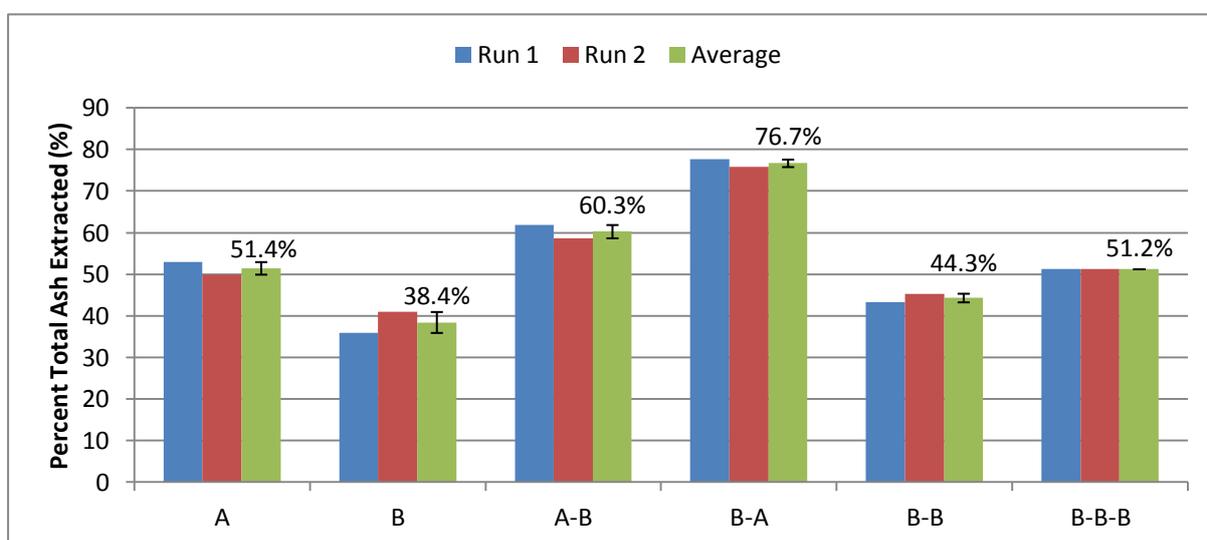
Figure 32:   **Analysis of the Effect of Acid-alkali Wash Sequence on Individual Lixiviant Ash Extraction Efficiency**

Table 46:   **Summary of the Effect of Acid-alkali Wash Sequence on Lixiviant Ash Extraction Efficiency**

Sequence	Ash Extracted by Sequence (%)	Ash Extracted by Acid (%)	Efficiency Reduction by Movement of Acid from Initial Wash to Final Wash (%)	Ash Extracted by Alkali/Alkali Combination (%)	Efficiency Reduction by Movement of Alkali/Alkali Combination from Initial Wash to Final Wash (%)
A-B	60.3	51.4	25.49	8.9	76.82
B-A	76.7	38.3		38.4	
A-BBB	76.1	51.4	40.47	24.9	51.76
BBB-A	81.8	30.6		30.6	

Additionally, the sulphurous smell released during PT-char X extraction with HCl lead to sulphur analysis of UPT-char. Sequential extraction combinations A-B-B-B and B-B-B-A were analysed for sulphur; however, the results were rendered semi-quantitative as they were outside the sulphur calibration range of the XRF machine. The results, therefore, cannot be compared to other reported sulphurous contents; however, comparing the two results is viable. XRF results show that sequential extraction combination B-B-B-A removed 0.94wt.% more sulphur than A-B-B-B.

The availability of reactive lixiviant in the first wash of the sequence is the limiting factor.
Certain ash components within PT-char X are amphoteric, and are able to react with both an acid and an alkali, while others are only able to react with either the acid or alkali [139]. Consequently, if the amphoteric components are greatly reactive within the system, the first lixiviant wash will be exhausted by the reaction and extraction of both amphoteric and target components [116] and, consequently, may not meet the required extraction capacity of its target components. Since there are three NaOH washes, the second and third washes are able to compensate for the target components which may not have been extracted in the first wash due to the additional extraction of the amphoteric components. There is no second or third HCl wash which is able to compensate for amphoteric component extraction; therefore the amphoteric compounds must be removed before the HCl wash so it is able to extract its target components. This is further substantiated by the sulphur extraction results. More sulphur is extracted from PT-char X when the HCl wash is last in the sequence. This shows that there is extra HCl available to react with the sulphur. It is postulated that the H^+ ions from HCl are able to react with sulphur within PT-char to form hydrogen sulphide gas (H_2S).

Analysis of HCl and NaOH Target Ash Components

To facilitate the understanding of which ash components are targeted by hydrochloric acid and which by sodium hydroxide, XRF analyses were completed for single HCl and NaOH washes.

Table 47 shows a comparison between the composition of PT-char X feed and UPT-char which has undergone one wash using 1.0M HCl, 60°C, 20min 20:100 (g/g). Two results are displayed: mineral content within PT-char X extracted by HCl (wt.%); and the mineral content of the feed PT-char X (wt.%).During the extraction process, the mass extracted by HCl consisted chiefly of iron, silicon/silicon dioxide, sodium and calcium; with low amounts of chromium, magnesium and manganese. Moreover, HCl was able to extract over 70% of the original content of iron, sodium, calcium, chromium, phosphorus and manganese from PT-char X. These results are in accordance to the metal reactivity series, as shown in figure 6, since most of the metals with PT-char X have the ability to be

displaced by an acid, with the most susceptible metals being potassium, sodium and calcium. Additionally, HCl is able to extract a large portion of iron since it is abundantly available within PT-char X and is able to react with HCl, although not the most reactive of the ash components. Interestingly, HCl extracts a portion of silicon/silicon dioxide components. According to J. Thomas [191], silicon is able to react halogens such as chlorine and fluorine, forming tetrahalides; and silicon is often reacted with chlorine gas to form silicon tetrachloride ($SiCl_4$). The chlorine ions from HCl may be reacting with silicon within PT-char X, forming a colourless gas at temperatures above 57.65°C; thus explaining the reduction in Si/SiO_2 mass. Additionally, it has been established that silicon dioxide is slightly acidic, and is only able to react with a strong alkali, such as strong NaOH at a high temperature (section 4.5). Therefore, the fact that HCl is able to extract a portion of the Si/SiO_2 content from PT-char X shows that there is, indeed silicon present within PT-char X which is not in its oxidised form. Refer to appendix N for relevant equations between HCl and PT-char ash components.

The presence of NaOH within a sample analysed by WD-XRF may cause expensive harm to the equipment and, thus, PT-char X extracted by NaOH could not be analysed using WD-XRF. Hence forth, UPT-char which has undergone one wash using 5.0M NaOH at 88°C for 60min at a C:L ratio of 20:100 (g/g) was analysed using SEM-EDX. The EDX detector was only able to analyse silicon and calcium as major inorganic components and, thus, a quantitative conclusion as to quantity metals extracted cannot be made. The analysis does, however, show that 44% Si/SiO_2 content has been extracted by 1 NaOH wash at the prescribed conditions, thus relating to 3.73% Si/SiO_2 extracted. Furthermore, the analysis shows that the UPT-char has a sulphur content of 1.26wt.%, thus showing a reaction between NaOH and sulphur occurs during extraction. From a literature survey, it is clear that NaOH is unable to react with Fe, Ca or Na since iron is basic and not amphoteric, and reactions with calcium and sodium require a temperatures of 600°C [142]. However, following NaOH extraction is a water wash, which will remove Ca and Na, as shown in figure 6. As previously discussed; aluminium, titanium and magnesium form oxides immediately upon exposure to air. NaOH is able to react with both elemental and oxide Al and Ti due to their amphoteric properties, however cannot react with MgO as it is slightly basic and not amphoteric. NaOH is able to react with potassium, chromium and silicon dioxide. Refer to appendix N for relevant equations between NaOH and PT-char ash components.

Table 47: **Compositional comparison of PT-char X feed and UPT-char submitted to 1.0M HCl Extraction at 60°C for 20min using a C:L ratio of 20:100 (g/g) (HCl-A as per Table 45)**

	Mineral Content in PT-char X (wt.%)	Mineral Content in UPT-char X (wt.%)	Mineral Content Extracted by HCl (wt.%)	Extraction Efficiency (%)
Fe	3.99	0.96	3.03	75.94
Si/SiO$_2$	8.47	6.10	2.37	27.98
Na	1.43	0.33	1.10	76.92
Ca	1.29	0.30	0.99	76.74
K	0.35	0.11	0.24	68.57
Al	0.23	0.12	0.11	47.83
P	0.11	0.03	0.08	72.73
Ti	0.10	0.05	0.05	50.00
Cr	0.04	0.01	0.03	75.00
Mg	0.07	0.04	0.03	42.86
Mn	0.03	0.01	0.02	66.67
Total	**16.11**	**8.07**	**8.05**	**-**

Development of Carbon Black from PT-char X through Acid-alkali Demineralisation

Figure 31 clearly illustrates that 1.0M HCl at 60°C for 20 minutes and 5.0M NaOH at 88°C for 60 minutes using an initial 20g char and 100g HCl in the sequence of B-B-B-A is unable to remove enough ash from PT-char X to meet the ash content requirement of CB N330, which is 1.95wt.% (or 87.51% ash removal). The process variables must, therefore, be augmented.

Analysing the HCl and NaOH variables, the first recognizable alteration would be to increase the temperature of the HCl wash since the HCl concentration is already particularly high and the NaOH variables are at their maximum. Using the previously discussed sequential extraction B-B-B-A, the extraction temperature for the HCl wash was increased from 60°C-80°C while keeping the other variables unchanged. This alteration proved to be sufficient as the final corrected ash content of the UPT-char tested to be 1.83wt.% ± 0.073. It must be noted that the lixiviant mass was kept at a constant 100g per wash, while the PT-char mass decreased from 20g in wash 1. A full characterisation comparison between CB N330, PT-char X and UPT-char follow.

Table 48 summarises the total mass percent extracted and the total ash percent extracted from PT-char X with each wash. These values were calculated from the results described in Figure 31 and Figure 32, and show the mass percent PT-char extracted rather than the percent ash extracted as previously described. As it can be seen, the first and last wash removes the most mass from PT-char.

Table 48: **Process Characteristics of PT-char Acid-alkali Demineralisation forming UPT-char (CB)**

Description	Unit	Total Mass Extracted		Total Ash Extracted	
		Value	Standard Deviation	Value	Standard Deviation
Wash 1: NaOH	wt.%	8.13	0.2105	6.19	0.4492
Wash 2: NaOH	wt.%	1.52	0.1794	0.95	0.1852
Wash 3: NaOH	wt.%	1.11	0.0091	1.11	0.0004
Wash 4: HCl	wt.%	8.71	0.7400	7.57	0.0728
Total	**wt.%**	**19.47**	**0.0030**	**15.82**	**0.0728**
NaOH: 5.0M, 88°C, 60minutes, 100g lixiviant per wash					
HCl: 1.0M, 80°C, 20minutes, 100g lixiviant per wash					

Due to the unavailability of a WD-XRF, a compositional analysis was performed using SEM-EDX, as shown in table 49 below. Utilising 12 area analyses, major elements analysed to be carbon, sulphur, silicon, chlorine and zinc. Carbon, sulphur and chlorine are the organic elements within PT-char, summating to a total of 100.145wt.%; while silicon and zinc are the inorganic components, comprising 1.38wt.%. Although in conformity, the small difference between the total SEM-EDX inorganic content summating to 1.38wt.% and the previously analysed ash content of 1.83wt.% can be attributed to a few factors: PT-char heterogeneity; zinc may be in chloride or oxide form and silicon may be in oxide form [91], thus adding to the overall weight percent; and the small sample size analysed by SEM-EDX. The SEM-EDX zinc content within UPT-char analysed to be 1.14wt.%. It must be noted that the initial zinc content within crude PT-char, however, is unknown due to lack of WD-XRF instrumental calibration, therefore the degree to which the acid-alkali demineralisation process extracts zinc is unknown.

The results show that approximately 8.23wt% Si/SiO_2 has been removed by the acid-alkali demineralisation process.

Table 49 clearly demonstrates the presence of chlorine as a major component. WD-XRF analysed chlorine to be a minor component within crude PT-char, with a total chlorine content of 1707ppm. However, the increase in chlorine content within UPT-char can be explained either by the large removal of impurities causing the chlorine content to hold a higher mass percent although not increasing in mass content; or the chlorine content has increased due to the presence of HCl. The former is most likely since chlorides are soluble.

Finally, UPT-char has a sulphur content of 1.13wt.%, which is much lower the sulphur content of CB N330, which is 1.8wt.%. The process is able to remove approximately 0.85wt.%. The acid-alkali demineralisation process is, thus, able to remove both ash and sulphur impurities, rendering the UPT-char purity comparable to that of CB N330.

Table 49:   **Compositional Analysis of UPT-char X**

	Unit	Value	Standard Deviation
C	wt.%	98.468	0.674
S	wt.%	1.126	0.329
Si/SiO_2	wt.%	0.24	0.030
Cl	wt.%	0.55	0.132
Zn	wt.%	1.14	0.009
Total	**wt.%**	**101.525**	**1.660**

SEM micrographs of UPT-char are illustrated in figure 33 below. As depicted by figure 33a, the particle sizes are much larger than that of CB N330, as shown in figure 10a. However, both particle populations of CB N330 in figure 10a and UPT-char in figure 33a are irregular shape and size. The UPT-char particle illustrated in figure 33b show the surface irregularity caused by the removal of ash, particularly SiO_2 as it is bulky filler. SEM-EDX analyses of the micrographs below show that the bright spots on the surface are rich in sulphur, with small quantities of metals present, as discussed thoroughly in section chapter 3.4.

(a)   (b)
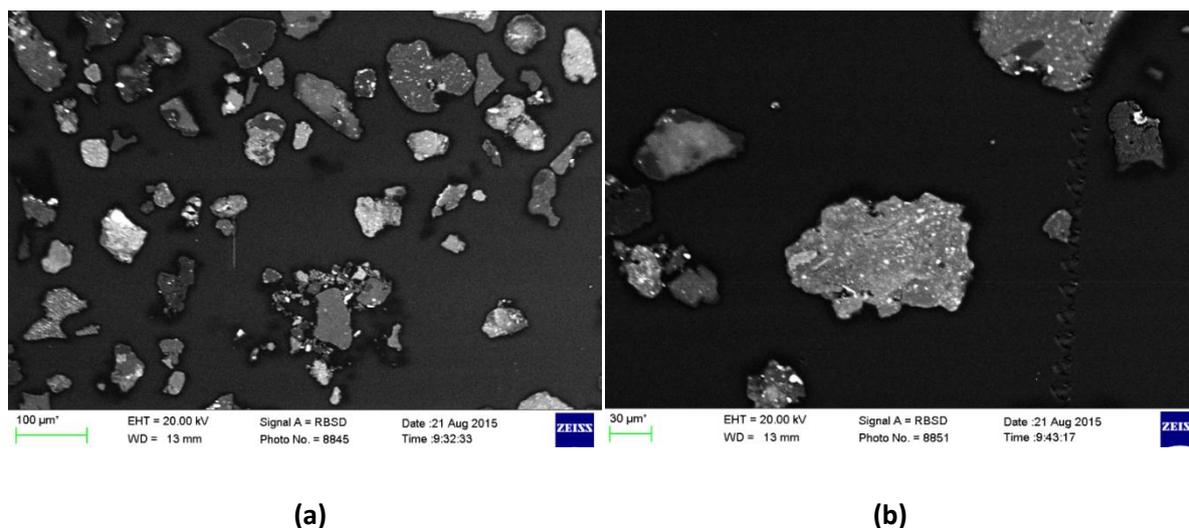
Figure 33:   **(a) SEM Micrograph of UPT-char Population; (b) SEM Micrograph of UPT-char Particle**

The particle size of UPT-char was analysed using the same nitrogen isotherms as described in section 3.3.1. The results are illustrated in figure 34 and table 50 below. The acid-alkali process was able to reduce the average particle size of PT-char X, but unable to reduce it to the required size of CB N330. The analysis results show that the average particle sizes of PT-char X, UPT-char and CB N330 are 153.2μm, 130.6μm, and 38.52μm respectively. Additionally, the median particle size analysed to be 139.2μm, 125.6μm and 3.585μm for PT-char X, UPT-char and CB N330 respectively. Since the particle size of UPT-char X is greater than 50μm, commercially, it cannot be described as reinforcing filler, and further size reduction is required. The overall particle size distribution is, also,

widespread, as shown in figure 35. The reduction in particle size is attributed to a combination of ash extraction from the PT-char structure, mechanical forces during the extraction process such as particle-wall or particle-particle collisions; and the conditions of WT-pyrolysis. Tyre crumb feed into WT-pyrolysis contains a variety of CB particle series and seizes, and the cracking of elastomers can cause the formation of tarry products on the surface of CB, binding the CB particles together [14][34][80][96] [161]. It must be noted that the available analytical techniques were unable to quantify the presence of tarry pyrolysis products. Additionally, particle size analyses are subject to great sampling error.
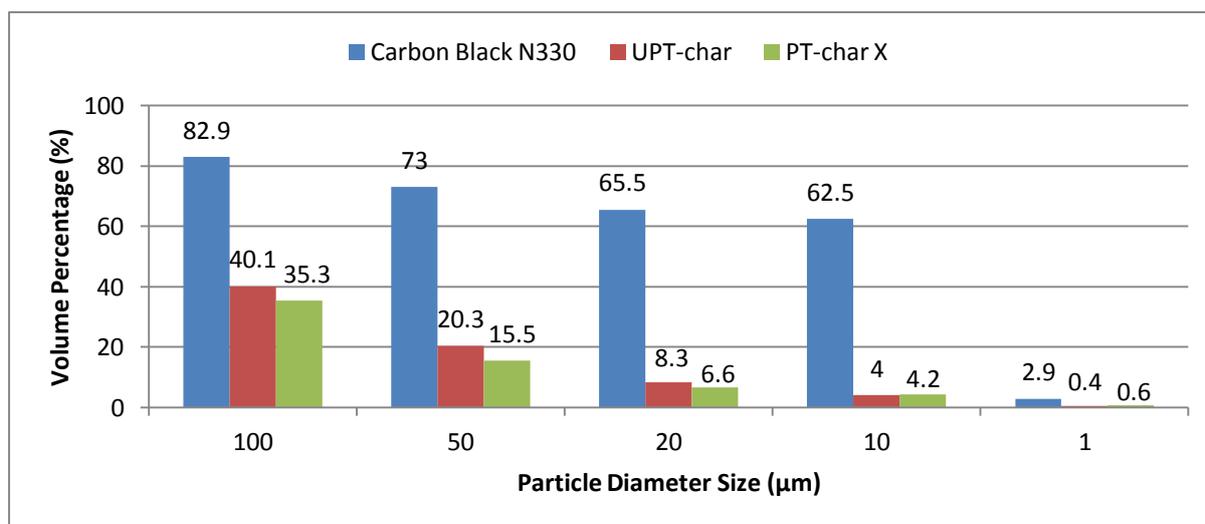
Figure 34:   **Particle Size Representation in terms of Percent Finer of Sampled Particle Populations CB N330, PT-char X and PT-char Y**

Table 50:   **Particle Size Distribution Statistics**

		PT-char X		UPT-char		Carbon Black N330	
	Unit	**Value**	**Standard Deviation**	**Value**	**Standard Deviation**	**Value**	**Standard Deviation**
Mean	µm	153.2	5.118	130.6	7.214	38.52	17.12
Median	µm	139.2	5.276	125.6	7.827	3.585	0.435
Mode	µm	212.6	19.87	212.6	25.25	2.677	0
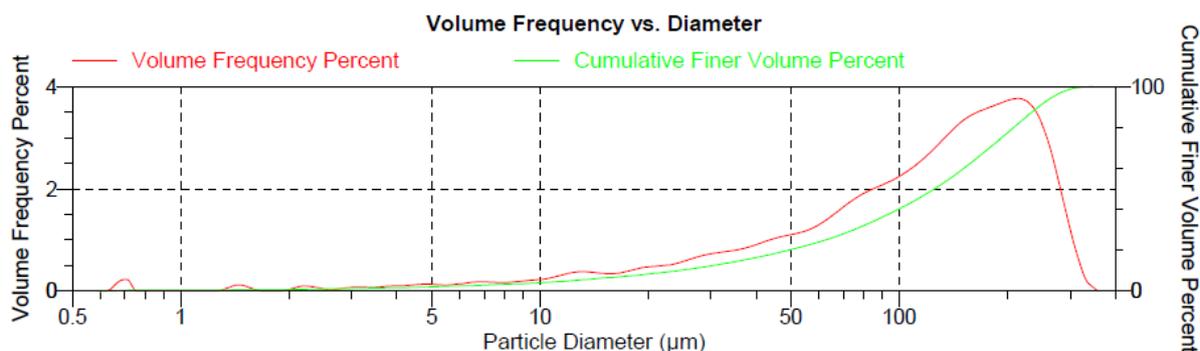
Figure 35:   **Particle Size Distribution of UPT-char X**

The BET surface area of UPT-char was analysed using nitrogen gas adsorption desorption isotherms, as discussed in the porosimetry paragraph of section 3.3.1. The BET surface area analysed to be 84.66m^2/g, thus showing that the process significantly increased the surface area by 30.73m^2/g. Additionally, the UPT-char has a BET surface area slightly higher than CB N330, which is 80.22m^2/g, as described in table 51. This renders it slightly more active than carbon black allowing for greater reinforcement within a tyre. The pore surface area of UPT-char analysed to be 74.73m^2/g, which is comparable to that of CB N330, which is 74.8m^2/g. The pore volume of UPT-char, however, is slightly less than that of CB N330, as described in table 51. This observation is in agreement with many authors who found the surface area to increase when inorganic impurities are removed [1][5][14][30][33][34][80][115]. The removal of these impurities by acid-alkali demineralisation increases the surface area of the UPT-char product. Furthermore, since the average particle size does not significantly decrease, it is clear that impurity removal is the predominant factor causing the increase in surface area of UPT-char. Impurity removal increases the interstitial spacing between the carbon black particles, allowing for an increase in surface area rather than particle size. This may be the reason why large particle sizes are observed by the particle size analysers. The interstitial space increase allows for the formation of large clusters of CB particles, which may improve adhesion with elastomers when utilised as tyre filler. It is recommended that further research be conducted so as to analyse the structure of these particles and their impact on adhesion between the elastomers and filler within the tyre, since this is a specialised area of expertise.

Table 51:   **Porosimetry Analysis of CB N330, PT-char X and UPT-char**

	Unit	PT-char X	UPT-char	CB N330
BET surface area	m^2.g^{-1}	58.9316	84.6629	80.2244
BJH adsorption cumulative pore surface area	m^2.g^{-1}	58.758	74.729	74.808
BJH adsorption cumulative pore volume	cm^3.g^{-1}	0.486442	0.515290	0.811579

Acid-alkali Demineralisation Process Validation

The acid-alkali demineralisation process was further tested by scaling-up the process using PT-char X, and repeating the original process using PT-char from another South African company (known as PT-char Z from here forth).

PT-char Z analysed to be a completely pyrolysed PT-char, with a volatiles content of 1.7wt.% and an ash content of 16.2wt.%. PT-char Z was subjected to the same acid-alkali process which was performed on PT-char X: 3x 5.0M NaOH washes at 88°C for 60minutes, followed by 1x 1.0M HCl wash at 80°C for 20minutes. The results show that UPT-char Z had an ash content of 4.1wt.%[61] on average, which is 2.27wt.% higher than when applying the process to PT-char X (1.83wt.%). This is due to the high silicon/ silicon dioxide content within PT-char Z, which 12.12wt.%, thus showing that the proposed acid-alkali demineralisation process is only able to extract a maximum of 8.4wt.% silicon/ silicon dioxide. The strength of the NaOH washes should be adapted to accommodate PT-char of greater impurity.

A 4x scale-up was performed using PT-char X using 3x 5.0M NaOH washes at 88°C for 60minutes, followed by 1x 1.0M HCl wash at 80°C for 20minutes. The scale-up experiment was able to remove approximately 0.15wt% more ash in comparison to the downsized experiment. However, due to equipment limitations, this experiment was conducted simply to analyse if scale-up is possible, and not to obtain quantitative results; therefore it can only be concluded that a scale-up by 4 is promising in terms of quantity ash extracted. It is recommended that a scale-up reactor be built so as to obtain quantitative scale-up results.

5.7. Conclusions and recommendations of process and product development

The objective of this chapter was to determine the kinetic influence of extraction temperature, extraction time and lixiviant concentration on the removal of ash from PT-char X. The trends were then utilised to create an upgraded PT-char with characteristics similar to that of CB N330. The study included kinetics and sequential extraction experiments using HCl and NaOH.

The kinetic experiments revealed that lixiviant concentration was the limiting factor, and extraction is most likely controlled by interfacial chemical reactions. The kinetic results demonstrated that an increase in concentration or temperature increased the quantity ash extracted. Using HCl as a

---

[61] Standard deviation of 0.053wt.%

lixiviant, an increase in concentration increased ash extraction more substantially compared to temperature augmentation, due to the strength of the acid allowing the extent to which the reaction proceeds to approach its maximum. The kinetics of a NaOH system illustrated that sufficient energy, in the form of heat, must be supplied to the system for the reaction between NaOH and SiO_2 to proceed, after which an increase in NaOH concentration will increase ash extraction further.

A combination of the kinetic and further sequential extraction experiments allowed for the determination of the most suitable process variable values and the development of acid-alkali wash sequence which aimed to extracted the greatest quantity ash. The results revealed that 3x 5.0M NaOH washes at 88°C for 60minutes followed by 1x 1.0M HCl at 60°C for 20minutes extracted the greatest quantity ash, with an ash extraction efficiency of 81.8wt.%. 20g PT-char was initially used; while each lixiviant wash consists of 100g lixiviant. The C:L ratio slowly decreased from 20:100 (g/g) as ash was removed from the PT-char.

Upgrading PT-char to a carbon black product required the removal of 87.51wt.% ash. The extraction process was strengthened by increasing the HCl extraction temperature to 80°C. This alteration proved sufficient as the resultant UPT-char had an ash content of 1.83wt.% on average. The entire process extracted 6.19wt.%, 0.95wt.%, 1.11wt.% and 7.57wt% during the first, second, third and fourth wash respectively. Similarly, the total mass extracted during each consecutive wash tested to be 8.13wt.%, 1.52wt%, 1.11wt%, and 8.7wt%. The final acid-alkali demineralisation process included 3x 5.0M NaOH washes at 88°C for 60minutes followed by 1x 1.0M HCl at 80°C for 20minutes. The initial lixiviant quantity of 100g used with 20g PT-char slowly decreased after each wash. Each lixiviant wash was followed by a thorough water wash.

Further characterisation studies were performed on the resultant UPT-char for increased comparison with CB N330. A compositional study showed illustrated conformity between the ash content as measured by the furnace, and the inorganics content. The acid-alkali process reduced the sulphur content within PT-char to 1.13wt.%. The process was able to reduce the initial average PT-char particle size from 153.2-130.6μm; however, the UPT-char had a much larger particle size than CB N330, which was, on average, 38.5μm. The process significantly enhanced the BET surface area of the PT-char from 58.9-84.7$m^2.g^{-1}$, while the BET surface area of CB N330 analysed to be 80.22$m^2.g^{-1}$. It has been hypothesised that the large particle size and large surface area may show the formation of large clusters of carbon black with increased interstitial spacing due to the removal of impurities. The widespread particle size distribution is attributed to the large array of carbon black series within the WT-pyrolysis feed and, thus, within crude PT-char.

In final conclusion, the acid-alkali process is able to render crude PT-char purity comparable to that of CB N330 by removing a large mass of sulphur and ash. Furthermore, the process is able to increase the surface area to that of an active carbon; however, although reducing the particle size, it is unable to render the particle size lower than 50μm, which is required for use as tyre filler. It is recommended that the particle structure of the current upgraded char product be analysed and tested within a tyre so as to see the reinforcing ability of the product, and deduce if further processing is required, particularly with regards to a particle size reduction process or a particle size separation process.

Chapter 6: Process Design & Economic Analysis of Pyrolytic Tyre Char Acid-alkali Demineralisation

6.1. PT-char acid-alkali demineralisation process design and economic analysis: study description

Within the previous chapters, this particular research has produced an experimental method for upgrading PT-char, fabricating a product with characteristics comparable to that of CB N330. An economic analysis on the proposed PT-char demineralisation process will enable the evaluation of the financial impact of a new or existing process, provided certain technical data is available [192].

In this study section, an industrial process will be proposed based on the experimental outcomes of the PT-char acid-alkali demineralisation formula previously explored in chapter 4 and chapter 5. The process design will include a relevant process flow diagram (PFD), complete mass balance, equipment description of major process units[62], and a process flow Gantt chart. Furthermore, based on the major equipment specifications, manufacturing costs and revenue, a preliminary design estimate will be performed so as to estimate the process profitability. The investment viability will be optimised by ensuring the NPV is positive and IRR is greater than 9.4% through the optimisation of high impact factors. A sensitivity analysis will be performed to analyse the risk associated with an increase or decrease in the high impact factors.

6.2. PT-char acid-alkali demineralisation process design and economic analysis: study substantiation

Previous chapters within this study have proposed an acid-alkali demineralisation method which is able to upgrade PT-char by increasing the surface area and reducing the ash content to meet specific carbon black standards. Using this foundation research, an industrial process can be designed in order to perform an economic analysis so as to gain insight into the profitability and investment viability of the project.

---

[62] Excluding pipe design

6.3. PT-char acid-alkali demineralisation process design and economic analysis: study objective ii.

To analyse the economic viability and appeal of the proposed crude pyrolytic tyre char upgrading process.

6.4. Discussion of PT-char acid-alkali demineralisation proposed process design and economic analysis

6.4.1. Process design

The PFD, as illustrated in figure 36, shows the flow of mass from left to right as the raw PT-char is upgraded to useful CB. As described by the experimental results of chapter 5, a batch process consisting of three hot NaOH washes followed by one hot HCl wash in series is required to remove all but 1.83wt.% ash from raw PT-char.

Each lixiviant wash is followed by a water wash. Process units T-1, T-2, T-3 and V-8 are distillation columns and neutralisation vessel, forming part of the NaOH, HCl and H2O recycling plant. It must be noted they have not been designed due to lack of technical information; however, they have been added to the PFD for process inclusiveness. It is recommended that further research be focussed on the recycling of lixiviants and water.

The entire process flow is aimed at simplicity. Firstly, as a supply specification, the feed PT-char provided must be free of any steel wires. Before the raw PT-char enters the first reactor, large particles must be removed. The process is unable to reduce large particles to an acceptable size, thus undesirably increasing the final particle size distribution. The solids within the process are transported using screw conveyors. Given that the solid particles are encased within the conveyor, there is minimal mass loss, thus increasing overall yield and decreasing the probability of a dust explosion since the PT-char particles easily able to elute into the surrounding atmosphere.

The NaOH and HCl feeds are both heated to their required temperatures of 88°C and 80°C using heated process water and plate heat exchangers. Plate heat exchangers are the preferred means of corrosive acid and alkali heating as the plates are easily removed and maintained, and the heaters are efficient.

All liquids are pumped using centrifugal pumps since large head is not required, the fluids are not highly viscous, and centrifugal pumps are associated with low capital costs and are easily maintained.

The reactors in which the extraction occurs are agitated Nutsche filter dryers, surrounded by a heating jacket. Nutsche filter dryers are process units which have the combined ability of a CSTR[63], a filter and a dryer. The combination of three major process units in one enables extensive capital savings. Additionally, the agitator is able to increase the filter cake movement, thus increasing the drying efficiency by increasing the contact area between the solids and the hot jacketed surface, as well as the drying air.

Vessels V-5, V-6 and V-7 are equalization tanks used to minimise control fluctuations and store liquid feed to the lixiviant/water recycling plant.

The flow summary of each stream shown in appendix O. The composition of each stream is described as kg/batch processed. The mass balance is based on the process specifications expressed in table 52. As previously said, the process specifications are largely based on the experimental results of chapter 5. No utility streams are illustrated in figure 36 or in appendix O; however, relevant utilities for each major process unit are described in appendix Q and appendix R. An input of 200kg raw PT-char per batch has been assigned for the study. The pressure of each stream is kept as low as possible for increased safety.

The overall process follows a precisely designed schedule, as shown in appendix P. To ensure the equipment is active for most of the time, four extraction stages precede simultaneously.

Table 52: **PT-char acid-alkali demineralisation process specifications**

Process Specification	S.I Unit	Value
PT-char: lixiviant ratio	kg/kg	2: 10
PT-char: water ratio	kg/kg	2: 10
PT-char feed	kg	200
PT-char feed ash content	wt.%	16.11
PT-char feed 'other' content	wt.%	7.28
UPT-char ash content	wt.%	1.83
Overall extraction: R-1	wt.%	8.13
Overall extraction: R-2	wt.%	1.52
Overall extraction: R-3	wt.%	1.11
Overall extraction: R-4	wt.%	8.71
Ash extraction: R-1	wt.%	6.19
Ash extraction: R-2	wt.%	0.95
Ash extraction: R-3	wt.%	1.11
Ash extraction: R-4	wt.%	7.57
'Other' extraction: R-1	wt.%	1.95
'Other' extraction: R-2	wt.%	0.57
'Other' extraction: R-3	wt.%	0.00
'Other' extraction: R-4	wt.%	1.14

---

[63] Continuously stirred tank reactor

Lixiviant removed by filter	wt.%	90.0
Lixiviant removed by water wash	wt.%	10.0
Water removed by filter	wt.%	90.0
Water removed by dryer	wt.%	9.90
Water within PT/ UPT-char output	wt.%	0.10
Lixiviant recycled	%	80.0
Water recycled	%	80.0

Figure 36:   **Process flow diagram of PT-char acid-alkali demineralisation**

6.4.2. Feasibility analysis

Five criteria were chosen to evaluate the feasibility of the project include: net present value (NPV); present value ratio (PVR); cumulative cash ratio (CCR); payback period (PPB); the rate of return on investment (ROROI); and the internal rate of return (IRR). The relevant equations are listed below.

$$NPV = \sum \left(\frac{Net\ Period\ Cash\ Flow}{(1+Rate\ of\ Return)^{Time\ Periods}} \right) - Initial\ Investment \qquad \text{[Equation 22]}$$

$$PVR = \frac{\sum(positive\ present\ values)}{\sum(negative\ present\ values)} \qquad \text{[Equation 23]}$$

$$CRR = \frac{\sum(positive\ cash\ flows)}{\sum(negative\ cash\ flows)} \qquad \text{[Equation 24]}$$

$$PPB = \frac{Initial\ Investment}{Cash\ Inflow\ per\ Period} \qquad \text{[Equation 25]}$$

$$ROROI = \frac{Average\ Annual\ Net\ Profit}{Fixed\ Capital\ Investment} \qquad \text{[Equation 26]}$$

$$IRR = The\ Rate\ of\ Return\ where\ NPV = 0 \qquad \text{[Equation 27]}$$

The positive NPV, which calculated to be ZAR 7 282 106.51, shows that the capital investment would add value to the project. The PVR calculated to be 1.04. This is just above unity, thus indicating that the project will break even and it will be profitable. The CCR of 3.75 further shows that the project has the potential to be profitable, since the ratio is greater than unity. The PBP on the fixed capital investment is 8.79years. The ROROI is 11.29% per annum. The internal rate of return is 9.67%, which shows that the project will attract South African investors if the UPT-char is sold for R21.48/kg (or $1810/t). This price of UPT-char is very high and may not be able to compete in the relevant markets. Table 53 described the criteria used to analyse economic feasibility of the proposed PT-char acid-alkali demineralisation process.

Table 53: **Criteria used to analyse Economic Feasibility**

Net present value	R7 282 106.51
Present value ratio	1.04
Cumulative cash ratio	3.75
Payback period	8.79 years
Rate of return on investment	11.29%
Internal rate of return	9.67%

6.4.3. Sensitivity analysis

The establishment of a process has risk associated with inflation, and supply and demand factors. A sensitivity analysis allows for the examination of such risks, including cost deviations in electricity, water, HCl, NaOH, labour, and UPT-char prices. These factors were chosen to be analysed for specific reasons. Firstly, the availability of electricity, produced by coal, and water are of great concern not only in South Africa, but worldwide, as they are finite resources. Finite resources are associated with price increases. The costs of HCl and NaOH raw materials, as well as the price of UPT-char product are directly influenced by the fluctuating price of commodities, such as fuel and oil reserves. Labour costs are affected by many factors, such as ability efficiency, unions and legislation; and fluctuation in labour costs, particularly in South Africa, occurs frequently.

The degree to which each factor affects the profit and NPV of the above proposed design is analysed using the slope of a fitted trendline. The sensitivity analysis results are illustrated in table 54. As can be seen by the largest trendline slope, in UPT-char price has the largest impact on NPV and profit; whereas alterations in electricity costs will have the lowest impact on project NPV and profit. The positive slope of UPT-char price shows that it has a direct influence on profit and NPV, while the negative slopes show the respective factor is inversely proportional to NPV and profit. Refer to appendix T for all graphical representation of sensitivity analyses.

Table 54:   **Sensitivity Analysis Results**

	Trendline Slope		Correlation Coefficient (R^2)	
	NPV	**Profit**	**NPV**	**Profit**
Electricity Costs	-6.71E+05	-1.26E+04	1	1
Water Costs	-5.88E+04	-1.10E+03	1	1
HCl Costs	-7.72E+04	-1.44E+03	1	1
NaOH Costs	-2.32E+05	-4.33E+03	1	1
Labour Costs	-2.83E+04	-5.30E+02	1	1
UPT-char Price	7.85E+05	1.39E+04	0.9971	1

6.5. Conclusions and recommendations of PT-char acid-alkali demineralisation process design and economic analysis

The objective of this research section was to develop an industrial process based on the previously established acid-alkali demineralisation process, with further economic analyses performed. The acid-alkali demineralisation process consisted of 3x 5.0M NaOH washes at 88°C for 60minutes followed by 1x 1.0M HCl at 60°C for 20minutes. The quantity of lixiviant used for each wash was

100g; while the 20g PT-char which was initially used, slowly decreased after each wash. Each lixiviant wash was followed by a thorough water wash.

A process flow diagram was established with major process units including storage vessels, plate heat exchangers, screw conveyors, agitated Nutsche filter dryers, centrifugal pumps and a sieve. The specifications of each process unit were calculated, allowing for an informative estimate of the total capital cost required to establish an acid-alkali demineralisation process on a pre-existing WT-pyrolysis plant. Using CEPCI forecasting, the total module cost estimated to be ZAR 37.62 million.

The overall production expenditure included annual utility costs (ZAR 3.56 million/year), annual labour costs (ZAR 4.24 million/year), raw material costs (ZAR 6.43 million/year) and annual maintenance and repair costs (ZAR 2.66 million/year). The overall production cost, thus, approximated to be ZAR 16.89million/year. The revenue produced by UPT-char sales is ZAR 21.48/kg, allowing an annual cash flow of ZAR 7.28million/year, with a tax rate of 28% included.

The NPV (ZAR 7.28 million), the PVR (1.04), the CCR (3.75) the PPB (8.79years) and the ROROI (11.29%) show that this particular 28 year project cannot be eliminated as unprofitable, however, investment in the project is not highly appealing since the PPB is high and the ROROI is low. The 9.67% IRR is appealing to South African investors if the UPT-char is sold for R21.48/kg (or $1810/t).

UPT-char must be sold for a very high price in order to render this project economically appealing to investors. However, this high price may render the UPT-char unable to compete in the relevant markets. The proposal of bylaws, which require tyre manufacturers to include a portion of UPT-char in their recipes, may be required to support this project and promote tyre recycling.

Chapter 7: Ultimate Conclusions & Recommendations for Future Research

7.1. Summary of research findings

The research statement, as described in section 1. 2, is "The current char produced by waste tyre pyrolysis is crude and has minimal market value or use which, in turn, reduces waste tyre pyrolysis sustainability and waste tyre recycling efforts".

The study consisted of three stages: the first stage included a thorough research survey; the second stage consisted of process and product development; while the third stage involved the design of an industrial process with a further economic analysis.

The research stage of this study included a thorough literature survey on waste tyre pyrolysis, the characteristics of pyrolytic tyre char, and processes by which pyrolytic tyre char can be upgraded. The analysis demonstrated that pyrolysis is a promising process by which waste tyres can be recycled. The products emerging from waste tyre pyrolysis have the potential to be greatly valuable, however, further processing is required. Pyrolytic tyre char, in particular, is a highly carbonaceous solid originating from the carbon black filler within tyres, constituting approximately 40% of the product mass produced by waste tyre pyrolysis. Pyrolytic tyre char has the potential to be upgraded to carbon black with the final objective of recycling it back into a tyre, thus completing the cradle-to-grave lifecycle of carbon black within a tyre. However, pyrolytic tyre char is highly contaminated, with contaminants consisting predominantly of ash and sulphur; however, its physical characteristics such as surface area and particle size further decrease its value and utility. The ash contains both metallic components as well as a highly stable silicon/ silicon dioxide portion. Many authors have successfully reduced the ash content within pyrolytic tyre char by means of solvent extraction (leaching) using acids or alkalis. However, the authors have utilised extreme extraction conditions, and have not focused on the demineralisation process itself, but rather their particular subsequent process, such as activation. Additionally, no authors have aimed at producing tyre carbon black from pyrolytic tyre char. In summation, the objective is to create a carbon black product from crude pyrolytic tyre char through acid-alkali leaching for the establishment of a cradle-to-cradle lifecycle of carbon black in tyres.

With the target product and upgrading process established, the experimental product and process development was the next research stage. Through a thorough characterisation of two crude

pyrolytic tyre chars (X and Y) and carbon black N330 supplied by the South African industry, the benchmark targets were established.

The study showed that crude pyrolytic tyre char produced 27.50MJ/kg when combusted, thus implying that it is able to be utilised as a solid fuel since it produces more energy than coal, which generates approximately 25.52MJ/kg during combustion.

Compositional studies analysed the organic, inorganic and volatile content within both pyrolytic chars and carbon black N330. The presence of 64.7wt.% volatile content confirmed that pyrolytic tyre char Y had not undergone complete pyrolysis. Furthermore, pyrolytic tyre char X had an organic hydrogen content of less than 1wt.% and a volatile content of 1.38wt.%, thus showing that it had undergone complete pyrolysis. Pyrolytic tyre char X was utilised for further experimentation within this study, while pyrolytic tyre char Y was dismissed. A comparison of the ash contents within pyrolytic tyre char X (16.24wt.%) and CB N330 (1.95wt.%) show that approximately 14.29wt.% ash must be removed from PT-char X in order to meet the target quality of CB N330. A further mineralogical study showed that the inorganic (ash) composition consisted predominantly of iron, silicon/ silicon dioxide, sodium and calcium; with approximately half the ash content dominated by a mixture of silicon and silicon dioxide, and the rest consisting of metals.

The structure of tyre carbon black is an important factor with regards to tyre reinforcement and the adhesion with the surrounding elastomers. Characterisation studies showed that upgrading pyrolytic tyre char X to a carbon black product would require the BET surface area to increase from $58.9m^2.g^{-1}$ to $80.22m^2.g^{-1}$, and a reduction in average particle size from 153.2-38.5µm.

With the benchmark properties of ash reduction from 16.24-1.95wt.%, surface area increase from $58.9-80.22m^2.g^{-1}$ and particle size reduction from 82.1-38.5µm established, process development was the next research stage. The process was developed to target the ash content within pyrolytic tyre char X since, according to authors; a reduction in ash allows for an increase in surface area. The ash consists of two types of components, namely metals and silicon/ silicon dioxide. Unless amphoteric in nature, the acidic or basic nature of the ash components render them reactive with either an acid or a base; therefore a combined acid-alkali demineralisation process is required, as additionally discussed by authors. In order to establish which lixiviant was most superior, a screening study was performed to analyse all the acids and alkalis discussed in literature with regards to pyrolytic tyre char demineralisation. The screening study included an analysis of the characteristics of each respective lixiviant, their demineralisation, or ash-removal, capacity and their raw material costs. The screening results proved that hydrochloric acid and sodium hydroxide were the most cost effective lixiviants. Nitric acid and sulphuric acid proved to be promising alternatives however, not as

superior as hydrochloric acid. Additionally, sequential extraction using an acid followed by sodium hydroxide was successful in reducing a large amount of ash from pyrolytic tyre char.

Since hydrochloric acid and sodium hydroxide proved to be superior during the screening study, they were used in further process development experimental studies. In order to analyse the effect of lixiviant concentration, extraction temperature and extraction time on ash extraction, kinetic studies performed. The kinetics of each system showed similar trends, with fast initial extraction rates, followed substantial reaction rate deceleration after approximately 5 minutes. Each system was governed by the interfacial chemical reaction control mechanism. In an HCl system, an increase in concentration resulted in greater ash extraction in comparison to a temperature increase. This is attributed to the strength of hydrochloric acid. The kinetics of a NaOH extraction system revealed that the system must first have enough energy, in the form of heat, for the reaction and extraction to occur, after which an increase in concentration will increase ash extraction further. The kinetic experiments showed that extraction times of 20minutes and 60minutes for hydrochloric acid and sodium hydroxide were optimal. Furthermore, at the selected extraction times, extraction temperatures of 60°C and 88°C for hydrochloric acid and sodium hydroxide were superior. Finally, using sequential extractions at these extraction times and temperatures, the lixiviant concentrations and wash requirements were determined: 1x 1.0M hydrochloric wash at 60°C for 20minutes and 3x 5.0M NaOH washes at 88°C for 60minutes were required. The wash sequence was, thereafter, determined to be 3x NaOH washes followed by 1x HCl wash, with thorough water washes between each lixiviant wash. Additionally, each lixiviant wash consisted of 100g lixiviant; which the C:L ratio slowly decreased from 20:100 (g/g) as ash was removed from the PT-char. The process was able to extract 81.8wt.% ash content from the pyrolytic tyre char.

Product development was the next research stage, with the aim to reduce the ash within pyrolytic tyre char X utilising the established acid-alkali demineralisation process. The process, however, was only able to reduce 81.8wt.% ash, and the required benchmark is 87.51wt.%, therefore the process was enhanced. The extraction temperature of the hydrochloric acid wash increased to 80°C, which proved sufficient as the resultant upgraded pyrolytic tyre char had an ash content of1.83wt.%, which is lower than the carbon black N330 benchmark of 1.95wt%. The entire process extracted 6.19wt.%, 0.95wt.%, 1.11wt.% and 7.57wt% during the first, second, third and fourth wash respectively. Similarly, the total mass extracted during each consecutive wash tested to be 8.13wt.%, 1.52wt%, 1.11wt.%, and 8.7wt.%. The final acid-alkali demineralisation process, thus, included 3x 5.0M NaOH washes at 88°C for 60minutes followed by 1x 1.0M HCl at 80°C for 20minutes. Characterisation of the upgraded pyrolytic tyre char showed that the acid-alkali demineralisation process was able to

increase the carbon content of pyrolytic tyre char to 98.47wt.%, which is in conformity to that of carbon black N330, which is 97.05wt.%. Furthermore, that the acid-alkali process reduced the sulphur content within pyrolytic tyre char to 1.13wt.%. The characterisation study confirmed the reduction in initial average pyrolytic tyre char particle size from 153.2-130.6μm; however, the upgraded char had a much larger particle size than CB N330, which was, on average, 38.5μm. The particle size distribution is widespread, due to the large spectrum of carbon black species within the waste tyre pyrolysis feed and, thus, within the pyrolytic tyre char. Furthermore, the process significantly enhanced the BET surface area of the pyrolytic tyre char from 58.9-84.7$m^2.g^{-1}$, with the carbon black BET surface area benchmark being 80.22$m^2.g^{-1}$. The increase in surface area is partially attributed to particle size reduction, but greatly accredited to the removal or inorganic (ash) impurities. Impurity removal increases the interstitial spacing between the carbon black particles, allowing for an increase in surface area rather than particle size. The interstitial space increase allows for the formation of large clusters of CB particles. It is unclear how the large particle size and surface area will affect adhesion with elastomers when utilised as tyre filler.

Finally, with the process and product developed, an economic analysis was performed. A process flow diagram based on he established acid-alkali demineralisation process, was designed with major process units including storage vessels, plate heat exchangers, screw conveyors, agitated Nutsche filter dryers, centrifugal pumps and a sieve. Using CEPCI forecasting, the total module cost estimated to be ZAR 37.62 million. The overall production expenditure, which included utility, raw material, labour and maintenance and repair costs, calculated to be ZAR 16.89 million/year with a tax rate of 28% included. The NPV (ZAR 7.28 million), the PVR (1.04), the CCR (3.75), the PPB (8.79years), the ROROI (11.29%), and the IRR (9.67%) show that this particular 28 year project cannot be eliminated as unprofitable, however, investment in the project is not highly appealing since this high UPT-char price (R21.48/kg) may render the UPT-char unable to compete in the relevant markets. Additionally, the PPB is high and the ROROI is low.

7.2.   General conclusions

In final conclusion, a baseline process consisting of three sodium hydroxide (5.0M, 88°C, 60min) washes followed by one hydrochloric acid (1.0M, 80°C, 20min) wash was able to reduce the ash content within crude pyrolytic tyre char and increase the surface area so as to render the upgraded pyrolytic char an active carbon black with properties similar to that of carbon black N330. The process reduces the particle size of crude pyrolytic tyre char; however, the upgraded char has a much larger average particle size than that of carbon black N330, with a widespread particle size distribution. The large particle size and high surface area shows that the removal of inorganic

impurities, or ash, has caused an increase in interstitial spacing between the particles. This further allows for carbon black cluster formation. The widespread particle size distribution is caused by the wide variety of carbon black species within the tyre crumb feed of waste tyre pyrolysis, and, thus, within crude pyrolytic tyre char. It is uncertain as to how the structure of the upgraded pyrolytic tyre char will affect the reinforcing within the tyre, however, the low ash content and large surface area are promising attributes. Particle size reduction or separation processes may resolve possible problems caused the large particle size and particle size distribution.

The economics of an industrially implemented process based on the current process shows that it cannot be eliminated as unprofitable; however investment in the project is not highly appealing. The high price at which the upgraded tyre char must be sold for to render the project attractive to investors may render it unable to compete within the market.

7.3.   Recommendations for further research

This research study lends itself to a number of future investigations that could be undertaken, as described below.

It is recommended that the current acid-alkali process be optimised. This could include the optimisation of each process variable, particularly lixiviant concentration and temperature, of each lixiviant wash. This will reduce the raw material expenditure in an industrially implemented process. Furthermore, it would be economically beneficial if the number of sodium hydroxide washes were to be reduced. Studies have utilised sodium hydroxide solution at high temperature, therefore, there an increase in temperature may allow for the reduction in sodium hydroxide washes. Additionally, including an economic analysis in the process optimisation will be greatly beneficial, with regards to raw material and fixed capital costs.

Further studies regarding the extract phase purification must be fulfilled as the process economics require lixiviant recycling since the raw material costs are high. This will lead to environmental benefits as the waste produced is toxic as it contains heavy metals. Additionally, there may be opportunity for income creation as the ash contains a large portion of silicon dioxide and iron. Additional studies should focus on the gases released during the extraction process as purification equipment, such as scrubbers, may be required.

The final, upgraded product has acceptable ash content and surface area; however its particle size is much larger in comparison to commercial carbon blacks. The large particle size may impede the reinforcing ability within the tyre; however, the increased interstitial surface area may increase the

reinforcing ability. It is recommended that the particle structure of the current upgraded char product be analysed and tested within a tyre so as to see the reinforcing ability of the product, and deduce if further processing is required, such as a particle size reduction process or a particle size separation process, such sieving.

For industrial implementation, a process scale-up is required. It is recommended that, after complete process analysis and optimisation is concluded, the process be scaled-up, if economically viable.

Although the principle aim of this project was to produce carbon black from crude pyrolytic tyre char, the upgraded char may have promising alternative applications, and research into these applications may be beneficial to other relevant projects. Another approach which could show promise is the production of carbon black from tyre derived oil.

Chapter 8: Bibliography

[1]   J. D. Martínez, N. Puy, R. Murillo, T. García, M. V. Navarro, and A. M. Mastral, "Waste tyre pyrolysis – a review," *Renew. Sustain. Energy Rev.*, vol. 23, pp. 179–213, Jul. 2013.

[2]   B. Danon, P. Van Der Gryp, C. E. Schwarz, and J. F. Görgens, "A review of dipentene (dl-limonene) production from waste tire pyrolysis," *J. Anal. Appl. Pyrolysis*, 2015.

[3]   J. Pilusa, M. Shukla, and E. Muzenda, "Economic Assessment of Waste Tyres Pyrolysis Technology: A Case study for Gauteng Province, South Africa," *Int. J. Res. Chem. Metall. Civ. Eng.*, vol. 1, no. 1, pp. 41–49, 2014.

[4]   N. Nkosi, E. Muzenda, J. Zvimba, and J. Pilusa, "The waste tyre problem in South Africa : an analysis of the REDISA Plan," 2013.

[5]   C. Roy, A. Chaala, and H. Darmstadt, "The vacuum pyrolysis of used tires end-uses for oil and carbon black products," *J. Anal. Appl. Pyrolysis*, vol. 51, pp. 201–221, 1999.

[6]   T. Amari, N. J. Themelis, and I. K. Wernick, "Resource recovery from used rubber tires," *Resour. Policy*, vol. 25, no. 3, pp. 179–188, 1999.

[7]   M. L. Mahlangu, "Waste tyre management problems in South Africa and the possible opportunities that can be created through the recycling thereof," University of South Africa, South Africa, 2009.

[8]   E. L. K. Mui, D. C. K. Ko, and G. McKay, "Production of active carbons from waste tyres: a review," *Carbon N. Y.*, vol. 42, no. 14, pp. 2789–2805, Jan. 2004.

[9]   P. R. Shakya, P. Shrestha, C. S. Tamrakar, and P. K. Bhattarai, "Studies on potential emission of hazardous gases due to uncontrolled open-air burning of waste vehicle tyres and their possible impacts on the environment," *Atmos. Environ.*, vol. 42, pp. 6555–6559, 2008.

[10]   J. L. Reisman, "Air emissions from scrap tire combustion: United States National Risk Management Environmental Protection Research Laboratory Report OH 45268," Agency Cincinnati, 1997.

[11]   S. Perry, R. H. Perry, D. W. Green, and J. O. Maloney, "Gasification," in *Perry's Chemical Engineers' Handbook, 7th Edition*, 7th ed., R. H. Perry, Ed. McGraw-Hill, 1997, pp. 25–94.

[12]   T. P. Wampler, "Analytical Pyrolysis: an overview," in *Applied Pyrolysis Handbook*, 2nd ed., T. P. Wampler, Ed. Boca Raton: CRC Press, 2006, p. 1.

[13]   M. Ryms, K. Januszewicz, W. M. Lewandowski, and E. Klugmann-Radziemska, "Pyrolysis process of whole waste tires as a biomass energy recycling," *Ecol. Chem. Eng. S*, vol. 20, no. 1, pp. 93–107, Jan. 2013.

[14]   N. Antoniou, G. Stavropoulos, and A. Zabaniotou, "Activation of end of life tyres pyrolytic char for enhancing viability of pyrolysis – Critical review , analysis and recommendations for a hybrid dual system," *Renew. Sustain. Energy Rev.*, vol. 39, pp. 1053–1073, 2014.

[15]   G.-G. Choi, S.-H. Jung, S.-J. Oh, and J.-S. Kim, "Total utilization of waste tire rubber through pyrolysis to obtain oils and CO2 activation of pyrolysis char," *Fuel Process. Technol.*, vol. 123, pp. 57–64, Jul. 2014.

[16]   S. Ucar, S. Karagoz, A. R. Ozkan, and J. Yanik, "Evaluation of two different scrap tires as hydrocarbon source by pyrolysis," *Fuel*, vol. 84, no. 14–15, pp. 1884–1892, Oct. 2005.

[17]   B. Rodgers and W. Waddell, "Tire engineering," in *The Science and Technology of Rubber, ed. V*, 2013, pp. 619–661.

[18]   C. Woolard, "Presentation: What makes a tyre." Stellenbosch, South Africa, 2014.

[19]   P. T. Williams, "Pyrolysis of waste tyres: a review.," *Waste Manag.*, vol. 33, no. 8, pp. 1714–28, Aug. 2013.

[20]   D. T. Norman, "Rubber grade carbon blacks," *Witco Corporation, Concarb Division Houston, Texas*. [Online]. Available: http://www.continentalcarbon.com/pdfs/What_Is_Carbon_Black.pdf. [Accessed: 15-May-2014].

[21]   C. M. Long, M. A. Nascarella, and P. A. Valberg, "Carbon black vs. black carbon and other airborne materials containing elemental carbon: physical and chemical distinctions," *Environ. Pollut.*, vol. 181, pp. 271–86, Oct. 2013.

[22]   P. Ariyadejwanich, W. Tanthapanichakoon, P. Japthong, K. Nakagawa, S. R. Mukai, and H. Tamon, "Adsorption-desorption characteristics of phenol and reactive dyes from aqueous solution on mesoporous activated carbon prepared from waste tires.," *Water Res.*, vol. 39, no. 7, pp. 1347–53, Apr. 2005.

[23]   P. Ariyadejwanich, W. Tanthapanichakoon, K. Nakagawa, and S. R. Mukai, "Preparation and characterization of mesoporous activated carbon from waste tires," *Carbon N. Y.*, vol. 41, pp. 157–164, 2003.

[24]   D. M. Money and G. Harrison, "Liquefaction of scrap automobile tyres in different solvents and solvent mixes," *Fuel*, vol. 78, no. 14, pp. 1729–1736, 1999.

[25]   Eskom, "Request for proposal GEN 3198 - appendix A: goods information." [Online]. Available: mp2mas17.eskom.co.za/tenderbulletin/File_Show.asp?ID=17333 .

[26]   J. Yang and C. Roy, "A new method for DTA measurement of enthalpy change during the pyrolysis of rubbers," *Thermochim. Acta*, vol. 288, pp. 155–168, 1996.

[27]   Cheung K-Y, Lee K-L, Lam K-L, Chan T-Y, Lee C-W, and Hui C-W, "Operation strategy for multi-stage pyrolysis," *J. Anal. Appl. Pyrolysis*, vol. 48, pp. 10222–33, 2011.

[28]   J. Rezaiyan and N. P. Cheremisinoff, *Gasification technologies: a primer for engineers and scientists*. CRC Press, 2005.

[29]   C. Yin, "Microwave-assisted pyrolysis of biomass for liquid biofuels production.," *Bioresour. Technol.*, vol. 120, pp. 273–84, Sep. 2012.

[30]   R. Helleur, N. Popovic, M. Ikura, M. Stanciulescu, and D. Liu, "Characterization and potential applications of pyrolytic char from ablative pyrolysis of used tires," *J. Anal. Appl. Pyrolysis*, vol. 58–59, pp. 813–824, Apr. 2001.

[31]   H. Pakdel, D. M. Pantea, and C. Roy, "Production of dl-limonene by vacuum pyrolysis of used tires," *J. Anal. Appl. Pyrolysis*, vol. 57, pp. 91–107, 2001.

[32]   J. Scheirs and W. Kaminsky, *Feedstock recycling and pyrolysis of waste plastics: converting waste plastics into diesel and other fuels*. John Wiley & Sons, Limited, 2006.

[33]   M. Bernardo, N. Lapa, M. Gonçalves, B. Mendes, F. Pinto, I. Fonseca, and H. Lopes, "Physico-chemical properties of chars obtained in the co-pyrolysis of waste mixtures.," *J. Hazard. Mater.*, vol. 219–220, pp. 196–202, Jun. 2012.

[34]   O. S. Chan, W. H. Cheung, and G. McKay, "Preparation and characterisation of demineralised tyre derived activated carbon," *Carbon N. Y.*, vol. 49, no. 14, pp. 4674–4687, Nov. 2011.

[35]   Li S-Q, Yao Q, Chi Y, Yan J-H, and Cen K-F, "Pilot-scale pyrolysis of scrap tires in a continuous rotary kiln reactor," *Ind. Eng. Chem. Res.*, vol. 43, pp. 5133–45, 2004.

[36]   P. T. Williams, R. P. Bottrill, and A. M. Cunliffe, "Combustion of tyre pyrolysis oil," *Trans. Inst. Chem. Eng.*, vol. 76, pp. 291–301, 1998.

[37]   M. Banar, V. Akyildiz, A. Ozkan, Z. Cokaygil, and O. Onay, "Characterization of pyrolytic oil obtained from pyrolysis of TDF (Tire Derived Fuel)," *Energy Convers. Manag.*, vol. 62, pp. 22–30, 2012.

[38]   D. Bunthid, P. Prasassarakich, and N. Hinchiranan, "Oxidative desulfurization of tire pyrolysis naphtha in formic acid/H2O2/pyrolysis char system," *Fuel*, vol. 89, no. 9, pp. 2617–2622, Sep. 2010.

[39]   R. Cypres and B. Bettens, "Production of benzoles and active carbons from waste rubber and plastic materials by means of pyrolysis with simultaneous postcracking," in *Pyrolysis and Gasification*, G. L. Ferrero, K. Maniatis, A. Buekens, and A. V. Bridgwater, Eds. London: Elsevier Applied Science, 1989, pp. 209–229.

[40]   X. Zhang, T. Wang, L. Ma, and J. Chang, "Vacuum pyrolysis of waste tires with basic additives," *Waste Manag.*, vol. 28, pp. 2301–10, 2008.

[41]   M. Kyari, A. Cunliffe, and P. T. Williams, "Characterization of oils, gases, and char in relation to the pyrolysis of different brands of scrap automotive tires," *Energy Fuel*, vol. 19, pp. 115–73, 2005.

[42]   A. G. Buekens, "Some observations on the recycling of plastics and rubber," *Conserv. Recycl.*, vol. 1, no. 3–4, pp. 247–71, 1977.

[43]   M. M. Barbooti, T. J. Mohamed, A. A. Hussain, and F. O. Abas, "Optimization of pyrolysis conditions of scrap tires under inert gas atmosphere," *J. Anal. Appl. Pyrolysis*, vol. 72, pp. 165–170, 2004.

[44] J. A. Conesa, R. Font, and A. Marcilla, "Gas from the pyrolysis of scrap tires in a fluidised bed reactor," *Energy and Fuels*, vol. 10, pp. 134–140, 1996.

[45] M. R. Islam, H. Haniu, and M. R. . Beg, "Liquid fuels and chemicals from pyrolysis of motorcycle tire waste: product yields, compositions and related properties," *Fuel*, vol. 87, pp. 3112–3122, 2008.

[46] G. Lopez, M. Olazar, R. Aguado, and J. Bilbao, "Continuous pyrolysis of waste tyres in a conical spouted bed reactor," *Fuel*, vol. 89, pp. 1946–52, 2010.

[47] J. Conesa, I. Martian-Gulloan, R. Font, and J. Jauhiainen, "Complete study of the pyrolysis and gasification of scrap tires in a pilot plant reactor," *Environ. Sci. Technol.*, vol. 38, pp. 3189–3194, 2004.

[48] P. T. Williams, S. Bresler, and D. T. Taylor, "Pyrolysis of scrap automotive tyres: the influence of temperature and heating rate on product composition.," *Fuel*, vol. 69, no. 1474–82, 1990.

[49] O. Senneca, P. Salatino, and R. Chirone, "A fast heating-rate thermogravimetric study of the pyrolysis of scrap tyres," *FUEL*, vol. 78, pp. 1575–1581, 1999.

[50] S. Ogasawara, M. Kuroda, and N. Wakao, "Preparation of activated carbon by thermal decomposition of used automobile tires," *Ind. Eng. Chem. Res.*, vol. 26, pp. 2552–2560, 1987.

[51] M. Betancur, J. D. Martinez, and R. Murillo, "Production of activated carbon by waste tire thermochemical degradation with CO2," *J. Hazard. Mater.*, vol. 168, pp. 882–7, 2009.

[52] A. Lucchesi and G. Maschio, "Semi-active carbon and aromatics produced by pyrolysis of scrap tires," *Conserv. Recycl.*, vol. 6, no. 3, pp. 85–90, 1983.

[53] G. Lopez, M. Olazar, R. Aguado, G. Elordi, M. Amutio, and M. Artetxe, "Vacuum pyrolysis of waste tires by continuously feeding into a conical spouted bed reactor," *Ind. Eng. Chem. Res.*, vol. 49, pp. 8990–7, 2010.

[54] C. Roy, H. Darmstadt, B. Benallal, and C. Amen-Chen, "Characterization of naphtha and carbon black obtained by vacuum pyrolysis of polyisoprene rubber," *Fuel Process. Technol.*, vol. 50, pp. 87–103, 1997.

[55] H. Aydin and C. Ilkilic, "Optimization of fuel production from waste vehicle tires by pyrolysis and resembling to diesel fuel by various desulfurization methods," *Fuel*, vol. 102, pp. 605–612, 2012.

[56] D. Y. C. Leung, X. L. Yin, Z. L. Zhao, Z. L. Xu, and Y. Chen, "Pyrolysis of tire powder: influence of operation variables on the composition and yields of gaseous product," *Fuel Process. Technol.*, vol. 79, pp. 141–155, 2002.

[57] M. Miranda, F. Pinto, I. Gulyurtlu, and I. Cabrita, "Pyrolysis of rubber tyre wastes: a kinetic study," *Fuel*, vol. 103, pp. 542–552, Jan. 2013.

[58] A. M. Cunliffe and P. T. Williams, "Composition of oils derived from the batch pyrolysis of tires," *J. Anal. Appl. Pyrolysis*, vol. 44, pp. 131–52.

[59]   M. F. Laresgoiti, B. M. Caballero, I. de Marco, A. Torres, M. A. Cabrero, and M. J. Chomon, "Characterization of the liquid products obtained in tyre pyrolysis," *J. Anal. Appl. Pyrolysis*, vol. 71, pp. 917–934, 2004.

[60]   Y. Kar, "Catalytic pyrolysis of car tire waste using expanded perlite," *Waste Manag.*, vol. 31, pp. 1772–1782, 2011.

[61]   R. M. Islam, M. U. Hossain Joardder, M. A. Kader, and M. R. Islam Sarker, "Valorization of solid tire wastes available in Bangladesh by thermal treatment," in *Proceedings of the WasteSafe - 2nd International Conference on Solid Waste Management in the Developing Countries*, 2011.

[62]   E. Aylon, A. Fernandez-Colino, R. Murillo, M. V. Navarro, T. Garcia, and A. M. Mastral, "Valorisation of waste tyre by pyrolysis in a moving bed reactor," *Waste Manag.*, vol. 30, pp. 1200–1224, 2011.

[63]   S. Galvagno, S. Casu, T. Casabianca, A. Calabrese, and G. Cornacchia, "Pyrolysis process for the treatment of scrap tyres: preliminary experimental results," *Waste Manag.*, vol. 22, pp. 917–23, 2002.

[64]   W. Kaminsky, C. Mennerich, and Z. Zhang, "Feedstock recycling of synthetic and natural rubber by pyrolysis in a fluidized bed," *J. Anal. Appl. Pyrolysis*, vol. 85, pp. 334–337, 2009.

[65]   P. T. Williams and A. J. Brindle, "Fluidised bed pyrolysis and catalytic pyrolysis of scrap tyres," *Environ. Technol.*, vol. 24, pp. 921–929.

[66]   X. Dai, X. Yin, C. Wu, W. Zhang, and Y. Chen, "Pyrolysis of waste tires in a circulating fluidized-bed reactor," *Energy*, vol. 26, pp. 385–399, 2001.

[67]   M. Olazar, R. Aguado, M. Arabiourrutia, G. Lopez, A. Barona, and J. Bilbao, "Catalyst effect on the composition of tyre pyrolysis products," *Energy and Fuels*, vol. 22, pp. 2909–16, 2008.

[68]   A. A. Zabaniotou and G. Stavropoulos, "Pyrolysis of used automobile tires and residual char utilization," *J. Anal. Appl. Pyrolysis*, vol. 70, pp. 711–722, 2003.

[69]   A. J. Marshall, "Commercial application of pyrolysis technology in agriculture," 2013. [Online]. Available: http://www.ofa.on.ca/uploads/userfiles/files/pyrolysis report final.pdf. [Accessed: 31-Mar-2014].

[70]   California environmental protection agency and Integrated waste management board, "Technology evaluation and economic analysis of waste tire pyrolysis, gasification and liquefaction." 2006.

[71]   T. Malkow, "Novel and innovative pyrolysis and gasification technologies for energy efficient and environmentally sound MSW disposal," *Waste Manag.*, vol. 20, pp. 848–89, 2006.

[72]   C. Clark, K. Meardon, and D. Russel, "Scrap tire technology and markets," *Environ. Prot. Agency Pacific Environ. Serv.*, 1993.

[73]   R. Murillo, A. Aranda, E. Aylon, and M. S. Callén, "Process for the separation of gas products from waste tire pyrolysis," *Ind. Eng. Chem. Res.*, vol. 45, pp. 1734–8, 2006.

[74]   C. Roy, R. C. Chaala, H. Darmstadt, B. de Caumia, H. Pakdel, and J. Yang, "Conversion of used tires to carbon black and oil pyrolysis. In: De SK, Isayev Al, Khait K, editors. Rubber Recycling.," *CRC Press Taylor Fr. Gr.*, 2005.

[75]   S. Kawakami, K. Inoue, H. Tanaka, and T. Sakai, "Pyrolysis process for scrap tires. IN: J. L. Jones, S. B. Radding (editors) Thermal conversion of solid wastes and biomass," in *American Chemical Society Symposium Series, Vol 130*, 1980, pp. 557–572.

[76]   J. Pilusa and E. Muzenda, "Beneficiation of Pyrolitic Carbon Black," *Int. J. Chem. Nucl. Mater. Metall. Eng.*, vol. 7, no. 10, pp. 392–396, 2013.

[77]   A. M. Cunliffe and P. T. Williams, "Properties of chars and activated carbons derived from the pyrolysis of used tyres," *Environ. Technol.*, vol. 19, no. 12, pp. 1177–1190, Dec. 1998.

[78]   E. Aylon, A. Fernandez-Colino, M. V. Navarro, R. Murillo, T. Garcia, and A. M. Mastral, "Waste tire pyrolysis: comparison between fixed bed reactor and moving bed reactor," *Ind. Eng. Chem. Res.*, vol. 47, pp. 4029–33, 2008.

[79]   G. Lopez, M. Olazar, M. Amutio, R. Aguado, and J. A. Bilbao, "Influence of tire formulation on the products of continuous pyrolysis in a conical spouted bed reactor," *Energy Fuel*, vol. 23, pp. 5423–31, 2009.

[80]   A. Quek and R. Balasubramanian, "Preparation and characterization of low energy post-pyrolysis oxygenated tire char," *Chem. Eng. J.*, vol. 170, no. 1, pp. 194–201, May 2011.

[81]   A. M. Fernandez, C. Barriocanal, and R. Alvarez, "Pyrolysis of a waste from the grinding of scrap tyres," *J. Hazard. Mater.*, vol. 203–204, pp. 236–43, 2012.

[82]   M. Hofman and R. Pietrzak, "Adsorbents obtained from waste tires for NO2 removal under dry conditions at room temperature," *Chem. Eng. J.*, vol. 170, no. 1, pp. 202–208, 2011.

[83]   F. A. Lopez, T. A. Centeno, F. J. Alguacil, and B. Lobato, "Distillation of granulated scrap tires in a pilot plant," *J. Hazard. Mater.*, vol. 190, pp. 285–92, 2011.

[84]   C. Diez, O. Martinez, L. F. Calvo, J. Cara, and A. Moran, "Pyrolysis of tyres: influence of the final temperature of the process on emissions and the calorific value of the products recovered," *Waste Manag.*, vol. 24, pp. 463–9, 2004.

[85]   A. Napoli, Y. Soudais, D. Lecomte, and S. Castillo, "Scrap tyre pyrolysis: are the effluents valuable products," *J. Anal. Appl. Pyrolysis*, vol. 40–41, pp. 373–82, 1997.

[86]   J. F. Gonzalez, J. M. Encinar, J. L. Canito, and J. J. Rodriguez, "Pyrolysis of automobile tyre waste. Influence of operating variables and kinetics study.," *J. Anal. Appl. Pyrolysis*, vol. 79, pp. 141–55, 2001.

[87]   S. Murugan, M. C. Ramaswamy, and G. Nagarajan, "The use of tyre pyrolysis oil in diesel engines," *Waste Manag.*, vol. 28, pp. 2743–49.

[88]   M. Bernardo, N. Lapa, M. Gonçalves, R. Barbosa, B. Mendes, F. Pinto, and I. Gulyurtlu, "Toxicity of char residues produced in the co-pyrolysis of different wastes.," *Waste Manag.*, vol. 30, no. 4, pp. 628–35, Apr. 2010.

[89]   H. Hu, Y. Fang, H. Liu, R. Yu, G. Luo, W. Liu, A. Li, and H. Yao, "The fate of sulfur during rapid pyrolysis of scrap tires," *Chemosphere*, vol. 97, pp. 102–107, 2014.

[90]   M. Kiminori and T. T. Takanohashi, "Extraction of coals with CS2-N-methyl-2- pyrrolidinone mixed solvent at room temperature: effect of coal rank and synergism of the mixed solvent," *FUEL*, vol. 67, pp. 1639–1647, 1988.

[91]   H. Darmstadt, C. Roy, and S. Kaliagljine, "From commercial tire pyrolysis plants," *Carbon N. Y.*, vol. 33, no. 10, pp. 1449–1455, 1995.

[92]   M. Bernardo, N. Lapa, M. Gonçalves, B. Mendes, and F. Pinto, "Study of the organic extraction and acidic leaching of chars obtained in the pyrolysis of plastics, tire rubber and forestry biomass wastes," *Procedia Eng.*, vol. 42, no. August, pp. 1739–1746, Jan. 2012.

[93]   M. Bernardo, M. Gonçalves, N. Lapa, R. Barbosa, B. Mendes, and F. Pinto, "Characterization of chars produced in the co-pyrolysis of different wastes: decontamination study.," *J. Hazard. Mater.*, vol. 207–208, pp. 28–35, Mar. 2012.

[94]   V. K. Gupta, M. R. Ganjali, A. Nayak, B. Bhushan, and S. Agarwal, "Enhanced heavy metals removal and recovery by mesoporous adsorbent prepared from waste rubber tire," *Chem. Eng. J.*, vol. 197, pp. 330–342, 2012.

[95]   C. Giavarini, "Active carbon from scrap tyres," *FUEL*, vol. 64, pp. 1331–1332, 1985.

[96]   A. Undri, B. Sacchi, E. Cantisani, N. Toccafondi, L. Rosi, M. Frediani, and P. Frediani, "Carbon from microwave assisted pyrolysis of waste tires," *J. Anal. Appl. Pyrolysis*, vol. 104, pp. 396–404, Nov. 2013.

[97]   C. Berrueco, E. Esperanza, F. J. Mastral, J. Ceamanos, and P. Garcia-Bacaicoa, "Pyrolysis of waste tyres in an atmospheric static-bed batch reactor: analysis of the gases obtained," *J. Anal. Appl. Pyrolysis*, vol. 74, pp. 245–53, 2005.

[98]   A. Aranda, R. Murillo, T. García, M. S. Callén, and A. M. Mastral, "Steam activation of tyre pyrolytic carbon black: kinetic study in a thermobalance," *Chem. Eng. J.*, vol. 126, no. 2–3, pp. 79–85, Feb. 2007.

[99]   D. Smo, "Heavy metals in fly ash from a coal-fired power station in Poland," *Polish J. Environ. Stud.*, vol. 15, no. 6, pp. 943–946, 2006.

[100]   Minex PTE LTD, "Activated Carbon Products." [Online]. Available: http://www.minex.sg/activatedcarbon.htm. [Accessed: 11-Jun-2014].

[101]   S. Brunauer, P. H. Emmett, and E. Teller, "Gases in multimolecular layers," *Am. Chem. Soc.*, vol. 60, pp. 309–19, 1938.

[102]   M. Streat, J. W. Patrick, and M. J. Comporro Perez, "Sorption of phenol and para-chlorophenol from water using conventional and novel activated carbons," *Water Res.*, vol. 29, no. 2, pp. 467–72, 1995.

[103] H. Teng, Y. Lin, and L. Hsu, "Production of Activated Carbons from Pyrolysis of Waste Tires Impregnated with Potassium Hydroxide," *J. Air Waste Manage. Assoc.*, vol. 50, pp. 1940–1946, Nov. 2000.

[104] N. K. Hamadi, X. Dong, M. M. Farid, and M. G. Q. Lu, "Adsorption kinetics for the removal of chromium (VI) from aqueous solution by adsorbents derived from used tyres and sawdust," *Chem. Eng. J.*, vol. 84, pp. 95–105, 2001.

[105] G. S. Miguel, G. D. Fowler, M. Dall'Orso, and C. J. Sollars, "Porosity and surface characteristics of activated carbons produced from waste tyre rubber," *J. Chem. Technol. Biotechnol.*, vol. 77, no. 1, pp. 1–8, Jan. 2002.

[106] T. A. Brady, M. Rostam-Abadi, and M. Rood, "Applications for activated carbons from waste tires: natural gas storage and air pollution control," *Gas Sep. Purif.*, vol. 10, no. 2, pp. 97–102, 1996.

[107] M. Myhre, S. Saiwari, W. Dierkes, and J. Noordermeer, "Rubber recycling: chemistry, processing, and applications," *Rubber Chem. Technol.*, vol. 85, no. 3, pp. 408–449, Sep. 2012.

[108] J. L. Allen, J. L. Gatz, and P. C. Eklund, "Applications for activated carbons from used tires: butane working capacity," *Carbon N. Y.*, vol. 37, pp. 1485–1489, 1999.

[109] A. M. Cunliffe and P. T. Williams, "Influence of process conditions on the rate of activation of chars derived from pyrolysis of used tires," *Energy Fuels*, vol. 13, no. 1, pp. 166–175, 1999.

[110] C. M. B. Lehmann, M. Rostam-abadi, and M. J. Rood, "Reprocessing and reuse of waste tire rubber to solve air-quality related problems," *Energy Fuels*, vol. 13, pp. 1095–1099, 1998.

[111] J. Sun, T. A. Brady, M. J. Rood, C. M. Lehmann, M. Rostam-abadi, and A. A. Lizzio, "Adsorbed natural gas storage with activated carbons made from Illinois coals and scrap tires," *Energy and Fuels*, vol. 11, pp. 316–322, 1997.

[112] A. A. Merchant and M. A. Petrich, "Pyrolysis of scrap tires and conversion of chars to activated carbon," *Am. Inst. Chem. Eng.*, vol. 39, no. 8, pp. 1370–6, 1993.

[113] A. A. Merchant and M. A. Petrich, "Preparation and characterization of activated carbons from scrap tires, almond shells and illinois coal," *Chem. Eng. Commun.*, vol. 118, pp. 251–63, 1992.

[114] C. I. Sainz-diaz and A. J. Griffiths, "Activated carbon from solid wastes using a pilot-scale batch flaming pyrolyser," *Fuel*, vol. 79, pp. 1863–71, 2000.

[115] H. Teng, M. A. Serio, M. A. Whjtowicz, R. Bassilakis, and P. R. Solomon, "Reprocessing of used tires into activated carbon and other products," *Ind. Eng. Chem. Res.*, vol. 34, pp. 3102–3111, 1995.

[116] A. Chaala, H. Darmstadt, and C. Roy, "Acid-base method for the demineralization carbon black of pyrolytic," *Fuel Process. Technol.*, vol. 46, pp. 1–15, 1996.

[117]   Sonepa, "Carbon black scrap,offgrade, prime, grade: N220, N330, N660, N550, mixed grade,"
2014. [Online]. Available: http://www.sonepa.com/carbon-black.html. [Accessed: 11-Jun-
2014].

[118]   Cancarb, "Physical and chemical properties of carbon black," 2014. [Online]. Available:
http://www.cancarb.com/docs/pdf/Physical_Chemical_Properties.pdf. [Accessed: 11-Jun-
2014].

[119]   J. B. Donnet, R. C. Bansal, and M. J. Wang, *Carbon Black: Science and Technology*, 2nd ed.
New York, USA, 1993.

[120]   New World Encyclopedia, "Activated Carbon," *New World Encyclopedia*, 2012. [Online].
Available: http://www.newworldencyclopedia.org/entry/Activated_carbon. [Accessed: 16-
Sep-2015].

[121]   CAREDDI, "Products / Tire/Plastic Pyrolysis Machine / Semi-Continuous Pyrolysis," 2013.
[Online]. Available:
http://www.careddi.com/Products/Tire_Plastic_Pyrolysis_Machine/Semi_Conti/. [Accessed:
11-Jun-2014].

[122]   A. Ruffini, "Coal compact necessary for SA's electricity sector | ESI-Africa.com," *ESI-
Africa.com*, 2013. [Online]. Available: http://www.esi-africa.com/coal-compact-necessary-for-
sa-s-electricity-sector/. [Accessed: 11-Jun-2014].

[123]   D. Gleason, "Eskom faces coal conundrum | Columnists | BDlive," *Business Day Live*, 2013.
[Online]. Available: http://www.bdlive.co.za/opinion/columnists/2013/09/20/eskom-faces-
coal-conundrum. [Accessed: 11-Jun-2014].

[124]   Evergreen Energy Inc., "Evergreen announces program to develop activated carbon product,"
2011. [Online]. Available: http://www.4-traders.com/news/Evergreen-Announces-Program-
to-Develop-Activated-Carbon-Product--13800148/. [Accessed: 24-Mar-2015].

[125]   N.-N. I. I. Corporation, "Activated carbon production," 2013. [Online]. Available:
http://novinkor.com/en/projects-en/industry-en/38-carbon.html. [Accessed: 11-Jun-2014].

[126]   Peat Resources Limited, "Welcome to peat resources." [Online]. Available:
http://www.peatresources.com/. [Accessed: 24-Mar-2015].

[127]   CP Consultants, "Market study on activated carbon carried out by CP Consultants, New
Delhi," *Bamboo Tech*, 2009. [Online]. Available: http://www.bambootech.org/files/Market
Study .pdf. [Accessed: 16-Sep-2015].

[128]   CABOT Corporation, "Speciality carbon blacks," 2014. [Online]. Available: http://www.cabot-
corp.com/Specialty-Carbon-Blacks/KBase. [Accessed: 11-Jun-2014].

[129]   E. Zhao, "Asia carbon industries, Inc. announces the completion of its speciality carbon black
production facility," *PRNewswire*, 2013. [Online]. Available:
http://www.prnewswire.com/news-releases/asia-carbon-industries-inc-announces-the-
completion-of-its-specialty-carbon-black-production-facility-214127141.html. [Accessed: 11-
Jun-2014].

[130]   The Freedonia Group, "World carbon black industry study with forecasts for 2013 & 2018," *The Freedonia Group*, 2013. [Online]. Available: http://www.freedoniagroup.com/brochure/25xx/2596smwe.pdf. [Accessed: 16-Sep-2015].

[131]   V. K. Gupta, B. Gupta, A. Rastogi, S. Agarwal, and A. Nayak, "Pesticides removal from waste water by activated carbon prepared from waste rubber tire," *Water Res.*, vol. 45, no. 13, pp. 4047–4055, 2011.

[132]   E. J. Henley, J. D. Seader, and D. K. Roper, "Leaching," in *Separation Process Principles*, 3rd ed., John Wiley & Sons, Limited, 2011, pp. 708–726.

[133]   T. Voeste, K. Weber, B. Hiskey, and G. Brunner, "Liquid – Solid Extraction," *Ullmann's Encyclopedia of Industrial Chemistry Vo. 21*. pp. 309–338, 2012.

[134]   J. R. Couper, W. R. Penney, F. J. R, and S. M. Walas, *Chemical Process Equipment: Selection and Design*, 3rd ed. Elsevier, 2012.

[135]   D. Dougherty, M. Fuhrmann, Y. Sanborn, L. Island, and N. E. W. York, "Leaching mechanisms of solidified low-level waste: the literature survey," *Nucelar Waste Res. Gr. - Dep. Nucl. Energy . United States Dep. Energy*, 1985.

[136]   M. S. Silberberg, "Elements in Redox Reactions," in *Principles of General Chemistry*, 2nd ed., New York, USA: McGraw-Hill, 2010, pp. 133–138.

[137]   M. S. Silberberg, "Acid-Base Reactions," in *Principles of General Chemistry*, 2nd ed., New York, USA: McGraw-Hill, 2010, pp. 123–129.

[138]   M. S. Silberberg, "Acids and Bases in Water," in *Principles of General Chemistry*, 2nd ed., New York, USA: McGraw-Hill, 2010, pp. 591–595.

[139]   D. Reger, S. Goode, and D. Ball, "Reactions between acids and bases," in *Chemsitry: Principles and Practice*, 3rd ed., Belmont, USA: Cengage Learning, 2009.

[140]   S. M. Bulatovic, *Handbook of Flotation Reagents: Chemistry, Theory and Practice: Volume 1: Flotation of Sulfide Ores*. Elsevier, 2007.

[141]   M. S. Silberberg, "Appendix D: standard electrode (half cell) potentials," in *Principles of General Chemistry*, 2nd ed., New York, USA: McGraw-Hill Companies, Incorporated, 2007, p. 829.

[142]   "Sodium hydroxide: all reactions." [Online]. Available: http://www.allreactions.com/index.php/group-1a/natrium/sodium-hydroxide. [Accessed: 10-Aug-2015].

[143]   Edurite, "How do Bases React with Metals," *Pearson India Education Services Pvt. Ltd*, 2015. [Online]. Available: http://www.edurite.com/kbase/how-do-bases-react-with-metals. [Accessed: 15-Jul-2015].

[144]   J. Clark, "Acid-base Behaviour of the Period 3 Oxides," *Chemguide*, 2014. [Online]. Available: http://www.chemguide.co.uk/inorganic/period3/oxidesh2o.html. [Accessed: 15-Jul-2015].

[145]   M. S. Silberberg, "Solubility as an Equilibrium Process," in *Principles of General Chemistry*, 2nd ed., New York, USA: McGraw-Hill, 2010, pp. 408–412.

[146]   J. Xue, H. Zhong, S. Wang, C. Li, and J. Li, "Kinetics of reduction leaching of manganese dioxide ore with Phytolacca americana in sulfuric acid solution," *J. SAUDI Chem. Soc.*, 2014.

[147]   V. S. Kislik, "Recent Advances in Solvent Extraction Processes and Techniques," in *Solvent Extraction: Classical and Novel Approaches*, 2012, pp. 483–524.

[148]   Y. Cengel and J. Cimbala, *Essentials of Fluid Mechanics: fundamentals and applications*. New York: McGraw-Hill Companies,Incorporated, 2009.

[149]   H. S. Stoker, "Laminar and turbulent boundary layers," in *General, Organic, and Biological Chemistry*, Shelton: Peoples Medical Publishing House-USA, 2010, pp. 208–209.

[150]   M. Teramoto, S. Tai, K. Nishii, and H. Teranishi, "Effects of pressure on liquid-phase mass transfer coefficients," *Chem. Eng. J.*, vol. 8, no. 3, pp. 223–226, Jan. 1974.

[151]   A. Pasipoularides, "Laminar and Turbulent Boundary Layers," in *Heart's Vortex: Intracardiac Blood Flow Phenomena*, Shelton: Peoples Medical Publishing House - USA, 2009, pp. 208–209.

[152]   G. W. Roberts, "Mechanisms of Diffusion," in *Chemical Reactions and Chemical Reactors*, John Wiley & Sons, 2009, pp. 319–325.

[153]   M. S. Silberberg, "Atomic Structure and Chemical Reactivity," in *Principles of General Chemistry*, 2nd ed., New York: The McGraw Hill Companies, Inc, 2010, pp. 267–273.

[154]   O. Levenspiel, "Fluid-particle Reactions: Kinetics," in *Chemical Reaction Engineering*, III., New York, USA: John Wiley & Sons, 1999, pp. 566–586.

[155]   S. Yagi and D. Kunii, "Fluidized-solids reactors with continuous solids feed - I: Residence time of particles in fluidized beds," *Chem. Eng. Sci.*, vol. 16, no. 3–4, pp. 364–371, 1961.

[156]   S. Yagi and D. Kunii, "Fluidized-solids reactors with continuous solids feed - II: Conversion for overflow and carryover particles," *Chem. Eng. Sci.*, vol. 16, no. 3–4, pp. 372–379, 1961.

[157]   S. Yagi and D. Kunii, "Fluidized-solids reactors with continuous solids feed - III: Conversion in experimental fluidized-solids reactors," *Chem. Eng. Sci.*, vol. 16, no. 3–4, pp. 380–391, 1961.

[158]   A. Sahuquillo, A. Rigol, and G. Rauret, "Overview of the use of leaching/extraction tests for risk assessment of trace metals in contaminated soils and sediments," *Trends Anal. Chem.*, vol. 22, no. 3, pp. 152–159, Mar. 2003.

[159]   R. Murillo, M. V. Navarro, J. M. López, T. García, M. S. Callén, E. Aylón, and a. M. Mastral, "Activation of pyrolytic tire char with CO2: kinetic study," *J. Anal. Appl. Pyrolysis*, vol. 71, no. 2, pp. 945–957, Jun. 2004.

[160]   Y. Shen, P. Zhao, and Q. Shao, "Microporous and Mesoporous Materials Porous silica and carbon derived materials from rice husk pyrolysis char," *Microporous Mesoporous Mater.*, vol. 188, pp. 46–76, 2014.

[161] H. Darmstadt, C. Roy, and S. Kaliaguine, "ESCA characterisation of commerical carbon blacks and of carbon blacks from vacuum pyrolysis of used tires," *Carbon N. Y.*, vol. 32, no. 8, pp. 1399–1406, 1994.

[162] M. Thommes and M. A. Thomas, "Micropore Size Calculations," *Quantachrome Instruments*. [Online]. Available: http://nanonet.rice.edu/research/BET/BET Seminar Part 2 afternoon.ppt. [Accessed: 28-Jun-2015].

[163] A. K. Bhowmick, M. M. Hall, and H. A. Benarey, "Fillers," in *Rubber Products Manufacturing Technology*, New York: Marcel Dekker, Inc., 1994, pp. 68–71.

[164] A. Samanta and R. Gupta, "Production and characterization of ash-free coal from low-rank Canadian coal by solvent extraction," *Fuel Process. Technol.*, vol. 115, pp. 88–98, 2013.

[165] M. H. Makgato, L. J. Moitsheki, L. Shoko, B. L. Kgobane, D. L. Morgan, and W. W. Focke, "Alkali-assisted coal extraction with polar aprotic solvents," *Fuel Process. Technol.*, vol. 90, no. 4, pp. 591–598, 2009.

[166] H. Seki, O. Ito, and M. Iino, "Caking properties of coal residues after extraction with mixed solvents," *Fuel*, vol. 68, no. 7, pp. 837–842, Jul. 1989.

[167] K. Sakanishi, E. Akashi, T. Nakazato, H. Tao, and H. Kawashima, "Characterization of eluted metal components from coal during pretreatment and solvent extraction," vol. 83, pp. 739–743, 2004.

[168] V. Singh, M. K. Purkait, V. K. Chandaliya, P. P. Biswas, P. K. Banerjee, and C. Das, "Development of membrane based technology for the separation of coal from organic solvent," *DES*, vol. 299, pp. 123–128, 2012.

[169] J. Wang, C. Li, K. Sakanishi, T. Nakazato, and H. Tao, "Investigation of the remaining major and trace elements in clean coal generated by organic solvent extraction," vol. 84, pp. 1487–1493, 2005.

[170] W. Wang, Y. Qin, F. Qian, L. Ye, W. Hao, L. Yuan, and F. Jin, "Partitioning of elements from coal by different solvents extraction," *FUEL*, no. February, 2014.

[171] D. Smook, "Removal of mineral material from solvent-refined coal by solvent extractions," *Fuel Process. Technol.*, vol. 88, pp. 795–798, 2007.

[172] A. S. Olawale, "Solid-liquid extraction of oils of African elemi's (Canarium schweinfurthii's) fruit," *Agric. Eng. Int. CIGR J.*, vol. 14, no. 2, pp. 155–160, 2012.

[173] E. Simeonov and V. Koleva, "Solid-liquid Extraction of Tannins from Geranium Sanguineum L . – Experimental Kinetics and Modelling," vol. 26, no. 3, pp. 249–255, 2012.

[174] H. G. Brittain, "Particle-Size Distribution II : Powdered Solids," *Pharm. Technol.*, pp. 67–73.

[175] D. O'Leary, "Sulphuric Acid," *University college Cork, Ireland*, 2000. [Online]. Available: http://www.ucc.ie/academic/chem/dolchem/html/comp/h2so4.html. [Accessed: 03-Aug-2015].

[176] Liquiflo, "Chemical Resistance Chart," *Liquiflo*. [Online]. Available: http://www.liquiflo.com/v2/files/pdf/lit/Chemical_Resistance_Chart.pdf. [Accessed: 01-Sep-2014].

[177] L. Cui, Y. Guo, X. Wang, Z. Du, and F. Cheng, "Dissolution kinetics of aluminum and iron from coal mining waste by hydrochloric acid," *Chinese J. Chem. Eng.*, vol. 23, no. 3, pp. 590–596, Mar. 2015.

[178] P. K. Parhi, K. H. Park, and G. Senanayake, "A kinetic study on hydrochloric acid leaching of nickel from Ni–Al2O3 spent catalyst," *J. Ind. Eng. Chem.*, vol. 19, no. 2, pp. 589–594, Mar. 2013.

[179] E. Olanipekun, "A kinetic study of the leaching of a Nigerian ilmenite ore by hydrochloric acid," pp. 1–10, 1999.

[180] R. T. Yang and K. Das, "Coal demineraiization using sodium hydroxide and acid solutions," *Fuel*, vol. 64, pp. 735–742, 1985.

[181] R. Wang, Y. Zhai, Z. Ning, and P. Ma, "Kinetics of SiO2 leaching from Al2O3 extracted slag of fly ash with sodium hydroxide solution," *Trans. Nonferrous Met. Soc. China*, vol. 24, no. 6, pp. 1928–1936, Jun. 2014.

[182] J. W. Van Der Merwe, C. Strydom, D. C. Odendaal, and M. I. Sampson, "A Comparison of the Effect of Chemical and Bioleaching on the Kinetics of Sphalerite Leaching," in *The Fourth Southern Africa Conference on Base metals*, no. 1999, pp. 211–222.

[183] O. Gerald, N. Christopher, O. Ayebatonworio, and O. Martin, "Comparative Kinetics of Iron Ore Dissolution in Aqueous HCl-HNO 3 System," *J. Miner. Mater. Charact. Eng.*, vol. 2013, no. July, pp. 153–159, 2013.

[184] Y. Cao, S. Harjanto, A. Shibayama, I. Naitoh, T. Nanami, K. Kasahara, Y. Okumura, and T. Fujita, "Kinetic Study on the Leaching of Pt , Pd and Rh from Automotive Catalyst Residue by Using Chloride Solutions," *Mater. Trans.*, vol. 47, no. 8, pp. 2015–2024, 2015.

[185] Y.-S. Ho, H. A. Harouna-Oumarou, H. Fauduet, and C. Porte, "Kinetics and model building of leaching of water-soluble compounds of Tilia sapwood," *Sep. Purif. Technol.*, vol. 45, no. 3, pp. 169–173, Oct. 2005.

[186] V. S. Gireesh, V. P. Vinod, S. Krishnan Nair, and G. Ninan, "Catalytic leaching of ilmenite using hydrochloric acid: A kinetic approach," *Int. J. Miner. Process.*, vol. 134, pp. 36–40, Jan. 2015.

[187] M. Marafi, A. Stanislaus, and E. Furimsky, "Section 7.1.2 Kinetics of Rejuvenation," in *Handbook of Spent Hydroprocessing Catalysts*, 1st ed., Amsterdam: Elsevier, 2010, pp. 207–208.

[188] G. W. Roberts, "Reaction Rates - Some Generalizations," in *Chemical Reactions and Chemical Reactors*, Hoboken: John Wiley & Sons, Inc, 2009, pp. 17–35.

[189] M. S. Silberberg, "Factors that Influence Reaction Rate," in *Principles of General Chemistry*, 2nd ed., New York: The McGraw Hill Companies, Inc, 2010, pp. 508–509.

[190]   M. S. Silberberg, "The Covalent Bonding Model," in *Principles of General Chemistry*, 2nd ed., New York: The McGraw Hill Companies, Inc, 2010, pp. 287–292.

[191]   J. Thomas, "How silicon reacts," in *The Elements: Silicon*, New York: Marshall Cavendish Corporation, 2002, pp. 15–19.

[192]   R. Turton, R. C. Bailie, W. B. Whiting, J. A. Shaeiwitz, and D. Bhattacharyya, *Analysis, Synthesis and Design of Chemical Processes*, 4th ed. New Jersey: Pearson, 2013.

[193]   O. Beaumont and Y. Schwob, "Influence of physical and chemical parameters on wood pyrolysis," *Ind. Eng. Chem. Res. Des. Dev.*, no. 23, pp. 637–641, 1984.

[194]   Y. Chang, "On pyrolysis of waste tire: degradation rate and product yields," *Resour. Conserv. Recycl.*, vol. 17, pp. 125–139, 1996.

[195]   R. Murillo, E. Aylon, M. V. Navarro, M. S. Callen, A. Aranda, and A. M. Mastral, "The application of thermal processes to valorise waste tyres," *Fuel Process. Technol.*, vol. 87, pp. 143–7, 2006.

[196]   M. Olazar, G. Lopez, M. Arabiourrutia, G. Elordi, R. Aguado, and J. Bilbao, "Kinetic modelling of tyre pyrolysis in a conical spouted bed reactor," *J. Anal. Appl. Pyrolysis*, vol. 81, no. 1, pp. 127–132, Jan. 2008.

[197]   R. Sinnot and G. Towler, *Chemical Engineering Design*, 5th ed. Oxford: Elsevier, 2009.

[198]   WageIndicator Network, "Mywage.co.za," 2015. [Online]. Available: http://www.mywage.co.za/main/salary/minimum-wages. [Accessed: 05-Aug-2015].

[199]   IMTE AG Power Consulting Engineers Switzerland, "Higher calorific values for some common fuels a coke , oil , wood , hydrogen and many more," 2005. [Online]. Available: http://www.mrsphoto.net/4-IMTE AG/2-2005-06.pdf. [Accessed: 16-Sep-2015].

[200]   M. Borkowski, "ChemBuddy," *Chembuddy*, 2005. [Online]. Available: http://www.chembuddy.com/?left=BATE&right=dissociation_constants. [Accessed: 02-Feb-2015].

[201]   Brewton-Parker College, "Brewton-Parker College Math & Natural Sciences," *Brewton-Parker College*, 2010. [Online]. Available: http://www.bpc.edu/mathscience/chemistry/table_of_monoprotic_acids.html. [Accessed: 02-Feb-2015].

[202]   M. S. Silberberg, "Precipitation Reactions," in *Principles of General Chemistry*, 2nd ed., New York, USA: McGraw-Hill, 2010, pp. 119–123.

[203]   E. J. Henley, J. D. Seader, and D. K. Roper, "Cascades and Hybrid Systems," in *Separation Process Principles*, 3rd ed., Hoboken: John Wiley & Sons, Inc, 2011, pp. 195–220.

Chapter 9: Appendices

Appendix A: **Mind-map illustrating the unravelling of the research problem and emerging themes**

Current status of PT char	Consideration of PT char as a low value product	Evaluation of enhancing PT char worth	Consideration of UPT char as a high value WT pyrolysis product
•What is it? •What is it used for? •How much is produced? •Price it is sold for? •Is there a market for the raw •Does it influence waste tyre recycling?	•Advantages? •Disadvantages? •Limitations of char? •Do limitations impact largely the selling price and market of char? •Does it need upgrading? •What will happen if not upgraded?	•How to enhance worth of PT char? •Advantages of a process? •Disadvantages of a process? •Will this process effect upstream and downstream processes? •Why does it need upgrading?	•Advantages? •Disadvantages? (limitations) •Does it impact the environment positively? •Does it add value to industry and economics? •Will it influence waste tyre recycling?

Appendix B: **Comprehensive list of ground tyre applications** [7]

- Tyre manufacturing
- Cover material for play grounds
- Synthetic turf
- Industrial flooring
- Soil conditioner
- Synthetic turf
- Mats and carpet backing
- Incorporation into rubber and plastic products
- Molded and extruded rubber products
- Protective coatings
- Road surfacing
- Floating breakwaters
- Erosion control
- Quarried gravel material replacement
- Artificial reefs
- Silage production
- Thermal insulator
- Landscaping
- Landfill leachate collection systems
- Landfill cell daily covers
- Septic systems leach fields
- Clean fill, gravel and sand
  - o Lightweight backfill

• Asphalt binding	○ Road embankment fill
• Rubberized bitumen and asphalt	○ Leachate collection system
• Traffic guide posts	○ Septic field drainage material
• Building materials	

Appendix C: Summary of central trends found in literature regarding the influence of pyrolysis process parameters on product characteristics and yields

Process Parameter	Central Trends discussed in Literature	Reference
Feedstock	Waste tyre type produced product yield difference of up to 10wt.%	[39]
	TDO yield for PT: 47.4wt.% TDO yield for TT: 55.6wt.%	[16]
	Different feedstock produced different product yields.	[40]
	Waste tyre type and origin effects TDO and PT-gas composition, not largely yield.	[41]
	Char ash content for TT: 14.3wt.% Char ash content for PT: 40.3wt.%	[42]
Feedstock particle size	Particle size effects product yield and characteristics. Large particles result in lower TDO and PT-gas yields and higher PT-char yields due to partial decomposition.	[1]
	At set pyrolysis time: smaller particles will almost reach complete degradation; coarser particles may contain rubber core.	[43]
	Larger particles require slower heating rates and lower temperatures	[193]
Temperature	Optimal pyrolysis temperature: 500°C 3 types (I, II, III) of behaviour dependencies of product yields on pyrolysis temperature: (I) Increased temperature causes increased TDO and PT-gas yield and decreased PT-char yield. (II) Increased temperature causes decreased TDO yield and increased PT-gas yield. (II) Increased temperature caused increased aromatic compounds and decreased aliphatic compounds and vice versa. (III) Temperature increase may cause PT-char yield due to carbonaceous deposits on surface.	[1]
	(II) Increased temperature causes TDO thermal cracking.	[194]
	(II)(III) Increased temperature (540°C - 740°C) caused decreased TDO yield and increase PT-gas and PT-char yields.	[75]
	(III) Increased temperature caused increased PT-char yield	[44]
	(III) Increased temperature caused increased PT-char yield due to heavy hydrocarbon deposits on surface.	[46]

Temperature	(III) At 1000°C, no TDO yielded, only PT-char (37wt.% PT-char, 25wt.% deposits) and PT-gas produced.	[47]
	Increased temperature caused decreased PT-char yield if oxygen present in carrier gas.	[48] [68]
	Increased temperature causes decreased PT-char calorific value.	[35]
	Increased temperature causes increased fixed carbon content.	[35]
	Increased temperature causes increased fixed surface area.	[48] [46]
Heating rate	Pyrolysis reactions start on surface of feed particle and move inwards. Low heating rates cause a resistance to heat and mass transfer and vice versa for high heating rates. High heating rates cause increased pyro-gas yield if the volatiles residence time is high. Heating rate related to pyrolysis reactor.	[1]
	Faster heat rates cause faster decomposition and an increase in volatiles cumulatively released.	[49]
	Pyro-gas composition is largely influenced by heating rate.	[48] [49]
	Increased heating rate caused increased pyro-gas yield, comparable to a temperature increase.	[86]
	Heating rate did not highly influence total tyre conversion and TDO yield and composition.	[195]
	Increased heating rate caused more aliphatic and less aromatic compounds in TDO.	[48]
	Lower heating rates need longer reaction times for complete degradation, but require less energy; while high heating rates need less time, but require more energy.	[27]
Pyrolysis time (feedstock particle residence time)	Pyrolysis time is directly proportional to particle size. Higher temperature or heating rates can decrease pyrolysis time. Longer pyrolysis times require larger reactor volumes. Pyrolysis time is related to volatiles residence time.	[1]
	Pyrolysis time can be decreased if temperature increases.	[27] [196]
Carrier gas flow rate and type	High carrier gas flow rate reduces volatiles residence time.	[1]
	Increased carrier gas flow rate increased TDO yields.	[58]
	Decreased carrier gas flowrate increased the PT-gas yield while TDO and PT-char yields decreased.	[45]
	Steam carrier gas caused low PT-char yield (9wt.%), high PT-char surface area (1260m^2/g), more aliphatic compounds in TDO, and large H_2 and CO quantities in PT-gas.	[50]
	CO_2 carrier gas caused PT-char oxidization at temperature higher than 760°C.	[51]
	CO_2 carrier gas caused sulphur content to shift to volatile fraction.	[52]

Volatiles residence time	Long volatiles residence time decreased TDO yield and increased PT-gas yield.	[78]
	Increased volatiles residence time increased production of H_2, CO and light hydrocarbon gases and decrease production of CO_2.	[66]
	Increasing volatile residence time increased H_2 and CH_4 production. PT-gas yield decreased while the solid yield increased from 800°C-900°C despite volatile residence time.	[44]
	Increasing residence time decreased TDO and PT-char yields and increased PT-gas yields.	[45]
Pressure	Decreasing pyrolysis pressure decreases undesirable secondary reactions.	[40]
	A vacuum pressure creates positive pressure gradient within a particle, thus increasing volatile diffusion towards the particle surface.	[53]
	Vacuum pressure increases TDO yield and decreases PT-gas and PT-char yields.	[1]
	Vacuum pressure increased D,L-limonene concentration, while PT-char has similar characteristics to commercial carbon black, although still containing high ash content.	[54] [40]
	Low pressure reduces process temperature, thus decreasing energy demands.	[1] [54]
	Vacuum pressure lessens carrier gas and volatile flow rates, thus improving process feasibility	[54]

Appendix D: Characteristic properties of differing carbon black series

Series	Property		Value
N234	Ash Content	[117]	$\leq 0.1\%$
	Sulphur Content	[117]	$\leq 1.1\%$
	Nitrogen Surface Area	[118]	$\sim 120 m^2/g$
	Surface Activity (CTAB Absorption)	[117]	$118 \pm 5 m^2/kg$
	Structure	[118]	High Structure
N220	Ash Content	[117]	$\leq 0.1\%$
	Sulphur Content	[117]	$\leq 1.1\%$
	Nitrogen Surface Area	[118]	$\sim 123 m^2/g$
	Surface Activity (CTAB Absorption)	[117]	$111 \pm 5 m^2/kg$
	Structure	[118]	High Structure

N375	Ash Content	[117]	$\leq 0.1\%$
	Sulphur Content	[117]	$\leq 1.1\%$
	Nitrogen Surface Area	[118]	$\sim 90 m^2/g$
	Surface Activity (CTAB Absorption)	[117]	$96 \pm 5 m^2/kg$
	Structure	[118]	High Structure
N339	Ash Content	[117]	$\leq 0.1\%$
	Sulphur Content	[117]	$\leq 1.1\%$
	Nitrogen Surface Area	[118]	$88 \sim m^2/g$
	Surface Activity (CTAB Absorption)	[117]	$93 \pm 5 m^2/kg$
	Structure	[118]	High Structure
N330	Ash Content	[117]	$\leq 0.1\%$
	Sulphur Content	[117]	$\leq 1.1\%$
	Nitrogen Surface Area	[118]	$\sim 85 m^2/g$
	Surface Activity (CTAB Absorption)	[117]	$82 \pm 5 m^2/kg$
	Structure	[118]	High Structure
N326	Ash Content	[117]	$\leq 0.1\%$
	Sulphur Content	[117]	$\leq 1.1\%$
	Nitrogen Surface Area	[118]	$\sim 83 m^2/g$
	Surface Activity (CTAB Absorption)	[117]	$83 \pm 5 m^2/kg$
	Structure	[118]	High Structure
N550	Ash Content	[117]	$\leq 0.1\%$
	Sulphur Content	[117]	$\leq 1.1\%$
	Nitrogen Surface Area	[118]	$38 - 46 m^2/g$
	Surface Activity (CTAB Absorption)	[117]	$42 \pm 5 m^2/kg$
	Structure	[118]	High Structure
N539	Ash Content	[117]	$\leq 0.1\%$
	Sulphur Content	[117]	$\leq 1.1\%$
	Nitrogen Surface Area	[118]	$\sim 44 m^2/g$
	Surface Activity (CTAB Absorption)	[117]	$41 \pm 5 m^2/kg$
	Structure	[118]	Moderate Structure
N660	Ash Content	[117]	$\leq 0.1\%$
	Sulphur Content	[117]	$\leq 1.1\%$
	Nitrogen Surface Area	[118]	$35 m^2/g$
	Surface Activity (CTAB Absorption)	[117]	$36 \pm 5 m^2/kg$
	Structure	[118]	Moderate Structure

Appendix E: Characteristic properties of differing activated carbon series

Series	Property		Value
B	Ash Content	[100]	$5-10\ wt\%$
	Moisture	[100]	$\leq 5wt.\%$
	Iodine Value	[100]	$600-1000\ mg/g$
F	Ash Content	[100]	$5-20\ wt\%$
	Moisture	[100]	$\leq 5wt.\%$
	Iodine Value	[100]	$700-1100\ mg/g$
G	Ash Content	[100]	$8-20\ wt\%$
	Moisture	[100]	$\leq 5wt.\%$
	Iodine Value	[100]	$1000-1200\ mg/g$
H	Ash Content	[100]	$8-20\ wt\%$
	Moisture	[100]	$\leq 5wt.\%$
	Iodine Value	[100]	-
J	Ash Content	[100]	$8-12\ wt\%$
	Moisture	[100]	$\leq 5wt.\%$
	Iodine Value	[100]	$850-1050\ mg/g$
P	Ash Content	[100]	$3-15\ wt\%$
	Moisture	[100]	$\leq 5wt.\%$
	Iodine Value	[100]	$600-1100\ mg/g$
Y	Ash Content	[100]	$5-12\ wt.\%$
	Moisture	[100]	$\leq 5wt.\%$
	Iodine Value	[100]	$600-1100\ mg/g$

Appendix F: Characteristic properties of differing fuel (coal) specifications

Eskom Specification	Property		Value
Spec 1	Ash Content	[25]	≤ 22.3%
	Sulphur Content	[25]	≤ 1.3%
	Calorific Value	[25]	≤ 24.1 MJ/kg
	Total Moisture	[25]	≤ 8.00%
	Volatiles	[25]	≤ 20.4%
Spec 2	Ash Content	[25]	≤ 27.2%
	Sulphur Content	[25]	$0.7\% \leq x \leq 1.3\%$
	Calorific Value	[25]	≤ 21.7 MJ/kg
	Total Moisture	[25]	≤ 7.00%
	Volatiles	[25]	≤ 20.4%
Spec 3	Ash Content	[25]	≤ 28.0%
	Sulphur Content	[25]	≤ 1.2%
	Calorific Value	[25]	≤ 20.3 MJ/kg
	Total Moisture	[25]	≤ 9.00%
	Volatiles	[25]	≤ 20.8%

Appendix G: Heating trend used for thermogravimetric analysis
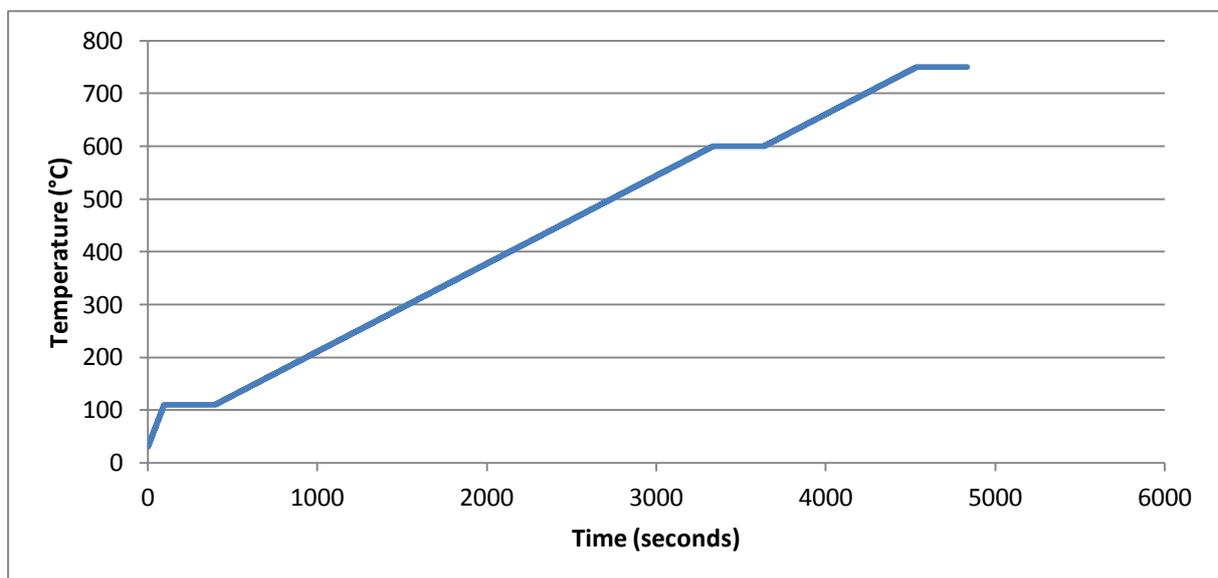
Appendix H: Data from Figure 11

Particle Size (µm)	PT-char X	PT-char Y	CB N330
100	60.8	3.2	82.9
50	31.3	1.8	73
20	15.4	1.2	65.5
10	9.3	1.1	62.5
1	1	0	2.9

Appendix I: Particle size analysis: volume frequency vs. diameter

Volume Frequency vs. Diameter for PT-char X
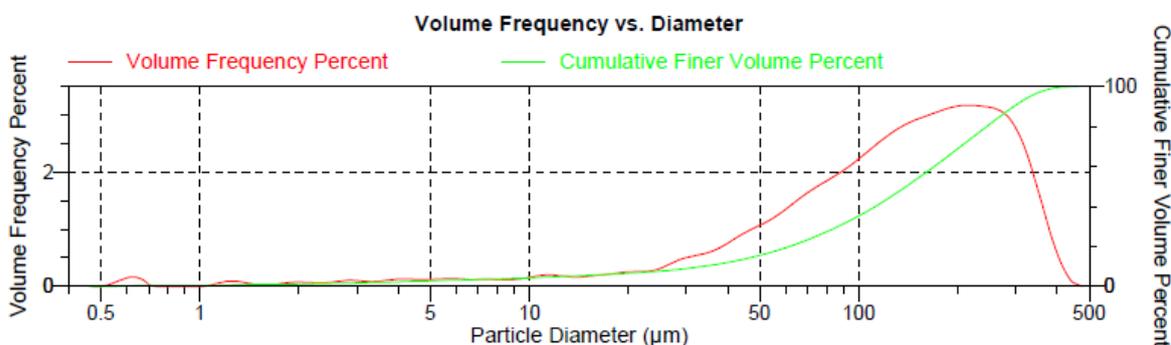
Volume Frequency vs. Diameter for PT-char Y
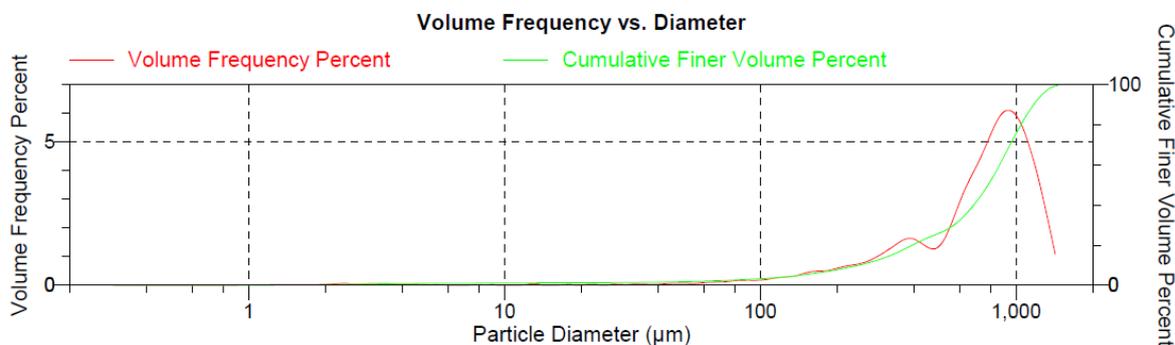
Volume Frequency vs. Diameter for CB N330
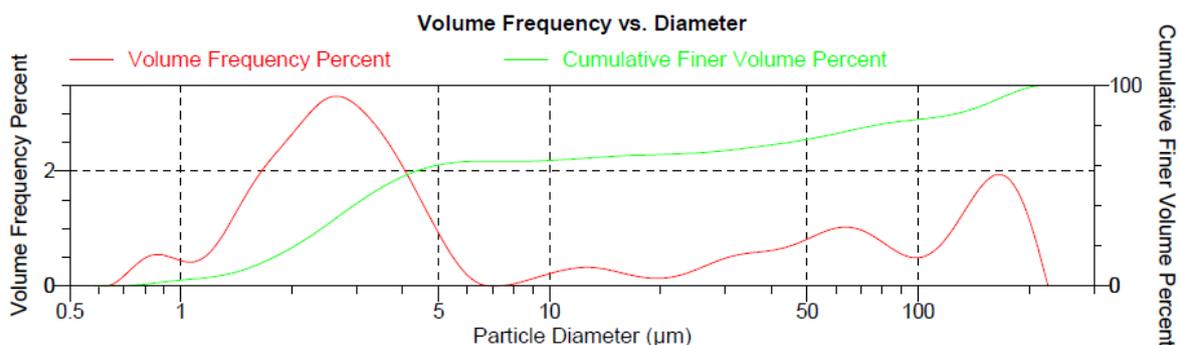
Appendix J: Nitrogen gas adsorption and desorption isotherm linear plots

Due to the presence of a small knee and a hysteresis loop, the isotherms for CB N330 and PT-char X show a type IV trend, further discussed in detail by Thommes and Thomas [162]. The absence of a knee in the PT-char Y isotherm renders the trend type V. In agreement, Miguel et al. [105] described PT-char to possess a type IV isotherm trend. Dissimilarly, Thommes and Thomas [162] said carbon black showed a type V trend. The hysteresis loop on all three isotherm plots has a distinct H3 shape, further discussed in Thommes and Thomas [162]. Pore size analysis must originate from the adsorption branch when the material has H3 isotherm nature due to the presence of capillary condensation in the meso- and macropores [162]. Since PT-char Y specifically portrays a type V isotherm, BET is not applicable and BJH is the appropriate measurement method.
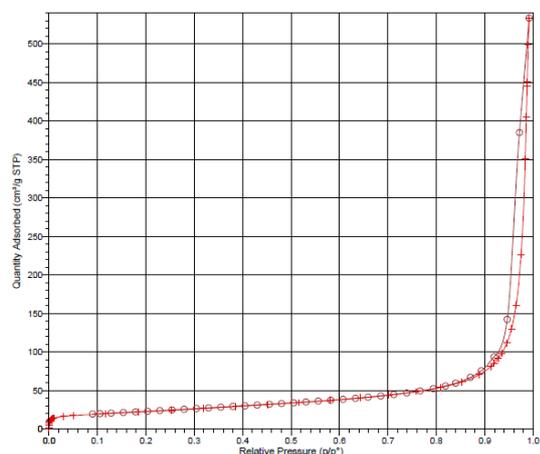
CB N330
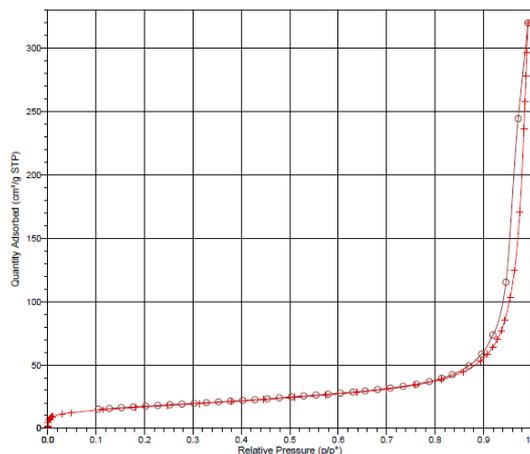
PT-char X
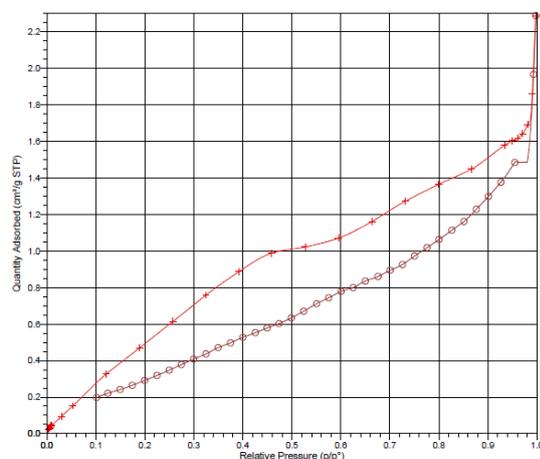
PT-char Y

Appendix K: Data from acid-alkali screening

Data from Screening by Lixiviant Demineralisation (refer to Figure 15 and Figure 16)

Lixiviant	Run Number	Quantity Mass Extracted from PT-char (wt.%)	Quantity Ash Extracted from PT-char X (wt.%)	Corrected Ash Content within PT-char (wt.%)	Quantity Mass Extracted Standard Deviation	Quantity Ash Extracted Standard Deviation
Nitric Acid	Run 1	13.306	11.217	5.022	0.035	0.024
	Run 2	12.603	11.264	4.974		
Hydrochloric Acid	Run 1	14.073	11.837	4.402	0.023	0.406
	Run 2	13.610	11.024	5.215		
Sulphuric Acid	Run 1	6.965	10.873	5.366	0.356	0.020
	Run 2	6.254	10.832	5.407		
Acetic Acid	Run 1	7.951	7.302	8.937	0.000	0.094
	Run 2	7.942	7.490	8.749		
Hydrogen Peroxide	Run 1	7.132	6.972	9.267	0.018	0.201
	Run 2	7.496	7.375	8.864		
Sodium Hydroxide	Run 1	9.447	3.691	12.548	0.080	0.260
	Run 2	9.608	3.171	13.068		

Data from Economic Screening

	Lixiviant Price: 10t lixiviant/1t PT-Char	CE Ratio (Ash)	CE Ratio (mass)
Hydrochloric Acid	7994	740	578
Sulphuric Acid	9757	954	1476
Nitric Acid	14480	1364	1118
Hydrogen Peroxide	12349	1885	1688
Acetic Acid	20502	3026	2580

Appendix L: **Hydrochloric acid kinetic model: linear correlations**

$$y = 0.0003x + 0.0321$$
$$R^2 = 0.8261$$

$$y = 0.0004x + 0.0294$$
$$R^2 = 0.9256$$

$$y = 0.0002x + 0.0318$$
$$R^2 = 0.9281$$

$$y = -1319.6x - 7.9922$$
$$R^2 = 0.3045$$
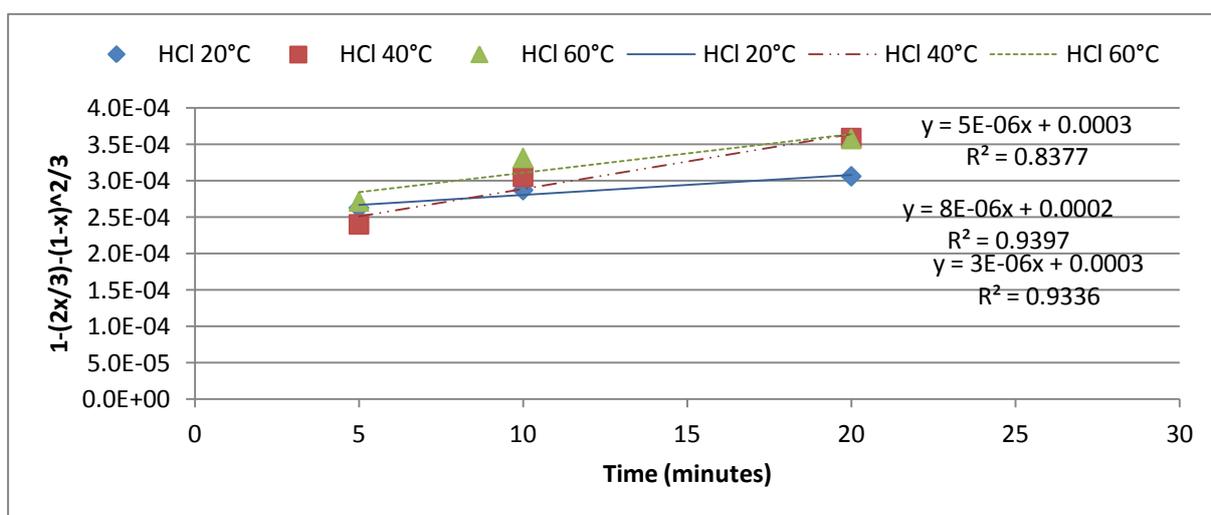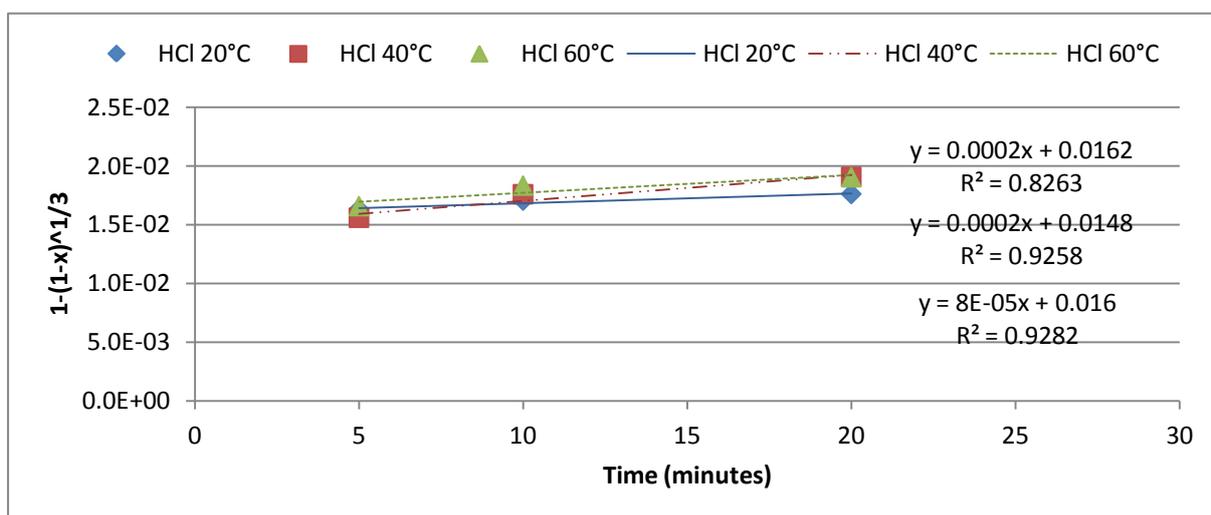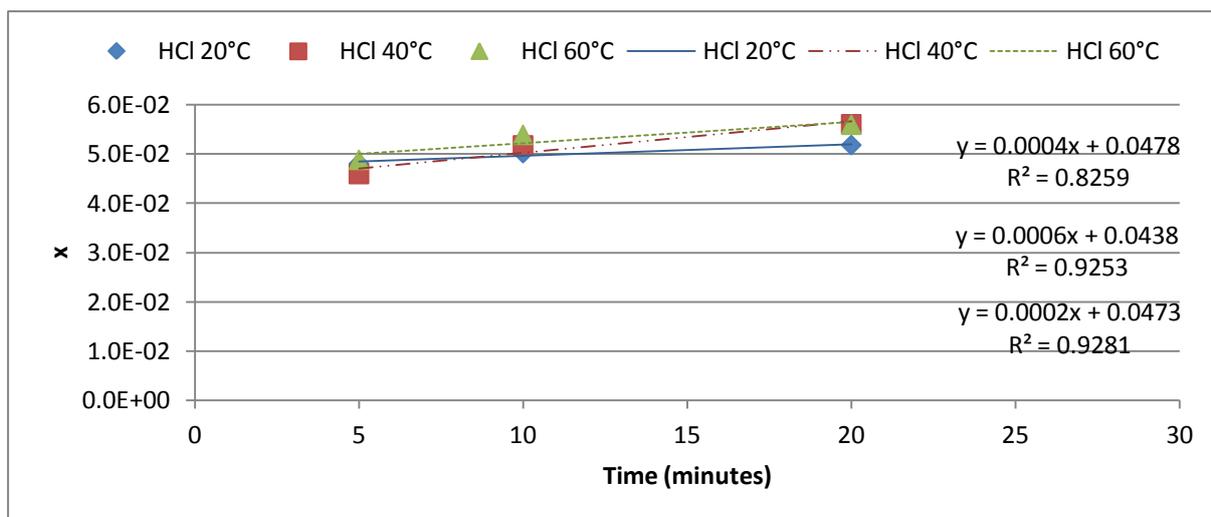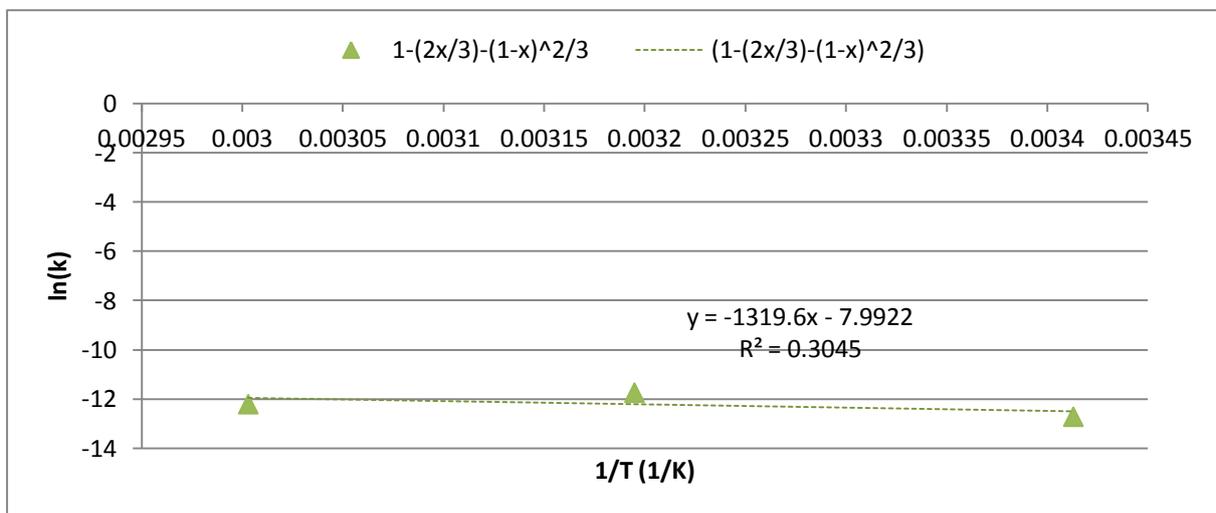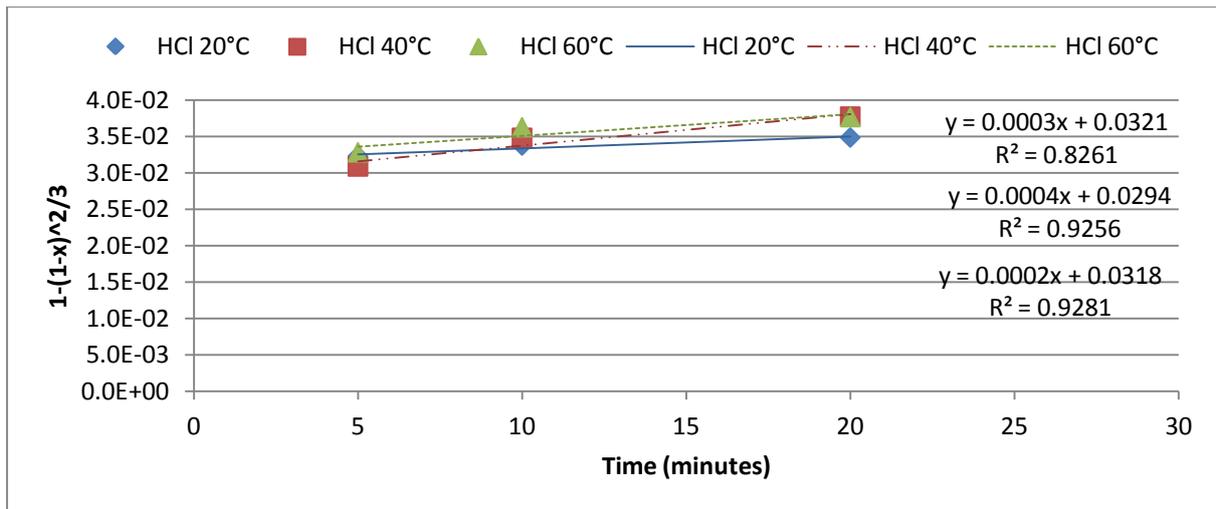
Appendix M: **Sodium hydroxide kinetic model: linear correlations**

$$y = 0.0003x + 0.0439$$
$$R^2 = 0.9665$$

$$y = 0.0004x + 0.0266$$
$$R^2 = 0.9954$$

$$y = 0.0005x + 0.0094$$
$$R^2 = 0.981$$
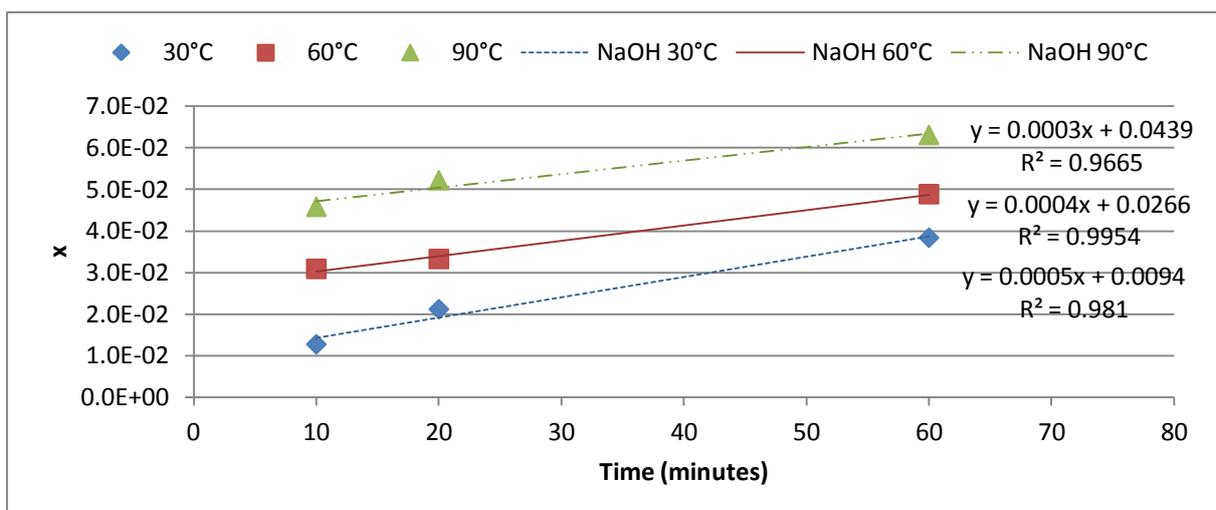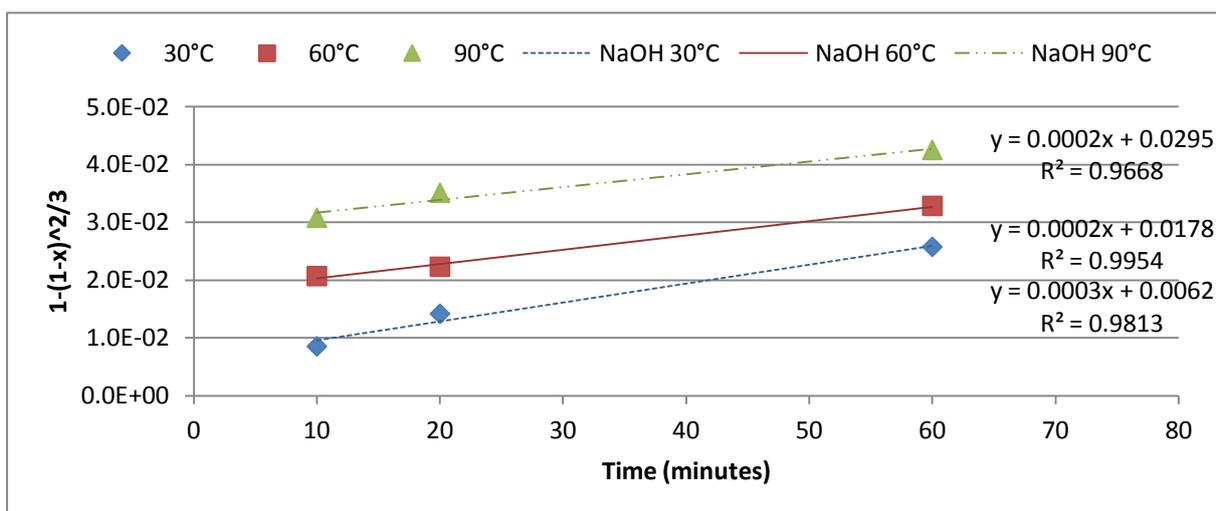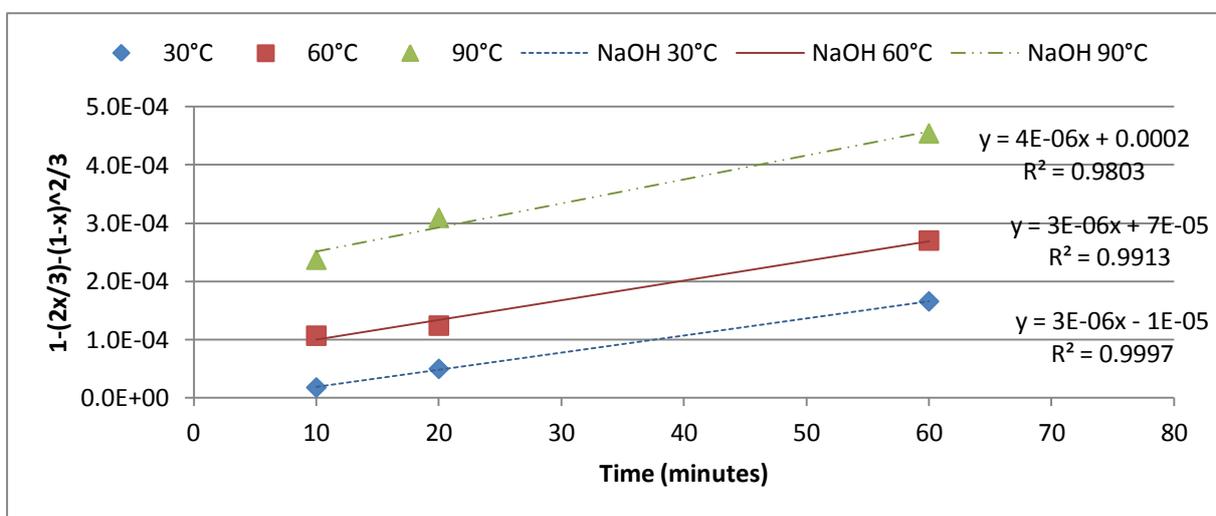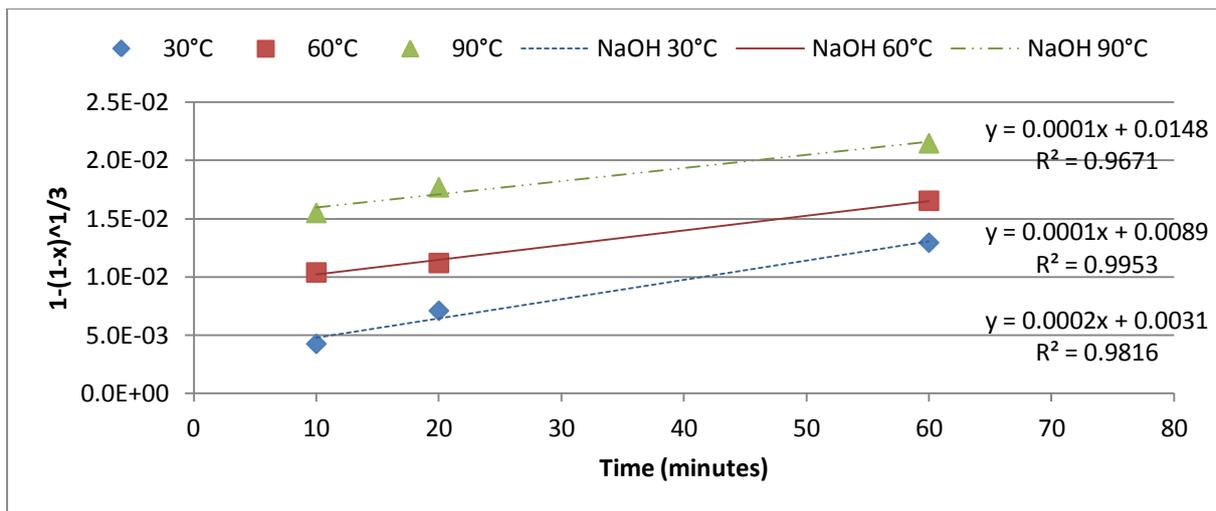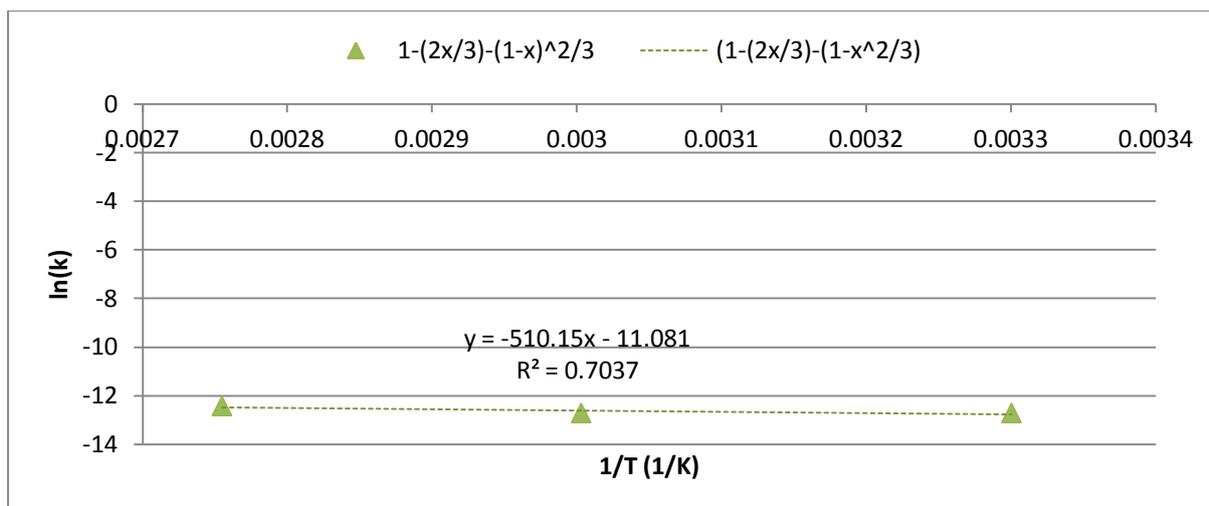
Appendix N: Reactions between ash components and HCl/ NaOH

Reactions with Hydrochloric Acid

Balanced Reaction	Complex Ion

$Fe_{(s)} + 2HCl_{(aq)} \rightarrow FeCl_{2(aq)} + H_{2(g)}$ $Cl_2[Fe(H_2O)_6]$

$2Ti_{(s)} + 6HCl_{(aq)} \rightarrow 2TiCl_{3(aq)} + 3H_{2(g)}$ $Cl_2[Ti(H_2O)_3]$

$Cr_{(s)} + 2HCl_{(aq)} \rightarrow CrCl_{2(aq)} + H_{2(g)}$ $Cl_2[Cr(H_2O)_6]$

$Mn_{(s)} + 2HCl_{(aq)} \rightarrow MnCl_{2(aq)} + H_{2(g)}$ $Cl_2[Mn(H_2O)_6]$

$2Na_{(s)} + 2HCl_{(aq)} \rightarrow 2NaCl_{(aq)} + H_{2(g)}$

$Ca_{(s)} + 2HCl_{(aq)} \rightarrow CaCl_{2(aq)} + H_{2(g)}$

$K_{(s)} + HCl_{(aq)} \rightarrow KCl_{(aq)} + H_{2(g)}$

$Mg_{(s)} + 2HCl_{(aq)} \rightarrow MgCl_{2(aq)} + H_{2(g)}$

$4Al_{(s)} + 6HCl_{(aq)} \rightarrow 2Al_2Cl_{3(aq)} + 3H_{2(g)}$

$Al_2O_{3(s)} + 6HCl_{(aq)} \rightarrow 2AlCl_{3(aq)} + 3H_{2(g)}$

$Si_{(s)} + Cl^-_{(aq)} \rightarrow SiCl_4$

$S^{2-}_{(aq)} + 2H^+ \rightarrow H_2S$
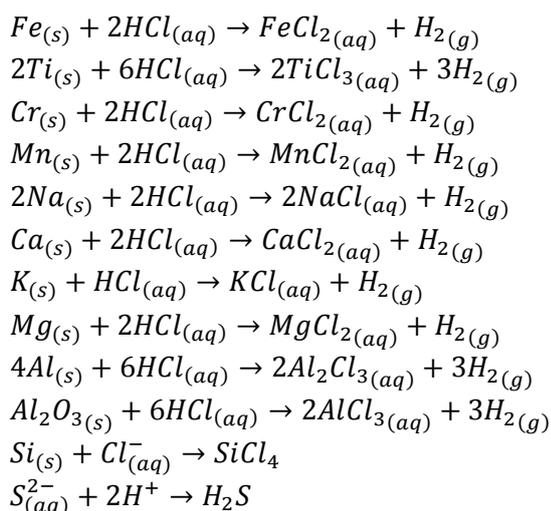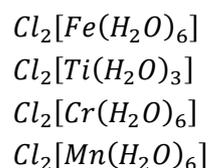
Reactions with Sodium Hydroxide

Balanced Reaction	Complex Ion

$Al_2O_{3(s)} + 2NaOH_{(aq)} + 3H_2O \rightarrow 2Na[Al(OH)_4] + 3H_{2(g)}$ $Al(OH)_4$

$2Al_{(s)} + 2NaOH_{(aq)} + 6H_2O \rightarrow 2Na[Al(OH)_4] + 3H_{2(g)}$ $Al(OH)_4$

$ZnO_{(s)} + 2NaOH_{(aq)} + H_2O \rightarrow 2Na[Zn(OH)_4] + H_{2(g)}$ $Zn(OH)_4$

$Zn_{(s)} + 2NaOH_{(aq)} + 2H_2O \rightarrow 2Na[Zn(OH)_4] + H_{2(g)}$ $Zn(OH)_4$

$SiO_{2(s)} + 4NaOH_{(aq)} \rightarrow Na_4SiO_4 + 2H_2O$

$4S + 6NaOH \rightarrow Na_2S_2O_3 + 2Na_2S + 3H_2O$

$2NaOH + 2Na \rightarrow 2Na_2O + H_2 \ (at\ 600℃)$

$4NaOH + 3Ca \rightarrow 3CaO + Na_2O + 2Na + 2H_2 \ (at\ 600℃)$

$NaOH + K \rightarrow KOH + Na$

$TiO_2 + NaOH + H_2O \rightarrow Ti(OH)_2 + NaO$

$Cr^{2+} + 3OH^- \rightarrow Cr(OH)_3$

$Mn^{2+} + 2OH^- \rightarrow Mn(OH)_2$
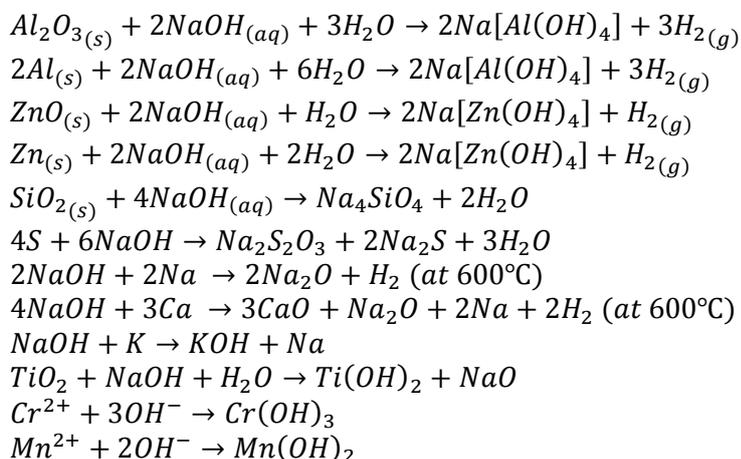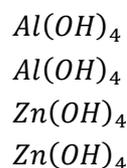
Appendix O: Flow summary table for PT-char acid-alkali demineralisation process shown in Figure 36

Streams 39a-45a are represent the flow of the lixiviant from the respective Nutsche filter dryer, and 39b-45b represent the flow of the water from the PT-char washing stage. The water, flows through the pipes after the respective lixiviant so as to clean the pipes for increased lifespan of the piping equipment.

	Temperature	Pressure	Vapour Fraction	Mass flow	PT-char: Carbon	Ash	Other	HCl	NaOH	H$_2$O
	°C	bar		Kg/batch						
1	25.00	1.20	0	800.00	-	-	-	-	-	800.00
2	25.00	1.60	0	800.00	-	-	-	-	-	800.00
3	25.00	1.54	0	200.00	-	-	-	200.00	-	-
4	25.00	1.36	0	200.00	-	-	-	200.00	-	-
5	25.00	1.01	0	600.00	-	-	-	-	600.00	-
6	25.00	1.22	0	600.00	-	-	-	-	600.00	-
7	25.00	1.00	0	210.00	160.88	33.83	15.29	-	-	-
8	25.00	1.00	0	200.00	153.22	32.22	14.56	-	-	-
9	25.00	1.22	0	2400.00	-	-	-	-	2400.00	-
10	25.00	1.36	0	800.00	-	-	-	800.00	-	-
11	25.00	1.60	0	3200.00	-	-	-	-	-	3200.00
12	25.00	1.22	0	3000.00	-	-	-	-	3000.00	-
13	88.00	1.12	0	3000.00	-	-	-	-	3000.00	-
14	88.00	1.12	0	3000.00	-	-	-	-	3000.00	-
15	88.00	1.12	0	1000.00	-	-	-	-	1000.00	-
16	88.00	1.12	0	2000.00	-	-	-	-	2000.00	-
17	88.00	1.12	0	1000.00	-	-	-	-	1000.00	-
18	88.00	1.12	0	1000.00	-	-	-	-	1000.00	-
19	25.00	1.36	0	1000.00	-	-	-	1000.00	-	-
20	80.00	1.11	0	1000.00	-	-	-	1000.00	-	-
21	80.00	1.49	0	1000.00	-	-	-	1000.00	-	-
22	25.00	1.60	0	4000.00	-	-	-	-	-	4000.00

23	25.00	1.60	0	1000.00	-	-	-	-	-	1000.00
24	25.00	1.60	0	3000.00	-	-	-	-	-	3000.00
25	25.00	1.60	0	1000.00	-	-	-	-	-	1000.00
26	25.00	1.60	0	2000.00	-	-	-	-	-	2000.00
27	25.00	1.60	0	1000.00	-	-	-	-	-	1000.00
28	25.00	1.60	0	1000.00	-	-	-	-	-	1000.00
29	100.00	1.01	1	99.00	-	-	-	-	-	99.00
30	100.00	1.01	1	99.10	-	-	-	-	-	99.10
31	100.00	1.01	1	198.10	-	-	-	-	-	198.10
32	100.00	1.01	1	99.10	-	-	-	-	-	99.10
33	100.00	1.01	1	297.20	-	-	-	-	-	297.20
34	80.00	1.01	1	101.38	-	-	2.28	-	-	99.10
35	110.00	1.01	0	184.74	153.22	19.85	10.67	-	-	1.00
36	110.00	1.01	0	181.69	153.22	17.95	9.53	-	-	1.00
37	110.00	1.01	0	179.47	153.22	15.72	9.53	-	-	1.00
38	110.00	1.01	0	162.06	153.22	0.59	7.25	-	-	1.00
39a	88.00	1.01	0	916.26	-	12.37	3.89	-	900.00	-
39b	60.31	1.01	0	1000.00	-	-	-	-	100.00	900.00
40a	88.00	1.37	0	916.26	-	12.37	3.89	-	900.00	-
40b	60.31	1.37	0	1000.00	-	-	-	-	100.00	900.00
41a	88.00	1.01	0	903.04	-	1.90	1.14	-	900.00	-
41b	60.31	1.01	0	1000.90	-	-	-	-	100.00	900.90
42a	88.00	1.38	0	903.04	-	1.90	1.14	-	900.00	-
42b	60.31	1.38	0	1000.90	-	-	-	-	100.00	900.90
43a	88.00	1.01	0	902.22	-	2.22	-	-	900.00	-
43b	60.31	1.01	0	1000.90	-	-	-	-	100.00	900.90
44a	88.00	1.37	0	902.22	-	2.22	-	-	900.00	-
44b	60.31	1.37	0	1000.90	-	-	-	-	100.00	900.90
45a	88.00	1.37	0	2721.53	-	16.50	5.03	-	2700.00	-
45b	60.31	1.37	0	3001.80	-	-	-	-	300.00	2701.80
46a	88.00	1.01	0	915.13	-	15.13	-	900.00	-	-
46b	60.31	1.01	0	1000.90	-	-	-	100.00	-	900.90

47a	88.00	1.37	0	915.13	-	15.13	-	900.00	-	-
47b	60.31	1.37	0	1000.90	-	-	-	100.00	-	900.90
48	80.00	1.37	0	915.13	-	900.00	-	900.00	-	-
49	60.31	1.37	0	1000.90	-	100.00	-	100.00	-	900.90
50	25.00	1.37	0	3001.80	-	-	-	-	300.00	2701.80
51	88.00	1.37	0	2721.53	-	-	5.03	-	2700.00	-
52	25.00	1.01	0	1239.37	-	200.00	5.03	200.00	600.00	402.70

Appendix P: Gantt chart for PT-char acid-alkali demineralisation process batch process shown in Figure 36[64]

The process allows for 21 batches of 4 washes each per 24hours with a 12 minute safety factor included. The HCl and NaOH are both heated to their required temperatures in 20minutes (stage 1 and 10 respectively in the Gantt chart below). The Nutsche filter dryers are first charged with their respective lixiviant in 10minutes (stage 2a and 11a for NaOH and HCl respectively), followed by the PT-char in 2 minutes (stage 2b and 11b for NaOH and HCl respectively). The NaOH extraction time is 60minutes (stage 2c), while the HCl extraction time is 20 minutes (stage 11c). The respective lixiviants both take approximately 20 minutes to filter sufficiently (stage 2d and 11d for NaOH and HCl respectively), after which, continuous washing and filtration occurs for 40 minutes (stage 2e and 11e for NaOH and HCl respectively). The washed filter cake is then dried for 60 minutes using the combination of air velocity, heating vessel walls and agitation stage 2f and 11f for NaOH and HCl respectively). Following drying, the PT-char is then discharged from the vessel in 12 minutes with help of the agitator curvature stage 3 and 12 for NaOH and HCl respectively). This process is repeated twenty-one times, three for NaOH (stages 1-3) and once for HCl (10-12).

---

[64] Grey shaded areas represent 2 minutes

Stage 1:											
Stage 2a:											
Stage 2b:											
Stage 2c:											
Stage 2d:											
Stage 2e:											
Stage 2f:											
Stage 3:											
Stage 10:											
Stage 11a:											
Stage 11b:											
Stage 11c:											
Stage 11d:											
Stage 11e:											
Stage 11f:											
Stage 12:											
Minutes:	20	40	60	80	100	120	140	160	180	200	224
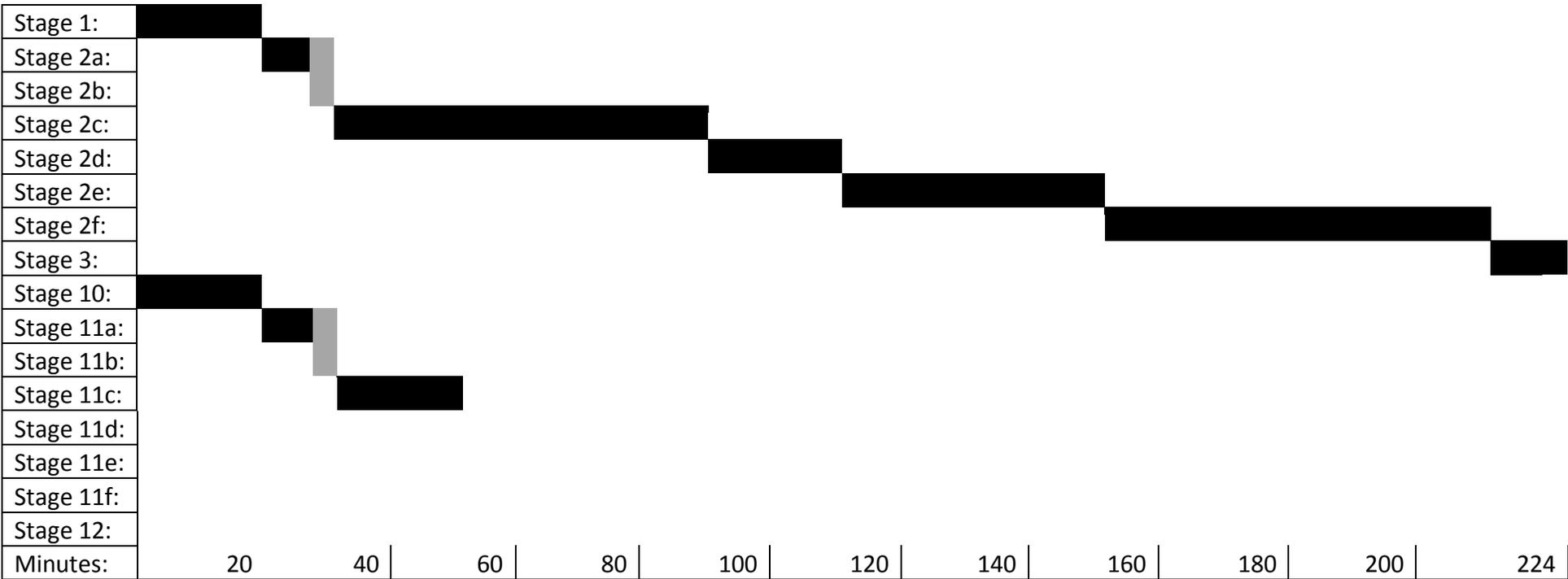
Appendix Q: Major Equipment Design Description and Specifications

The specifications of the major process units shown in the PT-char acid-alkali demineralisation process described in figure 36 are listed below in the tables below. Each process unit is designed according to methods outlined by Sinnot and Towler [197]. A design factor of 10% was utilised for the vessels, heat exchangers and screw conveyors; and a design factor of 20% was used for the Nutsche filter dryers.

Vertical storage vessels with a 5 day capacity (V-1 – V-4) are used to contain the feed materials, including PT-char, NaOH, HCl and water. The equalisation vessels (V-5 – V-7) have a storage capacity of 1.5days. The PT-char storage tank (V-4) and the H_2O storage tanks (V-1 V-6) are made of SS 304 which has a maximum stress capacity of 137.9N/mm^2 at room temperature. The HCl storage tanks, V-2 and V-7, are made of PVC[65] since it is cheaper than a nickel based alloy, and is compatible with acids. The NaOH storage tanks V-4 and V-5 area made of SS304L and alloy 800[66] respectively. The internal pressure of each storage tank is atmospheric, with a height to diameter ratio of 2. Additionally, the vessels have a joint efficiency of 85% and a corrosion allowance of 4mm for the NaOH and HCl tanks, 2mm for the H_2O and PT-char tanks. The specific specifications for each vessel are described below.

The plate heat exchangers were each designed to heat up their associated lixiviant to the required temperature before extraction. Hot process water was chosen as the heating liquid as it is inexpensive and readily available. The hot water enters both heat exchangers at 95°C, and has been assigned a fouling factor of 3.00E+4W/m^2°C. The lixiviants enter the heat exchangers at room temperature, and have fouling factors of 2857.14 W/m^2°C and 1.00E+4 W/m^2°C for NaOH and HCl respectively. Since these chemicals are highly corrosive, especially at high temperatures, nickel based alloys were chosen as the material of construction. The NaOH plate heat exchanger consists of alloy 800, which has a thermal conductivity of 12.9W/m°C, while the HCl plate heat exchanger comprises of alloy B2 which has a higher thermal conductivity of 110.69W/m°C. Port diameters for H-1 and H-2 were chosen to be 250mm and 100mm respectively. Detailed specifications for each plate heat exchanger are listed in the table below.

The agitated Nutsche filter dryers, as described previously, are single process units consisting of an agitated jacketed vessel, a sieve and a dryer combination. The Nutsche vessels, R-1, R-2 and R-3 are identical, while R-4 has associated dissimilarities. All Nutsche units are made of SS 316 coated with a

---

[65] PVC has a maximum stress capacity of 55.0N/mm^2

[66] Alloy 800 is a nickel based alloy with a maximum stress capacity of 91.7N/mm^2

nickel based alloy (alloy B2 for R-1,2,3 and alloy 800 for R-4) due to the corrosiveness of the lixiviants. Additionally, the vessels operate at atmospheric pressure and are designed to handle a solids content of 20%. The dimensions of the Nutsche vessels consist of a height to diameter ratio of 3 and a vessel thickness which includes a corrosion allowance of 4mm. The agitators are hub mounted curved-blade turbines made of the same respective material. The curvature enables PT-char discharge ease prior extraction. Additionally, there are no baffles within the vessel as the particles will entrap in dead zones. The Nutsche heating jacket is a spiralled around the exterior wall of the vessel and contains hot process water which enables the vessel to maintain the required extraction temperature. The latent heat supplied by the jacket assists the drying procedure prior extraction. The filter is a detachable pan filter situated at the bottom of the vessel, and made from chemically resistant polypropylene. The PT-char filter cake drying mechanism consists of a combination of latent heat provided by the jacket, the movement of the agitator thus increasing cake exposure, and the movement of warm air through the vessel. Energy required is the sum of temperature increase and water evaporation. Many Nutsche filters contained heated agitators to assist drying, however, the jacket surrounding the vessel and the air movement is sufficient. The specification details of each agitated Nutsche filter dryer are expressed in the table below.

The solids are handled by screw conveyors which automatically load and unload the PT-char from and to the respective process units. The screw conveyors are all at an approximate angle of 29°, conveying loads over an inclination distance of 5.75m. The screw conveyors are to load and unload their load volumes in 12 minutes, thus increasing the speed and power required. The specific requirements of each screw conveyor are listed in the relevant table below.

The particle size sorting sieve at the commencement of the process is a static sieve which allows dry screening. The objective is to expel larger particles from the PT-char extraction feed. It is enclosed to prevent the possibility of a dust explosion. The screen has an aperture diameter of 5mm, with a tolerance of 0.1mm. Refer to the relevant table below for the sieve specifications.

There are 9 small sized centrifugal pumps within the process, as shown in figure 34. The connecting pipes are smooth and include a corrosion allowance of 2mm for water pipes and 4mm for lixiviant pipes, with the material of construction being SS 304, PVC or a coating nickel based alloy, depending on the type and temperature of liquid contents. It must be noted that the respective pipe lengths are approximations. The pump is designed with an efficiency of 70%, and a joint efficiency of 97%. The velocity head include entries, exits, elbows, T-branches, T-lines and ball valves (100% open). Pumps P-2A/B and P-3A/B compensate for the pressure drops in heat exchanger H-1 and H-2 respectively. Comprehensive pump specifications are described in the relevant table below.

Vessel Specifications

		V-1	V-2	V-3	V-4	V-5	V-6	V-7
Volume	m³	6.00	1.40	11.09	2.00	15.10	26.50	5.50
Height	m	1.95	0.94	2.76	1.13	3.10	4.11	1.87
Diameter	m	0.98	0.47	1.38	0.56	1.55	2.05	0.94
Wall Thickness	mm	2.43	4.52	4.93	2.25	5.02	5.39	5.02
Holding Capacity	Days	5	5	5	5	1.5	1.5	1.5
MOC	-	SS 304	PVC	SS 304L	SS 304	Alloy 800	SS 304	PVC

Plate Heat Exchanger Specifications

			H-1	**H-2**
Hot Fluid	**Fluid Type**	-	Water	Water
	Flow	kg/hr	5994.54	7228.22
	Inlet Temperature	°C	95	95
	Outlet Temperature	°C	70	30
	Pressure Loss	Pa	0.15	45.96
Cold Fluid	**Fluid Type**	-	HCl	NaOH
	Flow	kg/hr	3000	9000
	Inlet Temperature	°C	25	25
	Outlet Temperature	°C	80	88
	Pressure Loss	Pa	0.17	55.72
Plate Specifications	**Total Heat Load**	kW	174.17	550.62
	Passes	-	1	1
	Pass Arrangement	-	1:1	1:1
	Total No. Plates	-	11.7	55.2
	MOC	-	Alloy B2	Alloy 800
	Overall Coefficient	W/m².°C	114.51	100.00
	Plate Length	m	2.3	4
	Plate Width	m	2.2	3.9
	Plate Spacing	mm	0.9	0.7
	Plate Thickness	mm	0.75	0.5

Nutsche Filter Dryer Specifications

			R-1, R-2, R-3	**R-4**
Vessel	**Volume**	m³	2.00	1.75
	Height	m	2.84	0.91
	Diameter	m	0.95	0.91
	Wall Thickness	mm	4.62	5.75
	Internal Pressure	Pa	101325	101325
	MOC	-	SS316 coated Alloy B2	SS316 coated Alloy 800
	Solids Content	wt.%	20	20
	Residence Time	hr	3	2.67
Impeller	**Type**	-	Hub mounted curved-blade turbine	Hub mounted curved-blade turbine
	Diameter	m	0.316	0.302
	Blade Width	m	0.063	0.060
	Level above Filter	m	0.237	0.226

	Speed	rpm	0.005	0.005
	Shaft power	kW	0.104	0.083
Heating Jacket	Total Heat Load	kW	69.12	45.43
	Baffle Type		Spiral	Spiral
	Pitch	mm	30.00	50.00
	Spiral Number		75.77	43.47
	Channel Length	m	225.43	123.67
	Height	m	2.273	2.174
	Jacket-wall spacing	mm	30	40.00
	Hydraulic Mean Diameter	mm	30	44.44
	Heating Liquid		Water	Water
	Inlet Temperature	°C	90	85
	Outlet Temperature	°C	86	75
	Liquid Flow Rate	kg/hr	2286.8	892.45
	Pressure Loss	Pa	0.048	0.001
Filter	Filter Type	-	Pan	Pan
	MOC	-	Polypropylene	Polypropylene
	Filter Area	m^2	0.704	0.906
	Pore Size	μm	10	10
	Cake Mass	kg	100	88.89
	Cake Volume	m^3	0.336	0.299
	Solids Loading	%	20	20
Drying Air	Heat Load	kW	13.215	39.40
	Inlet Temperature	°C	50	50
	Outlet Temperature	°C	20	20
	Solids Content	%	184.74	184.74
	Flow rate	kg/hr	26.194	78.09
	Velocity	m/s	2.01	11.61

Screw Conveyer Specifications

		C-1	C-2	C-3	C-4	C-5
Mass Flow	kg/hr	6000	5542.12	5450.83	5384.14	4861.78
Travelling Speed	m/s	6.00	5.84	5.81	5.79	5.59
Incline Length	m	5.75	5.75	5.75	5.75	5.75
Horizontal Length	m	5.00	5.00	5.00	5.00	5.00
Housing Area	m^2	1.45	1.37	1.36	1.35	1.26
Diameter	m	2.64	2.57	2.56	2.31	2.34
Screw Speed	rpm	150	150	150	150	150
Screw Pitch	m	2.40	2.34	2.32	2.31	2.24
Power	kW	0.235	0.217	0.159	0.157	0.138

Sieve Specifications

		S-1
Throughput	kg/hr	66.67
Particle Size Range	µm	1-10000
Material Characteristic	-	Free flowing
Screening Type	-	Dry screening
Sieve Type	-	Punctured
MOC	-	SS 304
Approximate Screen Area	m²	1.01
Screen Length	m	1.5
Screen Width	m	1.5
Aperture Diameter	mm	5
Aperture Tolerance	mm	0.1

Centrifugal Pump Specifications

		P-1	**P-2**	**P-3**	**P-4**	**P-5**	**P-6**	**P-7**	**P-8**	**P-9**
Flow Rate	kg/hr	20	20	60	20	60	25	25.02	25.02	25.02
Pipe Schedule	-	1"10	1"80	2"80	1"80	2"80	2"80	2"80	11/2"80	2"80
Line to Suction	m	0.5	0.5	0.5	0.5	0.5	1	1	1	0.5
Line from Suction	m	42.1	1.0	1.0	13.9	31.7	19.75	13.75	19.75	20.2
Inlet Pressure	Bar	1.20	1.53	1.01	1.50	1.12	1.01	1.01	1.01	1.01
Outlet Pressure	bar	1.60	1.84	1.16	2.25	1.53	1.37	1.38	1.37	1.37
Elevation	m	2.83	0.99	0.99	2.71	2.83	4.10	4.10	4.10	4.10
Total Head	m	5.47	2.81	1.37	7.44	3.94	4.51	4.39	4.50	4.51
Power	W	19.02	12.93	18.99	32.34	50.04	21.70	22.39	21.72	21.72
NPSH	m	12.29	14.33	8.74	13.91	9.67	10.34	10.344	10.34	10.33
Pipe MOC	-	SS304	PVC	PVC	SS316 coated Alloy 800	SS316, coated Alloy B2	SS316, coated Alloy B2	SS316, coated Alloy B2	SS316, coated Alloy B2	SS316 coated Alloy 800

Appendix R:　　　Economic Analysis

This particular economic analysis is based on the proposed acid-alkali demineralisation process design, and aims at producing informative estimates of the total capital cost and cash flow from Turton et al. [192][67]. It must be noted that this analysis is a study estimate, also known as a major equipment or factored estimate, used implicitly for feasibility or concept study as it has an expected inaccuracy range of 30-50% relative to the best index of 100%. This particular process is an extension to an existing WT-pyrolysis plant and, thus, the purchasing of land is not required. The overall cash flow includes revenue from the UPT-char product, savings from utilising PT-char from the onsite WT-pyrolysis plant, and associated manufacturing costs. The revenue has an associated 28% tax, with VAT excluded. The project has a 28 year project life; plant depreciation of 50%, 30% and 20% over three years, and a final salvage value of 20% at project termination. The economic analysis algorithm proceeds as demonstrated below.

The total capital cost calculation included the bare module cost (direct and indirect costs) for each major process unit, each adjusted for inflation using Chemical Engineering Plant Cost Index (CEPCI) forecast of 624.3765[68]. The cost of each process unit was first calculated for the base conditions[69], and then adjusted to account for specific requirements of this process, such as higher operating pressures and unusual materials of construction. All process units utilised in this process are standard, except the units within which extraction occurs: the agitated Nutsche filter dryer combines three process units, namely an agitated, jacketed CSTR, a filter and a dryer. It was calculated that for both the filter and the dryer, the cost of the vessel within with the respective process occurred, calculated to be half the total unit cost. Therefore, to account for the combination of three units in one, the cost estimation of the agitated Nutsche filter dryer included the complete cost of a jacketed, agitated reactor, and half the cost of a dryer and filter. A precise summary of the cost estimation of each process unit is summarised in the relevant table below. The overall bare module cost estimate, including CEPCI forecasting, is ZAR 37.62 million. For comparison, the cost[70] of building a new plant, which operates independently, calculated to be ZAR 66.59 million.

The true cost of utilities in a large process are difficult to estimate, therefore, this particular analysis assumes that the capital investment required to build the particular facility which supplies the utility has already been accounted for since this particular plant is an extension to an existing chemical

---

[67] An exchange rate of ZAR 11.87 per US $1 was utilised in all calculations
[68] Refer to appendix S for CEPCI forecast.
[69] Base conditions included near-ambient operating pressure and carbon steel material of construction. [192]
[70] The grassroots cost.

plant. The price of the particular utility and the utility cost of each process unit are described in the relevant table below. The overall cost of utilities, including ZAR 1061.65 for potable water, totalled to be ZAR 3.56 million/year.

The operating labour includes 9 operators, working 245 shifts/ year at 8hr/ shift. The plant operates 24hr/day, 344days/yr. In South Africa, the minimum monthly salary is approximately R 2610.00 [198]; however, considering the fact that the operating labourers on this plant must be skilled workers, the monthly salary was chosen to be ZAR 8000.00 as a first approximation. Hence forth, the overall labour cost approximated to be ZAR 4.24 million/year.

The raw material expenditure includes costs associated with 5.0M NaOH, 1.0M HCl, water and raw PT-char. Since the plant is an extension of an existing WT-pyrolysis plant which produces raw PT-char, this cost is included as a saving of ZAR 0.351 million/year rather than raw material expenditure. The same price margins described in the economic screening analysis, section 4.5, were ZAR 902.00/t for 5.0M NaOH and ZAR 1745.00/t for 1.0M HCl. Three 5.0M NaOH washes, one 1.0M HCl wash and 4 water washes per batch, at 21 batches per day including start-up, equated to ZAR 6.43 million/year. For comparison, if only two 5.0M NaOH washes were utilised, the raw material expenditure would total to R3.02 million/year.

The overall production expenditure is the summation of annual utility, labour, raw material, and maintenance and repairs costs. The annual maintenance and repair costs is approximately 6% of the total module cost, hence, ZAR 2.66 million/year. The overall production cost is approximated to be ZAR 16 895 227.30/year.

The fixed plant capital cost is the total module cost, which is ZAR 44.39 million; and the working capital is taken at 5% fixed capital. The fixed plant capital has a salvage value of 20% after 28 years. The overall cash flow, or profit, of the process plant over 28 years is determined by summating the overall revenue, savings incurred and production costs. As described above, the production cost is ZAR 16.895 million/year and the savings, which are brought about by utilising raw PT-char from the neighbouring WT-pyrolysis plant, are R0.351million/year. Revenue is produced by UPT-char sales and, since UPT-char is produced at a rate of 3403.26kg/day, it must be sold for ZAR 21.48/kg (US $1810/t) to produce positive cash flow of ZAR 7.282million/year and promote investment viability. After three years, 28% tax rate is levied, thus giving an after tax cash flow profit of ZAR 6.198million/year. A complete capital cost, cash flow, profit spreadsheets and cumulative cash flow diagram for non-discounted after-tax cash flows are described below.

Bare Module Cost of Major Equipment for PT-char Acid-alkali Demineralisation Process shown in Figure 36

Process Unit Description	Identification Number	Bare Module Equipment Cost (R million)
Plate Heat Exchanger	H-1	R6.59
Plate Heat Exchanger	H-2	R17.10
Total Cost including CEPCI		**R24.26**
Centrifugal Pump	P-1A/B	R 0.0134
Centrifugal Pump	P-2A/B	0.0167
Centrifugal Pump	P-3A/B	0.0210
Centrifugal Pump	P-4A/B	0.029`1
Centrifugal Pump	P-5A/B	0.0376
Centrifugal Pump	P-6A/B	0.0228
Centrifugal Pump	P-7A/B	0.0232
Centrifugal Pump	P-8A/B	0.0228
Centrifugal Pump	P-9A/b	0.0228
Total Cost including CEPCI		**0.2142**
Storage Vessel	V-1	R 0.77
Storage Vessel	V-2	0.35
Storage Vessel	V-3	1.21
Storage Vessel	V-4	0.42
Equalization Vessel	V-5	1.42
Equalization Vessel	V-6	2.14
Equalization Vessel	V-7	0.73
Total Cost including CEPCI		**7.21**
Sieve	S-1	0.206
Total Cost including CEPCI		**0.211**
Screw Conveyor	C-1	0.059
Screw Conveyor	C-2	0.058
Screw Conveyor	C-3	0.058
Screw Conveyor	C-4	0.058
Screw Conveyor	C-5	0.056
Total Cost including CEPCI		**0.295**
Agitated Nutsche Filter Dryer	R-1	1.346
Agitated Nutsche Filter Dryer	R-2	1.346
Agitated Nutsche Filter Dryer	R-3	1.346
Agitated Nutsche Filter Dryer	R-4	1.273
Total Cost including CEPCI		**5.438**

Utility Cost of Major Equipment for PT-char Acid-alkali Demineralisation Process shown in Figure 36

Process Unit Description	Identification Number	Utility Description	Utility Cost (R million/ annum)
Electricity: R0.86/kWh Heating Water: R20.00/1000kg Warm Air: R4.15/100m^3 Process Water: R0.80/1000kg			
Plate Heat Exchanger	H-1	Heating Water	R 0.982
Plate Heat Exchanger	H-2	Heating Water	R 1.194

Centrifugal Pump	P-1A/B	Electricity	R 0.00014
Centrifugal Pump	P-2A/B	Electricity	R 0.00009
Centrifugal Pump	P-3A/B	Electricity	R 0.00014
Centrifugal Pump	P-4A/B	Electricity	R 0.00023
Centrifugal Pump	P-5A/B	Electricity	R 0.00036
Centrifugal Pump	P-6A/B	Electricity	R 0.00015
Centrifugal Pump	P-7A/B	Electricity	R 0.00016
Centrifugal Pump	P-8A/B	Electricity	R 0.00015
Centrifugal Pump	P-9A/b	Electricity	R 0.00015
Screw Conveyor	C-1	Electricity	R 0.0017
Screw Conveyor	C-2	Electricity	R 0.0015
Screw Conveyor	C-3	Electricity	R 0.0011
Screw Conveyor	C-4	Electricity	R 0.0011
Screw Conveyor	C-5	Electricity	R 0.0010
Agitated Nutsche Filter Dryer	R-1	Electricity Heating Water Warm Air	R 0.00074 R 0.38 R 0.0158
Agitated Nutsche Filter Dryer	R-2	Electricity Heating Water Warm Air	R 0.00074 R 0.38 R 0.0158
Agitated Nutsche Filter Dryer	R-3	Electricity Heating Water Warm Air	R 0.00074 R 0.38 R 0.0158
Agitated Nutsche Filter Dryer	R-4	Electricity Heating Water Warm Air	R 0.00059 R 0.15 R 0.472

Capital Cost and Depreciation

Years	Plant (Fixed) Cost	Working Capital Cost	Total Capital Cost	Plant Depreciation
1	R -44 393 978.30	R -	R -44 393 978.30	R -
2	R -	R -2 219 698.92	R -2 219 698.92	R -
3	R -	R -	R -	R -
4	R -	R -	R -	R -17 757 591.32
5	R -	R -	R -	R -10 654 554.79
6	R -	R -	R -	R -7 103 036.53
7	R -	R -	R -	R -
8	R -	R -	R -	R -
9	R -	R -	R -	R -
10	R -	R -	R -	R -
11	R -	R -	R -	R -
12	R -	R -	R -	R -
13	R -	R -	R -	R -
14	R -	R -	R -	R -
15	R -	R -	R -	R -
16	R -	R -	R -	R -
17	R -	R -	R -	R -
18	R -	R -	R -	R -
19	R -	R -	R -	R -
20	R -	R -	R -	R -
21	R -	R -	R -	R -
22	R -	R -	R -	R -
23	R -	R -	R -	R -
24	R -	R -	R -	R -
25	R -	R -	R -	R -
26	R -	R -	R -	R -

| 27 | R   - | R   2 219 698.92 | R   2 219 698.92 | R   - |
| 28 | R   8 878 795.66 | R   - | R   8 878 795.66 | R   - |

Cash Flow

Years	Char Revenue	Char Savings	Production Cost	Cash Flow (Profit)
1	R -	R -	R -	R -
2	R -	R -	R -	R -
3	R 25 152 598.92	R 351 216.43	R -16 895 227.30	R 8 608 588.05
4	R 25 152 598.92	R 351 216.43	R -16 895 227.30	R 8 608 588.05
5	R 25 152 598.92	R 351 216.43	R -16 895 227.30	R 8 608 588.05
6	R 25 152 598.92	R 351 216.43	R -16 895 227.30	R 8 608 588.05
7	R 25 152 598.92	R 351 216.43	R -16 895 227.30	R 8 608 588.05
8	R 25 152 598.92	R 351 216.43	R -16 895 227.30	R 8 608 588.05
9	R 25 152 598.92	R 351 216.43	R -16 895 227.30	R 8 608 588.05
10	R 25 152 598.92	R 351 216.43	R -16 895 227.30	R 8 608 588.05
11	R 25 152 598.92	R 351 216.43	R -16 895 227.30	R 8 608 588.05
12	R 25 152 598.92	R 351 216.43	R -16 895 227.30	R 8 608 588.05
13	R 25 152 598.92	R 351 216.43	R -16 895 227.30	R 8 608 588.05
14	R 25 152 598.92	R 351 216.43	R -16 895 227.30	R 8 608 588.05
15	R 25 152 598.92	R 351 216.43	R -16 895 227.30	R 8 608 588.05
16	R 25 152 598.92	R 351 216.43	R -16 895 227.30	R 8 608 588.05
17	R 25 152 598.92	R 351 216.43	R -16 895 227.30	R 8 608 588.05
18	R 25 152 598.92	R 351 216.43	R -16 895 227.30	R 8 608 588.05
19	R 25 152 598.92	R 351 216.43	R -16 895 227.30	R 8 608 588.05
20	R 25 152 598.92	R 351 216.43	R -16 895 227.30	R 8 608 588.05
21	R 25 152 598.92	R 351 216.43	R -16 895 227.30	R 8 608 588.05
22	R 25 152 598.92	R 351 216.43	R -16 895 227.30	R 8 608 588.05
23	R 25 152 598.92	R 351 216.43	R -16 895 227.30	R 8 608 588.05
24	R 25 152 598.92	R 351 216.43	R -16 895 227.30	R 8 608 588.05

25	R	25 152 598.92	R	351 216.43	R	-16 895 227.30	R	8 608 588.05
26	R	25 152 598.92	R	351 216.43	R	-16 895 227.30	R	8 608 588.05
27	R	25 152 598.92	R	351 216.43	R	-16 895 227.30	R	8 608 588.05
28	R	25 152 598.92	R	351 216.43	R	-16 895 227.30	R	8 608 588.05

Profit

Years	Before Tax		Tax		After Tax		Project Cash Flow		Cumulative Cash Flow	
1	R	-	R	-	R	-	R	-44 393 978.30	R	-44 393 978.30
2	R	-	R	-	R	-	R	-2 219 698.92	R	-46 613 677.22
3	R	-	R	-	R	8 608 588.05	R	8 608 588.05	R	-38 005 089.17
4	R	-9 149 003.27	R	2 410 404.65	R	6 198 183.40	R	6 198 183.40	R	-31 806 905.77
5	R	-2 045 966.74	R	2 410 404.65	R	6 198 183.40	R	6 198 183.40	R	-25 608 722.38
6	R	1 505 551.52	R	2 410 404.65	R	6 198 183.40	R	6 198 183.40	R	-19 410 538.98
7	R	8 608 588.05	R	2 410 404.65	R	6 198 183.40	R	6 198 183.40	R	-13 212 355.59
8	R	8 608 588.05	R	2 410 404.65	R	6 198 183.40	R	6 198 183.40	R	-7 014 172.19
9	R	8 608 588.05	R	2 410 404.65	R	6 198 183.40	R	6 198 183.40	R	-815 988.80
10	R	8 608 588.05	R	2 410 404.65	R	6 198 183.40	R	6 198 183.40	R	5 382 194.60
11	R	8 608 588.05	R	2 410 404.65	R	6 198 183.40	R	6 198 183.40	R	11 580 377.99
12	R	8 608 588.05	R	2 410 404.65	R	6 198 183.40	R	6 198 183.40	R	17 778 561.39
13	R	8 608 588.05	R	2 410 404.65	R	6 198 183.40	R	6 198 183.40	R	23 976 744.79
14	R	8 608 588.05	R	2 410 404.65	R	6 198 183.40	R	6 198 183.40	R	30 174 928.18
15	R	8 608 588.05	R	2 410 404.65	R	6 198 183.40	R	6 198 183.40	R	36 373 111.58
16	R	8 608 588.05	R	2 410 404.65	R	6 198 183.40	R	6 198 183.40	R	42 571 294.97
17	R	8 608 588.05	R	2 410 404.65	R	6 198 183.40	R	6 198 183.40	R	48 769 478.37
18	R	8 608 588.05	R	2 410 404.65	R	6 198 183.40	R	6 198 183.40	R	54 967 661.76
19	R	8 608 588.05	R	2 410 404.65	R	6 198 183.40	R	6 198 183.40	R	61 165 845.16
20	R	8 608 588.05	R	2 410 404.65	R	6 198 183.40	R	6 198 183.40	R	67 364 028.55
21	R	8 608 588.05	R	2 410 404.65	R	6 198 183.40	R	6 198 183.40	R	73 562 211.95
22	R	8 608 588.05	R	2 410 404.65	R	6 198 183.40	R	6 198 183.40	R	79 760 395.35

23	R	8 608 588.05	R	2 410 404.65	R	6 198 183.40	R	6 198 183.40	R	85 958 578.74
24	R	8 608 588.05	R	2 410 404.65	R	6 198 183.40	R	6 198 183.40	R	92 156 762.14
25	R	8 608 588.05	R	2 410 404.65	R	6 198 183.40	R	6 198 183.40	R	98 354 945.53
26	R	8 608 588.05	R	2 410 404.65	R	6 198 183.40	R	6 198 183.40	R	104 553 128.93
27	R	8 608 588.05	R	2 410 404.65	R	6 198 183.40	R	8 417 882.31	R	112 971 011.24
28	R	8 608 588.05	R	2 410 404.65	R	6 198 183.40	R	15 076 979.06	R	128 047 990.30

Feasibility

Years	Project DCF		Cumulative Project Discounted Cash flow		Discounted Cash Flow Rate of Return	
1	R	-40 579 504.85	R	-40 579 504.85	R	-40 579 504.85
2	R	-38 947 422.39	R	-79 526 927.23	R	-38 947 422.39
3	R	-29 026 173.70	R	-108 553 100.93	R	-29 026 173.70
4	R	-22 205 069.37	R	-130 758 170.31	R	-22 205 069.37
5	R	-16 341 853.09	R	-147 100 023.40	R	-16 341 853.09
6	R	-11 322 274.06	R	-158 422 297.46	R	-11 322 274.06
7	R	-7 044 643.16	R	-165 466 940.62	R	-7 044 643.16
8	R	-3 418 517.81	R	-168 885 458.43	R	-3 418 517.81
9	R	-363 519.99	R	-169 248 978.42	R	-363 519.99
10	R	2 191 725.58	R	-167 057 252.84	R	2 191 725.58
11	R	4 310 545.10	R	-162 746 707.74	R	4 310 545.10
12	R	6 049 071.97	R	-156 697 635.77	R	6 049 071.97
13	R	7 457 015.31	R	-149 240 620.46	R	7 457 015.31
14	R	8 578 349.52	R	-140 662 270.95	R	8 578 349.52
15	R	9 451 932.79	R	-131 210 338.16	R	9 451 932.79
16	R	10 112 061.66	R	-121 098 276.50	R	10 112 061.66
17	R	10 588 968.02	R	-156 468 284.83	R	10 588 968.02
18	R	10 909 264.39	R	-151 837 443.35	R	10 909 264.39
19	R	11 096 342.75	R	-145 601 293.02	R	11 096 342.75
20	R	11 170 731.45	R	-138 069 889.01	R	11 170 731.45

21	R	11 150 414.65	R	-129 511 856.30	R	11 150 414.65
22	R	11 051 117.94	R	-145 417 166.88	R	11 051 117.94
23	R	10 886 563.75	R	-134 530 603.13	R	10 886 563.75
24	R	10 668 699.43	R	-123 861 903.70	R	10 668 699.43
25	R	10 407 900.99	R	-113 454 002.71	R	10 407 900.99
26	R	10 113 154.97	R	-135 304 011.91	R	10 113 154.97
27	R	9 988 478.11	R	-125 315 533.80	R	9 988 478.11
28	R	10 348 746.55	R	-114 966 787.25	R	10 348 746.55

Cumulative Cash Flow Diagram for Non-discounted After-tax Cash Flows
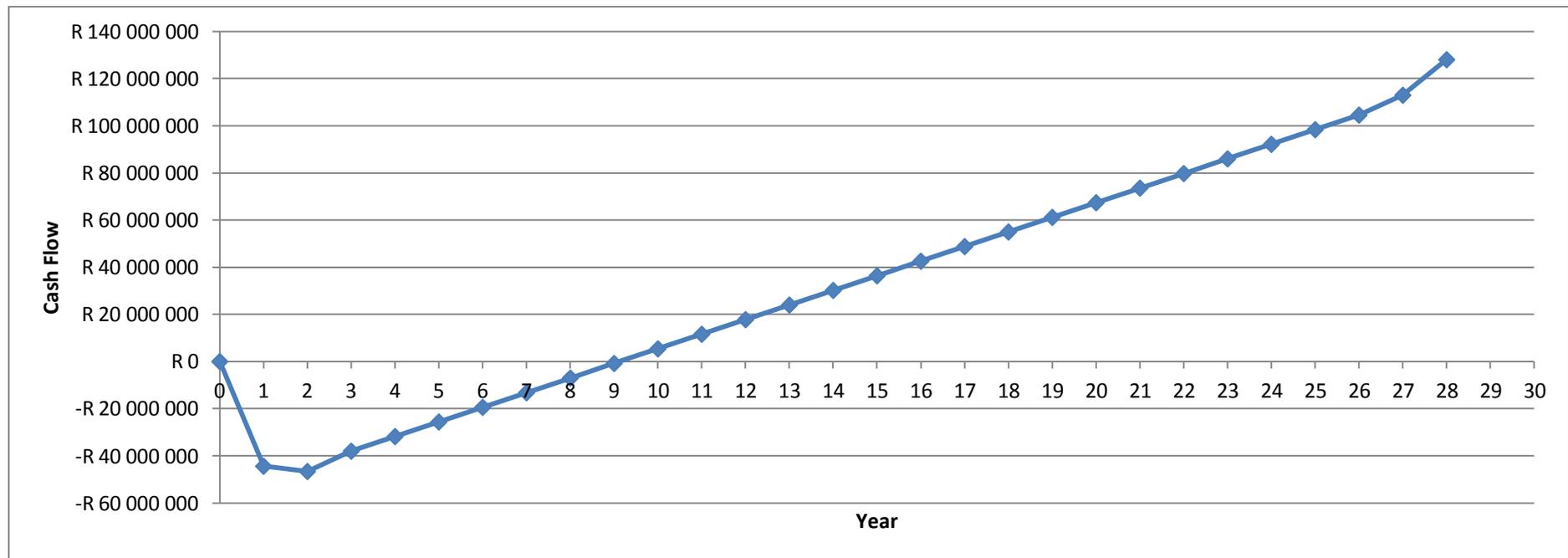
## Appendix S: Chemical engineering plant cost index projection

Values from 2012-2015 were forecasted using information from 1996-2011.

Year	CEPCI
1996	382
1997	387
1998	390
1999	391
2000	394
2001	394
2002	396
2003	402
2004	444
2005	468
2006	500
2007	525
2008	575
2009	521
2010	551
2011	582
2012	**580.55**
2013	**595.1588**
2014	**609.7676**
2015	**624.3765**

Chemical Engineering Plant Cost Index Trend
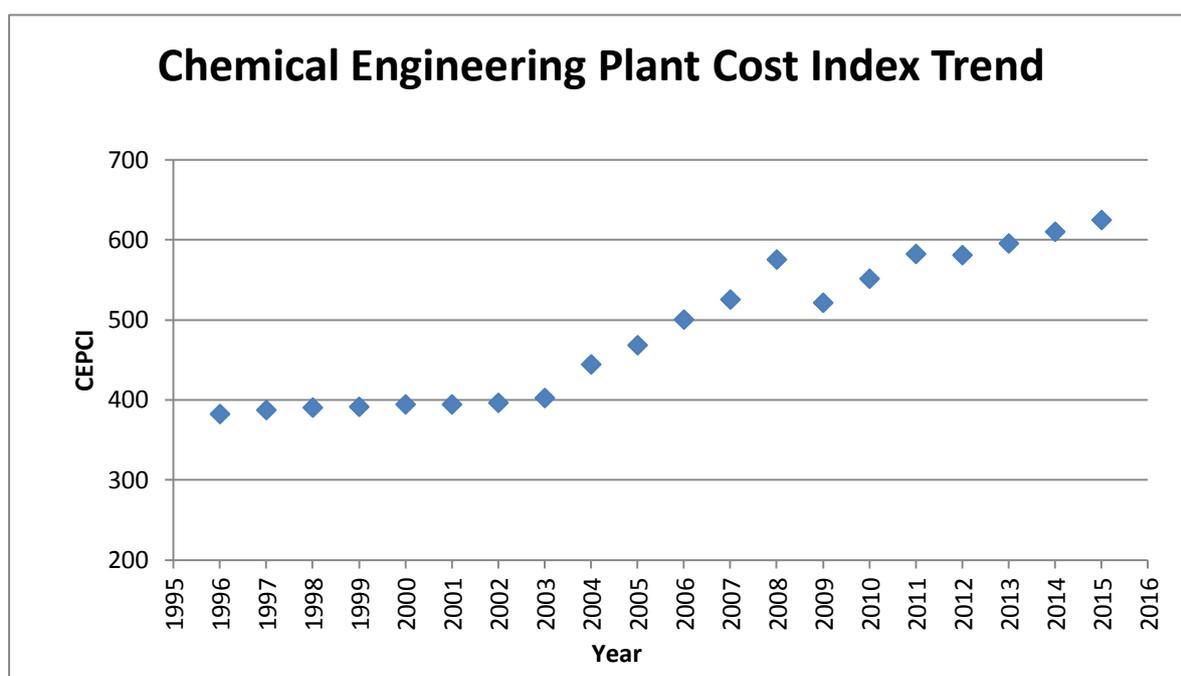
## Appendix T: Sensitivity analysis

The Effect of Fluctuating Electricity Costs
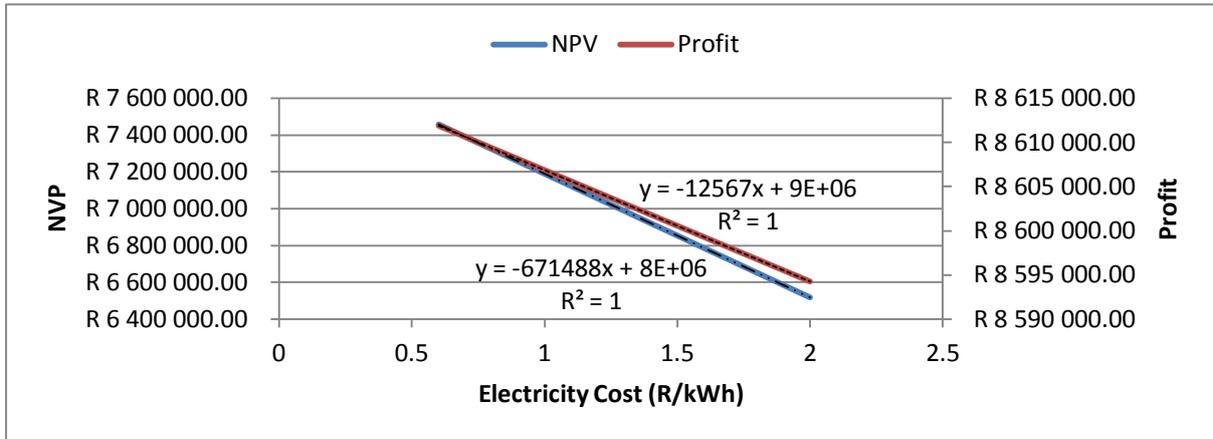

**The Effect of Fluctuating Water Costs**
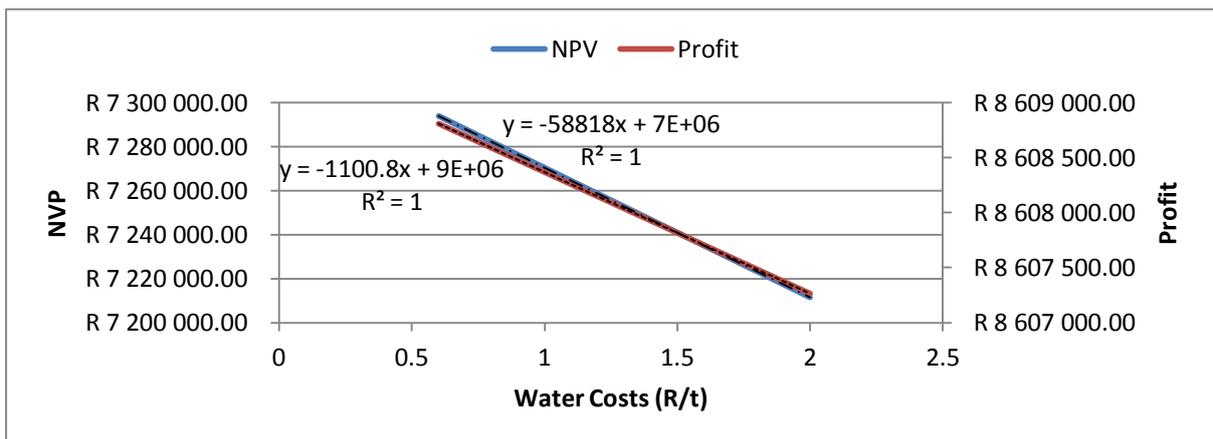
**The Effect of Fluctuating HCl Costs**
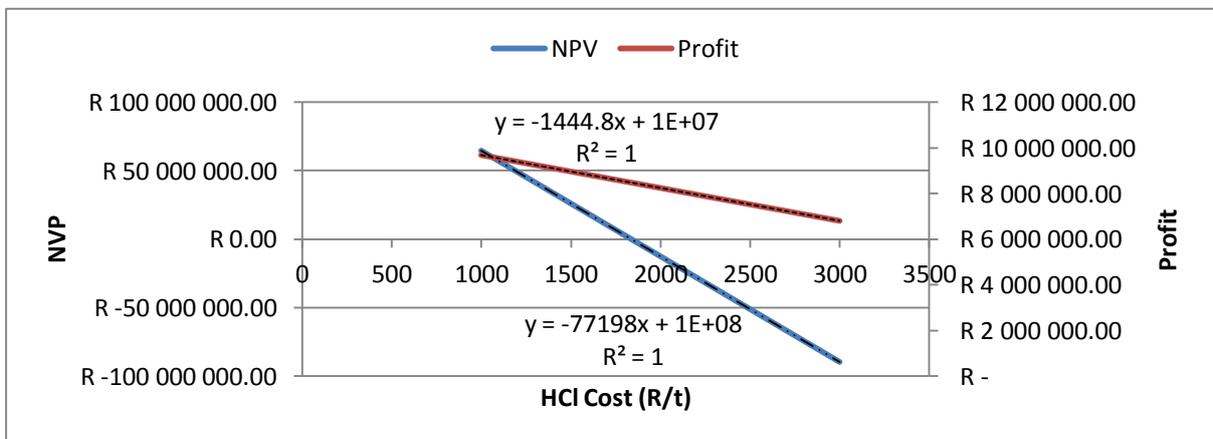
The Effect of Fluctuating NaOH Costs
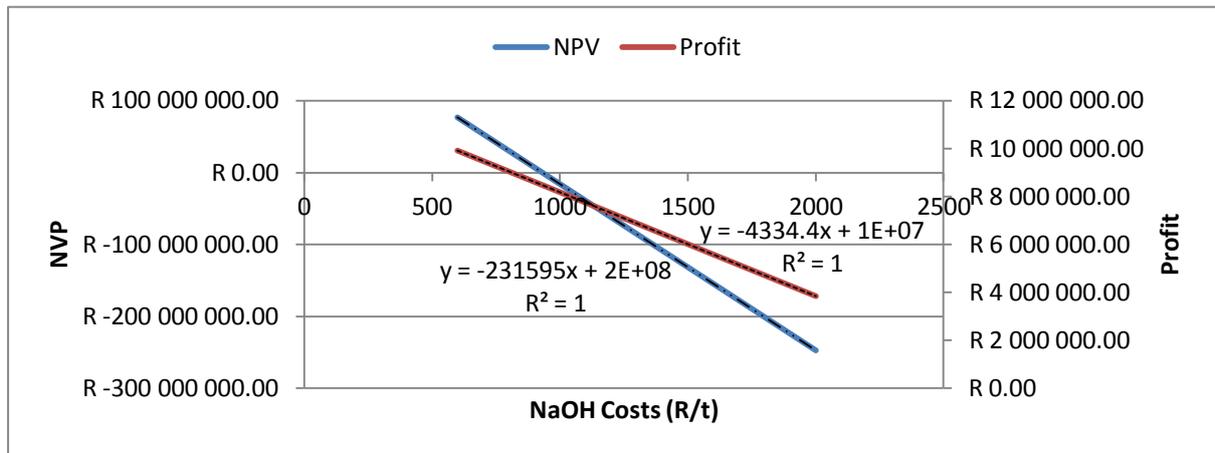
The Effect of Fluctuating UPT-char Price
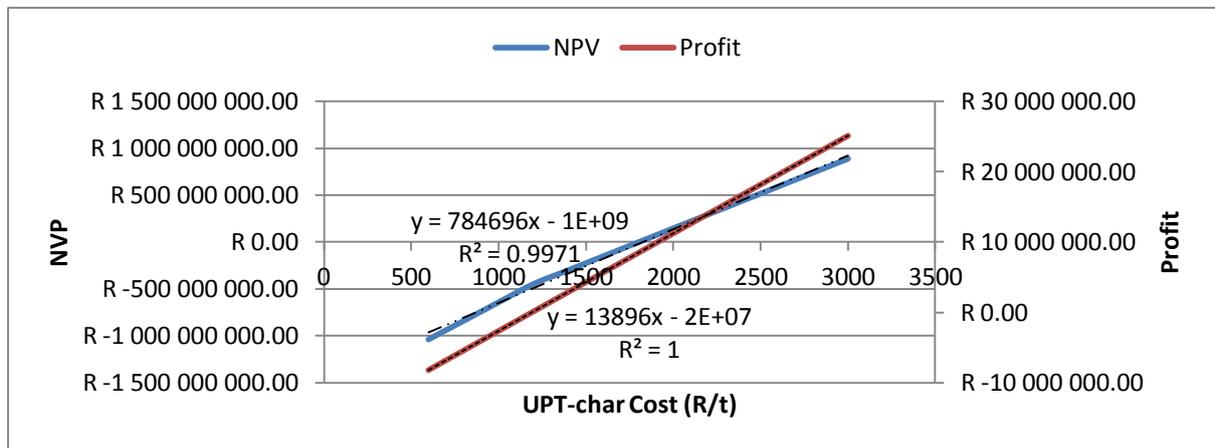
The Effect of Fluctuating Labour Costs

The Effect of Fluctuating Discount Rates

The Effect of Fluctuating Discount Rates. Chart with NPV (blue) and Profit (red) plotted against Labour Costs (R/month). Trendline equation:
$$y = 2E{+}13x^6 - 2E{+}13x^5 + 7E{+}12x^4 - 2E{+}12x^3 + 3E{+}11x^2 - 2E{+}10x + 9E{+}08$$
$$R^2 = 1$$